Engineering agnostic modules for the tuning of CAR T cell function

Thomas I Grothier

Cancer Institute

University College London

A thesis submitted for the degree of Doctor of Philosophy

2023

DECLARATION

I, Thomas I Grothier, confirm that the work presented in this thesis is my own. Where information has been derived from other sources, I confirm that this has been indicated in the thesis.

ACKNOWLEDGEMENTS

Firstly, I would like to thank Martin Pule and Shimobi Onuoha who interviewed me in 2015 for a role at Autolus. I'm fairly certain I got the job more as a result of my enthusiasm rather than knowledge or technical experience, so thanks for taking a gamble.

The four years of my PhD have been exciting, stressful, frustrating, inspiring and fun. I'm grateful for the experience of completing a PhD in a company setting and it is the people within Autolus, past and present, without whom I wouldn't have got to this point. Too many to thank by name for all the technical guidance, practical help, laughs and after work drinks.

I would like to thank Shaun Cordoba who was my first manager at Autolus and instrumental in securing my PhD position. More than this, he was a pleasure to work with and learn from, whilst taking the mick out of each other along the way. Thank you to Simon Thomas for picking up where Shaun left off and supporting me through the later stages of my PhD.

The cloning team within Autolus helped design and clone countless constructs, for which I am extremely grateful. They are James Sillibourne, Chris Allen, Kate Lamb, Abi Dolor and Farhaan Parekh. Other colleagues who contributed to the work in this thesis are Callum McKenzie, who engineered the $GD2^{+}$ cell lines and Mathew Robson who carried out the *in vivo* models. I'm thankful for the comradeship of both Matteo Righi and Ram Jha who have been here since day one.

A special thank you to Evangelia Kokalaki (Eva) who's support, knowledge, guidance and patience have been integral to this project. For listening to my rants and putting up with my dramatic side. I really can't thank you enough.

A huge thank you to my family for their unconditional love and constant encouragement. I'm incredibly lucky to have you. To my girlfriend Becky, thank you so much for your support, love, understanding and tolerance. You're just great.

To all my friends who have supported me throughout, I really am finished now.

ABSTRACT

Chimeric antigen receptor (CAR) T cells constitute an effective cancer immunotherapy, yet several challenges remain. For example, although CD22 is a promising B-ALL target, selective pressure from CAR T cells reduces CD22 expression resulting in patient relapse. To circumvent this hurdle, I aimed to develop a module to improve CAR T cell sensitivity. CSK is an inhibitory kinase that negatively regulates T cell signalling. I envisioned that a dominant-negative CSK might improve CAR T cell sensitivity. Therefore, I engineered a number of dominant-negative iterations of CSK (dnCSK). The co-expression of dnCSK modules in different CAR T cell platforms was seen to enhance sensitivity, improving cytotoxicity and cytokine release (IFN-γ and IL-2) against low antigen density target cells.

Another challenge for CAR T cell therapies is on-target off-tumour toxicity. The second aim was to develop a module enabling tuneable control of CAR T cell function. To do so, I employed a CSK mutant (CSK^{AS}) that is inhibited by a PP1 analogue, 3-IB-PP1. Co-expression of CSK^{AS} in CD22 and GD2 targeting CAR T cells dampened CAR function in the absence of 3-IB-PP1. However, after the addition of 3-IB-PP1, both CD22 and GD2 targeting CAR T cells displayed improved function compared to control CAR T cells. An advantage of this approach is the lack of CAR architecture re-engineering, permitting simple implementation into existing CAR platforms.

IMPACT STATEMENT

Cancer is one of the leading causes of death worldwide, accounting for nearly one in six deaths in 2020. Immunotherapies have emerged as encouraging treatment options for cancer patients, with CAR T cell therapy specifically demonstrating huge clinical success for the treatment of haematological malignancies. More recently, research focus has shifted to developing CAR T cell therapies for the treatment of solid tumours. However, there are a number of challenges facing CAR T cell therapy that are hindering its application to a broader range of indications. Such challenges include the lack of sensitivity of some CAR platforms against tumours expressing low levels of antigen as well as CAR-mediated toxicities such as CRS, neurotoxicity and on-target off-tumour toxicity.

The work in this thesis describes the identification and characterisation of standalone modules that were shown to improve CAR T cell sensitivity and enable tuneable control of CAR T cell function. With the aim of improving CAR T cell sensitivity, I described dnCSK modules that were able to lower the activation threshold of CAR T cells, improving the functional response against low antigen density target cells. These modules have the capacity to increase the sensitivity of CAR T cell platforms in which dimming of antigen density has led to tumour escape, and thus could potentially decrease the risk of relapse in these settings.

Toxicities associated with CAR T cell therapy have driven the engineering of numerous tuneable CARs, wherein CAR T cell function can be altered to respond to real-time adverse effects. In this thesis I described the CSK^{AS} module, which was shown to endow tuneable control over CAR T cell function in response to a small molecule drug. The CSK^{AS} module is expressed independently of the CAR, so in contrast to many existing tuneable CARs it requires no alteration of the CAR architecture, making its implementation into existing platforms straightforward. Moreover, it has the potential benefit to be used in the context of other receptors such as the TCR.

The drug used to control the function of the CSK^{AS} module is not clinically approved, thus it cannot currently be considered for use in a clinical product. However, the CSK^{AS} module demonstrates the feasibility of a CSK-based module to gain tuneable control of CAR T cell function. Engineering such a module would provide benefits in terms of reducing the adverse effects experienced by patients as well as reducing the financial burden associated with the management of CAR T cell-mediated toxicities.

TABLE OF CONTENTS

LIST OF FIGURES

LIST OF TABLES

ABBREVIATIONS

ACT	Adoptive Cell Therapy
ADCC	Antibody-Dependent Cell-Mediated Cytotoxicity
AICD	Antigen-Induced Cell Death
AKT	Protein Kinase B
ALL	Acute Lymphoblastic Leukaemia
APC	Antigen Presenting Cell
APC-Cy7	Allophycocyanin-Cyanine7
ATP	Adenosine Triphosphate
BCMA	B-Cell Maturation Antigen
BiTE	Bispecific T-cell Engagers
BSA	Bovine Serum Albumin
BV421	Brilliant Violet 421
CAIX	Carbonic Anhydrase IX
CAR	Chimeric Antigen Receptor
c-Cbl	Casitas B-lineage Lymphoma
CCR	Chimeric Cytokine Receptor
CD	Cluster of Differentiation
CDC	Complement-Dependent Cytotoxicity
CDR	Complementary Determining Region
CEACAM5	Carcinoembryonic antigen-related cell adhesion molecule 5
CLL	Chronic Lymphocytic Leukaemia
CLP	Common Lymphoid Progenitor

CMP	Common Myeloid Progenitor
CR	Complete Response
CRS	Cytokine Release Syndrome
C-terminal	Carboxyl terminal
CTL	Cytotoxic Lymphocyte
CTLA-4	Cytotoxic T-Lymphocyte Associated protein 4
CTV	Cell Trace Violet
DC	Dendritic Cells
DLBCL	Diffuse Large B Cell Lymphoma
DMSO	Dimethyl Sulfoxide
DNA	Deoxyribonucleic acid
E:T	Effector to Target Ratio
EGF	Epidermal Growth Factor
eGFP	Enhanced Green Fluorescent Protein
EGFR	Epidermal Growth Factor Receptor
EGFRvIII	Variant III of the Epidermal Growth Factor Receptor
ELISA	Enzyme-Linked Immunosorbent Assay
EpCAM	Epithelial Cell Adhesion Molecule
Fab	Fragment Antigen-Binding
FACS	Fluorescence-Activated Cell Sorting
FAK	Focal adhesion kinase
FAK2	Proline-rich tyrosine kinase 2
FBK	Flow-cytometry Based Killing

FDA	Food and Drug Administration
FITC	Fluorescein Isothiocyanate
FKBP	FK506-Binding Protein
FRB	FKBP12-Rapamycin Binding
FSC	Forward Scatter
GFP	Green Fluorescent Protein
GVHD	Graft Versus Host Disease
HA	Haemagglutinin
HER2	Human Epidermal Growth Factor Receptor 2
HLA	Human Leukocyte Antigen
HPV	Human Papilloma Virus
HRP	Horseradish Peroxidase
HSC	Haematopoietic Stem Cell
HSV-TK	Herpes Simplex Virus Thymidine Kinase
ICANS	Immune effector Cell-Associated Neurotoxicity Syndrome
IFN	Interferon
Ig	Immunoglobulin
IL	Interleukin
IMDM	Iscove Modified Dulbecco Media
IS	Immunological Synapse
ITAM	Immune-receptor Tyrosine-based Activation Motif
ITIM	Immune-receptor Tyrosine-based Inhibitory Motif
IV	Intravenous

JAK	Janus Kinase
Lag-3	Lymphocyte Activation Gene 3
LAT	Linker for Activation of T-Cells
Lck	Lymphocyte-specific Protein Tyrosine Kinase
mAbs	Monoclonal Antibodies
MCL	Mantle Cell Lymphoma
MFI	Mean Fluorescent Intensity
MHC	Major Histocompatibility Complex
MM	Multiple Myeloma
NHL	Non-Hodgkin Lymphoma
NK	Natural Killer
NSG	NOD SCID gamma
N-Terminal	Amino terminal
NT	Non-Transduced
ORR	Overall Response Rate
OVA	Ovalbumin
PAG	Phosphoprotein Associated with Glycosphingolipid-enriched microdomains
PBMCs	Peripheral Blood Mononuclear Cells
PBS	Phosphate Buffered Saline
PCR	Polymerase Chain Reaction
PD-1	Programmed-Death 1
PD-L1	Programmed Death Ligand 1
PE	Phycoerythrin

PI3K	Phosphoinositide 3-Kinase
PLC-γ1	Phospholipase C-γ1
PTPN22	Phosphotyrosine phosphatase, nonreceptor type 22
PVDF	Polyvinylidene Difluoride
RNA	Ribonucleic Acid
RPMI	Roswell Park Memorial Institute
scFv	Single Chain Variable Fragment
SDS-PAGE	Sodium Dodecyl Sulphate-Polyacrylamide Gel Electrophoresis
SFK	Src Family of protein tyrosine Kinases
SH	Src Homology
SHP-1	Src Homology region 2 domain-containing Phosphatase-1
SLP-7	SH2-domain-containing leukocyte protein of 76 kDa
SMAC	Supramolecular Activation Complex
SSC	Side Scatter
SYK	Spleen tyrosine Kinase
TAA	Tumour Associated Antigen
Tcm	Central memory T cells
TCR	T cells Receptor
Teff	Effector T cells
Tem	Effector memory T cells
Th	T Helper Cells
TILs	Tumour Infiltrated Lymphocytes
Tim-3	T-cell Immunoglobulin domain and Mucin domain 3

TM	Transmembrane
TME	Tumour Microenvironment
Tn	Naïve T cells
TNF	Tumour Necrosis Factor
TNFRSF	Tumour Necrosis Factor Receptor Superfamily
TRAF	TNFR Associated Factors
Treg	Regulatory T cells
TRUCKs	T cells Redirected for Antigen-Unrestricted Cytokine-Initiated Killing
TYRP	Tyrosinase-Related Protein 1
WT	Wild Type
ZAP-70	Zeta-Associated Protein of 70 kDa

1 INTRODUCTION

1.1 The immune system

The human immune system comprises many different cell types and molecules that work together to fight infection. The immune response to pathogens, toxins, or allergens can be split into two systems: Innate immunity and adaptive immunity. The innate immune response is the initial response to infection, with innate effector cells such as dendritic cells (DC), natural killer (NK) cells and macrophages able to recognise conserved molecular patterns of antigens (Chaplin 2010).

On the other hand, the effector cells of the adaptive immune response to infection are able to respond to a specific pathogen or antigen. B- and T- lymphocytes constitute the cells of the adaptive immune system (Cooper, Peterson, and Good 1965; Cooper et al. 1966). B cells have several functions, including antibody production and the regulation of T cell differentiation via the secretion of cytokines (Harris et al. 2000). Whereas T cells differentiate into subpopulations that have a variety of roles, although their main role is eliminating pathogen-infected cells or abnormal cells such as cancer cells (Reinherz and Schlossman 1980; Williams and Bevan 2007).

1.1.1 T Cells

1.1.1.1 T cell development and the T cell receptor

All human immune cells derive from pluripotent hematopoietic stem cells in the bone marrow, where they differentiate into either common myeloid progenitor (CMP) or common lymphoid progenitor (CLP) cells (Chaplin 2010). T cells arise from CLP cells, with precursor T cells migrating from the bone marrow to the thymus, where they undergo development. Here, T cells undergo a selection process and are challenged with self-peptides presented by Major Histocompatibility Complex (MHC) molecules. T cells that recognise self-peptide MHCs with optimal affinity receive a survival signal and are positively selected for, whereas those that recognise and bind with a

particularly high affinity undergo negative selection and apoptosis, to protect against autoimmunity (Aleksic et al. 2012).

T cells recognise antigen peptides on the surface of cells presented in the context of MHC class I (MHCI) and class II (MHCII) molecules. Specifically, proteins synthesised in the cytosol of nucleated cells are broken down into peptides and presented on the cell surface by MHCI molecules, identifying virally infected or cancerous cells for elimination by $CD8^+$ cytotoxic T cells. On the other hand, the MHCII molecules are expressed on the surface of Antigen Presenting Cells (APCs) and present peptides broken down from exogenous antigens, such as those from ingested bacteria. Peptides presented on the MHCII molecules are recognised by $CD4^+$ T cells (Rock, Reits, and Neefjes 2016). The T Cell Receptor (TCR) mediates recognition of peptides presented on MHC molecules, and binding of the TCR to nonself-peptides presented on MHCs triggers the T cell signalling pathway, enabling a cytotoxic response and elimination of the infected/tumour cell (Hennecke and Wiley 2001).

1.1.1.2 Structure of the T cell receptor

The TCR is a transmembrane protein residing on the surface of T-cells, which forms a heterodimer comprising either alpha/beta (αβ) or gamma/delta (γδ) polypeptide chains. 95-97% of the T cell population expressing the TCRαβ isoform (Brenner et al. 1986). The range of specificity of the TCR is attributed to the somatic rearrangement of different coding segments: variable (V), diversity (D), joining (J), and constant (C) (Davis and Bjorkman 1988; Fugmann et al. 2000), with the V and C regions forming the extracellular domain of the TCR.

The TCRα and TCRβ chains have short cytoplasmic domains with no signalling motifs, but they associate noncovalently with subunits of the CD3 complex (γ, δ, ε and ζ), all of which bear cytoplasmic tails containing Immunoreceptor Tyrosine-based Activation Motifs (ITAMs) (Clevers et al. 1988; Wucherpfennig et al. 2010; Reth 1989). ITAMs within the CD3ζ chains contain two YxxL/I sequences separated by seven or eight amino acid residues. Upon TCR engagement, the tyrosine residues within ITAMs are phosphorylated by kinases, enabling the docking of the ζ-chain Associated Protein tyrosine kinase of 70kDa (ZAP-70), an integral kinase in the TCR signalling pathway

(Reth 1989; Love and Hayes 2010). The current model of the TCR complex subunit composition is TCRαβ, CD3γε, CD3δε and ζζ. The γ, δ and ε chains each contain a single ITAM, whereas each ζ chain contains three ITAMs meaning the TCR complex contains ten ITAMs in total (Love and Hayes 2010). The benefit of multiple ITAMs is not fully understood and ITAM multiplicity is principally considered to be for the amplification of intracellular signalling, bestowing TCRs with high sensitivity. However, other models have been proposed: the ITAM discrimination model suggests that individual ITAMs recruit separate activation complexes, activating distinct downstream signalling pathways. Another model is the ITAM-mediated inhibition model, which suggests a negative regulatory role for ITAMs, with monophosphorylated ITAMs recruiting inhibitory phosphatases to the TCR (Love and Shores 2000).

To initiate TCR signalling, the TCR binds to the peptide-MHC (pMHC) with an affinity (K_D) range of 1-90 μM (Davis et al. 1998). Within the variable region of the TCR are three Complementarity Determining Regions (CDRs): CDR1, CDR2 and CDR3. The CDR3 loop sequence is the most variable, facilitating the recognition of a wide range of peptides (Chothia, Boswell, and Lesk 1988). After binding of the TCR to the pMHC, one of the co-receptors CD4 or CD8 can stabilise the TCR interaction further, binding pMHCII and pMHCI, respectively (Parnes 1989; Wooldridge et al. 2005).

1.1.1.3 Models of TCR triggering

The precise mechanism in which TCR binding to pMHC leads to ITAM phosphorylation, referred to as TCR triggering, remains a contentious topic. Three main models have been proposed to explain TCR triggering: aggregation, conformational change, and kinetic segregation. These models are not considered to be mutually exclusive.

According to the aggregation model, multimeric pMHC molecules cause engaging TCR complexes to cluster. Consequently, the amount of CD4/CD8 associated Lymphoid-specific Cytosolic protein tyrosine Kinase (Lck) increases, resulting in increased phosphorylation of ITAMs. Moreover, it has been suggested that this clustering

enables Lck to also phosphorylate and activate neighbouring Lck molecules, enhancing signalling (Cooper and Qian 2008).

The conformational change model is another model to describe TCR triggering. It has been suggested that conformational changes of the CD3ζ and ε cytoplasmic domains regulate triggering. One iteration of this model proposes that the cytoplasmic tail of CD3ζ is folded and bound to the plasma membrane, protected from phosphorylation. Upon engagement of the TCR, the CD3ζ unfolds from the membrane exposing the ITAMs for phosphorylation (Aivazian and Stern 2000). Similarly, it has been proposed that TCR engagement causes a conformational change in CD3ε, exposing a proline-rich motif, resulting in the recruitment of the Non-Catalytic tyrosine Kinase (Nck) before the activation of Lck and other tyrosine kinases (Gil et al. 2002). However, it has been demonstrated that this proline-rich motif plays a role in the expression of TCR and CD3 subunits, and Nck is not required for T cell activation (Mingueneau et al. 2008; Szymczak et al. 2005). Although conformational changes may play a role in TCR triggering, further research is required to understand the underlying mechanism of such changes.

Lastly, kinetic segregation is another model proposed to explain the activation of T cells upon TCR engagement. This model is based on segregation of the TCR complex from membrane-associated phosphatases. Upon TCR engagement to the pMHC, an immunological synapse (IS) forms between the T cell and the APC. The size of the TCR-MHC complex within the synapse determines the distance between the two membranes, which is approximately 14 nm (van der Merwe et al. 1995). The membrane bound tyrosine phosphatases CD45 and CD148 both bear large ectodomains, with the ectodomain of CD45 estimated to be between 28-51 nm long (McCall, Shotton, and Barclay 1992), while the ectodomain of CD148 has been estimated to be 47-55 nm (van der Merwe et al. 2000). As both these ectodomains exceed the size of the IS, CD45 and CD148 are segregated from the synapse site.

TCR signalling relies on a balance of molecules that promote signalling, such as Lck and ZAP-70, and molecules that inhibit signalling, such as the tyrosine phosphatases CD45 and CD148. In the absence of ligand, the TCR is constitutively phosphorylated and dephosphorylated, with the dynamic equilibrium between these signals

maintaining the T cell in a non-active resting state (O'Shea et al. 1992; Imbert et al. 1994; Secrist et al. 1993). However, the phosphatase segregation removes the inhibitory parameter from the synapse resulting in phosphorylation of the CD3 ITAMs, triggering the TCR. Evidence in support of this model shows that truncation of both CD45 and CD148 ectodomains to prevent their segregation from the synapse hinders T cell triggering (Lin and Weiss 2003; Irles et al. 2003; Cordoba et al. 2013).

1.1.1.4 TCR signalling

Protein tyrosine phosphorylation is fundamental to TCR signalling. The ITAMs within the cytoplasmic tails of the TCR complex are phosphorylated by members of the Src Family of protein tyrosine Kinases (SFKs). Lck is a member of the SFKs and a key positive regulator of TCR signalling. The CD4 and CD8 co-receptors are known to recruit Lck to the TCR complex, facilitating the phosphorylation of the ITAMs (Veillette et al. 1988; Rudd et al. 1988). However, more recently it has been suggested that this proximal phosphorylation event is carried out by a pool of "free", constitutively active Lck that can associate directly with the CD3 chains (Nika et al. 2010; Casas et al. 2014). The phosphorylation of the tyrosine residues within the ITAMs provides a docking site for ZAP-70 (Chan et al. 1992) which, upon binding to doubly phosphorylated ITAMs, becomes phosphorylated and hence activated by Lck. Upon activation, ZAP-70 phosphorylates numerous substrates including the Linker for Activation of T-Cells (LAT) (Figure 1), an adaptor protein that recruits numerous mediators crucial to downstream signalling (Wange 2000; Courtney, Lo, and Weiss 2018).

There are a number of negative regulatory proteins that phosphorylate and dephosphorylate tyrosine residues on the positive regulators of TCR signalling, Lck and ZAP-70. The phosphatases CD45 and CD148 play both an activatory and inhibitory role in the regulation of TCR signalling. They inhibit TCR signalling by dephosphorylating the activatory tyrosine residue in Lck, but they also dephosphorylate the inhibitory tyrosine of Lck, directing it towards a partially-active, "primed" state (Figure 2b) (Tangye et al. 1998; Zikherman et al. 2010; Stepanek et al. 2011; McNeill et al. 2007). C-terminal Src Kinase (CSK), negatively regulates TCR signalling by phosphorylating the inhibitory C-terminal tyrosine residue in Lck

(Bergman et al. 1992). This equilibrium between the phosphorylation and dephosphorylation of the TCR and Lck dictates the activation state of the T cell.

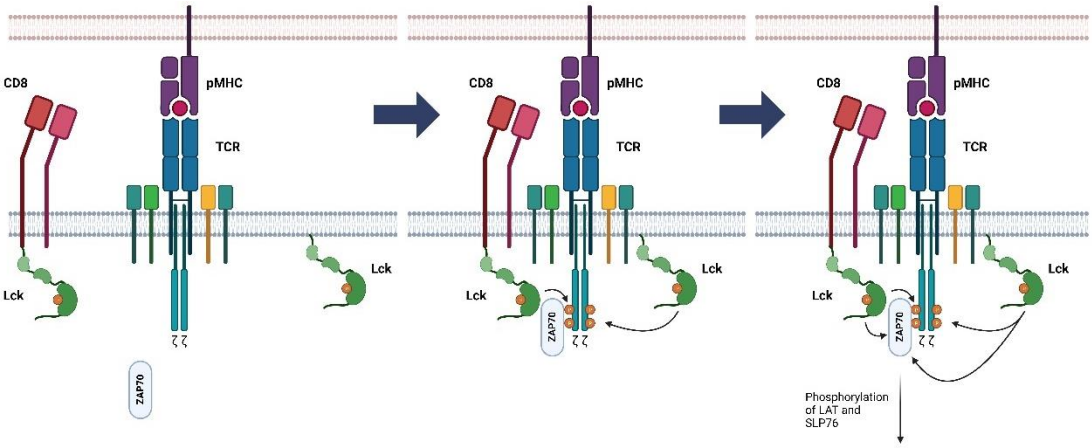

Figure 1. Proximal T cell signalling. After TCR engagement, free Lck or Lck associated with CD4 or CD8 phosphorylates CD3 ITAMs. Subsequently, ZAP-70 is recruited to doubly phosphorylated ITAMs and is then phosphorylated by Lck. Phosphorylation of ZAP-70 by Lck results in ZAP-70 activation and autophosphorylation. Activated ZAP-70 then phosphorylates the downstream adapter proteins LAT and SLP-76.

1.1.1.5 Proximal regulators of TCR signalling

TCR signalling is strictly regulated to ensure appropriate cellular responses to external stimuli. Without such stringent regulation, T cells can cause toxicities, such as targeting healthy tissues, leading to autoimmune diseases. TCR signalling is regulated by protein tyrosine kinases and phosphatases that directly interact with each other. The equilibrium between these regulators defines the activation threshold of the T cell and is therefore vital for normal T cell function (Hermiston et al. 2002).

The TCR complex itself does not possess catalytic function, however, the phosphorylation of the CD3 ITAMs by the SFKs initiates downstream signal cascades that lead to T cell activation (Weiss and Littman 1994). SFKs share a common structure (Figure 2a) comprising an Src homology (SH) 4 domain with myristoyl and palmitoyl groups attached that permit membrane localisation. Following the SH4 domain is an SH3 domain, an SH2 domain, a protein tyrosine kinase domain (SH1 domain) and a short C-terminal regulatory tail. All SFKs contain two regulatory tyrosine residues, one in the activation loop of the kinase domain and one in the C-terminal tail (Thomas and Brugge 1997). Solving the crystal structure of Lck and other SFKs led to the proposal of a common model for activation (Figure 2b) (Xu et al. 1999; Yamaguchi and Hendrickson 1996).

1.1.1.5.1 Lck

The SFK members Lck and Fyn play integral roles in T cell activation and can be associated either with the TCR itself (Samelson et al. 1990), with the CD4 and CD8 co-receptors (Veillette et al. 1988) or in lipid rafts within the plasma membrane (Janes et al. 2000). It is established that Lck is responsible for the phosphorylation of the ITAMs in the CD3ζ chains of the TCR complex. Jurkat cells lacking Lck have been shown to be unable to phosphorylate the CD3ζ chains, yet upon reintroduction of Lck by transfection, phosphorylation was re-established (Straus and Weiss 1992).

Lck exists in three forms: closed-inactive, open-primed, and open-active (Figure 2b). The specific conformation of Lck is determined by the phosphorylation state of two tyrosine residues, one in the C-terminal tail (Y505) and the other in the activatory loop (Y394). When the C-terminal tyrosine residue of Lck (Y505) is phosphorylated, it

interacts with its own SH2 domain, resulting in Lck adopting a closed-inactive conformation. The deletion or mutation of Y505 in Lck supports this regulatory model, as it resulted in a constitutively active form of Lck, that was no longer able to adopt this closed conformation (Marth et al. 1988). CSK negatively regulates Lck by phosphorylating the Y505 residue (Bergman et al. 1992).

The CD45 phosphatase dephosphorylates the tyrosine residues in both the activation loop and in the C-terminal tail, thus both positively and negatively regulating Lck (McNeill et al. 2007). This directs Lck towards a partially active, open and “primed” state.

Phosphorylation of the activation loop tyrosine of Lck (Y394) directs it towards an open-active conformation which has a 2-4-fold greater catalytic activity than Lck in an open-primed state. This can occur due to the clustering of co-receptors triggering Lck to phosphorylate the activatory tyrosine on neighbouring Lck molecules (Palacios and Weiss 2004).

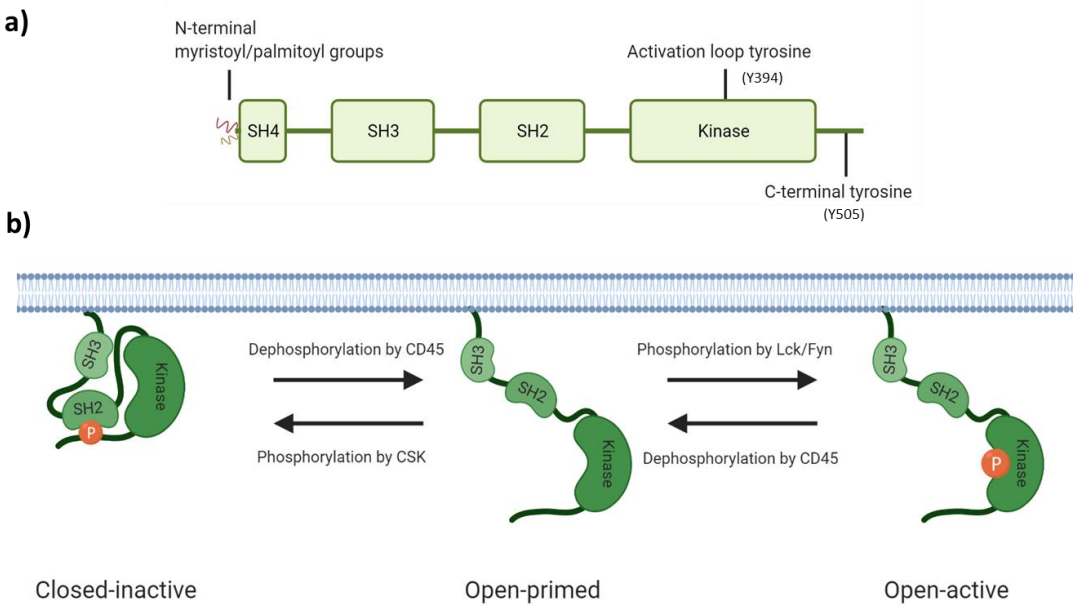

Figure 2. Structure and regulation of SFKs. a) Structure of Lck. Lck shares a common structure with other SFK members, with N-terminal myristoyl and palmitoyl groups that are required for membrane localisation, an SH4 domain, SH3 domain, SH2 domain, a protein tyrosine kinase domain (SH1 domain) and a short C-terminal regulatory tail. SFKs contain a regulatory tyrosine residue in the activation loop of the kinase domain and in the C-terminal tail. b) The regulation of Lck. Lck can be found in three states of activation: a closed-inactive state, in which the inhibitory C-terminal tyrosine residue is phosphorylated, an open-primed state in which Lck is mildly active but neither the C-terminal tyrosine or the tyrosine in the activation loop of the kinase domain are phosphorylated, and an open-active state in which the tyrosine residue in the activation loop is phosphorylated, resulting in full activation of Lck. The regulation of other SFKs is also dependent on the phosphorylation state of the tyrosine residues within the activation loop and the C-terminal tail.

1.1.1.5.2 Fyn

Fyn is another SFK member, which directly interacts with the TCR (Samelson et al. 1990) and ITAMs in the ζ chain (Gauen et al. 1992), but is also found in lipid rafts (Janes et al. 2000; Filipp et al. 2003). Fyn causes phosphorylation of the CD3ζ ITAMs resulting in ZAP-70 recruitment and subsequent activation of downstream signalling molecules (Gauen et al. 1994).

Fyn differs from Lck in its cellular distribution, with immunofluorescence analysis indicating that only a small portion of Fyn is associated with the TCR complex (approximately 5%), with the majority localised to the microtubule cytoskeleton (Ley et al. 1994). This localisation of Fyn suggests it also plays a role in cytoskeletal regulation. In support of this, Fyn phosphorylates Proline-rich tyrosine kinase 2 (FAK2) after TCR stimulation, a protein tyrosine kinase involved in actin cytoskeleton rearrangement (Qian et al. 1997).

In a similar manner to Lck and in accordance with the SFK regulatory model proposed by Xu and colleagues, the activation of Fyn is regulated by the phosphorylation state of a C-terminal tyrosine and a tyrosine in the activation loop (Figure 2b). Specifically, Fyn is activated upon phosphorylation of the activation loop tyrosine, Y420. On the other hand, upon phosphorylation of its C-terminal tyrosine, Y531, Fyn adopts a closed inactive conformation (Mustelin et al. 1992; Xu et al. 1999). As observed with Lck, the phosphorylation of the inhibitory C-terminal tyrosine is mediated by CSK (Okada et al. 1991). Moreover, phosphatases such as CD45 and CD148 also direct Fyn towards a primed state via the dephosphorylation of both Y420 and Y531 tyrosine residues (McFarland et al. 1993).

1.1.1.5.3 ZAP-70

As previously mentioned, activation of both Lck and Fyn causes the phosphorylation of ITAMs in the cytoplasmic tails of the TCR complex, resulting in the recruitment of ZAP-70. ZAP-70 is a member of the spleen tyrosine kinase family. It consists of two SH2 domains and a C-terminal kinase domain. Unlike the SFKs, ZAP-70 is not myristoylated or palmitoylated for membrane localisation (Chan et al. 1992). After Lck/Fyn mediated phosphorylation of the ITAMs in the cytoplasmic tails of the TCR

complex, ZAP-70 localises to the TCR by binding to doubly phosphorylated ITAMs via its tandem SH2 domains. Subsequent phosphorylation of ZAP-70 by Lck and Fyn causes ZAP-70 to become activated, which in turn phosphorylates a number of downstream proteins, culminating in T cell activation.

Within the kinase domain of ZAP-70 there are two regulatory tyrosine residues, Y492 and Y493. These are both phosphorylated after TCR engagement, with Y493 phosphorylated first by Lck/Fyn, followed by phosphorylation of Y492 by Lck, Fyn or ZAP-70 itself. The phosphorylation of Y493 is considered to be fundamental to ZAP-70 activation with Y492 potentially playing a negative regulatory role (Chan et al. 1995).

After activation, ZAP-70 phosphorylates and activates LAT and SH2-domain-containing Leukocyte Protein of 76 kDa (SLP-76). LAT and SLP-76 are both adaptor proteins that act as scaffolds to recruit numerous other molecules involved in the downstream transmission of the activation signal (Au-Yeung et al. 2009; Zhang et al. 1998).

In addition to the two regulatory tyrosine residues within the kinase domain of ZAP-70, there are three more tyrosine residues in the region between the second SH2 domain and the kinase domain that are known sites of phosphorylation: Y292, Y315 and Y319. These tyrosine residues are also phosphorylated by Lck/Fyn after TCR engagement, facilitating the interaction of ZAP-70 with other signalling regulators. Phosphorylation of Y292 on ZAP-70 facilitates the recruitment of the E3 ubiquitin ligase protein Casitas B-lineage Lymphoma (c-Cbl), which promotes the ubiquitination and thus degradation of the CD3ζ chain, Lck and Fyn, inhibiting TCR signalling (Wang et al. 2001; Lupher et al. 1997; Tanaka et al. 1995). The phosphorylation of Y315 and Y319 prevents ZAP-70 from returning to an autoinhibited conformation. Furthermore, substitution of Y319 to a phenylalanine reduces the phosphorylation of both LAT and SLP-76, inhibiting downstream signalling, indicating that Y319 is an important residue in the positive regulation of ZAP-70-dependent signals (Au-Yeung et al. 2009; Di Bartolo et al. 1999).

1.1.1.5.4 CD45

CD45 is a transmembrane protein tyrosine phosphatase, covering up to 10% of the surface of T cells (Thomas 1989). It possesses a large ectodomain (28-51 nm), a transmembrane domain, two intracellular tandem phosphatase domains (D1 and D2) and a C-terminal tail. The ectodomain exists in multiple isoforms with varying degrees of glycosylation, attributing to the range in size (McCall, Shotton, and Barclay 1992; Thomas and Lefrançois 1988; Hermiston, Xu, and Weiss 2003). Of the two phosphatase domains, only the membrane proximal D1 domain has phosphatase activity. Although both domains are required for optimal phosphatase activity, the role of the D2 domain is not fully understood (Desai et al. 1994; Hermiston, Zikherman, and Zhu 2009).

It was initially reported that CD45 is a positive regulator of TCR signalling, as CD45 was found to dephosphorylate the inhibitory tyrosine of both Lck and Fyn (Y505 and Y531, respectively), directing them towards the partially-active primed state (Mustelin et al. 1992; Mustelin, Coggeshall, and Altman 1989). Moreover, it was observed that CD45 was necessary for TCR signal transduction, with Lck and Fyn displaying increased phosphorylation of their inhibitory tyrosine residues in CD45 deficient cell lines (Pingel and Thomas 1989; McFarland et al. 1993; Sieh, Bolen, and Weiss 1993). Furthermore, due to the decrease in the amount of primed Lck, loss of CD45 in T cells impaired phosphorylation of the CD3ζ chain and ZAP-70 (Courtney et al. 2019).

CD45 also has an inhibitory effect on T cell signalling as it dephosphorylates the tyrosine residue in the activation loop of Lck (Y394), directing it towards a primed state and preventing its full activation (McNeill et al. 2007). Moreover, CD45 dephosphorylates the ITAMs of the CD3ζ chain (Furukawa et al. 1994; Hui and Vale 2014). Although complete loss of CD45 impairs TCR signalling, downregulation of CD45 expression to 10-60% of WT levels leads to optimal TCR signalling (McNeill et al. 2007).

1.1.1.5.5 CD148

CD148 is another transmembrane protein tyrosine phosphatase expressed on the surface of T cells, however, it differs in structure from CD45. CD148 consists of a large ectodomain, a transmembrane domain and a single intracellular phosphatase domain. Although the precise structure of the ectodomain has not been determined, it is known to have 8-10 N-glycosylated fibronectin domains and a mucin-like N-terminal region, indicating a total length of 47-55 nm (van der Merwe et al. 2000; Ostman, Yang, and Tonks 1994). The phosphatase domain contains a cysteine residue at position 1239 that is crucial for the catalytic activity of CD148 (Baker et al. 2001).

In a similar manner to CD45, CD148 has both an activatory and inhibitory role in TCR signalling, as it dampens the activity of Lck by dephosphorylating the tyrosine residue in the activation loop but also increases Lck activation through the dephosphorylation of the C-terminal tyrosine (Stepanek et al. 2011). As mentioned previously, TCR engagement leads to the activation of ZAP-70, which activates the adaptor protein LAT. In turn, LAT recruits and phosphorylates Phospholipase C-γ1 (PLC-γ1). Activation of PLC-γ1 results in the production of the secondary messenger molecules Diacylglycerol (DAG) and Inositol 1,4,5-trisphosphate (IP3), both of which are essential for T cell function. CD148 negatively regulates TCR signalling as it dephosphorylates both LAT and PLC-γ1, resulting in abrogation of TCR signalling (Baker et al. 2001).

1.1.1.5.6 PTPN22

Phosphotyrosine phosphatase, nonreceptor type 22 (PTPN22) is a cytosolic protein tyrosine phosphatase that contains an N-terminal phosphatase domain, interdomain and C-terminal domain with four proline-rich regions (Cohen et al. 1999; Matthews et al. 1992). PTPN22 is known to have an inhibitory effect on both Lck and ZAP-70 by dephosphorylating their activatory tyrosine residues, Y394 and Y493, respectively. However, it does not dephosphorylate their inhibitory tyrosine residues, Y505 in Lck and Y292 in ZAP-70. PTPN22 also dephosphorylates the activating tyrosine in Fyn (Y420) and inhibits TCR signalling further by direct dephosphorylation of the CD3ε and ζ chains (Wu et al. 2006; Cloutier and Veillette 1999). On the other hand, PTPN22

also plays a positive role in the regulation of TCR signalling. As previously mentioned, c-Cbl inhibits TCR signalling by promoting the ubiquitination and degradation of the CD3ζ chain, Lck and Fyn. PTPN22 binds and dephosphorylates c-Cbl, inhibiting this degradation and promoting TCR signalling (Tanaka et al. 1995; Cohen et al. 1999; Thien and Langdon 2005).

1.1.1.5.7 CSK

CSK is a protein tyrosine kinase that has a structural arrangement similar to SFKs. It contains an SH3 domain, SH2 domain and a C-terminal kinase domain. However, CSK lacks myristylation/palmitoylation sites that enable membrane localisation of SFKs. It also lacks the regulatory tyrosine residues in the activation loop and C-terminal tail, indicating it is regulated differently to the SFKs (Nada et al. 1991; Ogawa et al. 2002). CSK phosphorylates the C-terminal tyrosine of the SFKs, including Lck and Fyn directing them to a closed conformation and rendering them inactive (Figure 2b) (Bergman et al. 1992; Okada et al. 1991). In studies using mice with mutations in CSK to disrupt its function, SFK activity was observed to increase up to 14.7-fold, highlighting CSK as a negative regulator of TCR signalling (Nada et al. 1993).

CSK is a cytosolic protein, yet its substrates, Lck and Fyn, are localised at the plasma membrane, therefore, recruitment to the plasma membrane is a crucial step for the regulatory activity of CSK and is achieved primarily through its binding to Phosphoprotein Associated with Glycosphingolipid-enriched microdomains (PAG).

PAG is a transmembrane protein that is present alongside Lck and Fyn in lipid rafts within the plasma membrane and this close proximity to the SFKs results in the phosphorylation of a numerous tyrosine residues within PAG. Binding of the SH2 domain of CSK to PAG is dependent on phosphorylation of the Y317 residue. Once associated with PAG, CSK is able to access and phosphorylate the inhibitory C-terminal tyrosine residues of both Lck and Fyn, directing them to a closed-inactive conformation, inhibiting TCR signalling (Figure 3). However, upon TCR engagement, PAG becomes dephosphorylated, resulting in the dissociation of CSK (Brdicka et al. 2000; Davidson et al. 2003). Chow and colleagues generated a membrane-bound CSK by adding an N-terminal myristylation site, which increased the inhibition of Lck and

Fyn in T cells, highlighting the importance of membrane localisation to the negative regulatory effect of CSK (Chow et al. 1993). Once localised to the membrane, CSK is phosphorylated on a serine residue (S364) by Protein kinase A (PKA), resulting in a 2-4-fold increase in CSK activity (Vang et al. 2001).

In addition to the direct inhibition of SFKs, CSK also inhibits TCR signalling by recruiting PTPN22 to the plasma membrane (Figure 3). CSK binds to phosphorylated PAG via its SH2 domain and to PTPN22 via its SH3 domain. The recruitment of PTPN22 to the membrane facilitates the dephosphorylation and subsequent inactivation of Lck and Fyn (Cloutier and Veillette 1996). Some groups have suggested a synergistic function of the association between CSK and PTPN22, by demonstrating that PTPN22 mutants unable to interact with CSK inhibit TCR signalling less potently than wild-type PTPN22 (wtPTPN22) (Cloutier and Veillette 1999; Gjörloff-Wingren et al. 1999; Zikherman et al. 2009).

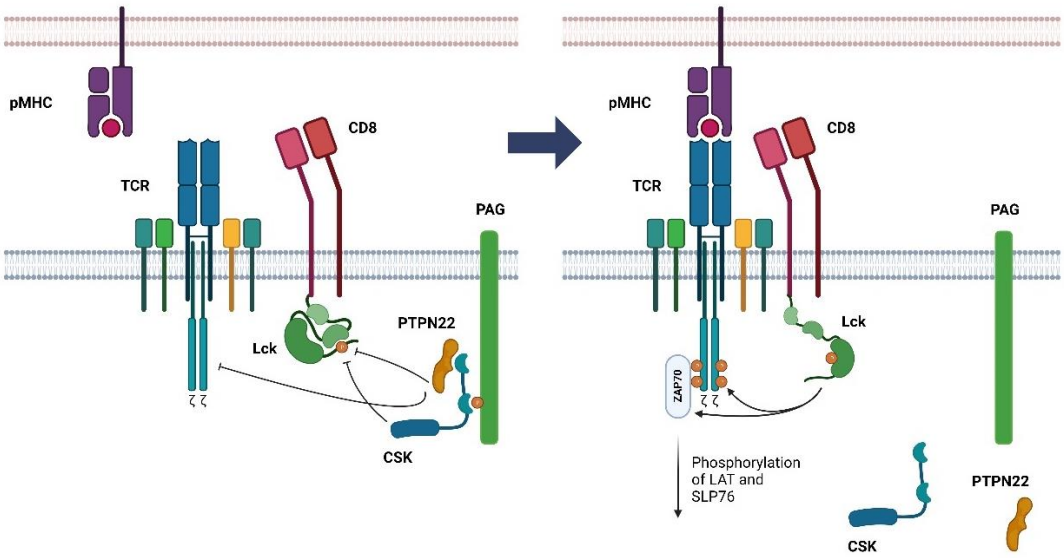

Figure 3. CSK in T cell signalling. Left: CSK localises to the plasma membrane via the interaction of its SH2 domain with phosphorylated transmembrane anchors, primarily PAG. At the membrane CSK inhibits T cell signalling by phosphorylation of the inhibitory residue of Lck (Y505). CSK-mediated recruitment of PTPN22 to the plasma membrane further inhibits signalling. PTPN22 dephosphorylates the activatory tyrosine residue of Lck (Y394) as well as ITAMS within the CD3ζ chains. Right: Upon engagement of the TCR with a pMHC complex, PAG becomes dephosphorylated, resulting in the dissociation of CSK (and subsequently PTPN22) from the plasma membrane. As CSK is no longer in the proximity of Lck it is unable to inhibit its activity, allowing for activated Lck to phosphorylate the CD3ζ chains of the TCR, promoting the docking of ZAP-70 and downstream T cell signalling.

1.1.1.6 Co-stimulation of T cells

Signalling through the TCR complex is insufficient to fully activate T cells. Additional co-stimulatory signals are required for full activation, with the discovery of CD28 providing evidence for the two-signal model of T cell activation. In this model, engagement of the TCR complex provides “signal 1”, transmitting through the CD3 chains. After which, binding of co-stimulatory receptors to their cognate ligands on APCs provides “signal 2”, promoting T cell activation and proliferation (Mueller, Jenkins, and Schwartz 1989; June et al. 1987; Lafferty and Cunningham 1975).

CD28 is a co-stimulatory receptor on the surface of T cells that binds primarily to members of the B7 family on APCs (Sharpe and Freeman 2002). Acuto and Michel reviewed the numerous studies demonstrating CD28 to promote T cell proliferation, cytokine production and cell survival (Acuto and Michel 2003). One key event upon CD28 binding is the association of Phosphatidylinositol 3-Kinase (PI3K) with a motif (pY173-M-N-M) in the cytoplasmic tail of CD28, leading to PI3K activation. This facilitates the activation of protein Kinase B (AKT), which phosphorylates multiple downstream proteins, activating the T cell (Parry et al. 1997).

In addition to CD28, numerous other co-stimulatory molecules have also been discovered. 4-1BB and OX40 are both co-stimulatory molecules and members of the Tumour Necrosis Factor Receptor Super Family (TNFRSF). Upon binding to their respective ligands, 4-1BBL and OX40L, a number of signalling proteins become activated, including PI3K and AKT. However, unlike CD28, 4-1BB and OX40 do not associate directly with signalling proteins but do so indirectly via TNFR-Associated Factor (TRAF) adaptor proteins. In addition to promoting T cell activation, co-stimulation via 4-1BB and OX40 also promotes T cell survival by upregulating anti-apoptotic molecules such as Bcl-XL (Lee et al. 2002; Rogers et al. 2001).

1.2 Adoptive Cell Therapy

As cancer cells arise from self, a hurdle in cancer immunotherapy is the tolerance of the immune system to tumour associated self-antigens (Pardoll 2003). TCRs with high affinity to self-antigens are subjected to thymic elimination, resulting in TCRs targeting tumour associated self-antigens having a 1.5-log lower affinity for pMHCs

than corresponding viral-peptide specific TCRs (Aleksic et al. 2012). Therefore, the endogenous T cell repertoire is often insufficient in managing cancer. Adoptive Cell Therapy (ACT) is the administration of immune cells with antitumour activity to cancer-bearing patients, such as Tumour-Infiltrating Lymphocytes (TILs), T cells with engineered TCRs, and T cells bearing Chimeric Antigen Receptors (CARs).

1.2.1 TIL based therapy

TILs are extracted from tumour biopsies and expanded *in vitro* before being adoptively transferred into patients. It was first demonstrated in 1988 that ACT using autologous TILs could mediate regression of cancer, as observed in 9 of 15 patients with metastatic melanoma (Rosenberg et al. 1988). Since then, TIL-based therapies have been used to treat a variety of different solid tumours including breast (Lee et al. 2017; Dadmarz et al. 1995), gastrointestinal (Turcotte et al. 2014), kidney (Hanada et al. 2001; Andersen et al. 2018), lung (Djenidi et al. 2015; Ben-Avi et al. 2018), and uveal melanoma (Chandran et al. 2017).

Despite promising studies demonstrating clinical efficacy, difficulties with the *in vitro* expansion and manufacturing of TILs persist. For instance, during *in vitro* expansion, the TCR repertoire can change drastically, resulting in loss of dominant tumour-specific T cell clones (Poschke et al. 2020). Such challenges have limited the widespread implementation of TIL therapy.

1.2.2 TCR based therapy

An alternative adoptive cell therapy to TILs is the use of T cells engineered to express TCRs specific for tumour associated antigens (TAAs). In 2006 it was demonstrated for the first time in humans that the adoptive transfer of T cells with an engineered TCR could mediate an anti-tumour response, although only 2 out of 15 patients treated for metastatic melanoma achieved sustained objective regression (Morgan et al. 2006). Clinical efficacy of engineered TCR-based immunotherapies for the treatment of other malignancies has also been demonstrated, including multiple myeloma (Rapoport et al. 2015) and colorectal cancer (Parkhurst et al. 2011).

A major benefit of TCR-based immunotherapies is that they are able to recognise a huge repertoire of peptides, including those derived from endogenous cytosolic proteins, tumour-associated mutated proteins, as well as peptides from microbial or viral antigens (Tsimberidou et al. 2021).

However, there are some risks associated with TCR-based therapies. Firstly, the viral transfer of exogenous TCRs into T cells could lead to mis-paired TCRs being expressed on the cell surface, whereby the α chain of the endogenous TCR pairs with the β chain of the exogenous TCR, or vice versa. Such mixed TCRs pose a toxicity risk as they may be reactive against self-antigens, as reported in one study that observed lethal graft versus host disease (GVHD) in a syngeneic mouse model following the adoptive transfer of engineered TCR cells (Bendle et al. 2010).

Secondly, another risk of TCR-based immunotherapies is the engineering of high affinity TCRs. This approach has led to lethal toxicity after accidental cross-reactivity of the TCRs against antigens on vital tissues (Linette et al. 2013; Morgan et al. 2013).

TCRs recognise antigens in the context of MHC molecules, however, MHC molecules are extremely polymorphic with thousands of alleles identified (Robinson et al. 2015). As TCRs only recognise antigens in the context of a specific MHC isoform, only patients expressing the correct isoform would be suitable for the administration of T cells with engineered TCRs (MHC-restriction). This limitation of TCR-based immunotherapy, in addition to the aforementioned risks, drove the development of CAR T cells. Unlike TCRs, CARs are able to recognise an antigen on the surface of target cells in an MHC-independent manner (Chmielewski, Hombach, and Abken 2013; Eshhar et al. 1993).

1.2.3 Chimeric antigen receptor T cell therapy

1.2.3.1 Structure of CARs

CARs comprise an extracellular binding domain that bestows the antigen specificity, a spacer region, transmembrane (TM) domain and an intracellular signalling domain (Figure 4). The extracellular domain consists of a Single-Chain Variable Fragment (scFv) and a spacer. The scFv is made up of the variable heavy (V_H) and variable light

(V_L) chains of an antibody tethered together by a flexible linker. The scFv bestows the specificity of the CAR, enabling the recognition of a wide range of cell surface antigens (Eshhar et al. 1993). The spacer region dictates the distance of the scFv from the plasma membrane and confers flexibility to the extracellular domain (Guest et al. 2005). The TM domain anchors the protein on the plasma membrane. Incorporating the CD3ζ intracellular domain into the CAR endodomain constitutes the first generation of CAR design and permits T cell activation (Figure 4) (Irving and Weiss 1991; Eshhar et al. 1993).

Eshhar and colleagues developed the first CAR construct, by expressing a scFv specific for 2,4,6-trinitrophenyl (TNP) linked to the CD3ζ chain in T cells. These T cells specifically lysed and secreted interleukin-2 (IL-2) in response to TNP positive target cells (Eshhar et al. 1993).

scFv domains are the most common binding domains used by CARs to endow specificity against a particular antigen. Features of the scFv such as affinity and antigen epitope location can dictate the functionality of the CAR T cell, although the topic of scFv affinity is contentious as most studies claim that high affinity CAR T cells are superior at recognising low antigen density targets compared to low affinity CARs (Hudecek et al. 2013; Chames et al. 2002; Lynn et al. 2016; Caruso et al. 2015; Liu et al. 2015; Chmielewski et al. 2004). However, one group reported CAR T cells with a low affinity scFv performed better against low antigen density targets (Turatti et al. 2007). Moreover, CAR T cells with a lower affinity scFv showed improved cytotoxicity and proliferation, which was attributed to a faster off-rate resulting in shorter receptor-ligand interactions, enabling serial triggering (Ghorashian et al. 2019).

In addition to affinity, the distance of the epitope from the target cell membrane is also a consideration of scFvs, with CARs targeting membrane-proximal epitopes found to be superior to those targeting membrane-distal epitopes (Hombach et al. 2007; James et al. 2008; Zhang et al. 2019). Targeting different epitopes alters the distance between the T cell and target cell, with a larger distance allowing for inhibitory phosphatases to infiltrate the synapse (Davis and van der Merwe 2006). To date, all FDA-approved CAR T cells target membrane proximal epitopes, with approximate synapse distances between CAR T cell and target cell to be 12-15 nm

(Xiao et al. 2022), which is small enough to exclude phosphatases such as CD45 (22 to 51 nm) (McCall, Shotton, and Barclay 1992).

The spacer and transmembrane regions are also important considerations of CAR structure. As mentioned above, the size of the CAR T cell synapse is important for functionality. To maintain the optimal synapse size, changes in spacer length must take into account whether the scFv targets a membrane-proximal or -distal epitope, with a short spacer being optimal for scFvs targeting distal epitopes and a longer spacer required for those targeting membrane-proximal epitopes (Guest et al. 2005). A recent study increased the size of a CAR spacer by adding tandem Ig domains of CEACAM5 and observed that increasing the size of the spacer domain diminished CAR T cell activation *in vitro* and *in vivo* (Xiao et al. 2022).

The type of spacer can also impact CAR T cell function, as some linkers are less flexible than others, potentially restricting access to epitopes. This was highlighted by Wilkie and colleagues who switched a CD28 hinge spacer for a flexible IgD hinge to improve recognition of a sterically hindered epitope on MUC1 (Wilkie et al. 2008). A more recent study has shown that both the hinge and transmembrane domain are important to CAR T cell function, by replacing the CD8 hinge/transmembrane region with a CD28 hinge/transmembrane region CAR T cells had a more stable synapse and a lower activation threshold (Majzner et al. 2020).

The endodomain of first generation CARs solely consists of the CD3ζ chain (Eshhar et al. 1993), however despite demonstrating effective cytotoxicity against tumour cells, these CAR T cells lacked sufficient IL-2 production, proliferation and persistence *in vivo* (Gong et al. 1999; Thomas Brocker 2000).

In order to achieve optimal activation, T cells require both “signal 1” and “signal 2”. The absence of a signal 2 can result in T cell anergy, a state of unresponsiveness (T. Brocker and Karjalainen 1995). To avoid T cell anergy and improve proliferation, second generation CARs were developed with intracellular domains comprising CD3ζ to provide signal 1, fused to co-stimulatory domains such as CD28 that provide signal 2. CAR T cells bearing a CD28 co-stimulatory domain displayed improved production of IL-2 and Interferon-γ (IFN-γ) (Maher et al. 2002). In addition to CD28, other co-

stimulatory domains have also been incorporated into CARs, including 4-1BB and OX40 (Finney, Akbar, and Lawson 2004).

CAR T cells bearing 4-1BB and the CD3ζ chain (4-1BBz) have displayed improved persistence compared to CAR T cells bearing CD28 and the CD3ζ chain (CD28z) in a clinical trial for the treatment of B cell Acute Lymphoblastic Leukaemia (B-ALL) (Zhao et al. 2020). Moreover, comparison of 4-1BBz and CD28z CAR T cells for the treatment of Non-Hodgkin's Lymphoma (NHL) found the 4-1BBz CAR T cells to be better tolerated with less severe adverse effects observed compared to patients who received CD28z CAR T cells (Ying et al. 2019). However, CD28z CAR T cells have been shown to be more sensitive against tumours with low antigen density than 4-1BBz CAR T cells *in vivo* (Majzner et al. 2020).

Third generation CARs have an intracellular domain comprising two co-stimulatory domains in addition to CD3ζ and have displayed improved proliferation and survival signals (Wilkie et al. 2008; Carpenito et al. 2009). Specifically, Pule and colleagues engineered a third generation CAR expressing CD28-OX40z, which produced 10-fold more IL-2 compared to second generation CAR T cells expressing CD28z (Pule et al. 2005). Overall, the precise CAR configuration and co-stimulatory domain selection for optimal CAR T cell functionality remains a topic of discussion. For instance, Abate-Daga and colleagues found that a second generation CAR with a CD28 endodomain displayed superior antitumour efficacy than a third generation CAR with a CD28 and 4-1BB endodomain (Abate-Daga et al. 2014).

Lastly, fourth generation CARs have been engineered to contain endodomains that enable the secretion of cytokines such as IL-12 upon CAR stimulation. The secretion of IL-12 after antigen engagement has been shown to recruit other immune cells such as macrophages to the tumour microenvironment, resulting in the lysis of tumour cells lacking antigen that would have ordinarily been spared (Chmielewski et al. 2011).

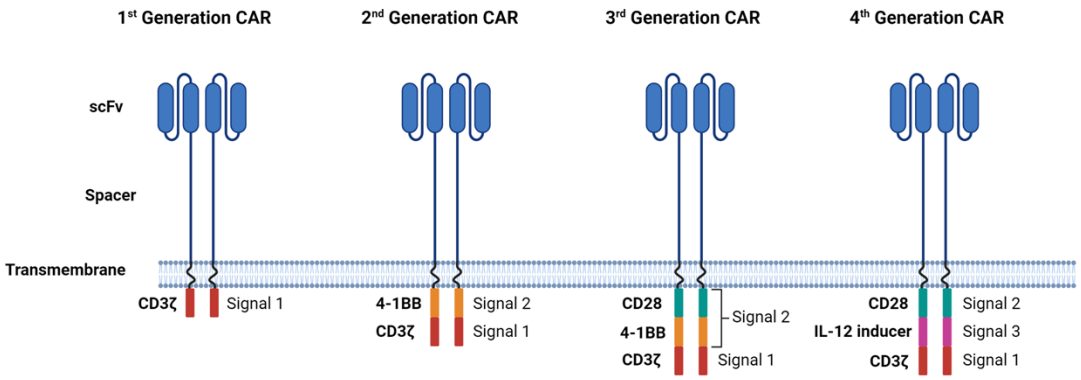

Figure 4. CAR structures. CARs consist of an scFv binding domain that bestows specificity, a spacer region that confers flexibility and length, a transmembrane domain, and an intracellular signalling domain. First generation CARs bear only a single signalling domain, typically CD3ζ. Second generation CARs bear CD3ζ and one co-stimulatory domain, such as CD28, 4-1BB or OX40. Third generation CARs bear CD3ζ and two co-stimulatory domains and fourth generation CARs have the additional ability to express a key cytokine, such as IL-12.

1.2.3.2 CAR signalling

To initiate signalling after antigen engagement, conventional CARs utilise the CD3ζ chain usually associated with the TCR. Recent studies have shown that after stimulation, both CARs and TCRs signal via a similar network of proximal signalling proteins. By employing a mass spectrometry approach, Salter and colleagues analysed phosphorylation events after the stimulation of second generation CAR T cells containing either a CD28 or 4-1BB co-stimulatory domain (Salter et al. 2018). After CAR-mediated stimulation, CAR T cells were observed to have increases in the activation of key signalling proteins including ZAP-70, LAT and PLC-γ1. A study by Tousley and colleagues also demonstrated that CAR T cells utilise signalling proteins key to TCR-mediated signalling (Tousley et al. 2023). In this study, they showed that knocking out one of Lck, ZAP-70, LAT or SLP-76, resulted in ablation of CAR T cell activity, highlighting their importance to CAR-mediated signalling.

Although CARs and TCRs have been shown to utilise common signalling proteins there remains a discrepancy in their sensitivity to antigen. While TCRs are able to elicit an activation response and secrete IL-2 after engagement with a single pMHC complex (Sykulev et al. 1996; Huang et al. 2013), the antigen density required for CAR-mediated cytokine production is estimated to be in the range of 770-5,320 molecules/cell (Stone et al. 2012; Watanabe et al. 2015).

This difference in sensitivity could be due to the difference in number of ITAMs in the TCR compared to a CAR, with the TCR having a total of ten ITAMs, yet conventional homodimeric CARs only have six (Harris and Kranz 2016). In support of the idea increased number of ITAMs improve T cell sensitivity, Majzner and colleagues reported that an anti-CD19 CAR bearing two consecutive CD3ζ chains demonstrated improved proliferation and cytotoxicity against low density targets (963 molecules/cell) (Majzner et al. 2020). In addition to the number of ITAMs, Feucht and colleagues reported that the position of each ITAM also influences T cell function, with second generation CARs expressing a CD28 co-stimulatory domain followed by CD3ζ containing a single membrane proximal functional ITAM shown to perform better *in vivo* than CARs expressing CD3ζ containing all three ITAMs (Feucht et al. 2019).

Another reason for the discrepancy between TCR and CAR sensitivity could be attributed to differences in their synapse formation. After TCR interaction with pMHC, the IS forms and consists of concentric rings called supramolecular activation clusters (SMACs). At the centre of the IS is the central-SMAC (cSMAC), which is formed by clustering of TCRs and has also been shown to be enriched for Lck (Monks et al. 1998). Surrounding the cSMAC is the peripheral-SMAC (pSMAC), which is enriched with lymphocyte function antigen-1 (LFA-1). LFA-1 binds intercellular adhesion molecule-1 (ICAM-1) on target cells, which contributes to both adhesion and co-stimulation (Bromley et al. 2001; Monks et al. 1998). The outermost ring is called the distal-SMAC (dSMAC) and is enriched for CD45, where it is spatially separated from the TCR and proximal signalling kinases such as Lck (Freiberg et al. 2002). Conversely, CAR T cells form an IS lacking a distinct LFA-1-enriched ring and Lck appears in multiple disorganised microclusters rather than clustering at the centre of the synapse (Davenport et al. 2018). Recent work by Burton and colleagues suggests the inefficient utilisation of adhesion receptors is a factor contributing to the lower sensitivity of CAR T cells. In this study they reported that engagement of LFA-1 with ICAM-1 increased the sensitivity of TCRs by 22-fold, whereas CAR sensitivity only increased 4.7-fold (Burton et al. 2023).

1.2.3.3 CAR T Cell therapy in the clinic

Despite CARs first being designed in the late 1980s, they were not tested clinically as a cancer therapy until the mid-2000s. The success of these trials was limited due to poor persistence of the CAR T cells (Kershaw et al. 2006; Park et al. 2007; Till et al. 2008). To address the issue of persistence, second generation CARs were developed containing co-stimulatory domains.

CD19 is a transmembrane protein expressed on B cells throughout their development and is also expressed on nearly all B cell malignancies (Wang, Wei, and Liu 2012). Early clinical trials of second generation CARs targeting CD19 showed promise, with a complete response (CR) observed to be ongoing > 10 months after treatment in two out of three patients treated for Chronic Lymphocytic Leukaemia (CLL) (Kalos et al. 2011) and in one of two patients treated for Acute Lymphoblastic Leukaemia (ALL) (Grupp et al. 2013).

Since these landmark trials, CD19 has become the most well-established target for CAR T cell therapy. In addition to ALL and CLL, CAR T cell treatment of other haematological malignancies has proved successful, as anti-CD19 CAR T cells have been utilised for the treatment of multiple myeloma (MM) leading to a CR or progression free disease in 6 of 10 patients (Garfall et al. 2015). Additionally, 63 of 77 patients (82%) with Diffuse Large B Cell Lymphoma (DLBCL) obtained a partial response or CR after treatment with an anti-CD19 CAR (Neelapu et al. 2017). Of the six CAR T cell therapies that have been approved by the FDA, all are for the treatment of haematological malignancies with four targeting CD19 (Maude et al. 2018; Neelapu et al. 2017; Wang et al. 2020; Abramson et al. 2020) and two targeting B-Cell Maturation Antigen (BCMA) (Munshi et al. 2021; Berdeja et al. 2021).

The success of CAR T cell therapies observed in haematological malignancies is yet to be emulated in the treatment of solid tumours. There have however been a number of promising clinical trials for the treatment of solid tumours such as neuroblastoma, prostate, lung and ovarian (Marofi et al. 2021). Although CAR T cell therapy has seen success in the treatment of haematological malignancies, there are a number of hurdles to be overcome before its widespread application for the treatment of other indications.

1.2.3.4 Clinical hurdles of CAR T Cell therapy

Despite the clinical efficacy of CAR T cell therapy, there are a number of challenges preventing its application for the treatment of a broader range of cancers. These challenges include suboptimal efficacy against low antigen density targets, or toxicities such as: Cytokine Release Syndrome (CRS), neurotoxicity, and on-target off-tumour toxicity.

1.2.3.4.1 Suboptimal function against low antigen density targets

The importance of antigen density to CAR sensitivity was emphasized in a phase I clinical trial of an anti-CD22 CAR for the treatment of patients with relapsed/refractory B-ALL. The overall rate of complete remission was 72.5%, but of the 12 patients who attained remission, 8 patients relapsed. Before the infusion of the CAR T cells, the median CD22 density was 2,839 molecules/cell. However, 7 of

the 8 reported relapses were associated with diminished CD22 density, resulting in tumour escape (Fry et al. 2018). Relapses attributed to dimming of CD22 antigen have also been observed in a clinical trial of a CAR T cell targeting both CD19 and CD22. Of the 13 patients that responded to treatment, 9 relapsed, with the majority of relapses attributed to poor CAR T cell persistence. However, one relapse was attributed to tumour escape via the complete loss of CD19 expression and diminished CD22 expression (Cordoba et al. 2021).

To prevent tumour escape by diminishing of antigen density, improving CAR T cell sensitivity to low antigen density has become a research focus. One strategy employed to increase sensitivity is adjusting the CAR affinity.

A number of studies reported an increase in CAR affinity to be positively correlated with function against low antigen density targets (Hudecek et al. 2013; Chames et al. 2002; Lynn et al. 2016; Caruso et al. 2015; Liu et al. 2015; Chmielewski et al. 2004). However, there are a number of caveats within these studies which highlight that the relationship between CAR affinity and sensitivity is not straightforward. For example, a number of these studies only compared two CARs, rather than investigating a range of different CAR affinities (Chames et al. 2002; Hudecek et al. 2013; Caruso et al. 2015). Moreover, some groups compared the affinity of CARs containing two distinct scFvs, whilst not taking into account other features that may vary between the constructs, such as stability (Hudecek et al. 2013; Caruso et al. 2015). Chmielewski and colleagues studied CARs with a range of affinities: 15 pM, 0.12 nM, 1 nM, 16 nM and 320 nM. However, they observed a binary response between affinity and cytotoxicity, as CARs with an affinity ≤ 16 nM effectively lysed target cells to comparable levels, whereas the CAR T cells with the 320 nM affinity demonstrated limited cytotoxicity (Chmielewski et al. 2004). Thus, a more comprehensive range of affinities is required to better understand the relationship between CAR affinity and functionality.

Despite the majority of studies demonstrating a positive correlation between CAR affinity and function against low antigen density targets, one study found that a CAR with low affinity (1.6 μM) had superior function against low antigen density targets than a CAR with a higher affinity (1 nM) (Turatti et al. 2007). In addition to the caveats

mentioned above, conflicting conclusions on the correlation between CAR affinity and sensitivity render it a challenging approach.

Another approach to improve CAR sensitivity is by increasing the CAR density. However, this strategy also carries limitations, as increasing CAR density above a threshold is associated with tonic signalling and AICD. The specific threshold was observed to vary depending on the CAR platform (Gomes-Silva et al. 2017).

More recently, approaches to improve the sensitivity of CAR T cells have focused on modifying other features of CAR architecture other than the scFv, such as the transmembrane and signalling domains. For instance, anti-CD19 CARs expressing two copies of the CD3ζ chain showed improved proliferation and cytotoxicity against targets with a low antigen density. Furthermore, in an *in vivo* model of CD19 low leukaemia, these "double zeta" CARs demonstrated superior antitumour activity compared to single zeta CAR T cells, resulting in prolonged survival (Majzner et al. 2020). In the same study, replacing the CD8-derived hinge/transmembrane domain with a CD28 hinge/transmembrane domain was also reported to significantly improve CAR function against low antigen density targets. To improve CAR T cell sensitivity, Salter and colleagues modified the signalling domains of two distinct CARs to contain elements of the CD3ε chain fused to the CD3ζ chain. This led to improved IFN-γ and IL-2 production in response to low antigen density target cells compared to conventional CARs (Salter et al. 2021).

1.2.3.4.2 CRS and Neurotoxicity

CRS is a systemic inflammatory response characterised by elevated levels of cytokines, most notably Tumour Necrosis Factor-alpha (TNFα), IFN-γ and IL-6 (Teachey et al. 2016). CRS is the most common toxicity induced by CAR T cell therapy and can range from mild to life threatening (grade 1-5), with symptoms including high fever, nausea, fatigue, tachycardia, cardiac dysfunction, organ failure and sometimes death (Lee et al. 2014). The FDA-approved CAR T cell product Kymriah observed CRS of ≥ grade 3 in 46% of patients treated for B-ALL (Maude et al. 2018), while 13% of patients treated with Yescarta for DLBCL experienced ≥ grade 3 CRS (Neelapu et al. 2017).

An ideal treatment for CRS would alleviate symptoms without adversely and irreversibly impacting the antitumour efficacy of the CAR T cells. IL-6 is a suitable target for managing CRS, since it is increased during CRS and is unnecessary for T cell function. Blocking the IL-6 Receptor (IL-6R) using tocilizumab, an FDA-approved monoclonal antibody (mAb), enabled rapid reversal of CRS (Maude et al. 2014; Grupp et al. 2013). Furthermore, CAR T cells remained efficacious as were still observed in patients who received tocilizumab (Maude et al. 2014). Currently, the administration of tocilizumab is considered the gold standard in the management of CAR-mediated CRS.

If CRS is not reversed upon the administration of tocilizumab, the administration of corticosteroids is a common secondary treatment (Lee et al. 2014). Corticosteroids are immunosuppressive and have successfully reversed CRS in patients undergoing CAR T cell therapy. However, their administration over a prolonged period or at high doses has also been reported to impair CAR T cell expansion and efficacy (Davila et al. 2014).

Neurotoxicity is another adverse side effect associated with CAR T cell therapy and is commonly referred to as immune effector cell-associated neurotoxicity syndrome (ICANS). Symptoms range from hallucinations, headaches and confusion to aphasia and seizures (Neelapu et al. 2018). Neurotoxicity has been observed in patients after treatment with CARs targeting different antigens, including CD19 (Davila et al. 2014; Maude et al. 2014) and BCMA (Munshi et al. 2021). In one anti-CD19 CAR T cell trial for the treatment of B-ALL, severe neurotoxicity arose in 50% of patients (Turtle et al. 2016). In a phase 1/2 clinical trial of another anti-CD19 CAR, 38% of patients experienced ≥ grade 3 ICANS, with one case of fatal cerebral oedema (Shah et al. 2019). Although the precise mechanism responsible for these neurological toxicities is unknown, it is speculated that it is due to general CAR T cell-mediated inflammation as opposed to specific targeting of Central Nervous System (CNS) tissue. This is based on the observation that neurotoxicity also arose in patients treated with blinatumomab, a bispecific antibody that binds CD3 on T cells and CD19 on tumour cells (Topp et al. 2014).

In severe cases, neurotoxicity is managed with corticosteroids. The administration of corticosteroids rather than tocilizumab for the treatment of severe neurotoxicity is favoured due to the ability of steroids, such as dexamethasone, to cross the blood-brain barrier (Lee et al. 2014; Mitchell et al. 2005). However, as mentioned above, administration of corticosteroids can reduce CAR T cell efficacy. Specifically, in one B-ALL study, the administration of corticosteroids reduced CAR T cell expansion, with patients experiencing disease recurrence (Davila et al. 2014). Therefore, a treatment that enables direct, reversible control over CAR T cell efficacy *in vivo* would be hugely beneficial for the management of CRS/ICANS.

Dasatinib is an FDA-approved immunosuppressive that has been identified as a drug with potential use in the management of both CAR-mediated CRS and neurotoxicity (Weber et al. 2019). It is a kinase inhibitor that blocks the adenosine triphosphate (ATP) binding sites of SFKs such as Lck, thereby inhibiting the phosphorylation of the ITAMs in the CD3ζ chains, preventing the recruitment of ZAP-70 and hindering T cell signalling (Tokarski et al. 2006).

Recent experiments have demonstrated the administration of dasatinib rapidly and reversibly inhibits CAR T cell activation, proliferation, cytotoxicity, and cytokine production both *in vitro* and *in vivo*. Titration of the dasatinib dose was demonstrated to confer complete or partial inhibition of CAR T cell functionality. Furthermore, CAR T cell viability was unaffected by the administration of dasatinib and a potent anti-lymphoma effect was observed in mice after the removal of dasatinib (Weber et al. 2019; Mestermann et al. 2019). As the administration of dasatinib has been shown to directly and reversibly control CAR T cell function without damaging cell viability, it poses an intriguing option for the future management of CRS and ICANS.

1.2.3.4.3 On-target off-tumour toxicity

A crucial consideration in CAR T cell therapy is the selection of the target antigen. An optimal target antigen would be one that is exclusively expressed on tumour cells. Tumour specific antigens can arise from mutations of surface proteins in tumour cells, referred to as neoantigens. Variant III of the Epidermal Growth Factor Receptor (EGFRvIII) is a neoantigen exclusively expressed on glioblastoma cells (Gan, Kaye, and

Luwor 2009). Its absence from healthy tissue makes EGFRvIII an ideal target for CAR T cell therapy. A number of anti-EGFRvIII CARs for the treatment of glioblastoma has been developed and validated *in vitro* and *in vivo* (Johnson et al. 2015; Sampson et al. 2014). However, neoantigens are rare.

A major obstacle is the dearth of tumour specific target antigens, leading to many CAR T cell therapies targeting TAAs. The scarcity of tumour specific target antigens is a result of cancer cells originating from self, with the vast majority of tumour antigens also being expressed on healthy tissue. As TAAs are generally overexpressed on tumours but also expressed on healthy tissues, there are concerns over safety. This pattern of expression is observed in a plethora of the TAAs targeted for the treatment of solid tumours, including PSMA, MUC1, and HER2 (Junghans et al. 2016; Zhou et al. 2019; Ahmed et al. 2015). In one case, a patient infused with anti-HER2 CAR T cells for treatment of metastatic colon cancer developed fatal CRS. This was attributed to on-target off-tumour toxicity, wherein the CARs recognised low levels of HER2 on lung epithelial cells (Morgan et al. 2010).

A number of different approaches have been developed to improve the safety of CAR T cell therapy. Suicide switches allow for the selective destruction of CAR T cells if CAR-mediated toxicities arise. One example of a suicide switch is the expression of Herpes Simplex Virus Thymidine Kinase (HSV-TK) in adoptively transferred T cells which makes them susceptible to elimination via the administration of ganciclovir. However, as HSV-TK is a virally derived protein there are concerns over immunogenicity, limiting its clinical application (Ciceri et al. 2009). An alternative suicide switch was developed by Straathof and colleagues, termed inducible Caspase-9 (iCasp9) which permits selective elimination of CAR T cells via apoptosis after the administration of a small molecule drug (Straathof et al. 2005). Other suicide switches have been engineered which enable elimination of CAR T cells via the administration of antibodies which bind to a marker on the cell surface. One such approach is to express a truncated form of EGFR (EGFRt) on engineered T cells, with the administration of cetuximab shown to result in effective elimination of EGFRt expressing cells (Wang et al. 2011; Paszkiewicz et al. 2016). Similarly, Phillip and colleagues developed a marker gene which could also be utilised as a suicide switch,

by fusing epitopes from CD34 and CD20 (RQR8). In this study, administration of rituximab was shown to selectively eliminate transgene expressing T cells (Philip et al. 2014).

Although shown to be effective, suicide switches share a major limitation, which is the permanent elimination of the CAR T cells eliminating their antitumour response. This limitation has prompted the development of a number of alternative strategies that address the issue of CAR-mediated on-target off-tumour toxicity.

Two research groups have independently developed affinity-tuned CARs that are able to distinguish between targets expressing high- and low-density antigen (Caruso et al. 2015; Liu et al. 2015). Liu and colleagues reported that anti-EGFR CARs with a high affinity (0.94 nM) did not discriminate between targets expressing varying levels of EGFR, with comparable responses against K562 cells electroporated with a 200-fold range of EGFR mRNA. However, the reactivity of CARs with lower affinity (88 nM and 217 nM) correlated with the expression level of EGFR on target cells (Liu et al. 2015). Similarly, Caruso and colleagues demonstrated that a 10.7-fold decrease of the affinity of an anti-EGFR CAR resulted in a 3.8-fold decrease in IFN-γ production against low density EGFR target cells (Caruso et al. 2015). Both of these studies reported that affinity tuning is an effective, albeit cumbersome, approach to shift the antigen density recognition window or CAR T cells, reducing the risk of on-target off-tumour toxicity.

Numerous research groups have applied Boolean logic gating to CAR T cells to enable more accurate distinction between malignant and healthy cells (Kloss et al. 2013; He et al. 2020; Lajoie et al. 2020; Lanitis et al. 2013; Fedorov, Themeli, and Sadelain 2013; Srivastava et al. 2019; Roybal et al. 2016; Tousley et al. 2023). Rather than targeting a single antigen, logic gate CAR T cells get activated once exposed to a specific combination of antigens. One approach using logic gates is to expresses two distinct CARs that target separate antigens, with one CAR expressing the CD3ζ chain, while the other CAR expresses a co-stimulatory endodomain. Thus, engagement of both CARs leads to full T cell signalling (Lanitis et al. 2013). However, this model still has the potential for on-target off-tumour toxicity, as CAR constructs expressing only the CD3ζ chain are still capable of activation in response to antigen expressing cells

(Eshhar et al. 1993). Another logic gate strategy was proposed by Roybal and colleagues, in which antigen engagement of the first CAR triggers the transcription of a second CAR which triggers signalling after engagement with a separate antigen (Roybal et al. 2016). However, as this strategy relies on transcription, there is a delay of approximately 6 hours after engagement of the first CAR before the second CAR is expressed on the cell surface.

Logic gates have also been engineered to prevent signalling in the presence of a specific antigen. Fedorov and colleagues developed a system called the inhibitory-CAR (iCAR), in which CARs expressed inhibitory signalling domains derived from CTLA-4 or PD-1 (Fedorov, Themeli, and Sadelain 2013). In this setting two CARs are expressed, one which binds a TAA and the iCAR which binds an antigen expressed on healthy tissues. Therefore, when both CARs are engaged with antigen, the inhibitory domain of the iCAR prevents the CAR T cell from being activated by healthy cells, preventing on-target off-tumour toxicity.

Several tuneable systems have been developed to improve the safety of CAR T cells, in which CAR T cell activity is controlled by the presence of a small molecule drug. Tuneable CARs can be characterised as drug-ON systems, wherein the CAR requires both antigen engagement and the small molecule for activation (Wu et al. 2015; Juillerat et al. 2016; Leung et al. 2019; Labanieh et al. 2022; Sahillioglu et al. 2021). Wu and colleagues engineered a tuneable CAR in which the antigen binding domain and intracellular signalling domains are expressed as separate peptides. Only upon the administration of a heterodimerizing small molecule, the rapamycin analogue (rapalog) AP21967, do the separate components of the CAR assemble. The functionality of this “ON-switch” CAR was tested *in vivo* in a mouse xenograft model, and in the absence of the small molecule, similar levels of tumour cell survival were observed when comparing the ON-switch CAR T cells condition and the condition in which no T cells were given. Yet, upon administration of the small molecule, ON-switch CAR T cells achieved significantly higher levels of target cell lysis (Wu et al. 2015). However, the small molecule rapalog used in this platform is an experimental drug used in research and is thus not suitable in a clinical setting.

Rapamycin could be used in place of the rapalog to dimerise the binding and signalling domains of a split CAR platform, but as rapamycin is an immunosuppressive drug using it in a drug-ON system would be problematic. Since this study, a number of other drug-ON CAR systems have been developed that also utilise rapamycin/rapalog to induce CAR T cell function (Juillerat et al. 2016; Leung et al. 2019). More recently, tuneable drug-ON CAR platforms have been developed that contain the hepatitis C virus (HCV) NS3 protease, and are activated via the administration of FDA-approved HCV protease inhibitors (Labanieh et al. 2022; Sahillioglu et al. 2021). However, the use of a virally derived protease in these platforms raises concerns over immunogenicity.

A disadvantage of drug-ON systems is that regular administration of the small molecule drug is required to maintain CAR T cell efficacy. To address this, a number of tuneable CAR systems have been developed in which administration of a small molecule disrupts CAR efficacy (drug-OFF systems) (Giordano-Attianese et al. 2020; Sun et al. 2020; Hotblack et al. 2021). In a similar fashion to the tuneable CAR developed by Wu and colleagues (Wu et al. 2015), another group engineered a split CAR system in which the binding domain and signalling domains are expressed as separate peptides (Giordano-Attianese et al. 2020). However, in this study the intracellular domain of each peptide contained one monomer from a protein pair (chemically disruptable heterodimer) that spontaneously assemble to form a heterodimer, bringing together the binding domain of the CAR with the signalling domains and facilitating activation. This heterodimer was successfully disrupted upon the administration of a small molecule drug, inhibiting the activation of CAR T cells *in vitro* and *in vivo*, regardless of antigen engagement (Giordano-Attianese et al. 2020).

Sun and colleagues engineered an alternative drug-OFF system in which the administration of a small molecule drug recruits Src homology region 2 domain-containing phosphatase-1 (SHP-1) to the CAR synapse. This leads to SHP-1-mediated dephosphorylation of the CD3ζ chains of the CAR, attenuating activation. The administration of the small molecule drug was observed to reduce IFN-γ release by CAR T cells in a reversible manner both *in vitro* and *in vivo* (Sun et al. 2020).

Affinity tuning, logic gate CARs and tuneable CAR systems all represent promising strategies to improve the safety of CAR T cell therapy. However, in addition to some of the caveats highlighted, the majority require cumbersome reengineering of the CAR structure, and thus are not easily transferrable into existing CAR platforms.

2 RESEARCH PROPOSAL

As discussed, CAR T cell therapy faces a number of hurdles. In this project I address two of these challenges: CAR T cell sensitivity and on-target off-tumour toxicity. To address these challenges this research has two primary aims:

Aim 1: To develop agnostic modules capable of improving CAR T cell sensitivity.

Aim 2: To engineer a module that enables tuning of CAR T cell function in response to a small molecule drug.

3 MATERIALS AND METHODS

3.1 Molecular biology

3.1.1 Engineering of DNA constructs

Constructs were designed on SnapGene® software, with oligonucleotides purchased from IDTDNA. Utilising the gammaretroviral (γRV) vector SFG (Büeler and Mulligan 1996), the constructs used in this research were generated by splicing overlap Polymerase Chain Reaction (PCR), referred to as Phusion PCR (3.1.2), restriction enzyme digest, which is also referred to as "cut and paste cloning" (3.1.11) or Golden Gate DNA assembly (3.1.12). Expression of multiple transgenes within the same vector was achieved by the inclusion of the *Thosea asigna* virus 2A (T2A) and *Porcine teschovirus-1* 2A (P2A) self-cleaving peptides, resulting in equimolar expression of transgenes either upstream or downstream of these peptides (Liu et al. 2017). All constructs contained a scaffold attachment region which enhances transgene expression (Agarwal et al. 1998). To confirm successful cloning, all new constructs generated were verified by DNA sequencing (Beckman Coulter) with analysis of the sequencing results to confirm sequence alignment performed using SnapGene®.

3.1.2 Phusion Polymerase Chain Reaction

Phusion PCR is a two-step protocol which enables two or more DNA fragments to be fused together at specific locations. The first step is the primary PCR, in which a sequence incorporated in the 5' overhang of each primer, is complementary to the end of the other DNA fragment. During the primary PCRs, these complementary overhangs are incorporated into the DNA fragments. The resultant DNA fragments are complementary and can thus anneal and extend during the second step, which is the Phusion PCR. The enzyme used in these reactions is the Phusion High-Fidelity (HF) DNA polymerase (NEB, M0530L) with the required Phusion HF 5X buffer (NEB, B0518S). PCR reaction mixes for the primary PCR and the Phusion PCR are described in Table 1 and Table 2, respectively. The thermocycling conditions for the PCRs are outlined in Table 3.

Table 1. Primary PCR reaction mix (Step 1)

Reagent	**Volume (µl)**	**Final Concentration**
Water (nuclease free)	Up to 50 µl	N/A
10 µM Forward Primer	2.5	0.5 µM
10 µM Reverse Primer	2.5	0.5 µM
10 mM dNTPs	1	200 µM (each)
Template Plasmid DNA (1 - 100 ng)	1	0.1 - 2 ng / µl
Phusion HF or GC Buffer, 5X*	10	1X
Phusion DNA Polymerase	0.5	0.02 units

Table 2. Phusion PCR reaction mix (Step 2)

Reagent	**Volume (µl)**	**Final Concentration**
Water (nuclease free)	Up to 50 µl	N/A
10 µM Forward Primer	2.5	0.5 µM
10 µM Reverse Primer	2.5	0.5 µM
10 mM dNTPs	1	200 µM (each)
DNA fragment from primary PCR 1 (1 - 100 ng)	1	0.1 - 2 ng / µl
DNA fragment from primary PCR 2 (1 - 100 ng)	1	0.1 - 2 ng / µl
Phusion HF or GC Buffer, 5X*	10	1X
Phusion DNA Polymerase	0.5	0.02 units

Table 3. Thermocycling conditions for PCR using Phusion polymerase

Step	**Temp**		**Time**
Initial Denaturation	98°C		30 - 90 seconds
Denaturation		98°C	5 - 15 seconds

Annealing Extension	25 - 35 cycles	50 - 72°C 72°C	10 - 30 seconds 20 - 30 seconds / kb
Final Extension	72°C		2 minutes
Hold	12°C		∞

3.1.3 DNA digestion using restriction endonucleases

Restriction endonucleases recognise specific DNA sequences called restriction sites. Digestion of DNA using restriction endonucleases (creates complementary overhangs on the PCR product DNA (insert) and the vector backbone. These complementary overhangs enable the digested DNA insert(s) and vector backbone to ligate together, forming the desired plasmid construct. Restriction digestions were performed based on the instruction provided by New England Biolabs (NEB), making sure to use a buffer compatible with the enzymes used. The master mix for the digestion of DNA inserts is outlined in Table 4 and the master mix for the digestion of the vector backbone DNA is outlined in Table 5.

Table 4. Master mix for restriction endonuclease digestion of insert DNA

Reagent	**Volume (µl)**
Insert DNA	40
Restriction Enzyme 1	1
Restriction Enzyme 2	1
Buffer	4

Table 5. Master mix for endonuclease digestion of vector DNA

Reagent	**Volume (µl)**
Vector DNA (1 µg/mL)	3
Water (nuclease free)	24
Restriction Enzyme 1	1

Restriction Enzyme 2	1
Buffer	4

Each reaction master mix was incubated at a suitable temperature (usually 37°C for HF enzymes) in a thermocycler for 1 hour and then stored at 4°C.

3.1.4 Dephosphorylation of vector backbone

To decrease the amount of the linearised (digested) vector backbone that re-circularises during the ligation step a dephosphorylation step is often utilised. In turn, this decreases the number of background colonies observed during the transformation step. A 50 µl reaction mix using a heat sensitive dephosphorylating phosphatase (Antarctic Phosphatase – NEB, M0289) was set up as outlined in Table 6 and run in a thermocycler as described in Table 7.

Table 6. Reaction mix for dephosphorylation of vector backbone DNA

Reagent	Volume (µl)	Final concentration
Vector DNA (digested)	30 – 44	1 - 5 µg
Antarctic Phosphatase	1	5 units
10X Buffer	5	1 X
Water (nuclease free)	to 50	N/A

Table 7. Thermocycling conditions for dephosphorylation of vector backbone DNA

Step	Time	Temperature
Incubate	30 – 60 mins	37°C
Heat Inactivate	2 mins	80°C
Hold	∞	12°C

3.1.5 Gel electrophoresis

To verify DNA fragments based on size, a 1-2% agarose gel was prepared by dissolving 1.5-2g of Agarose powder (Bioline BIO-41025) in 1x TAE (Tris-acetate-EDTA) buffer, with 10 µl SYBR Safe (Thermo Fisher; S33102) added. The gel was then left to solidify

in a gel template with a comb to allow well formation. Each DNA sample was mixed with loading dye and added into the wells in the gel. The gel was run at 140V until the dye was approximately 75-80% of the way down the gel.

3.1.6 DNA extraction from agarose gels

Following gel electrophoresis, the DNA fragments were excised from the gel and placed in a 1.5 ml centrifuge tube. 3x volume of Buffer QG Solubilization buffer (Qiagen; 19063) were added to 1x volume of gel and incubated at 50°C for 10 min. After the gel was fully dissolved, 1x gel volume of isopropanol (Thermo Fisher; 10284250) was mixed with the sample. The sample was added to a DNA spin column (Qiagen; 27115) and centrifuged at 13000 rpm for 1 minute. The flow through was discarded and 750 µl of Buffer PE (Qiagen; 19065) was added to the DNA spin column which were then centrifuged at 13000 rpm for 1 minute. The flow through was again discarded and the DNA spin column was centrifuged at 13000 rpm for 1 minute once more, discarding any more flow through. To elute the DNA, the spin column was placed in a new 1.5 ml centrifuge tube and 35 µl nuclease free water (IDT DNA; 11-05-01-04) was added to the centre of the spin column. The DNA spin column was left to incubate for 1 minute before centrifuging at 13000 rpm for 1 minute.

3.1.7 DNA purification using spin columns

To purify the DNA extracted from the agarose gel, 5 parts Binding Buffer PB (Qiagen; 19066) were mixed with 1 part DNA and added to a DNA spin column to be centrifuged at 13000 rpm for 1 minute. The flow through was discarded and 750 µl Buffer PE added to the column, which was then centrifuged at 13000 rpm for 1 minute. After discarding the flow through, the spin columns were centrifuged again at 13000 rpm for 30-60 seconds. To elute the DNA, 35 µl of nuclease free water was added to the spin column, left to left to incubate for 1 minute before centrifuging at 13000 rpm for 1 minute.

3.1.8 DNA ligation and transformation

After digestion of PCR fragments and an appropriate vector backbone with NEB restriction enzymes, the PCR fragments are inserted into the vector backbone using

T4 DNA ligase (Roche; 10716359001). The ligation reactions were set up in 0.2 ml PCR tubes as outlined in Table 8.

Table 8. Ligation master mix using T4 DNA ligase

Reagent	Volume (20µl total)
T4 DNA Ligase Buffer (10X) (Roche; 11243292001)	2 µl
Vector DNA (digested)	50 ng
Insert DNA (digested)	37.5 ng
Water (nuclease free)	to 20 µl
T4 DNA Ligase	1 µl

Ligation reactions were incubated at 16°C for minimum of 1 hour in a thermocycler. NEB 5-alpha competent high-efficiency *E. coli* (NEB; C2987U) were transformed by mixing 25 µl cells with 2-4 µl ligation mix (containing 0.001-100ng plasmid DNA) in a 0.2 ml PCR tube and incubated on ice for 30 minutes. This transformation mix was then heat shocked at 42°C for 35 seconds, before being returned to ice for a further 3 minutes. 25-100 µl SOC media (NEB; supplied with E. coli cells) was then added to the transformation mix, which was then placed into a shaking incubator set at 37°C and 250 rpm for 1 hour. 50-100 µl of the transformation mix was spread onto agar plates containing an appropriate antibiotic and incubated overnight at 37°C.

3.1.9 Plasmid DNA purification by Mini prep

For small scale DNA preparation (minipreps), we used the NucleoSpin® Plasmid EasyPure kit (Machery-Nagel; 740727.250). After bacterial transformation, a single colony was picked from the agar plate and placed in a culture tube with 5 ml of Luria-Bertani (LB) Medium (MP Biomedicals LLC; 3002-031) supplemented with an appropriate antibiotic. The tubes were incubated in a shaking incubator at 37°C and 250 rpm for 12-16 hours. 1.5 ml of the bacterial culture was removed and centrifuged at 13000 rpm for 5 minutes. The supernatant was discarded, then the pellet was resuspended in 150 µl A1 buffer. To lyse the bacterial cells, 250 µl A2 buffer was added, mixed well, and left to incubate for 2 minutes at room temperature. 350 µl of the A3 buffer (a neutralising buffer) was then added to the cell lysate and the tubes were then centrifuged at 13000 rpm for 3 minutes. The supernatant containing

the plasmid DNA was transferred to a Nucleospin column and centrifuged at 13000 rpm for 1 minute. The flow through was discarded and 450 µl AQ buffer was added to each column, which were then centrifuged at 13000 rpm for 1 minute. The flow through was discarded and columns centrifuged at 13000 rpm for a further 2 minutes. The columns were placed in a new 1.5 ml centrifuge tube and the DNA was eluted by adding 50 µl of the elution buffer.

3.1.10 Plasmid DNA purification by Midi Prep

For large scale DNA preparation (midipreps), we used the NucleoBond® Xtra Midi Kit (Machery-Nagel; 740410.100). As with the miniprep protocol (3.1.9), a single colony was picked from an agar plate and placed in a culture tube with 5 ml of LB media supplemented with an appropriate antibiotic. This “starter culture” was incubated in a shaking incubator at 37°C and 250 rpm for 8 hours. The starter culture was diluted 1:500-1000 to inoculate the overnight culture of LB media supplemented with appropriate antibiotic, which was placed in a shaking incubator at 37°C and 250 rpm for 12-16 hours. The bacterial cells were pelleted by centrifugation at 4,200 x g for 30 minutes at 4°C. The pellet was resuspended in 8 ml resuspension buffer RES + RNase A. Once the pellet was fully resuspended, the cells were lysed by adding 8 ml LYS buffer and left to incubate at room temperature for 5 minutes. In the meantime, the NucleoBond® Xtra column filter was equilibrated with 12 ml EQU buffer. The cell lysate was the neutralised with 8 ml NEU buffer before being transferred into column filter. The column filter was left to empty by gravity flow and then washed once with 5 ml EQU buffer. The filter was removed from the column and discarded. The column was then washed once with 8 ml WASH buffer. The plasmid DNA was eluted by adding 5 ml ELU buffer. To precipitate the eluted DNA, 3.5 ml room-temperature isopropanol was added, vortexed and left to incubate for 2 minutes. The plasmid DNA was pelleted by centrifuging at 4,200 x g for 30 minutes at 4°C. The DNA was then washed with room-temperature 70% ethanol and centrifuged at 4,200 x g for 20 minutes. The pellet was dried at room temperature, with any remaining traces of ethanol absorbed using a sterile cotton bud.

3.1.11 Plasmid cloning by restriction enzyme digest (cut and paste)

Traditional cut and paste cloning, is a technique in which a vector and insert DNA are digested with restriction enzymes (3.1.3). The digested DNA fragments are then verified via gel electrophoresis (3.1.5), excised from the gel and purified (3.1.6 and 3.1.7). To form a new recombinant DNA plasmid, the vector backbone was then dephosphorylated as outlined in 3.1.4 before ligating the DNA insert into the vector backbone using T4 ligase. After ligation, *E. coli* cells were transformed with the ligation mix and spread on agar plates containing an appropriate antibiotic (3.1.8). Colonies were then picked for further growth and purification of the plasmid DNA (3.1.9 or 3.1.10).

3.1.12 Golden Gate DNA assembly

Golden gate DNA assembly was the primary method used for multi-fragment DNA assembly. Golden gate assembly permits the sequential ligation of multiple inserts into a vector backbone utilising a single type IIS restriction enzyme such as: BsaI (NEB, R3733), BsmBI (NEB, R0739) or BbsI (NEB, R0539). One of these restriction enzymes was used to digest DNA fragments generated by PCR (as described in 3.1.2) and the vector backbone. The fragment-specific sequence of each DNA overhang generated by these type IIS restriction enzymes allows sequential assembly of multiple fragments simultaneously. The digested DNA was then ligated together and transformed into *E. coli* cells (3.1.8). As previously described in 3.1.9 and 3.1.10, bacterial colonies were then picked to expand, from which the plasmid DNA was purified.

3.2 Tissue culture

3.2.1 Basic cell culture techniques

3.2.1.1 Culturing of adherent cell lines

HEK293T cells (ATCC; ATCC®CRL-11268™) (293Ts) were cultured in Iscove's Modified Dulbecco's Medium (IMDM) (Lonza; LZBE12-726F) supplemented with 10% heat inactivated foetal bovine serum (FBS) (Biosera; FB-1001) and 10 mM glutamine

(Sigma-Aldrich; g7513-100ml) (I10). 293T cells were maintained in T175 tissue culture treated flasks at 37°C and 5% CO_2. Upon reaching 90% confluency, cells were passaged by washing with Phosphate Buffer Saline (PBS) (Sigma-Aldrich; D8537). To detach the 293T cells from the flask, 5 ml trypsin/EDTA (Sigma-Aldrich; T4049) was added, then the flasks were incubated for 5 minutes at 37°C and 5% CO_2. Once detached, cells were reseeded in fresh medium and cultured as above.

3.2.1.2 Culturing of non-adherent cell lines

Non-adherent cell lines were all cultured in Roswell Park Memorial Institute (RPMI)1640 (Fisher Scientific; 11879020) supplemented with 10% heat inactivated FBS and 10 mM glutamine (Sigma-Aldrich; g7513-100ml) (R10). Cells were maintained in T175 flasks at 37°C and 5% CO_2. Cell passage was carried out by resuspending the cells in fresh R10 media to achieve a density of less than $1x10^6$ cells/ml.

3.2.1.3 Cryopreservation of cell lines

Cell lines to be cryopreserved were centrifuged at 400xg for 5 minutes, then resuspended at $5x10^6$ cells/ml in chilled freezing medium made up of FBS + 10% DMSO (Sigma-Aldrich; D2650-100ML). Resuspended cells were then aliquoted into cryovials (1 ml per vial), which were placed into a CoolCell™ LX Cell Freezing Container (Corning®) and transferred to a -80°C freezer. The next day the cryovials were moved to a liquid nitrogen tank for storage.

3.2.1.4 Recovery of cell lines post cryopreservation

The frozen cryovials were thawed in a 37℃ water bath. As the DMSO in the freezing media is toxic to metabolising cells, cells were then quickly washed in 20 ml of suitable pre-warmed complete media. Cells were then centrifuged at 400xg for 5 minutes, resuspended in complete media and maintained in appropriate flasks in an incubator at 37°C and 5% CO_2.

3.2.2 Retroviral transductions

3.2.2.1 Retroviral supernatant production

293T cells were seeded at $3x10^6$ cells per 10 cm plate in 10 ml I10 ($3x10^5$ cells/ml). The 293Ts were incubated overnight at 37°C, 5% CO_2 to allow the cells to adhere to the plate and achieve a confluency of 50%-60%. Per 10 cm plate, 30 µl GeneJuice (Millipore; 70967-4) was mixed with 470 µl plain IMDM and incubated at room temperature for 5 minutes. After which, three plasmids were added to the GeneJuice mix: an SFG plasmid containing the transgene of interest (4.7ug), a plasmid encoding the viral gag/pol genes (4.7 µg), and an RD114 envelope expression plasmid (RDF) (3.1ug). This transfection mixture was then left to incubate for a further 15 minutes at room temperature. The transfection mixture was then added to the 293T cells in a dropwise manner and incubated at 37°C and 5% CO_2. Supernatant was harvested at both 48- and 72-hour timepoints post transfection, pooled and stored at -80°C until required.

3.2.2.2 Coating tissue culture plates with RetroNectin

When coating non-tissue culture treated 6-well plates with RetroNectin (Takara Clonetech; T100B), 8 µl of RetroNectin was added per 1 ml of sterile PBS (final concentration of 8 µg/ml), with 2 ml diluted RetroNectin added to each well. For coating non-tissue culture treated 24-well plates, 0.5 ml of diluted RetroNectin was added per well. Plates were sealed and stored at 4 °C overnight before use.

3.2.2.3 Retroviral transduction of suspension cells

The day before transduction, the cells in suspension were split to ensure they were in exponential growth the following day. Diluted RetroNectin was aspirated from 24 well plates and 1.5 ml of retroviral supernatant was added to each well and incubated for 30 minutes at room temperature. The suspension cells to be transduced were resuspended at $0.6x10^6$ cells/ml in R10, with 0.5 ml added per well. The plates were then centrifuged at 1000xg for 40 minutes then incubated at 37°C and 5% CO_2 for 2-3 days.

3.2.3 Engineering of target cell lines

SupT1 (ATCC; ATCC®CRL-1942™) cells were used as the parental cell line for all target cell lines used for *in vitro* assays in this study. We engineered a number of SupT1 cell

lines expressing human CD22, CD19 or GD2 on the cell surface at different densities. The CD22 antigen comprised a CD22 ectodomain, CD19 TM domain and CD19 endodomain. Whereas the CD19 antigen comprised a CD19 ectodomain, CD19 TM domain and a GFP endodomain. To express GD2 on the cell surface, both GD2 and GD3 synthase are required (Battula et al. 2012). Supernatants containing retrovirus encoding the CD22 antigen, CD19 antigen or GD2 and GD3 synthase genes were produced as described in 3.2.2.1. These supernatants were used to transduce SupT1 cells (as described in 3.2.2.3), generating target cell lines expressing CD22, CD19 or GD2 on the cell surface. After transduction, some target cell lines were sorted using the BD FACSMelody™ cell sorter for cells with the desired level of RQR8, the transduction marker developed by Philip and colleagues (Philip et al. 2014). Additionally, Target cell lines were sometimes sorted for RQR8 expression using anti human CD34 MicroBeads, as per the manufacturer's instructions (Miltenyi Biotec; 130-100-453).

The expression of antigen on target cell lines was detected by flow cytometry (described in 3.2.6.2). Quantification of the antigen density on the surface of the target cell lines was calculated using Quantibrite-PE Beads (BD Biosciences; 340495) (Table 13). The target cell lines used in this study and the method(s) employed to engineer them are described in Table 9.

3.2.3.1 STOPSKIP technology

One method we used to obtain cell lines expressing low levels of antigen was to engineer vectors containing a "STOPSKIP" motif upstream of the antigen encoding transgene. A STOPSKIP motif reduces the translational efficiency of any downstream transgene, it contains a stop codon (e.g. TGA) followed by a read-through sequence (e.g. CATG) (Sillibourne et al. 2022). The presence of the stop codon prevents mRNA translation, however, the read-through sequence causes inefficient termination of protein synthesis, resulting in a low level of translational read-through and thus low level protein synthesis (Loughran et al. 2014; Cassan and Rousset 2001). Utilising this STOPSKIP technology, we engineered a number of cell lines with low target antigen density.

3.2.3.2 Signal sequence mutations

An alternative method to the STOPSKIP technology to generate cell lines with reduced antigen expression is to introduction mutations in the signal sequence. Cell surface proteins are trafficked to the cell membrane through the secretion pathway. A signal sequence in the N-terminal of transmembrane and secreted proteins identifies them for entry into this pathway, with signal sequences of newly formed peptide chains recognised by the Signal Recognition Particle (SRP). The binding of the SRP to the signal sequence results in translation being paused. The SRP then also binds to the SRP-receptor, recruiting the peptide/ribosome complex to the Endoplasmic Reticulum (ER). Subsequently, the polypeptide is inserted into a pore within the ER, with the signal peptide cleaved in the ER lumen. This permits continued translation and the polypeptide chain to pass across the membrane of the ER (Nothwehr and Gordon 1990). The introduction of mutations within the signal sequence can reduce the efficiency of polypeptide transfer into the ER. Therefore, the expression of the protein on the cell surface can also be reduced.

3.2.3.3 Single cell cloning by limiting dilution

After retroviral transduction, a cell line can exhibit a heterogeneous range of transgene expression, and subsequently display a range of antigen density. In order to achieve a target cell line of very homogenous expression, we identified single cell clones by limiting dilution. Firstly, cells were resuspended at a concentration of $1x10^6$ cells/ml in R10. From this cell suspension, 39 µl was taken and diluted in 30 ml R10, labelled “Dilution 1” (773-fold dilution). From Dilution 1, 39 µl was taken and diluted in 30 ml R10, labelled “Dilution 2”. From dilution 2, 200 µl was added per well into a flat-bottom 96-well plate. Using this method, on average, each third well contained only a single cell. Plates were then incubated for 1-2 weeks at 37°C and 5% CO_2, until the colonies took up approximately 25% of the well. The single cell clones were then transferred to 24 well plates with 2 ml of R10 per well. Once confluent, the new homogenous cell populations can be screened by flow cytometry for antigen density (as described in 3.2.6.2).

Table 9. Target cell lines.

Cell line	AU Number	Antigen	Antigen density (molecules/cell)	Description
SupT1 NT	37873	N/A	N/A	Parental T cell lymphoblastic lymphoma-derived cell line naturally negative for CD19/CD22. Used as a negative control.
SupT1 $CD22^{High}$	84347	CD22	53,866	Parental SupT1 NT cell line transduced to artificially express CD22 antigen.
SupT1 $CD22^{Mid}$	41583	CD22	6,309	Parental SupT1 NT cell line transduced to artificially express CD22 antigen.
SupT1 $CD22^{Low}$	45194	CD22	1,968	Parental SupT1 NT cell line transduced with a cassette bearing a STOPSKIP sequence to achieve low density CD22 expression. The cells were then sorted on the FACSMelody™ cell sorter for very low levels of expression.
SupT1 $CD22^{Low(b)}$	68868	CD22	1,946	Parental SupT1 NT cell line transduced with a cassette bearing a STOPSKIP sequence to achieve low density CD22 expression. The cells were then sorted on the FACSMelody™ cell sorter for low levels of expression and sorted again for RQR8 using anti-human CD34 MicroBeads.

SupT1 CD22^{VL} (Very Low)	68867	CD22	284	Parental SupT1 NT cell line transduced with a cassette bearing a STOPSKIP sequence to achieve low density CD22 expression. The cells were then sorted on the FACSMelody™ cell sorter for low levels of expression and sorted again for RQR8 using anti-human CD34 MicroBeads.
SupT1 CD19^{High}	42187	CD19	100,830	Parental SupT1 NT cell line transduced to artificially express CD19 antigen.
SupT1 CD19^{Mid}	84642	CD19	11,846	Parental SupT1 NT cell line transduced with a cassette bearing a STOPSKIP sequence to achieve low density CD19 expression. A single cell clone was then identified by limiting dilution.
SupT1 CD19$^{Mid(b)}$	73529	CD19	16,357	Parental SupT1 NT cell line transduced with a cassette bearing a STOPSKIP sequence to achieve low density CD19 expression. Cells were then sorted for RQR8 expression using anti-human CD34 MicroBeads.
SupT1 CD19^{Low}	84645	CD19	4,282	Parental SupT1 NT cell line transduced with a cassette bearing a STOPSKIP sequence to achieve low density CD19 expression. A single cell clone was then identified by limiting dilution.

SupT1 $CD19^{Low(b)}$	62635	CD19	4,754	Parental SupT1 NT cell line transduced with a cassette bearing mutations in the signal sequence to achieve low density CD19 expression.
SupT1 $CD19^{VL}$ (Very Low)	62635	CD19	3,032	Parental SupT1 NT cell line transduced with a cassette bearing mutations in the signal sequence to achieve low density CD19 expression.
SupT1 $GD2^{High}$	56468	GD2	220,834	Parental SupT1 NT cell line transduced with a cassette expressing both GD2 and GD3 synthase required for surface expression of GD2.
SupT1 $GD2^{Mid}$	82724	GD2	28,903	SupT1 $GD2^{+}$ cell line (AU56468) transduced with a cassette expressing B3GALT4, which downregulates GD2 expression. The cassette also contained eBFP, which was inversely correlated to GD2 expression. The cells were then sorted on the FACSMelody™ cell sorter for high levels of eBFP expression. Following cell sorting, single cell clones were identified by limiting dilution.

SupT1 $GD2^{Low}$	82720	GD2	14,920	SupT1 $GD2^{+}$ cell line (AU56468) transduced with a cassette expressing B3GALT4, which downregulates GD2 expression. The cassette also contained eBFP, which was inversely correlated to GD2 expression. The cells were then sorted on the FACSMelody™ cell sorter for mid-levels of eBFP expression. Following cell sorting, single cell clones were identified by limiting dilution.
SupT1 $GD2^{VL}$ (Very Low)	82716	GD2	415	SupT1 $GD2^{+}$ cell line (AU56468) transduced with a cassette expressing B3GALT4, which downregulates GD2 expression. The cassette also contained eBFP, which was inversely correlated to GD2 expression. The cells were then sorted on the FACSMelody™ cell sorter for mid-levels of eBFP expression. Following cell sorting, single cell clones were identified by limiting dilution.

3.2.4 Primary cell culture

3.2.4.1 Isolation and culture of PBMCs

Whole blood was purchased from National Health Service Blood and Transplant (NHSBT; Colindale, UK). Peripheral blood mononuclear cells (PBMCs) were isolated from whole blood by density gradient sedimentation. The blood was mixed 1:1 with

sterile RPMI, with 25 ml of diluted blood carefully layered on top of 15 ml of Ficoll-Paque PLUS (ficoll) (GE Healthcare; 17-1440-03) in SepMate™-50 (STEMCELL Technologies; 85460) tubes. The SepMate™ tubes were then centrifuged at 1200xg for 20 minutes at 20°C with the acceleration and deceleration of the centrifuge set at 6. The PBMC layer (buffy coat) was harvested using a Pasteur pipette and then washed twice with RPMI, with cells centrifuged at 400xg for 5 minutes at 20°C after each wash. PBMCs were either used fresh or frozen down and stored in liquid nitrogen until required (as outlined in 3.2.1.3).

PBMCs thawed or freshly isolated from whole blood were resuspended at $0.7x10^6$ cells/ml in R10. To activate the T cells, 0.5 µl/ml of cells of anti-CD3 antibody (clone OKT3. Miltenyi Biotec; 130-093-387) and 50 µl/ml of cells of anti-CD28 antibody (clone 15E8. Miltenyi Biotec; 130-093-375) were added (final concentration of each was 50 ng/ml) and PBMCs were then incubated overnight at 37°C and 5% CO_2. 24 hours after activation, 100U/ml of recombinant human IL-2 (GenScript; Z00368-1) was added to maintain the cells.

3.2.4.2 Retroviral transduction of PBMCs

Diluted RetroNectin was aspirated from the wells of 6-well plates before the addition of 3 ml retroviral supernatant to each well, with plates then incubated at room temperature for 30 minutes. Activated PBMCs were harvested and resuspended at $1x10^6$ cells/ml in R10 supplemented with 400 U/ml of IL-2. From this master-mix, 1 ml was added per well (final concentration of IL-2 was 100U/ml). The plates were then centrifuged at 1000xg for 40 minutes then incubated at 37°C and 5% CO_2 for 72 hours.

PBMCs were assessed for transduction efficiency by measurement of binding of CAR to soluble CD22 (R&D systems; 1968-SL) or soluble CD19-Rabbit Fc produced by K652 cells (Autolus; K562 cells transduced with AU19818), followed by labelling with appropriate secondary antibodies. PBMCs were also labelled with an anti-CD34 antibody for the detection of the RQR8 transduction marker (Table 10 and Table 11).

3.2.5 NK cell depletion

$CD56^+$ NK cells present in PBMCs isolated from whole blood can increase the background cytotoxicity observed in *in vitro* immunological assays such as Flow-cytometry Based Killing assays (FBKs). To reduce this potential background cytotoxicity, we depleted $CD56^+$ cells from the PBMCs the day prior to assay set-up. PBMCs were depleted of $CD56^+$ cells using Stemcell Technologies EasySep™ Human CD56 Positive Selection Kit II, in accordance with the manufacturer's instructions (STEMCELL Technologies; 17855).

3.2.6 Flow cytometry

3.2.6.1 General labelling protocol

Cells for labelling were counted, washed once in 100 µl PBS and centrifuged at 1000xg for 2 minutes. $2x10^5$ cells were resuspended in 100 µl of PBS with an appropriate concentration of primary antibody/dye and incubated in the dark at room temperature for 10 minutes. If a secondary antibody was required, cells were washed once in PBS as before and resuspended in 100 µl of PBS with an appropriate concentration of secondary antibody/dye. Cells were then washed once with PBS and labelled with 7AAD viability dye (Biolegend; 420404) diluted in PBS in a final volume of 100 µl. All data was acquired on a MACSQuant® Analyzer 10 or MACSQuant® X flow cytometer (Miltenyi Biotec) and analysed on FlowJo v10.

Table 10. Labelling of CD22 targeting CAR T cells

Labelling Step	Antigen	Conjugate	Supplier; Catalogue number	Dilution
Primary	soluble CD22 (sCD22)	N/A	R&D systems; 1968-SL	1:1000
Secondary	Human-Fc	AF647	Jackson ImmunoResearch; 109-605-098	1:1000
	CD34(RQR8)	AF488	RnD Systems; FAB7227G	1:50
Viability	7AAD	N/A	Biolegend; 420404	1:50

Table 11. Labelling of CD19 targeting CAR T cells

Labelling Step	Antigen	Conjugate	Supplier; Catalogue number	Dilution
Primary	soluble CD19 (sCD19)	N/A	Autolus; K562 cells transduced with plasmid to secrete soluble CD19 (AU19818)	Neat (100 µl)
Secondary	Rabbit IgG	PE	Jackson ImmunoResearch; 111-116-144	1:200
	CD34(RQR8)	APC	RnD Systems; FAB7227A	1:50
Viability	7AAD	N/A	Biolegend; 420404	1:50

Table 12. Labelling of GD2 targeting CAR T cells

Labelling Step	Antigen	Conjugate	Supplier; Catalogue number	Dilution
Primary	CD34(RQR8)	AF488	RnD Systems; FAB7227G	1:50
Viability	7AAD	N/A	Biolegend; 420404	1:50

3.2.6.2 Antigen quantification with QuantiBrite-PE

To determine the cell surface antigen density of engineered target cell lines (Table 9), we used a PE Fluorescence Quantitation Kit (BD Quantibrite™) which contains a lyophilised pellet of beads conjugated with four levels of PE. These beads were used in parallel with cells labelled with anti-PE monoclonal antibodies against the antigen of interest. The QuantiBrite™ bead number of PE molecules/beads and the corresponding Mean Fluorescence Intensity (MFI) are plotted into a standard curve to correlate MFI with density. To allow for a more accurate PE quantification, we ran isotype controls for the PE monoclonal antibody to eliminate background binding. Therefore, we labelled plates in duplicate, with “Set 1” labelled with a mAb-PE against the antigen of interest and “Set 2” is labelled using the isotype-PE (Table 13, Table 14 and Table 15).

Table 13. Labelling for CD22 antigen quantification

Labelling Step	Antigen	Conjugate	Supplier; Catalogue number	Dilution

Set 1: Primary	CD22	PE	Biolegend; 302506	1:50
	CD34(RQR8)	APC	RnD Systems; FAB7227A	1:50
Set 2: Primary	Isotype	PE	Biolegend; 400112	1:50
	CD34(RQR8)	APC	RnD Systems; FAB7227A	1:50
Viability	7AAD	N/A	Biolegend; 420404	1:50

Table 14. Labelling for CD19 antigen quantification

Labelling Step	Antigen	Conjugate	Supplier; Catalogue number	Dilution
Set 1: Primary	CD19	PE	Biolegend; 302208	1:50
	CD34(RQR8)	APC	RnD Systems; FAB7227A	1:50
Set 2: Primary	Isotype	PE	Biolegend; 400112	1:50
	CD34(RQR8)	APC	RnD Systems; FAB7227A	1:50
Viability	7AAD	N/A	Biolegend; 420404	1:50

Table 15. Labelling for GD2 antigen quantification

Labelling Step	Antigen	Conjugate	Supplier; Catalogue number	Dilution
Set 1: Primary	GD2	PE	Biolegend; 357304	1:50
	eBFP	N/A	N/A	N/A
Set 2: Primary	Isotype	PE	Biolegend; 400112	1:50
	eBFP	N/A	N/A	N/A
Viability	7AAD	N/A	Biolegend; 420404	1:50

3.2.7 *In vitro* assays

3.2.7.1 Flow-cytometry Based Killing (FBK) assay

Transduced T cells (effectors) were counted and normalised to 30% transduction level (unless specified otherwise) with the addition of non-transduced (NT) T cells. Transduced effector cells and target cells were harvested, counted, and resuspended

in R10 to a concentration of $5x10^5$ cells/ml. To achieve an effector to target ratio (E:T) of 1:1, 100 µl of transduced effector cells ($5x10^4$ cells) and 100 µl of target cells ($5x10^4$ cells) were added per well in a 96-well round-bottom tissue culture plate, with a final volume of 200 µl. The number of target cells remained constant at $5x10^4$ cells per well in a 96-well plate. Therefore, in order to achieve E:T ratios of 1:2, 1:4, and 1:8, the number of transduced effector cells per well was diluted to $25x10^4$, $12.5x10^4$, and $6.25x10^4$ cells respectively.

In some conditions the analogue of PP1, 3-IB-PP1 (Merck; 529598) was added to co-cultures. 3-IB-PP1 was diluted in R10 before the addition of 50 µl of the 3-IB-PP1 master-mix to each well. To maintain a final co-culture volume of 200 µl, the concentration of the target cells or transduced effector cells had to be reduced in order to plate the desired/final number of cells in a 50µl volume instead of 100µl. The final concentration of 3-IB-PP1 is indicated on the relevant figures in the results section. The co-cultures were then incubated at 37°C and 5% CO_2 for 72 hours.

Before analysis by flow-cytometry, an equal number of fluorescent counting beads (Invitrogen; C36950) were added to each co-culture to enable calculation of absolute cell numbers. 72 hours post co-culture set up CAR T cell-mediated cytotoxicity was analysed by flow-cytometry. The T cells were differentiated from the target cells by labelling for CD3, CD2 and CD8, with target cells identified by their lack of CD3, CD2 and CD8 expression. Cell viability was assessed by labelling with the dead cell exclusion dye 7AAD (Biolegend; 420404) (Table 16). Viable target cells were then enumerated for each condition and the percentage of target cell survival calculated by normalising the number of viable target cells compared to the condition in which the targets were co-cultured with NT T cells (100%). All data was acquired on either a MACSQuant® Analyzer 10 or a MACSQuant® X flow cytometer (Miltenyi Biotec) and analysed on FlowJo v10.

Table 16. Labelling for analysis of FBK co-cultures

Labelling Step	Antigen	Conjugate	Supplier; Catalogue number	Dilution
Primary	CD2	PE	Biolegend; 300208	1:50
	CD3	PE/Cy7	Biolegend; 344816	1:50
	CD8	APC/Cy7	Biolegend; 301016	1:50
	Counting beads	N/A	Invitrogen; C36950	1:33
Viability	7AAD	N/A	Biolegend; 420404	1:50

3.2.7.2 Cytokine ELISA

At 72 hours post co-culture set up, the 96-well plates were centrifuged at 1000xg for 2 minutes, 100 µl supernatant was then collected and frozen at -20°C for later analysis. To detect the production of cytokines by CAR T cells, the supernatants were thawed and analysed by ELISA. ELISAs for the detection of IFN-γ and IL-2 were carried out using the Human IFN-γ ELISA MAX Deluxe (Biolegend; 431704) and Human IL-2 ELISA MAX Deluxe (Biolegend; 431804) kits as per the manufacturer's instructions.

3.2.7.3 Proliferation assay

$3x10^6$ transduced T cells were aliquoted into a 15 ml Falcon tube (Corning; CLS430791) and resuspended at a concentration of $1x10^6$ cells/ml in PBS containing 5 µM CellTrace Violet (CTV) (Invitrogen; C34571). The cells were then incubated in the dark at 37°C for 20 minutes. To quench the CTV, 5x volume of R10 was added and left to incubate at room temperature for 5 minutes. The cells were then washed and resuspended in pre-warmed R10 and incubated for a further 10 minutes before co-culture set up.

3.2.7.4 CAR T cell memory phenotyping

On day 4 after the setup of a co-culture, as described in 3.2.7.1, CAR T cells were labelled for the markers of memory differentiation, CD45RA and CCR7. The panel for the differentiation labelling is shown in Table 17. Using this labelling panel, four different subsets of T cell memory phenotype were identified: naïve (Tn), central memory (Tcm), effector memory (Tem) and effector (Teff) T-cells. An example of the different memory populations present in healthy donor PBMCs is shown in Figure 5.

Table 17. Panel for T-cell memory phenotyping

Labelling Step	Antigen	Conjugate	Supplier; Catalogue number	Dilution
Primary	CCR7	PE	Biolegend; 353204	1:50
	CD45RA	PE Texas Red	Life Technologies; MHCD45RA17	1:50
	CD3	PE/Cy7	Biolegend; 344816	1:50
	CD8	APC/Cy7	Biolegend; 301016	1:50
	CD34(RQR8)	APC	RnD Systems; FAB7227A	1:50
Viability	Sytox	N/A	ThermoFisher; S10274	1:1000

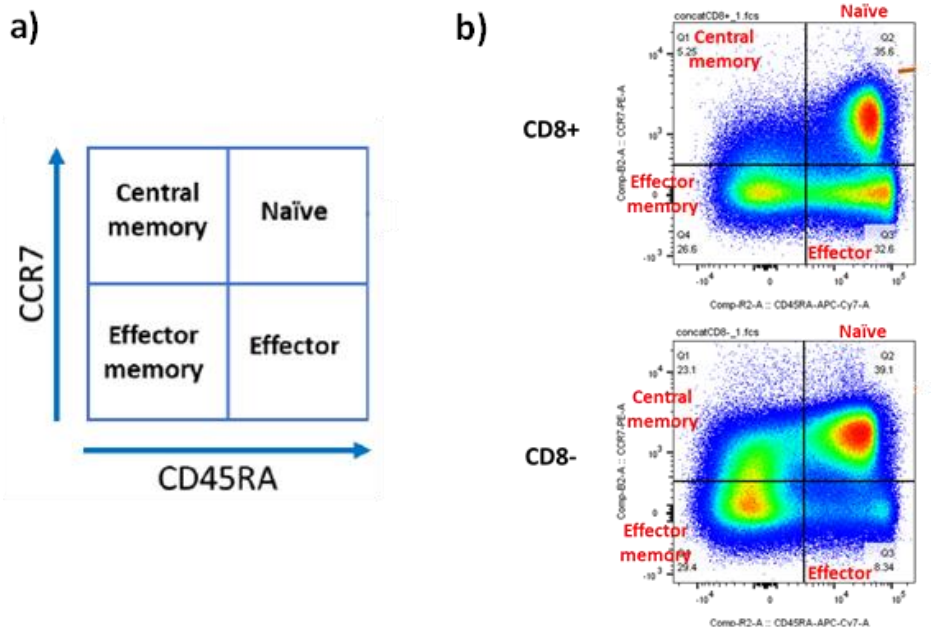

Figure 5. T cell memory populations based on the expression of CCR7 and CD45RA. a) Gating of T cell subsets based on the expression of CCR7 and CD45RA. b) Different memory populations present in a healthy donor PBMCs

3.2.7.5 CAR T cell exhaustion phenotyping

As in 3.2.7.4, on day 4 after co-culture setup, CAR T cells were labelled for the markers of T cell exhaustion Tim-3, Lag-3, and PD-1. The labelling panel for these exhaustion markers is shown in Table 18. The severity of T cell exhaustion was analysed based on the expression of these markers, with the expression of only one marker not considered to constitute an exhausted T cell population. However, the expression of two (double positive) or three (triple positive) of these markers was used to indicate more exhausted T cell populations.

Table 18. Panel for T-cell exhaustion phenotyping

Labelling Step	Antigen	Conjugate	Supplier; Catalogue number	Dilution
Primary	Tim-3	BV421	Biolegend; 345008	1:50
	Lag-3	FITC	Enzo Life Sciences; ALX-804-806F-C100	1:50
	PD-1	PE	Biolegend; 329906	1:50
	CD3	PE/Cy7	Biolegend; 344816	1:50
	CD34(RQR8)	APC	RnD Systems; FAB7227A	1:50
	CD8	APC/Cy7	Biolegend; 301016	1:50
Viability	7AAD	N/A	Biolegend; 420404	1:50

3.2.7.6 Plate-bound assays

Anti-CD3 antibody diluted in PBS was added 96-well non-treated plates (StarLab; CC7672-7596) and incubated overnight at 4°C. The plates were then washed two times in PBS in a sterile environment prior to assay set up. $1x10^5$ T cells were added to each well in media (R10) or media supplemented with 10 µM 3-IB-PP1. 24h after initiation of the assay, the supernatant from each well was harvested and analysed for IFN-γ (as described in 3.2.7.2).

3.3 Protein work

3.3.1 Sample preparation, quantification, and electrophoresis

Prior to activation, CAR T cells were incubated at 37°C for 30 minutes in either plain media (RPMI) or media supplemented with the CSK^{AS} inhibitor 3-IB-PP1 (10 µM). T cells were then activated with sCD22 (4-8 µg/ml) or anti-CD3 and anti-CD28 antibodies (5 µg/ml each). After a set time of activation, the cells were harvested in a 2 ml microcentrifuge tube and pelleted at 13000 rpm for 1 minute. The supernatant was discarded, and the samples were washed in 1 ml of ice-cold PBS. The tubes were centrifuged again at 13000 rpm for 1 minute. After discarding the supernatant, the cells were resuspended in 50 µl 1x RIPA buffer (Merck Millipore; 20-188) containing 1x protease and phosphatase inhibitor cocktail (AbCam; ab201119). The cells were then incubated on ice for 15 minutes. Each sample was then vortexed before being incubated on ice for a further 15 minutes. The samples were then centrifuged at 13000 rpm for 10 minutes at 4°C. The lysate samples were then transferred to PCR tube strips and stored at -80. The protein concentration of each lysate was quantified using the Pierce™ BCA Protein Assay Kit (Thermo Fisher; 23227), by following the manufacturer's instructions.

Prior to electrophoresis (SDS-PAGE), 1x loading buffer (Thermo Fisher; NP007) was added to each to each lysate and boiled at 95°C for 5 minutes. 4 µg of each lysate sample was run on a premade 4–20% Mini-PROTEAN® TGX™ Precast Gel (Bio-Rad; 4561095) at 180V for 35 minutes. 8 µl of protein ladder was run alongside the lysate samples as size marker (1:1 mix of Bio-Rad; 1610374 and Bio-Rad; 1610373). After electrophoresis the gels were used for Western blotting.

3.3.2 Western Blots

The SDS-PAGE gels were transferred to a PVDF membrane (Bio-Rad; 1704157) using the Bio-Rad Trans-Blot® Turbo™ transfer system. After transfer, the membranes were blocked with 1x Tris-Buffered Saline containing 0.05% Tween (TBST) (Pierce; 28360) supplemented with 5% Bovine Serum Albumin (BSA) (Sigma-Aldrich; A7906) and placed on a rotating plate shaker at 4°C overnight. The following day the membranes

were washed three times in TBST for 10 minutes per wash before antibody staining. Membrane staining was carried out with primary antibodies diluted as per manufacturer's recommendations in TBST supplemented with 5% BSA for 1 hour on a rotating plate shaker at room temperature. The primary antibodies used in this research were the Phospho-Zap-70 (Tyr319)/Syk (Tyr352) Antibody (pZAP-70 (Y319)) (Cell Signalling Technology; 2701S) and the GAPDH (14C10) Rabbit mAb (GAPDH) (Cell Signalling Technology; 2118L). The membranes were washed three times in TBST for 10 minutes per wash. The membrane was then stained with Anti-rabbit IgG, HRP-linked secondary antibody (aRb-HRP) (Cell Signalling Technology; 7074S) diluted in TBST supplemented with 5% BSA as per manufacturer's recommendations and placed on a rotating plate shaker for 1 hour at room temperature. The membranes were washed again three times in TBST for 10 minutes per wash. The use of an HRP-conjugated secondary antibody allowed the detection of bound antibody via chemiluminescence if an appropriate HRP-substrate is added. Thus, after washing, the membranes were developed by adding Pierce™ ECL Plus Western Blotting Substrate (Thermo Fisher; 34580) and incubating for 3 minutes. After incubation the membranes were removed from the substrate and visualisation of protein bands was achieved using the Azure 200 Gel Imaging Workstation.

3.3.3 PamGene peptide microarray

$2x10^6$ CAR T cells with 30% transduction were incubated at 37°C for 30 minutes in either media (R10) or media supplemented with the CSK^{AS} inhibitor 3-IB-PP1 (10 µM). After which, all T cells were activated by spiking in sCD22 (4 µg/ml) and incubated at 37°C for 15 minutes. The cells were harvested in a 2 ml microcentrifuge tube and pelleted by centrifugation (8 minutes at 500xg at 4°C). Cell pellets were prepared and shipped PamGene as per PamGene's SOP (protocol 1161).

At PamGene, the cells were lysed and then protein concentration was determined using the standard Bradford assay as per PamGene SOPs. Lysates were then run on the PamChip® microarrays, which contain immobilised protein tyrosine kinase (PTK)-specific conserved peptides, representative of kinase targets/substrates (phosphosites). Active kinases in the cell lysate sample will phosphorylate their target

on the array. Using fluorescently labelled antibodies that recognize phosphorylated residues, the extent of the phosphorylation of each phosphosite can be visualised and quantified to generate PTK activity profiles. PamGene used its in-house bioinformatics toolbox to generate list of top altered kinases.

3.4 *In vivo* assays

All procedures were performed in accordance with the United Kingdom Home Office Animals (Scientific Procedures) Act 1986 and in adherence to Imperial College London SOPs. For the animal models we used 6-8 weeks old female NOD SCID gamma (NSG) mice supplied by Charles River Laboratories.

3.4.1 3-IB-PP1 toxicology model

3-IB-PP1 (in RPMI) was administered to NSG mice via intraperitoneal (IP) injections three times a week at a range of concentrations (1-500 ng/g). Three control groups were also included in which injections of RPMI containing equivalent amounts of DMSO as three of the 3-IB-PP1 concentrations tested (1 ng/g, 50 ng/g and 500 ng/g). Mice were weighed periodically up to day 23 from their first injection. Mice were also monitored for changes in physical appearance or behaviour. Mice were culled on day 23.

3.4.2 CAR T cell efficacy model

On day -7, NSG mice were injected with $1x10^6$ Nalm6 CD19KO cells Intravenously (IV). On day 0, the mice were injected IV with the $1x10^6$ of transduced CAR T cells. Tumour growth was measured 3 times a week by bioluminescent imaging (BLI). On day 0 the mice received their first dose of either vehicle (1.1% DMSO in RPMI) or drug (500 ng/g 3-IB-PP1), which they received three times per week until day 14. The mice were culled on day 14 or before if BLI exceeded $1x10^{10}$ photons/s/cm2/sr.

3.4.3 Bone marrow harvesting and preparation

200 µl centrifuge tubes with holes pierced at the bottom were placed into 1.5 ml centrifuge tubes. Femurs and tibias were harvested from the mice and immediately transferred to chilled PBS. The bone edges were removed with scissors, and the

bones were then placed into the 200 µl tubes. The tubes were then centrifuged at 10,000xg for 2 minutes to pellet the bone marrow cells. The cells were then resuspended in 500 µl ACK lysis buffer (Lonza; 10-548E) and incubated at room temperature for 5 minutes. 1 ml PBS was then added before centrifugating the cells at 10,000xg for 2 minutes. The cells were then counted, and equal numbers labelled following the protocol outlined in Table 19.

Table 19. Labelling of cells harvested from bone marrow

Labelling Step	Antigen	Conjugate	Supplier; Catalogue number	Dilution
Primary	Human TruStain FcX	N/A	Biolegend; 422302	1:33
	Murine TruStain FcX	N/A	Biolegend; 101320	1:33
	Counting beads	N/A	Invitrogen; C36950	1:33
Secondary	Murine CD45	BV421	Biolegend; 103134	1:50
	CD34(RQR8)	AF488	RnD Systems; FAB7227G	1:50
	CD3	PE/Cy7	Biolegend; 344816	1:50
	HA tag	AF647	Biolegend; 682404	1:50
Viability	7AAD	N/A	Biolegend; 420404	1:50

3.5 Statistical analysis

Statistical analysis was carried out on Prism Version 8 (GraphPad). When comparing multiple data sets to one reference data set, we used one-way ANOVA statistical analysis. However, when comparing two data sets, we implemented an unpaired t-test. For all the statistical analysis done in this study, the statistical significance values were: *P<0.05, **P<0.01, ***P<0.001, ****P<0.0001.

3.6 Illustrations

Unless otherwise specified, all illustrations were created with BioRender.com.

4 RESULTS: VALIDATION OF CSK AS A MODULE TO ALTER CAR T CELL FUNCTION

4.1 Introduction

4.1.1 Limitations in the field

CAR T cell therapies have demonstrated impressive clinical efficacy for the treatment of relapsed/refractory B cell malignancies (Maude et al. 2018; Neelapu et al. 2017; Abramson et al. 2020) and myeloma (Raje et al. 2019; Munshi et al. 2021). Despite this clinical success, there are a number of challenges hindering its widespread implementation, particularly for the treatment of solid tumours. One of these challenges is suboptimal efficacy against targets with low antigen density. The need to improve CAR T cell sensitivity was brought to the fore after data was published from a phase 1 trial for the treatment of B-ALL with anti-CD22 CAR T cells (Fry et al. 2018; Shah et al. 2020). Of 8 patients that relapsed after treatment, 7 of the relapses were attributed to decreases in CD22 expression, leading to escape of B-ALL cells (Fry et al. 2018).

A second challenge for CAR T cell therapy is the identification of tumour specific antigens. The majority of antigens that are targeted by immunotherapies are expressed on normal tissue as well as the cancer (TAAs), posing the risk of on-target off-tumour toxicity. In some cases, CAR T cell-mediated on-target off-tumour toxicity results in the acceptable loss of healthy tissue such as CD19 or CD22 targeting in B-cell malignancies leading to B cell aplasia, which can be clinically managed by immunoglobulin replacement (Maude et al. 2014). The management of B-cell aplasia is the exception, and the occurrence of on-target off-tumour for the majority of antigens would be highly toxic. In one case, the administration of HER2 targeting CAR T cells for the treatment of colon cancer caused rapid respiratory failure, multi-organ dysfunction and subsequent death due to expression of HER2 on lung epithelial cells (Morgan et al. 2010).

These challenges indicate the need for a strategy to enhance CAR T cell activation to low antigen density targets whilst maintaining control over CAR T cell activation to avoid on-target off-tumour toxicity.

4.1.2 Scope of this project

To achieve this, proteins that regulate the T cell signalling pathway can be exploited to alter T cell function. Protein tyrosine phosphorylation is fundamental to T cell activation and there are a number of enzymes that positively and negatively regulate this process. The interaction between, and phosphorylation state of these enzymes dictate many aspects of T cell function. Thus, tuning the activity of these regulatory enzymes involved in proximal TCR signalling would also tune T cell function.

To address both the low-density antigen expression as well as the on-target off-tumour challenges, I identified CSK and PTPN22 as enzymes that could be utilised to either increase sensitivity to low-density targets (by engineering dominant-negative iterations) or dampen CAR T cell function, to avoid recognition of low-density antigen on healthy tissues.

As previously described (1.1.1.5.7), CSK in an inhibitory tyrosine kinase capable of negatively regulating T cell signalling. CSK is a cytosolic enzyme that primarily localises to the cell membrane by binding to the transmembrane protein PAG, specifically via the interaction of the SH2 domain of CSK and a phosphorylated tyrosine residue (Y317) in PAG (Brdicka et al. 2000). As PAG is situated in lipid rafts within the plasma membrane, it is in close proximity to SFKs such as Lck and Fyn. The association of CSK with PAG allows CSK to phosphorylate the C-terminal tyrosine residue in Lck and other SFKs, rendering them inactive and thus inhibiting T cell signalling (Brdicka et al. 2000; Bergman et al. 1992; Okada 2012).

Similar to CSK, PTPN22 also negatively regulates T cell signalling (discussed in 1.1.1.5.6). PTPN22 is a phosphatase, which inhibits T cell signalling via dephosphorylation of the activatory tyrosine residues of Lck (Y394) and ZAP-70 (Y493) in addition to the dephosphorylation of the CD3ε and ζ chains within the TCR complex (Wu et al. 2006; Cloutier and Veillette 1999).

Therefore, the first goal of this work was to investigate, as a proof of concept, whether the co-expression of either wild-type CSK (wtCSK) or wtPTPN22 in CAR T cells impacted their functionality by reducing sensitivity to antigen.

4.2 Aim

The overall aim of this project was to develop agnostic modules that enable tuning of CAR T cell function to address two challenges facing CAR T cell therapy: lack of function against low antigen density targets, and on-target off-tumour activity. The approach I took was to firstly, identify an inhibitor of T cell activation which would enable dampening of CAR T cell function, reducing response to antigen. Secondly, engineer dominant-negative iterations of this protein to improve CAR T cell sensitivity. Lastly, engineer a module that enables tuning of CAR T cell function in response to a small molecule drug, avoiding on-target off-tumour toxicity whilst generating efficient function against low antigen density targets.

The aim of this chapter was to investigate the effect of co-expressing wtCSK or wtPTPN22 in CAR T cells to screen them as candidate modules to dampen CAR T cell function.

4.3 Results

4.3.1 Dampening of CAR T cell function with wtCSK or wtPTPN22

4.3.1.1 Structure of LT22 CARs co-expressing wtCSK or PTPN22

In order to investigate the impact of wtCSK or wtPTPN22 on the functionality of CAR T cells, each enzyme was co-expressed with a second generation anti-CD22 CAR (Figure 6). The LT22 CAR is a component of the AUTO3 CD19/CD22 dual targeting product which is in a Phase 1/2 trial for the treatment of paediatric and young adult patients with relapsed/refractory B-ALL (NCT03289455) (Cordoba et al. 2021). The LT22 CAR is comprised of a scFv derived from the LT22 antibody, the pentameric coiled-coil domain from cartilage oligomeric matrix protein (COMP) as a spacer, a TM domain derived from Tyrosinase Related Protein 1 (Tyrp-1), a 4-1BB co-stimulatory domain and CD3ζ signalling domain. The RQR8 marker, which contains epitopes from

both CD34 and CD20 antigens (Philip et al. 2014) was included upstream of the CAR transgene as an independent marker of transduction. RQR8 and the CAR transgene were separated by the T2A self-cleaving peptide (Liu et al. 2017), which facilitates equal expression both. A second 2A peptide (P2A) was used to separate the CAR from either wtCSK or wtPTPN22 (Figure 6a).

To detect the surface expression of the LT22 CAR in PBMCs, cells were labelled with soluble CD22 (sCD22) in addition to an anti-CD34 antibody for the detection of the RQR8 transduction marker (Figure 6b). NT T cells were included as a negative control. The expression level of RQR8 and the CAR in all of the constructs in PBMCs were comparable.

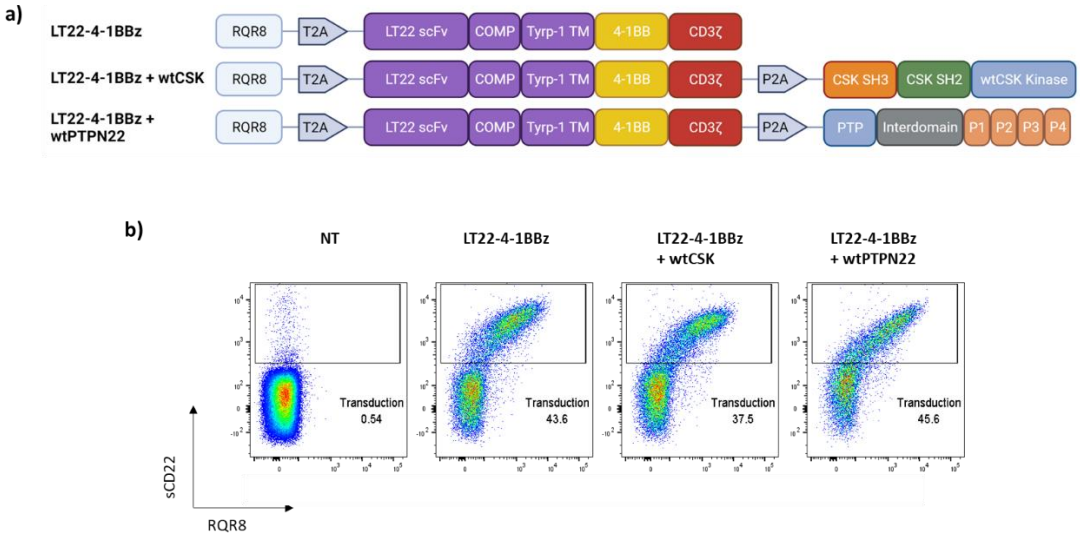

Figure 6. Co-expression of wtCSK or wtPTPN22 in LT22 CAR T cells. a) Construct maps of the LT22 CAR alone or the LT22 CAR co-expressing either wtCSK or wtPTPN22 b) PBMCs were labelled with sCD22 to test for expression of the LT22 CAR. To detect the RQR8 transduction marker, PBMCs were also labelled with an anti-CD34 antibody. One representative donor is shown.

4.3.1.2 Function of LT22 CAR T cells co expressing either wtCSK or PTPN22

Co-cultures of CAR T cells and SupT1 target cells were set up to assess the impact co-expressing either wtCSK or wtPTPN22 had on CAR T cell function. The T cells were challenged with either SupT1 NT or SupT1 $CD22^{Mid}$ targets, expressing 6,309 molecules/cell (Figure 10), at an effector to target (E:T) ratio of 1:1. The expression of all constructs was confirmed by flow cytometry (Figure 6b) and transduction was normalised to 30% before co-culture set up. After 72-hours, the cytotoxicity of the T cells was measured, viable target cells were counted by flow cytometry and normalised to counting beads as well as to the NT T cell condition. This was done to mitigate for any non-CAR mediated lysis of target cells.

Against SupT1 NT targets, there was negligible background lysis observed by any of the T cells (Figure 7a). When challenged with the SupT1 $CD22^{Mid}$ targets, the LT22 CAR T cells displayed moderate cytotoxicity, with a median target cell survival of 46.9%. The co-expression of wtCSK reduced the cytotoxicity of CAR T cells against SupT1 $CD22^{Mid}$ target cells to a median target cell survival of 79.2% compared to the LT22 CAR, although no statistical significance was achieved. However, the co-expression of wtPTPN22 only reduced the target cell survival to a median of 59.3% (Figure 7b). Based on these results I subsequently focused solely on CSK to engineer modules to alter CAR T cell function.

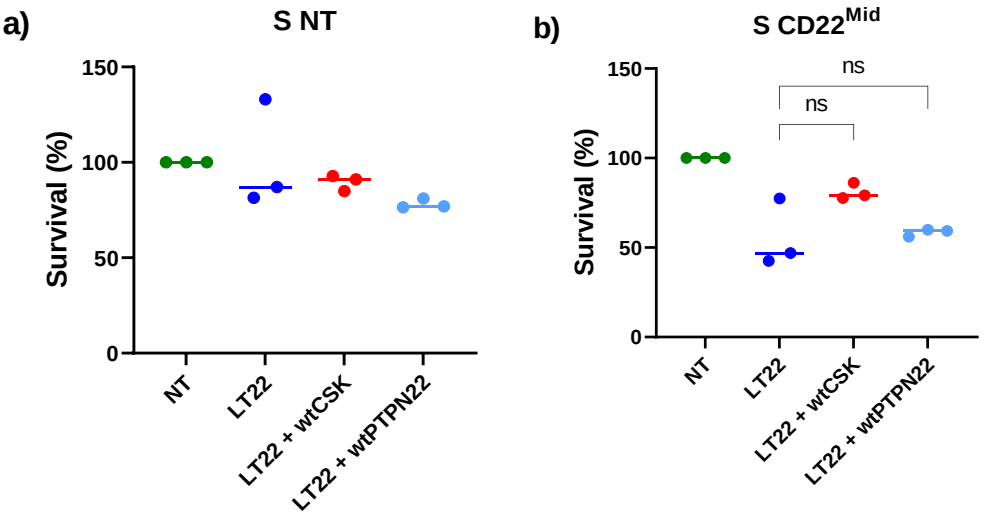

Figure 7. Cytotoxicity of LT22 CAR T cells co-expressing either wtCSK or wtPTPN22. Analysis of target cell survival by flow cytometry was carried out at 72h post co-culture set up. Each condition was tested with 3 donors (n=3), with median indicated and all data was normalised to NT T cells. Co-cultures were set up with an E:T ratio of 1:1, with either SupT1 NT (a) or SupT1 $CD22^{Mid}$ (b) targets. The LT22 CAR was compared to LT22 CAR T cells expressing wtCSK or wtPTPN22 using one-way ANOVA statistical analysis. *P<0.05, **P<0.01, ***P<0.001, ****P<0.0001.

4.3.2 Dampening of CARs with different endodomains

The choice of co-stimulatory domain affects the potency of the CAR T cells and thus how easy or difficult it is to alter their activity. Therefore, I chose to explore the effect of wtCSK on CAR T cells with different endodomains. The inclusion of 4-1BB in the CAR has been linked to the expression of granzyme B, TNFα, IFN-γ and the anti-apoptotic protein Bcl-XL (Zhong et al. 2010), in addition to improved persistence and antitumour activity (Song et al. 2011). Alternatively, the incorporation of a CD28 co-stimulatory domain has shown to improve CAR T cell cytokine production and proliferation (Maher et al. 2002). Compared to 4-1BB CAR T cells, CD28 CAR T cells have shown rapid and profound changes in the phosphorylation state of hundreds of proteins involved in TCR signalling, whilst displaying improved cytokine production and enhanced lysis of targets with low antigen density (Majzner et al. 2020).

4.3.2.1 Structure of LT22 CARs with different co-stimulatory domains

I initially co-expressed wtCSK in T cells alongside second generation anti-CD22 CARs with different endodomains. The CARs both contained the LT22 scFv, COMP spacer, Tyrp-1 TM domain and CD3ζ signalling domain. One of the CARs had a 4-1BB co-stimulatory domain, while the other contained CD28. In both constructs, RQR8 was positioned upstream of the CAR transgene (Figure 8).

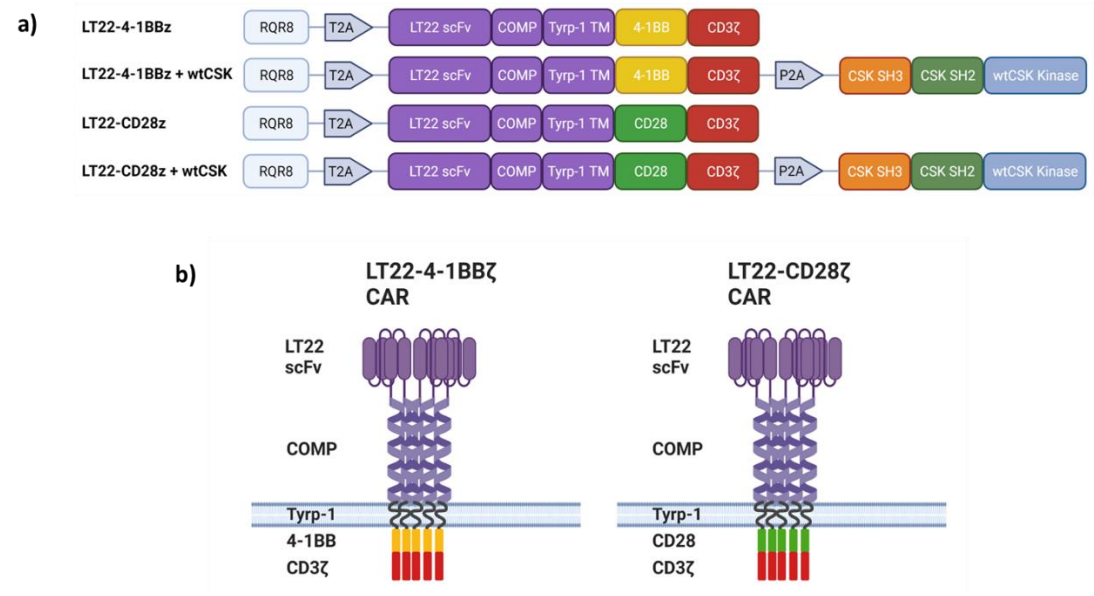

Figure 8. Structure of LT22 CARs bearing different co-stimulatory domains a) Construct maps showing the LT22 CAR with either 4-1BB or CD28 co-stimulatory domains and with or without wtCSK. b) Schematic of the two LT22 CARs, consisting of the LT22 scFv, COMP spacer, Tyrp-1 transmembrane domain, either a 4-1BB (left) or CD28 (right) co-stimulatory and a CD3ζ signalling domain. The COMP spacer forms a coiled coil structure resulting in the formation of a pentamer.

4.3.2.2 LT22 CARs transduction efficiency

On day 3 after retroviral transduction, PBMCs were analysed for surface expression of RQR8 and the LT22 CAR (Figure 9a). Analysis of the MFI ratio of the CAR/RQR8 showed that the expression of the LT22 CAR containing the 4-1BB co-stimulatory domain was 3.2-fold higher compared to the LT22-CD28 CAR (Figure 9b). However, the retroviral supernatants used were not titrated, thus this difference of expression could potentially be due to a difference in multiplicity of infection (MOI) values. Both constructs bearing CD28 had a reduced MFI ratio in comparison to the corresponding 4-1BB containing CAR, suggesting they had lower CAR expression on the cell surface. More importantly, cells co-expressing the wtCSK modules had comparable CAR expression to cells expressing the respective CAR in the absence of wtCSK.

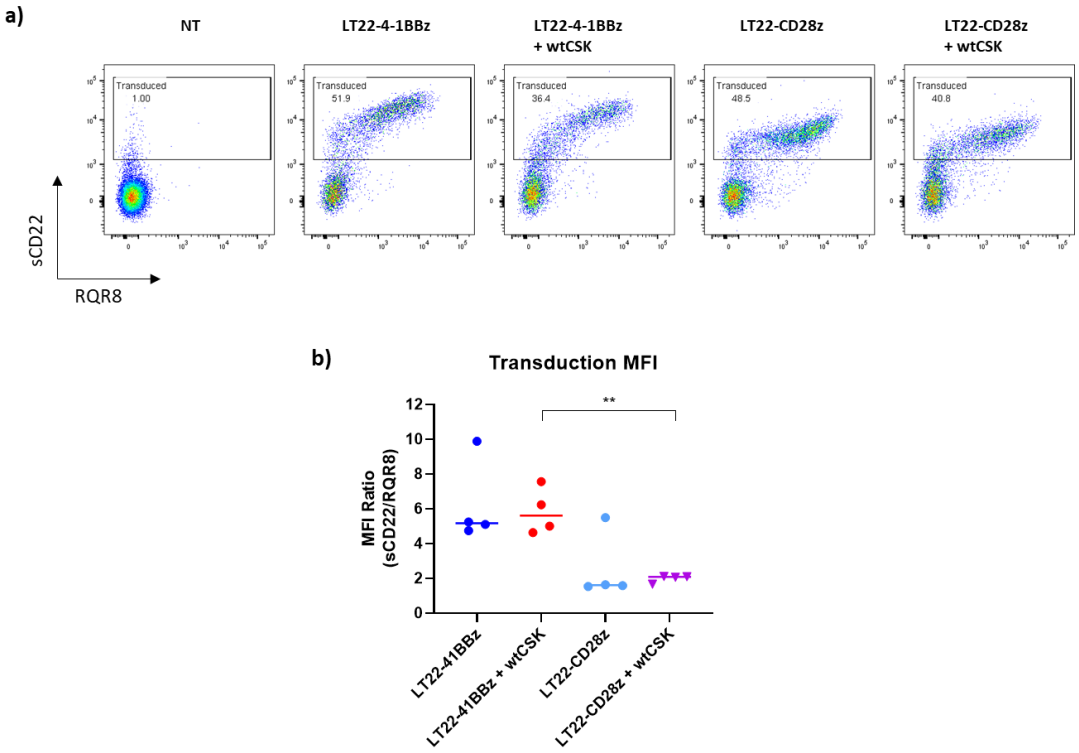

Figure 9 Expression of LT22 CARs in PBMCs. a) All PBMCs were labelled with sCD22 for expression of the LT22 CAR and an anti-CD34 antibody for detection of the RQR8 transduction marker. One representative donor is shown (n=4). b) The MFI ratio of sCD22/aCD34 shows that constructs with CD28 had markedly reduced MFI compared to constructs with 4-1BB co-stimulatory domain. Statistics were run using an unpaired t-test (*P<0.05, **P<0.01, ***P<0.001, ****P<0.0001).

4.3.2.3 CD22 targets antigen density: Mid and Low

I previously challenged LT22 CAR T cells against SupT1 $CD22^{Mid}$ target cells (4.3.1.2) with an antigen density of 6,309 molecules/cell. To investigate the dampening effect of wtCSK further, I wanted to challenge CAR T cells against more than one antigen positive cell line. Therefore, I engineered an additional cell line, termed SupT1 $CD22^{Low}$ (methodology outlined in 3.2.3), with a lower antigen density of 1,968 molecules/cell (Figure 10).

a)

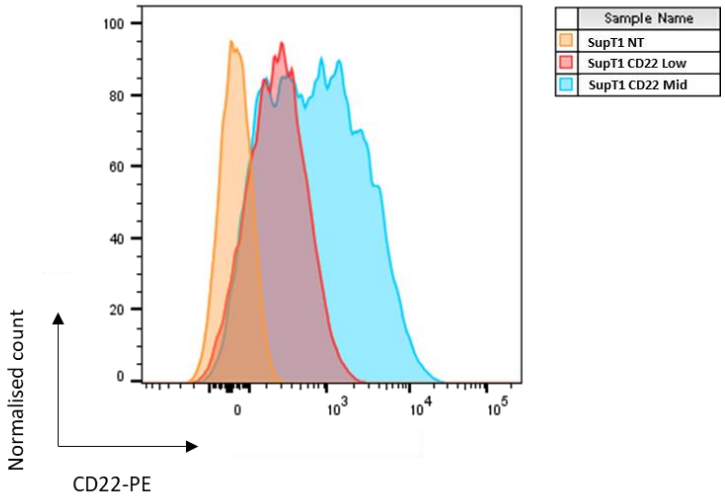

b)

Target cell line	CD22/cell
SupT1 NT	0
SupT1 $CD22^{Mid}$	6,309
SupT1 $CD22^{Low}$	1,968

Figure 10. Antigen density of SupT1 CD22 target cells: Mid and Low. SupT1 cells were transduced with a retroviral vector to express a chimeric CD22 antigen, with CD22 ectodomain and CD19 TM and endo-domains. a) To verify the CD22 antigen density on two engineered target cell lines the cells were labelled with an anti-CD22-PE antibody. b) To quantify the CD22 antigen density, Quantibrite^{TM} beads were used to create a standard curve on PE MFI and molecules/cell. I obtained $CD22^{Mid}$ and $CD22^{Low}$ cell lines, expressing 6,309 and 1,968 molecules/cell, respectively.

4.3.2.4 LT22 CARs function

72-hour co-cultures were set up to assess the functionality of the LT22-4-1BB and LT22-CD28 CARs, with or without co-expression of wtCSK. T cells were challenged with SupT1 NT, SupT1 $CD22^{Mid}$ and SupT1 $CD22^{Low}$ target cells, at two effector to target ratios (E:T of 1:2 and 1:4) (Figure 11). There was a trend of LT22-4-1BB CAR displaying higher background lysis against antigen negative SupT1 NT compared to the LT22-CD28 CAR. Both CARs showed reduced background cytotoxicity when co-expressed with wtCSK (Figure 11a). Regarding antigen specific lysis, the LT22-CD28 CAR T cells showed a substantially greater degree of target cell lysis than the LT22-4-1BB CAR T cells. The co-expression of the wtCSK module significantly reduced the cytotoxicity of both the LT22-4-1BB or LT22-CD28 CAR T cells against SupT1 $CD22^{Mid}$ target cells (Figure 11b and e).

The ability of the LT22-4-1BB CAR to recognise and lyse SupT1 $CD22^{Low}$ targets was modest, whereas the LT22-CD28 CAR T cells were able to eliminate these targets (Figure 11c and f). Against the $CD22^{Low}$ targets, the co-expression of wtCSK inhibited the cytotoxicity of the CD28 CAR T cells, eliciting a 5.8-fold decrease in target cell lysis (Figure 11f), but unlike the 4-1BB CAR T cells it was not reduced to background levels of cytotoxicity. Although wtCSK significantly reduced the cytotoxicity of the CAR against both $CD22^{Mid}$ and $CD22^{Low}$ targets, it did not fully ablate the CAR function.

The inhibitory effect of the wtCSK module was also analysed by measuring the secretion of the cytokines IFN-γ and IL-2 (Figure 12 and Figure 13 respectively). All CAR T cells displayed minimal levels of IFN-γ release in the presence of antigen negative SupT1 NT target cells (Figure 12a). Against both the SupT1 $CD22^{Mid}$ and $CD22^{Low}$ target cells, the introduction of wtCSK significantly reduced the level of IFN-γ secretion of both CARs (Figure 12b, c, e and f).

Against the $CD22^{+}$ target cells, IL-2 secretion by both the LT22-4-1BB and LT22-CD28 CAR T cells was minimal (Figure 13b, c, e and f). However, the low levels of IL-2 produced were abrogated upon co-expression of wtCSK.

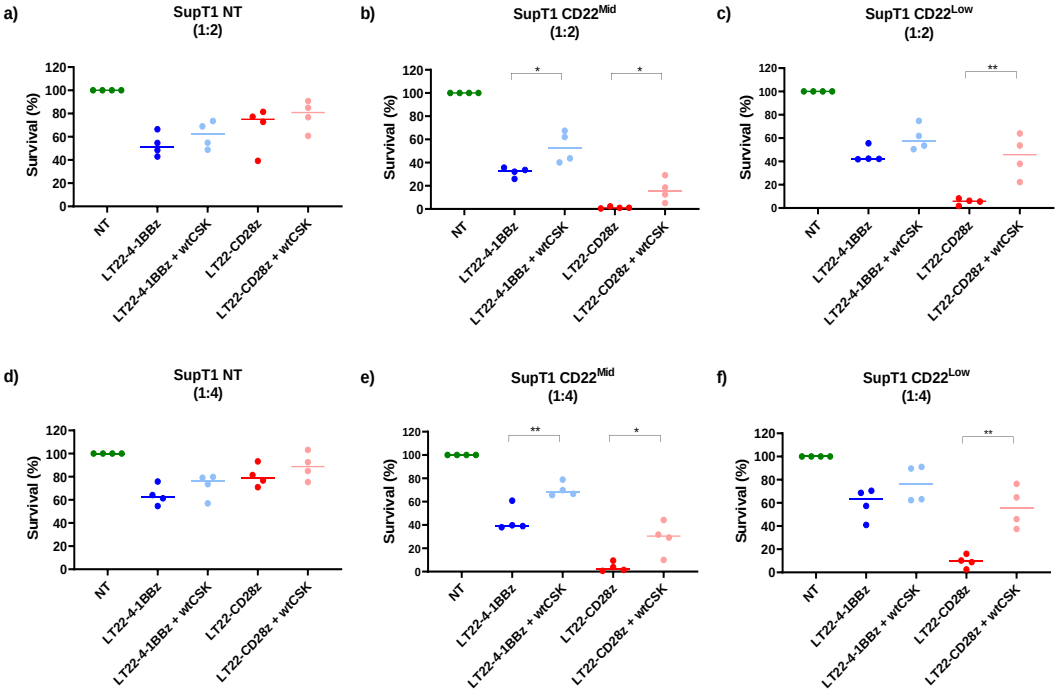

Figure 11. Cytotoxicity of LT22 CARs with either 4-1BB or CD28 co-stimulatory domain. Analysis of target cell survival by flow cytometry was carried out following 72h co-culture. Each condition was tested with a minimum of 4 donors (n=4), with median indicated and all data was normalised to NT T cells. Co-cultures were set up with an E:T ratio of 1:2 (a-c) or 1:4 (d-f), with either SupT1 NT (a/d), SupT1 CD22^{Mid} (b/e) or SupT1 CD22^{Low} (c/f) targets. Cytotoxicity of each CAR was compared with and without wtCSK by an unpaired t-test. *P<0.05, **P<0.01, ***P<0.001, ****P<0.0001.

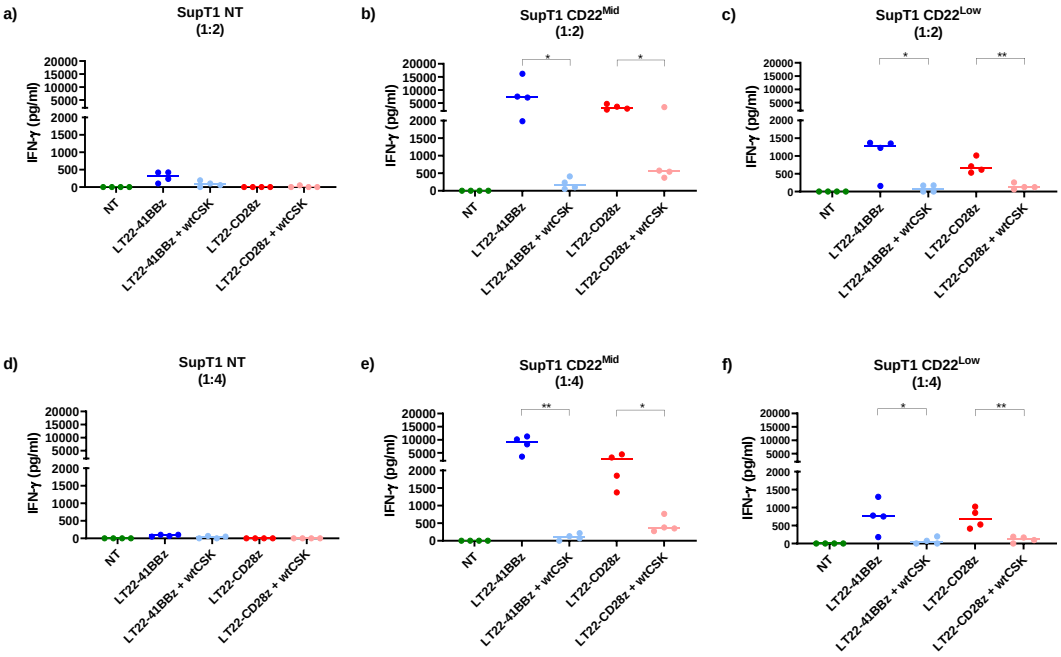

Figure 12. IFN-γ release by LT22 CARs with either 4-1BB or CD28 co-stimulatory domain. Supernatant taken at 72h post co-culture initiation was analysed by ELISA for the presence of IFN-γ. Each condition was tested with a minimum of 4 donors (n=4), with median indicated. The target cell lines used were SupT1 NT (a/d), SupT1 $CD22^{Mid}$ (b/e) or SupT1 $CD22^{Low}$ (c/f) cells and co-cultures were set up with either an E:T ratio of 1:2 (a-c) or 1:4 (d-f). Cytokine secretion by each CAR was compared with and without wtCSK by an unpaired t-test. * P<0.05, **P<0.01, ***P<0.001, ****P<0.0001.

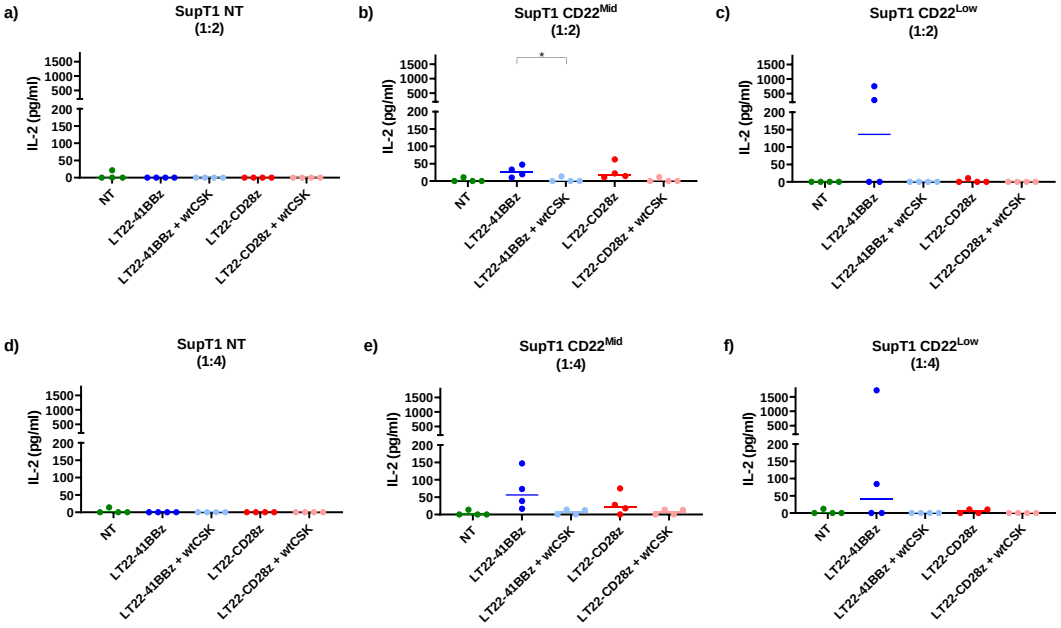

Figure 13. IL-2 release by LT22 CARs with either 4-1BB or CD28 co-stimulatory domain. Supernatant taken at 72h post co-culture initiation was analysed by ELISA for the presence of IL-2. Each condition was tested with a minimum of 4 donors (n=4), with median indicated. The target cell lines used were SupT1 NT (a/d), SupT1 CD22^{Mid} (b/e) or SupT1 CD22^{Low} (c/f) cells and co-cultures were set up with either an E:T ratio of 1:2 (a-c) or 1:4 (d-f). Cytokine secretion by each CAR was compared with and without wtCSK using an unpaired t-test. * P<0.05, **P<0.01, ***P<0.001, ****P<0.0001.

4.3.3 Dampening of an alternative anti-CD22 CAR

As observed in 4.3.2.4, the introduction of the wtCSK module is effective in dampening the function of CAR T cells with different co-stimulatory domains, especially in relation to cytokine secretion. To investigate the scope of this dampening effect, I sought to co-express the wtCSK module in an alternative CD22 targeting CAR. A range of new aCD22 binders were tested and characterized within Autolus, leading to the development of the 9A8 CAR. 9A8 is a non-humanised aCD22 scFv, developed from immunized rats (Kokalaki et al. 2023).

4.3.3.1 9A8 CAR structure

The 9A8 CAR was designed as a second-generation CAR, with the retroviral vector directing expression of the aCD22 9A8 scFv, human CD8α spacer (CD8αSTK) and TM domain (CD8αTM), 4-1BB co-stimulatory domain, and CD3ζ signalling domain. The RQR8 marker gene was placed upstream of the CAR transgene, separated by a T2A peptide. In the second construct, the wtCSK module was co-expressed downstream of the 9A8 CAR, separated by a P2A peptide (Figure 14a). A schematic of the 9A8 CAR as a dimer on the cell surface is shown in Figure 14b.

4.3.3.2 9A8 CAR transduction efficiency

PBMCs were transduced with the retroviral supernatant and analysed on day 3 post transduction for surface expression of RQR8 and the 9A8 CAR (Figure 14c), the former was detected by anti-CD34 labelling and latter was detected by sCD22 labelling.

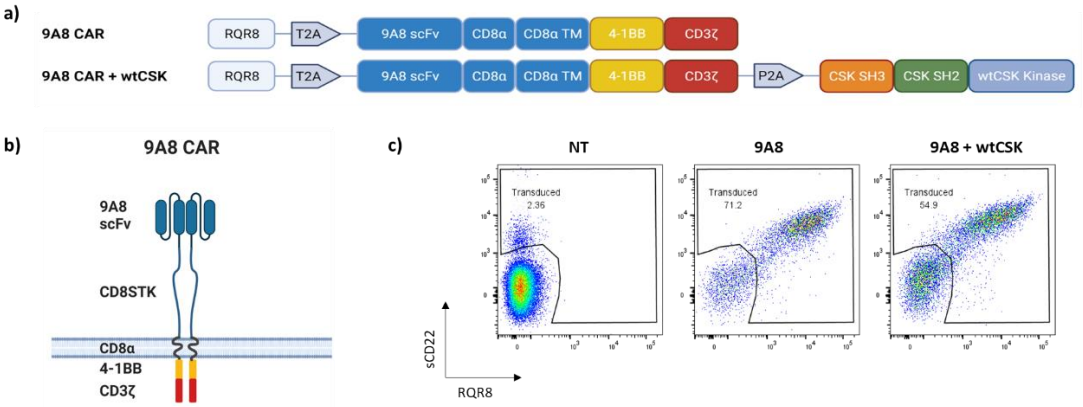

Figure 14. 9A8 CAR structure and expression. a) The construct map of the 9A8 CAR, with and without wtCSK. RQR8 is included as a transduction marker b) The 9A8 CAR consists of an anti-CD22 scFv, with a CD8αSTK spacer, CD8αTM domain, a 4-1BB co-stimulatory domain and a CD3ζ signalling domain. c) All PBMCs were labelled with sCD22 to test for expression of the LT22 CAR. PBMCs were also labelled with an anti-Human CD34 for detection of the RQR8 transduction marker. One representative donor is shown.

4.3.3.3 9A8 CAR function

To assess the effect of the wtCSK module on the functionality of the 9A8 CAR, I co-cultured T cells for 72 hours with one of three target cell lines: SupT1 NT, SupT1 $CD22^{Mid}$ or SupT1 $CD22^{Low}$ cells (Figure 15). In agreement with the LT22 CAR results, when challenged with SupT1 NT control targets, the co-expression of wtCSK was able to reduce background cytotoxicity levels (Figure 15a).

When challenged with SupT1 $CD22^{Mid}$ targets, the 9A8 CAR T cells efficiently lysed the targets at both the 1:2 and 1:4 E:T ratios, (Figure 15b and e). The co-expression of the wtCSK module significantly impaired the lysis of the target cells. The inhibitory effect of the wtCSK module on target cell lysis was more profound against the low density SupT1 $CD22^{Low}$ targets than against the $CD22^{Mid}$ targets. At an E:T ratio of 1:2, the wtCSK dampened lysis of the $CD22^{Mid}$ target cells by 25.7% (median) (Figure 15b), whereas against the $CD22^{Low}$ targets, cytotoxicity was reduced by 54.9% (Figure 15c).

Additionally, I measured the inhibitory effect of the wtCSK module by assessing CAR T cell cytokine secretion in response to target cells (Figure 16 and Figure 17). Against SupT1 NT targets, I observed background secretion of IFN-γ by the NT T cells at both the 1:2 and 1:4 ratios (Figure 16a and d). This is likely to be a technical artefact of the assay as increases were not seen against SupT1 CD22 positive cells (Figure 16b, c, e and f). Although IFN-γ (Figure 16c and f) and IL-2 (Figure 17c and f) secretion was not detectable in $CD22^{Low}$ targets, I observed wtCSK expression to completely abrogate secretion of both these cytokines when CAR T cells were co-cultured with $CD22^{Mid}$ targets (Figure 16b and e and Figure 17b and e).

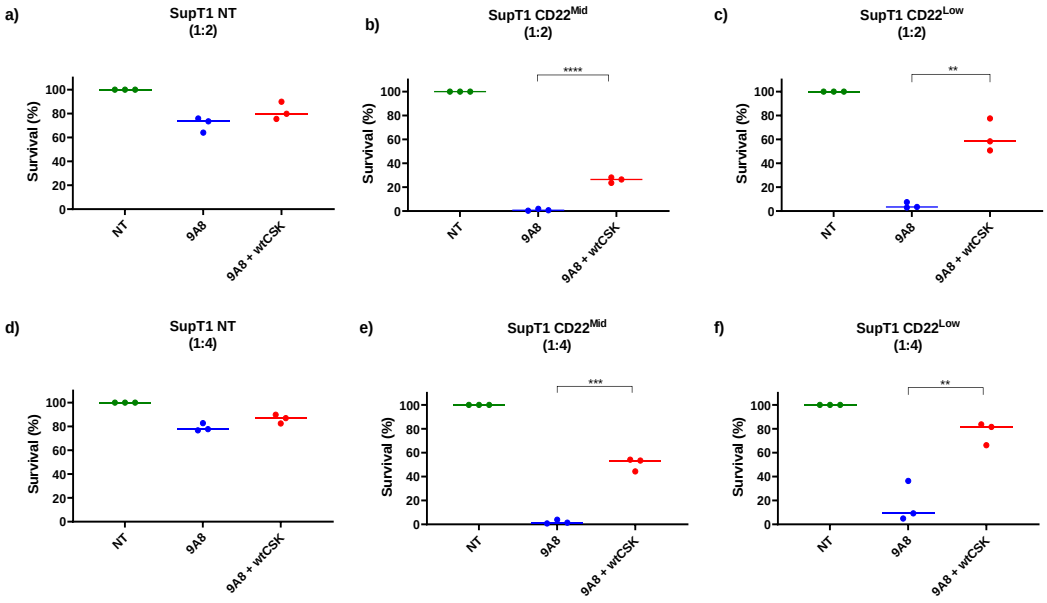

Figure 15. Cytotoxicity of 9A8 co-expressed with wtCSK. Analysis of target cell survival by flow cytometry was carried out at 72h post co-culture set up. Each condition was tested with 3 donors (n=3), with median indicated. All data was normalised to NT T cells. Co-cultures were set up with an E:T ratio of 1:2 (a-c) or 1:4 (d-f), with either SupT1 NT (a/d), SupT1 $CD22^{Mid}$ (b/e) or SupT1 $CD22^{Low}$ (c/f) targets. Cytotoxicity of 9A8 CAR T cells was compared with and without wtCSK using an unpaired t-test. * P<0.05, **P<0.01, ***P<0.001, ****P<0.0001.

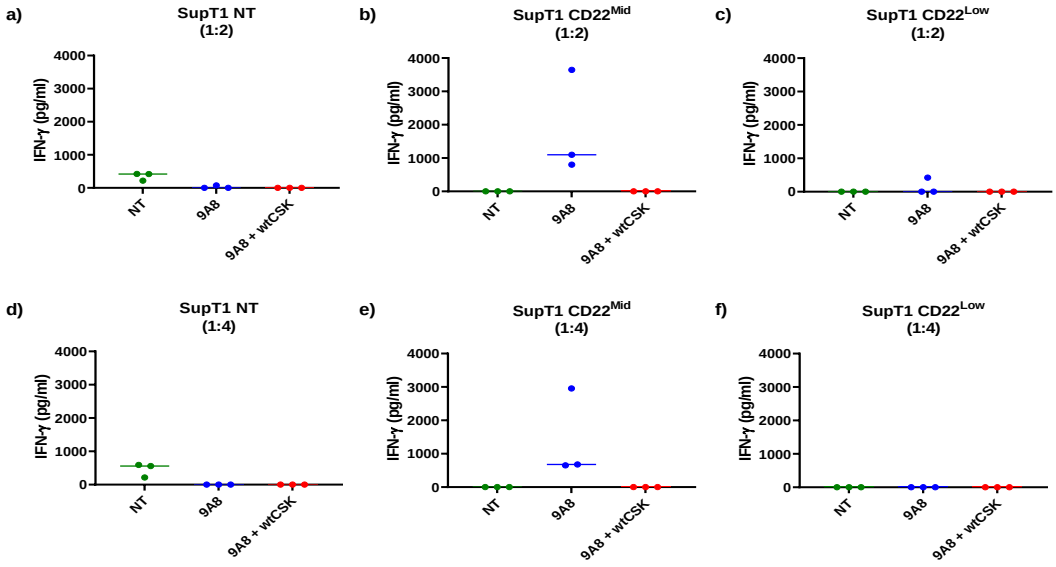

Figure 16. IFN-γ release by 9A8 CAR co-expressed with wtCSK. Supernatant taken at 72h post co-culture initiation was analysed by ELISA for the presence of IFN-γ. Each condition was tested with 3 donors (n=3), with median indicated. Co-cultures were set up with an E:T ratio of 1:2 (a-c) or 1:4 (d-f), with either SupT1 NT (a/d), SupT1 $CD22^{Mid}$ (b/e) or SupT1 $CD22^{Low}$ (c/f) targets. 9A8 CARs were compared with and without wtCSK by an unpaired t-test. * P<0.05, **P<0.01, ***P<0.001, ****P<0.0001.

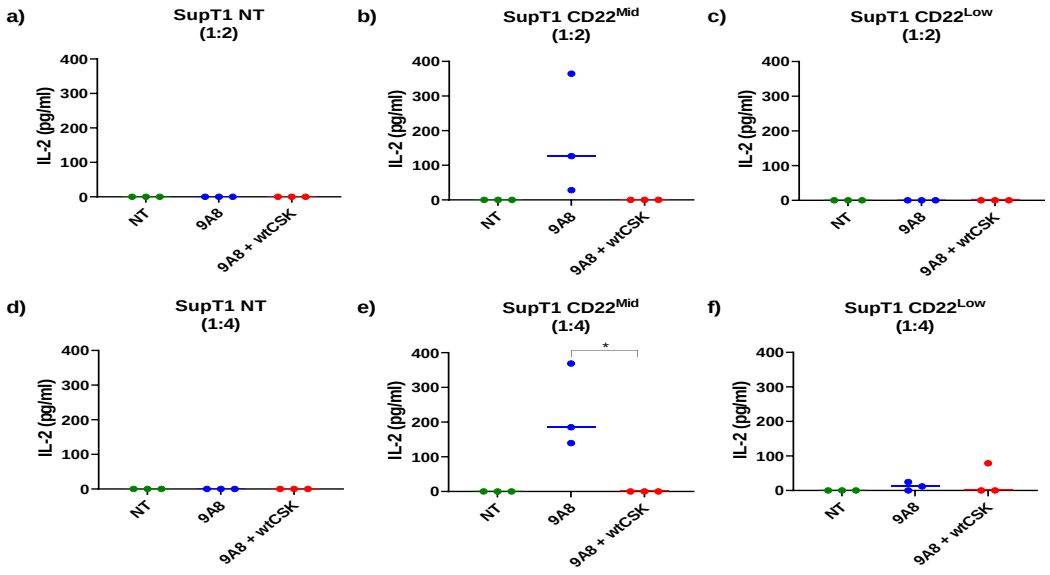

Figure 17. IL-2 release by 9A8 CAR co-expressed with wtCSK. Supernatant taken at 72h post co-culture initiation was analysed by ELISA for the presence of IL-2. Each condition was tested with 3 donors (n=3), with median indicated. Co-cultures were set up with an E:T ratio of 1:2 (a-c) or 1:4 (d-f), with either SupT1 NT (a/d), SupT1 $CD22^{Mid}$ (b/e) or SupT1 $CD22^{Low}$ (c/f) targets. 9A8 CARs were compared with and without wtCSK using an unpaired t-test. *P<0.05, **P<0.01, ***P<0.001, ****P<0.0001.

4.3.4 Dampening of an anti-CD19 CAR

After testing the wtCSK module in CD22 targeting CAR T cells, I further investigated the robustness of the module by incorporating it into CD19 targeting CAR T cells. CD19 is a very well-established target in the CAR T therapy field and has been proven as an effective target in the treatment of CLL, ALL, MM and B cell lymphoma (Porter et al. 2015; Maude et al. 2014; Garfall et al. 2015; Kochenderfer et al. 2015; Shah et al. 2021). The aCD19 FMC63 scFv was developed by Nicholson et al. from a mouse hybridoma cell line (Nicholson et al. 1997). This scFv was incorporated into CAR T cells in 2009 (Kochenderfer et al. 2009), and has since become the most common aCD19 scFv used in clinical trials. Based on the success of these clinical trials, a number of FMC63 containing CAR T cell products have been FDA-approved (Maude et al. 2018; Neelapu et al. 2017; Wang et al. 2020; Abramson et al. 2020).

4.3.4.1 FMC63 CAR structure

The FMC63 CAR used in these experiments was the same as the one used in the FDA-approved Kymriah product (Maude et al. 2018; Milone et al. 2009), consisting of the aCD19 FMC63 scFv, CD8αSTK and CD8αTM domain, with a 4-1BB co-stimulatory domain and CD3ζ signalling domain (Figure 18a). In both constructs, the RQR8 marker gene was located upstream of the CAR transgene. In the second construct, the wtCSK module was located downstream of the CAR transgene. Figure 18b depicts the FMC63 CAR as a dimer on the cell surface.

4.3.4.2 FMC63 CAR transduction efficiency

On day three post transduction, PBMCs were analysed by flow cytometry for the surface expression of the FMC63 CAR and the RQR8 marker gene through labelling with soluble CD19 (sCD19) and an anti-CD34 antibody respectively (Figure 18c).

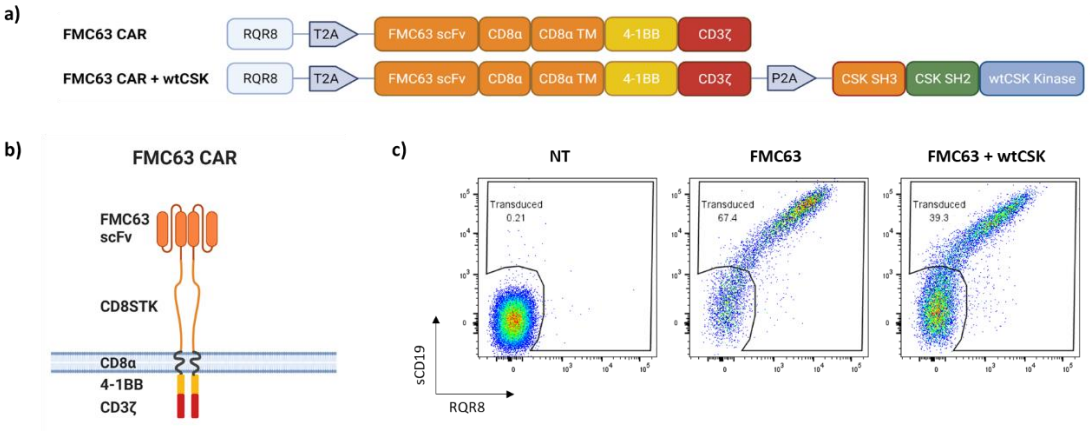

Figure 18. FMC63 CAR Structure and expression. a) The FMC63 CAR is depicted in the construct map in the presence or absence of wtCSK. RQR8 is included as a transduction marker b) The schematic illustrates the structure of FMC63 CAR. The FMC63 CAR consists of an anti-CD19 scFv, with a CD8αSTK spacer, CD8α TM domain, a 4-1BB co-stimulatory domain, and a CD3ζ signalling domain. c) following transduction, all PBMCs were labelled with soluble CD19 to test for expression of the FMC63 CAR. PBMCs were also labelled with an anti-CD34 antibody for detection of the RQR8 transduction marker. One representative donor is shown.

4.3.4.3 CD19 target antigen density

Two CD19^{+} target cell lines were engineered to express different densities of antigen (Figure 19). SupT1 cells are a T cell line that is naturally CD19 negative and were engineered to express CD19 at densities of 100,830 molecules/cell and 3,032 molecules/cell. These lines are referred to as CD19^{High} and CD19^{VL} respectively.

a)

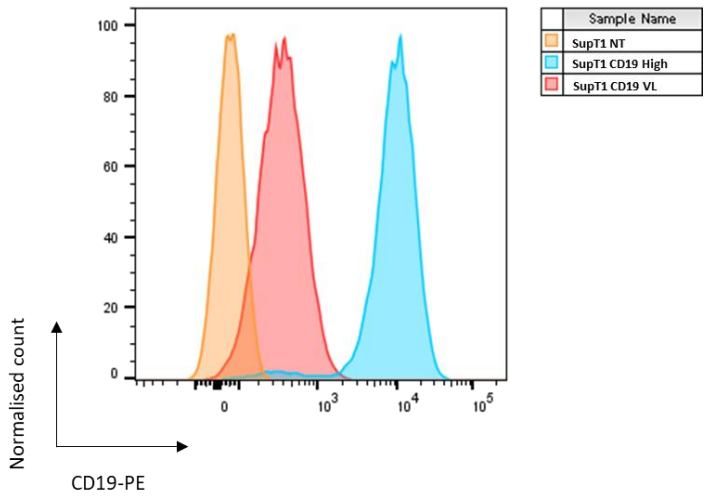

b)

Target cell line	CD19/cell
SupT1 NT	0
SupT1 CD19^{High}	100,830
SupT1 CD19^{VL}	3,032

Figure 19. Antigen density of SupT1 CD19 target cells. a) To verify the expression of CD19 on the target cell lines, the cell lines were labelled with an anti-CD19-PE antibody. b) To quantify the CD19 antigen density, Quantibrite™ beads were used to create a standard curve on PE MFI and molecules/cell. CD19^{High} and CD19^{VL} cell lines express 100,830 and 3,032 molecules/cell, respectively.

4.3.4.4 FMC63 CAR function

To assess the inhibition of FMC63 CAR function mediated by wtCSK, CAR T cells were challenged with SupT1 NT, $CD19^{High}$ and $CD19^{VL}$ target cells and cytotoxicity and cytokine secretion measured (Figure 20). In contrast to the CD22 targeting CARs, I observed only negligible background lysis of the SupT1 NT control target cell line that was not further reduced with the introduction of wtCSK (Figure 20a and d). When challenged with the SupT1 $CD19^{High}$ cells, FMC63 CAR T cells completely ablated the target cells at both the 1:2 and 1:4 E:T ratios (Figure 20b and e), and the expression of wtCSK failed to inhibit this cytotoxicity. In contrast, under the suboptimal condition of low antigen density, the wtCSK module had a significant effect on the CAR-mediated cytotoxicity. Specifically, the co-expression of wtCSK was seen to decrease cytotoxicity by 46% (Figure 20c).

In terms of cytokine secretion, SupT1 NT control target cells evoked only negligible levels of background IFN-γ and IL-2 secretion at both the 1:2 and 1:4 ratio (Figure 21a and d and Figure 22a and d). Despite failing to inhibit the cytotoxic capacity of FMC63 CAR T cells challenged with SupT1 $CD19^{High}$ targets, the co-expression of the wtCSK module significantly reduced both IFN-γ (66% decrease) and IL-2 production (89% decrease) (Figure 21b and Figure 22b). Against targets with low antigen density (SupT1 $CD19^{VL}$), I also observed a reduction in IFN-γ production upon the introduction of wtCSK (Figure 21c and f).

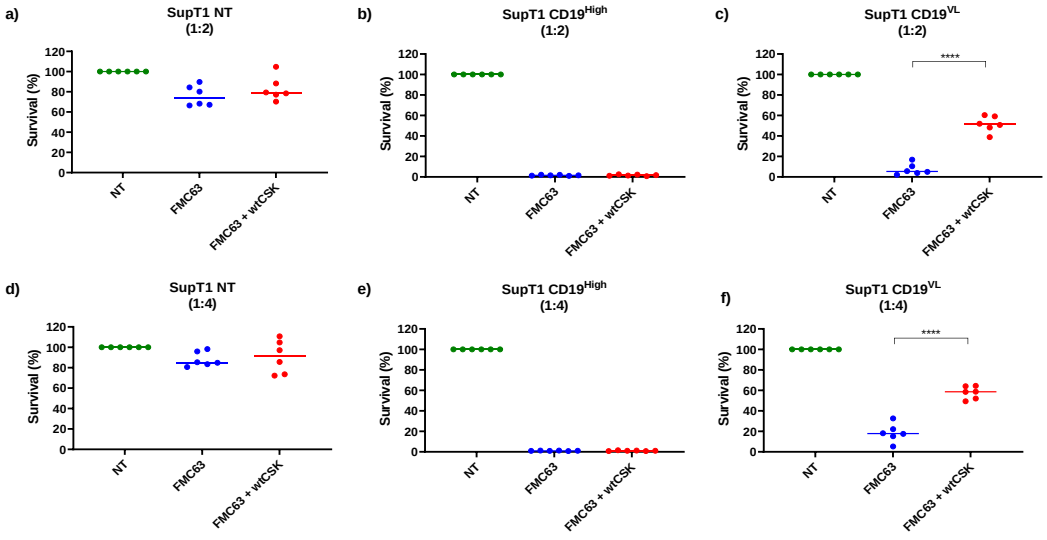

Figure 20. Cytotoxicity of FMC63 CAR co-expressed with wtCSK. FMC63 CAR T cell cytotoxicity was analysed by flow cytometry at 72h post co-culture set up. Each condition was tested with 6 donors (n=6), with median indicated and all data was normalised to NT T cells. CAR T cells were co-cultured with an E:T ratio of 1:2 (a-c) or 1:4 (d-f), with either SupT1 NT (a/d), SupT1 $CD19^{High}$ (b/e) or SupT1 $CD19^{VL}$ (c/f) targets. FMC63 CARs were compared with and without wtCSK by an unpaired t-test. * P<0.05, **P<0.01, ***P<0.001, ****P<0.0001.

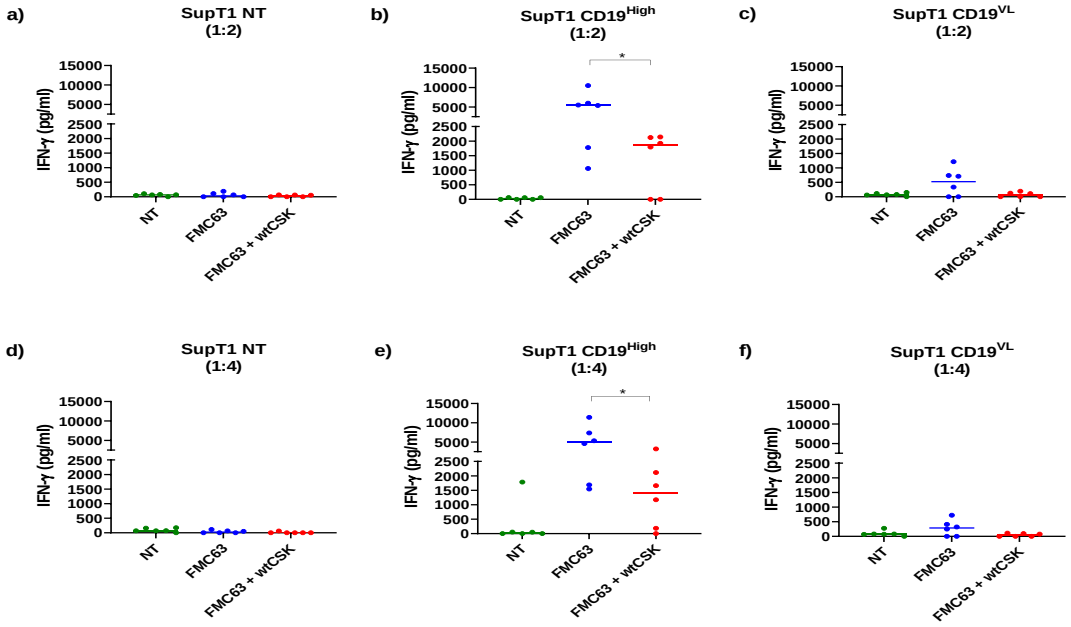

Figure 21. IFN-γ release by FMC63 CAR co-expressed with wtCSK. Supernatant taken at 72h post co-culture set up was analysed by ELISA for the presence of IFN-γ. Each condition was tested with a minimum of 6 donors (n=6), with median indicated. The target cell lines used were SupT1 NT (a/d), SupT1 $CD19^{High}$ (b/e) or SupT1 $CD19^{VL}$ (c/f) cells and co-cultures were set up with either an E:T ratio of 1:2 (a-c) or 1:4 (d-f). FMC63 CARs were compared with and without wtCSK by an unpaired t-test. *P<0.05, **P<0.01, ***P<0.001, ****P<0.0001.

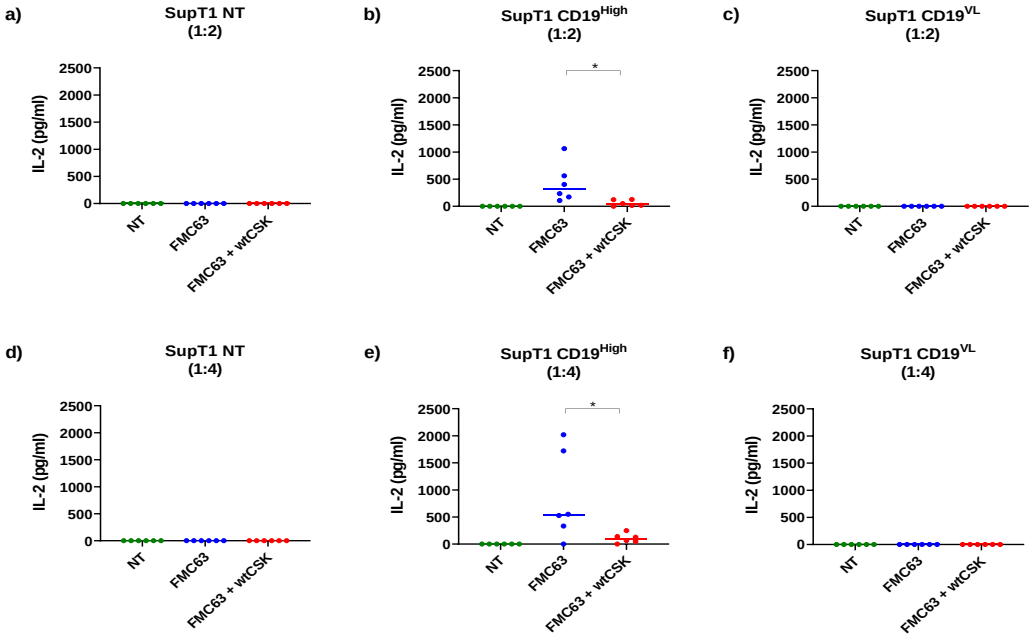

Figure 22. IL-2 release by FMC63 CAR co-expressed with wtCSK. Supernatant taken at 72h post co-culture set up was analysed by ELISA for the presence of IL-2. Each condition was tested with a minimum of 6 donors (n=6), with median indicated. The target cell lines used were SupT1 NT (a/d), SupT1 CD19^{High} (b/e) or SupT1 CD19^{VL} (c/f) cells and co-cultures were set up with either an E:T ratio of 1:2 (a-c) or 1:4 (d-f). FMC63 CARs were compared with and without wtCSK by an unpaired t-test. *P<0.05, **P<0.01, ***P<0.001, ****P<0.0001.

4.4 Summary

Despite the impressive clinical efficacy of many CAR T cell therapies (Maude et al. 2018; Neelapu et al. 2017; Abramson et al. 2020; Raje et al. 2019; Munshi et al. 2021), there are a number of hurdles limiting its broader application. Suboptimal sensitivity of CAR T cells against low antigen density targets represents one such challenge, as reported in clinical trials for treatment of relapsed/refractory B-ALL (Fry et al. 2018; Shah et al. 2020). A second challenge is the risk of on-target off-tumour toxicity, wherein CAR T cells attack healthy tissues due to low-level expression of antigen (Morgan et al. 2010; Lamers et al. 2013; Thistlethwaite et al. 2017).

To address both these challenges, the overarching aim of this project was to develop a module which is co-expressed independently of the CAR and enables tuneable control of CAR T cell function. I envisioned a module with dual functionality, which could dampen CAR T cell function to avoid the risk of on-target off-tumour toxicity yet also have the capacity for improved T cell function in response to low antigen density targets. As the first step towards this goal, in this chapter I aimed to investigate the dampening effect of co-expressing wtCSK or wtPTPN22 on CAR T cell function, specifically with regards to sensitivity to antigen.

CSK and PTPN22 are both negative regulators of T cell signalling and hence were logical choices as candidate modules to dampen CAR T cell function (discussed in 1.1.1.5.7 and 1.1.1.5.6). CSK negatively regulates SFKs via phosphorylation of inhibitory tyrosine residues in their C-terminal tails. Lck and Fyn are both SFKs that are involved in TCR-mediated signalling and are inhibited this way by CSK (Bergman et al. 1992; Okada 2012). PTPN22 also has an inhibitory effect on Lck and Fyn, in addition to other proteins involved in TCR signalling, such as ZAP-70, CD3ε and CD3ζ (Wu et al. 2006; Cloutier and Veillette 1999).

As an initial proof of concept study to demonstrate the ability of wtCSK and wtPTPN22 to dampen CAR T cell sensitivity, each protein was co-expressed alongside the CD22 targeting LT22 CAR (Figure 6). The co-expression of wtCSK was observed to dampen LT22 CAR T cell cytotoxicity to a greater degree than wtPTPN22, increasing median target cell survival by 32.3% compared to 12.4% (Figure 7b).

It has been indicated that PTPN22 also negatively regulates c-Cbl (Cohen et al. 1999), the E3-ubiquitin ligase that has an inhibitory effect on TCR signalling via the ubiquitination of SFKs such as Lck, Src and Fyn (Duan et al. 2004; Tanaka et al. 1995; Thien and Langdon 2005). This suggests that PTPN22 is not a strict negative regulator of T cell signalling, as inhibition of c-Cbl by PTPN22 would lead to less degradation of Lck and Fyn. The difference I observed in the dampening of T cell function observed between wtPTPN22 and wtCSK could be attributed to this positive impact of PTPN22 on T cell signalling (Figure 7). This considered, only wtCSK was taken forward for further investigation.

The second aim of this chapter was to investigate the dampening effect of wtCSK on the sensitivity of CAR T cells to antigen, in order to determine whether dominant-negative iterations of CSK would be a viable approach to improving CAR sensitivity. To this end, I first tested wtCSK in a CAR platform that had previously demonstrated lack of efficacy to low-antigen density targets, the LT22 CAR.

LT22 CAR is the anti-CD22 component of the AUTO3 CD19/CD22 dual targeting product. In a phase 1/2 trial for the treatment of relapsed/refractory B-ALL, of 13 patients that responded to AUTO3 treatments, 9 relapsed. The main reason for relapse was poor long-term persistence of the CAR T cells, however in one instance relapse was observed in which tumour cells had completely lost CD19 expression and had diminished CD22 expression (from 4,649 molecules/cell pre-treatment to 1,416 molecules/cell) (Cordoba et al. 2021). Relapses attributed to dimming of CD22 expression have also been observed in other CAR T cell clinical trials (Fry et al. 2018; Shah et al. 2020), supporting the selection of an anti-CD22 CAR in which to co-express modules that improve sensitivity.

As the overall aim was to engineer agnostic modules to enable tuning of CAR T cell function, they must be generalizable to work in CAR T cell platforms with different architectures. To test the generalizability of wtCSK, it was initially co-expressed in LT22 CARs with either a 4-1BB or CD28 co-stimulatory domain (Figure 8). The CD28 containing CAR T cells displayed a higher cytotoxic capacity than the 4-1BB containing CAR T cells against low antigen density targets (Figure 11). The co-expression of wtCSK efficiently inhibited the cytotoxic function of both CAR T cell populations,

irrespective of co-stimulatory domain. In the case of the 4-1BB endodomain, cytotoxicity was reduced to levels similar to those observed with NT targets. However, cytotoxicity was only moderately reduced with the CD28 endodomain CAR. Stimulated CD28 and 4-1BB containing CAR T cells have been shown to activate similar proteins involved in signalling, but CD28 CAR T cells increase phosphorylation of these proteins more quickly and to a larger magnitude. An increase in basal phosphorylation of the CAR-associated CD3ζ chains and Lck was shown to contribute to the increased signal observed in CD28 CAR T cells (Salter et al. 2018). It is likely that the LT22-41BB T cells produce a less potent signal than the LT22-CD28 CAR T cells, which is easier for wtCSK to overcome.

To investigate the generalizability of CSK as a CAR regulating candidate, I co-expressed wtCSK with the 9A8 CAR. 9A8 is a CAR that recognizes CD22 and has been shown to be a highly sensitive CAR, that can specifically lyse target cells expressing approximately 490 CD22 molecules/cell (Kokalaki et al. 2023). Although, 9A8 CAR cytotoxicity was superior to the LT22 CAR (Figure 15f; Figure 11f), wtCSK was able to significantly inhibit 9A8 cytotoxicity, IFN-γ, and IL-2 release (Figure 15; Figure 16; Figure 17). These data demonstrated that wtCSK can also dampen CAR T cells with different binding domains.

After assessing the inhibitory capacity of wtCSK in CD22 targeting CAR T cells, I then implemented the wtCSK module in an anti-CD19 CAR. CAR T cell trials targeting CD19 show that the most common cause of remission is CD19 loss, and not dimming of antigen density (Grupp et al. 2015; Cordoba et al. 2021; Turtle et al. 2016). Therefore, technology to improve anti-CD19 CAR sensitivity against low antigen-density targets may seem unwarranted. However, inter- and intra-patient heterogeneity of CD19 expression has been observed in some B cell malignancies (Majzner et al. 2020). Therefore, lack of CAR T cell sensitivity in cases where CD19 expression is low could lead to tumour escape. In this chapter I aimed to test the generalisability of wtCSK, so the FMC63 CAR served the purpose of a well-characterised platform for targeting CD19 (Maude et al. 2018; Milone et al. 2009).

The FMC63 CAR T cells lysed > 98% of the $CD19^{High}$ targets (Figure 20b and e). However, against the $CD19^{VL}$ targets at an E:T ratio of 1:4, median target cell survival

increased to 17.8% (Figure 20f). wtCSK expression led to efficient inhibition of function against the $CD19^{VL}$ targets, in a similar trend to both LT22 and 9A8 CARs. Although inhibition of cytokine release was observed against $CD19^{High}$ targets, inhibition of cytotoxicity was not.

The above observations support the idea that there are separate thresholds in T cells for cytokine release and cytotoxicity. Huppa and colleagues reported that prolonged TCR signalling was required for IL-2 release and proliferation (Huppa et al. 2003). Moreover, other groups have reported that CAR T cells require a higher antigen density for cytokine production (770-5,320 molecules/cell) than for cytotoxicity (240 molecules/cell) (Stone et al. 2012; Watanabe et al. 2015).

It is clear from these experiments that overexpression of wtCSK can affect cytokine secretion and cytotoxicity of CAR T cells. However, the magnitude of the dampening effect depends on the target density, with reduced cytotoxic inhibition against high antigen density. Overall, the dampening effect of wtCSK was seen to be generalisable, enabling inhibition of CAR T cells with different endodomains, binding domains, and targeting different antigens.

5 RESULTS: IMPROVING CAR T CELL SENSITIVITY

5.1 Introduction

Limitations in CAR sensitivity to tumour-expressed antigens have been shown to result in reduced efficacy and to lead to relapses in clinical trials (Fry et al. 2018; Shah et al. 2020; Cordoba et al. 2021). Therefore, there is a clear need to increase CAR sensitivity to prevent such relapses and as CAR therapy expands to encompass a growing number of different antigens it seems likely that this need will become even more critical.

A number of approaches have been tested with the aim of improving the sensitivity of CAR T cells to low density targets. One approach to address the issue of CAR sensitivity is to directly tune the affinity of the CAR T cell, with numerous research groups demonstrating a positive correlation between affinity and sensitivity (Hudecek et al. 2013; Chames et al. 2002; Lynn et al. 2016; Caruso et al. 2015; Liu et al. 2015). Conversely, one study observed a negative correlation between CAR affinity and sensitivity, with a low-affinity CAR demonstrating superiority against low-density targets (Turatti et al. 2007). The inconsistent conclusions on the relationship between CAR affinity and sensitivity (in addition to the caveats discussed in 1.2.3.4.1) make affinity tuning a challenging approach.

Other approaches to improve CAR sensitivity are centred around structural changes in CAR design. One study has demonstrated that including two copies of the CD3ζ chain or including the CD28 hinge/transmembrane domain can improve the cytotoxicity of CAR T cells in response to targets with a low antigen density (963 molecules/cell) (Majzner et al. 2020). However, as such approaches require re-engineering of CAR architecture, they do not represent a strategy that can be easily introduced into existing CAR platforms.

To improve CAR sensitivity, I aimed to decrease the activation threshold of the CAR T cells through the co-expression of a standalone module structurally independent of the CAR. The activation threshold in CAR T cells is regulated by the equilibrium of a network of phosphatases and kinases that positively and negatively regulate T cell

signalling. As I have shown the effect of wtCSK on CAR T cell function, I aimed to explore whether I could counter this negative regulation with a dominant-negative CSK module (dnCSK).

CSK is an inhibitory kinase made up of three distinct domains, SH3, SH2 and a kinase domain. The kinase domain of CSK suppresses TCR signalling by phosphorylating the inhibitory tyrosine residue (Y505) of the key T cell triggering protein, Lck (Bergman et al. 1992). CSK further impedes T cell signalling by recruiting PTPN22 to the membrane via the CSK SH3 domain (Cloutier and Veillette 1996). CSK localises to the membrane via its SH2 domain binding to phosphorylated PAG (Brdicka et al. 2000; Davidson et al. 2003). This interaction with PAG is the primary mechanism by which CSK localises to the plasma membrane. However, one study detected small amounts of lipid raft-associated CSK present in the thymocytes of PAG KO mice, suggesting PAG-independent recruitment of CSK to the plasma membrane (Xu et al. 2005). A number of alternative membrane anchors have been identified that bind CSK and are present in lipid rafts post T cell activation, such as DOK1 (Schoenborn et al. 2011), paxillin and FAK (Sabe et al. 1994), SIT1 (Pfrepper et al. 2001), LIME (Brdicková et al. 2003) and caveolin-1 (Cao, Courchesne, and Mastick 2002).

I envisioned that dnCSK modules, lacking kinase activity, could compete with endogenous CSK for the binding of these membrane anchors. This would lead to a reduction in the amount of functional CSK in proximity to Lck, reducing the level of inactive Lck and thus reducing the signalling threshold.

5.2 Aim

In this chapter I aimed to engineer modules that decrease the activation threshold of CAR T cells, increasing their sensitivity.

To achieve this, the balance of the positive and negative signals within the CAR T cell would have to be shifted towards the positive. Impeding the inhibitory function of endogenous CSK would skew the balance towards a more activatory signal. Thus, I co-expressed a series of dnCSK modules alongside the CD22-targeting LT22 CAR and the CD19-targeting FMC63 and CAT19 CARs.

5.3 dnCSK Results

5.3.1 dnCSK: LT22 CAR

5.3.1.1 LT22-dnCSK CAR constructs: structure and transduction efficiency

I engineered three dnCSK modules to be co-expressed in LT22 CAR T cells (Figure 23). The modules lacked the kinase activity of wtCSK, but all retained the SH2 domain necessary for membrane anchor binding. Therefore, the dnCSK modules compete with endogenous CSK for binding to the membrane anchors, reducing the amount of CSK localised to the plasma membrane (Figure 23d). Consequently, less Lck will be inhibited and the negative effect of CSK on CAR signalling reduced.

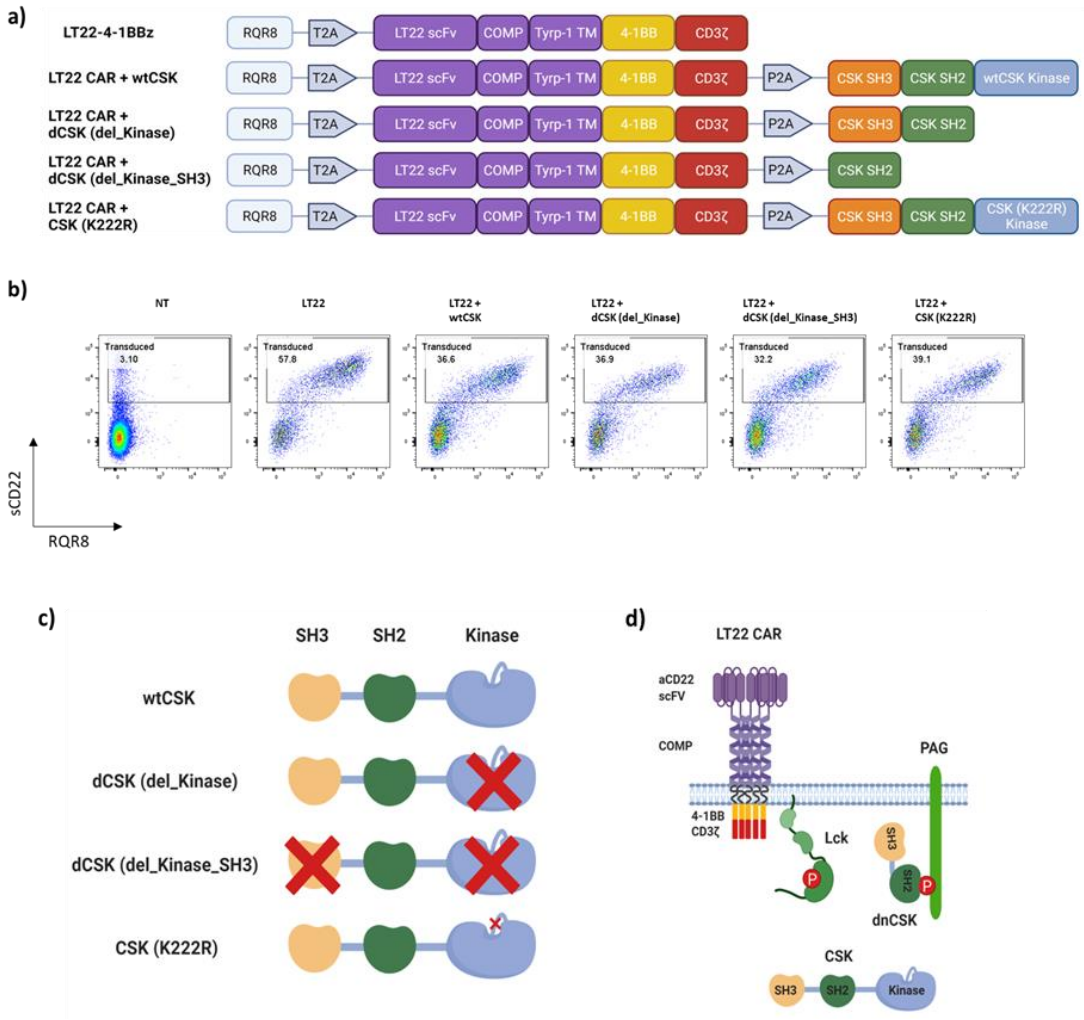

Figure 23. LT22-dnCSK CAR constructs: Structure and transduction efficiency. a) The construct maps of the LT22 CAR alone, LT22 CAR co-expressing wtCSK and the LT22 CAR constructs containing the dnCSK modules. All constructs include the RQR8 transduction marker upstream of the CAR. b) To test for the expression of the LT22 CAR on the cell surface, PBMCs were labelled with soluble CD22. Cells were also labelled with an anti-Human CD34 antibody for detection of the RQR8 transduction marker. One representative donor is shown. c) Structure of the dnCSK modules. d) Schema of the theoretical mechanism of action of action of the dnCSK modules, displaying the dnCSK blocking endogenous CSK from binding phosphorylated PAG and thus preventing inactivation of Lck.

Each dnCSK module was positioned downstream of the LT22 CAR transgene, after a 2A self-cleaving peptide. The plasmid maps of each are shown in Figure 23a. A negative control construct was also included, wherein wtCSK was expressed downstream of the transgene.

For the first dnCSK module, dCSK(del_kinase), I truncated CSK by deleting the kinase domain, whilst retaining the SH3 domain, thus PTPN22 could potentially still be recruited to the membrane to inhibit T cell signalling. For the second dnCSK module, dCSK(del_kinase_SH3), I truncated CSK by deleting both the kinase and SH3 domains. The deletion of these domains bore a dual role: the first was to prevent the inhibition of Lck via phosphorylation of its inhibitory tyrosine by CSK and the second was to abrogate association to the inhibitory phosphatase, PTPN22. The third dnCSK module, CSK(K222R), is a full-length CSK bearing a substitution of a lysine (K) residue for an arginine (R) residue at position 222. This mutation renders CSK catalytically inactive (Bergman et al. 1995). The structures of wtCSK and the three dnCSK modules are shown in Figure 23c. The expression and transduction levels of all the LT22-dnCSK constructs were comparable in PBMCs (Figure 23b).

5.3.1.2 LT22-dnCSK CAR function

The functionality of the LT22-dnCSK CAR T cells was assessed through a 72-hour cytotoxicity assay against SupT1 NT, SupT1 $CD22^{Mid}$ (6,309 molecules/cell) and SupT1 $CD22^{Low}$ (1,968 molecules/cell) target cells (Figure 10), at an effector to target (E:T) ratio of 1:4 (Figure 24). The LT22 CAR alone and wtCSK-bearing LT22 CAR were included in all the assays as positive and negative controls of cytotoxicity, respectively.

Overall, the background lysis of SupT1 NT targets was low (Figure 24a). However, the LT22 CAR bearing the dCSK(del_kinase_SH3) module lysed a higher percentage of non-specific targets compared to the LT22 CAR alone control. Although these background differences were small this may reflect greater alloreactivity due to reduced T cell thresholds with the dnCSK modules.

As expected, the introduction of wtCSK was able to significantly reduce cytotoxicity of CAR T cells when challenged with either SupT1 $CD22^{Mid}$ or $CD22^{Low}$ targets

comparable to levels observed with NT target controls (Figure 24b and c). When challenged with SupT1 $CD22^{Mid}$ target cells, CAR T cells bearing wtCSK reduced cytotoxicity by 40.2% (Figure 19b). Comparing the three dnCSK bearing CAR T cells to LT22 CAR, the dCSK(del_kinase_SH3) and CSK(K222R) modules showed significant increases in cytotoxicity against both the SupT1 $CD22^{Mid}$ and $CD22^{Low}$ targets (Figure 24b and c). Specifically, against the $CD22^{Low}$ targets, the dCSK(del_kinase_SH3) and CSK(K222R) modules caused a reduction in median target cell survival by 17% and 19.7%, respectively (Figure 24c).

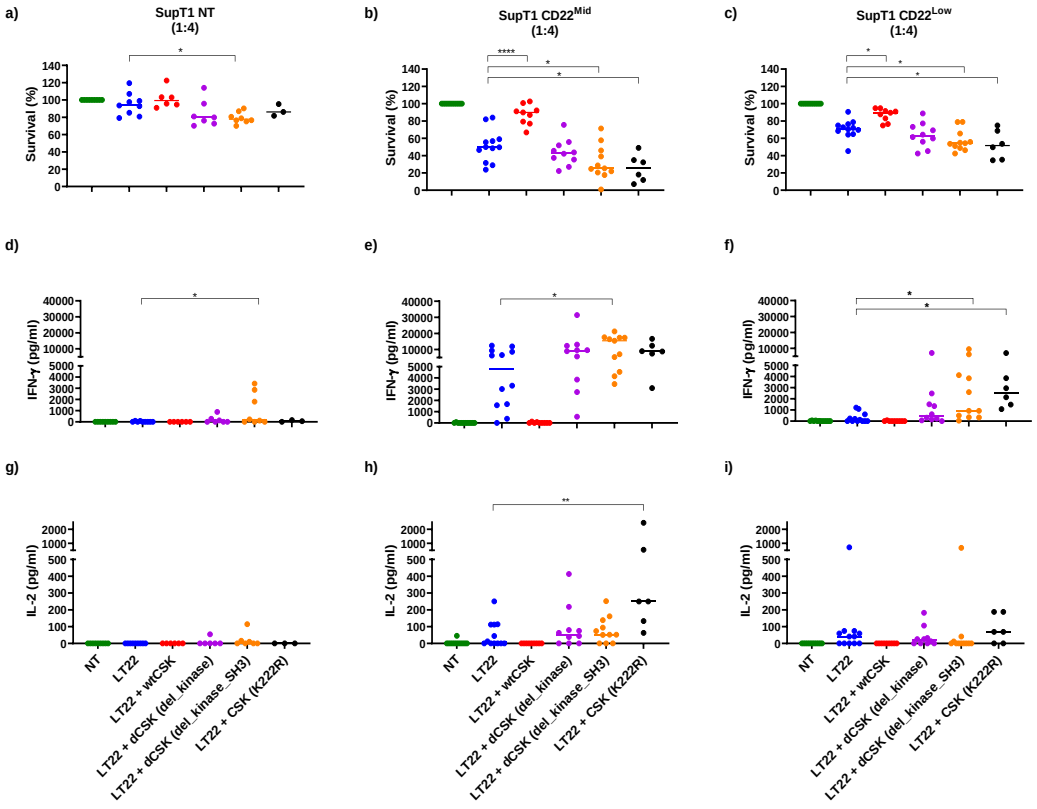

Figure 24. Cytotoxicity and cytokine production of LT22-dnCSK CAR T cells. a-c) Analysis of CAR T cell cytotoxicity by flow cytometry was carried out at 72h post co-culture set up. Each condition was tested with a minimum of 3 donors (n=3-12), with median indicated. All data was normalised to NT T cells. Co-cultures were set up with an E:T ratio of 1:4. SupT1 NT target cells were used in the left column, SupT1 CD22^{Mid} target cells were used in the middle column and SupT1 CD22^{Low} target cells were used in the right column. Supernatant taken at 72h post co-culture set up was analysed by ELISA for the presence of IFN-γ (d-f) or IL-2 (g-i). For the cytotoxicity assay (a-c), IFN-γ (d-f) and IL-2 (g-i) release, all constructs were compared to LT22 CAR alone condition (red squares) by one-way ANOVA statistical analysis. *P<0.05, **P<0.01, ***P<0.001, ****P<0.0001.

When challenged against SupT1 NT targets, T cells expressing the dCSK(del_kinase_SH3) module displayed some background release of IFN-γ compared to the CAR alone (Figure 24d). In accordance with the cytotoxicity against CD22 positive targets, the introduction of the wtCSK completely abrogated the secretion of IFN-γ even when challenged with $CD22^{Mid}$ targets, highlighting its potency as a negative inhibitor of CAR signalling (Figure 24e). All three dnCSK modules tested displayed a trend of increased IFN-γ secretion when co-cultured with CD22 positive targets compared to CAR T cells expressing LT22 alone. This reached significance for the dCSK(del_kinase_SH3) module against the $CD22^{Mid}$ and $CD22^{Low}$ targets and the CSK(K222R) module against the $CD22^{Low}$ targets. In the co-culture with the $CD22^{Mid}$ target cells, the dCSK(del_kinase_SH3) module resulted in a 3.2-fold increase in median IFN-γ release compared to the LT22 CAR (Figure 24e).

As shown in Figure 24g, IL-2 secretion by T cells against SupT1 NT targets was negligible. However, against SupT1 $CD22^{Mid}$ targets, the secretion of IL-2 was increased for all dnCSK-bearing T cells, compared to LT22 CAR alone T cells (Figure 24h). The introduction of the CSK(K222R) module displayed the biggest difference compared to the LT22 alone T cells. As was the case for IFN-γ release, I observed that the inclusion of the wtCSK module inhibited the functionality of the LT22 CAR, completely abrogating IL-2 release (Figure 24h and i).

5.3.2 dnCSK: FMC63 CAR

5.3.2.1 FMC63-dnCSK CAR constructs: structure and transduction efficiency

In order to test whether the dnCSK modules could provide an agnostic approach to improving CAR T cell function against low antigen density targets, I went on to co-express them in a second CAR platform. Although lack of functionality in response to low antigen density targets is not a major challenge facing anti-CD19 CAR T cell therapies, CD19 represents an extremely well characterised target. Therefore, I opted to investigate the dnCSK modules in the anti-CD19 CAR, FMC63.

The FMC63 CAR structure was previously outlined in 4.3.4.1. I aimed to increase the function of the FMC63 CAR against low antigen density targets by co-expressing different dnCSK modules. As described in 5.3.1.1, I engineered three dnCSK modules,

which were co-expressed with the FMC63 CAR (Figure 25a). wtCSK was used as a negative control. To confirm the surface expression of the FMC63 CAR in PBMCs, all cells were labelled with sCD19 as well as an anti-CD34 antibody for the detection of the RQR8 marker (Figure 25b).

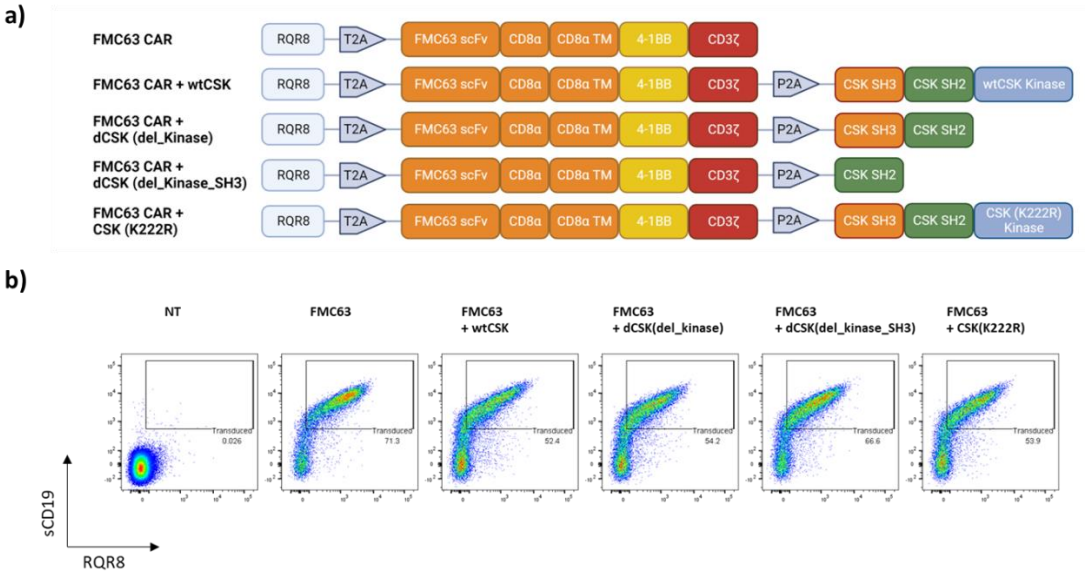

Figure 25. FMC63-dnCSK CAR constructs: Structure and transduction efficiency. a) Construct maps displaying the FMC63 CAR alone, co-expressing one of the three dnCSK modules or co-expressing wtCSK as a negative control. The RQR8 transduction marker is expressed in all constructs upstream of the CAR. b) FMC63 CAR and RQR8 expression on the surface of one representative PBMC donor. PBMCs were labelled with sCD19 to test for expression of the CAT19 CAR. For detection of RQR8, PBMCs were labelled with an anti-Human CD34 antibody.

5.3.2.2 CD19 targets antigen density: Mid and Low

Previously, two $CD19^{+}$ target cell lines were engineered to express different densities of antigen (Figure 19). However, when challenged against the $CD19^{High}$ targets, the CAR T cells completely ablated the target cells (Figure 20b and e). As the aim of the dnCSK modules was to improve CAR T cell function, I used target cells which are sub-optimally lysed by the CAR T cells. Furthermore, CD19 expression in the majority of B cell leukaemias ranges from 10,000-16-000 molecules/cell (Ginaldi et al. 1998), hence I engineered a cell line within this range. To test the dnCSK modules in the FMC63 CAR platform I used SupT1 $CD19^{Mid}$ and $CD19^{Low}$ target cell lines, with antigen densities of 11,846 molecules/cell and 4,282 molecules/cell, respectively (Figure 26).

a)

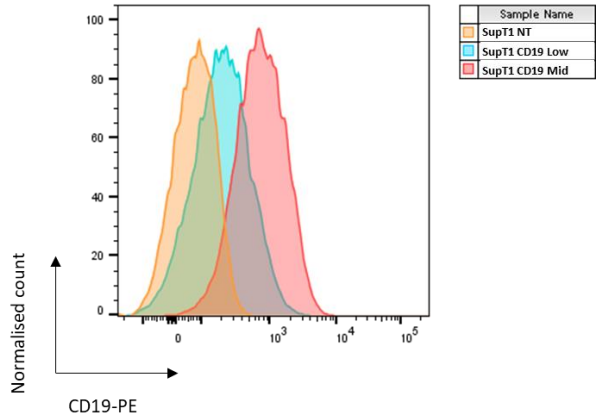

b)

Target cell line	CD19/cell
SupT1 NT	0
SupT1 CD19^{Mid}	11,846
SupT1 CD19^{Low}	4,282

Figure 26. FMC63-dnCSK CARs: Antigen density of SupT1 CD19 target cells. The cell lines were labelled with an anti-CD19-PE antibody to verify the expression of CD19 on the target cell lines. b) Quantibrite^{TM} beads were used to quantify the CD19 antigen density. I obtained a CD19^{Mid} and CD19^{Low} cell lines expressing 11,846 and 4,282 molecules/ cell, respectively.

5.3.2.3 FMC63-dnCSK CAR function

Co-expression of the dnCSK modules led to an increase in the background lysis of SupT1 NT targets (Figure 27a). However, against the $CD19^{Mid}$ and $CD19^{Low}$ cell lines, cytotoxicity of the dnCSK constructs was comparable to the FMC63 CAR and showed little to no improvement whilst wtCSK significantly inhibited target cell lysis (Figure 27b and c).

In terms of cytokine production by the CAR T cells, those bearing the dnCSK(del_kinase) module saw the most notable increase in IFN-γ production compared to the FMC63 CAR, achieving a 1.7-fold increase in median production when challenged with the $CD19^{Mid}$ targets (Figure 27e) and a 3.7-fold increase when challenged with the $CD19^{Low}$ targets (Figure 27f). However, IL-2 production by dnCSK CAR T cells was comparable to FMC63 CAR T cells, with no increases observed (Figure 27h and i).

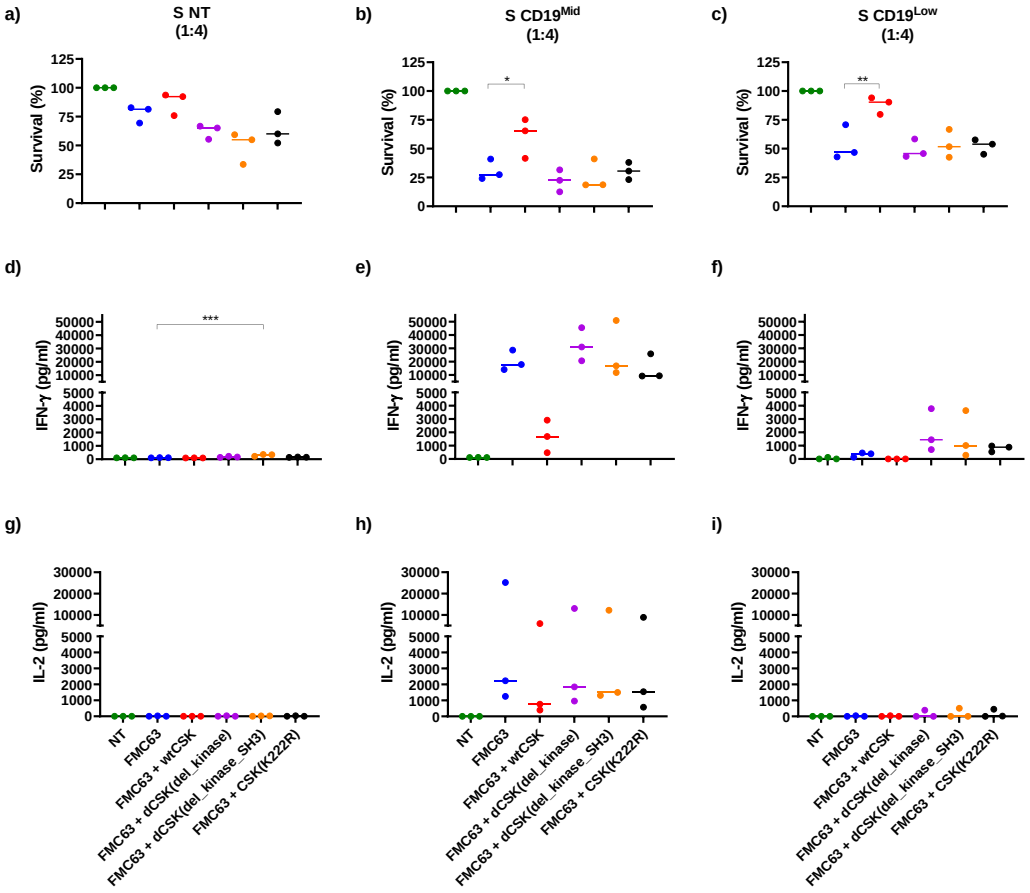

Figure 27. Cytotoxicity and cytokine production of FMC63-dnCSK CAR T cells. a-c) Cytotoxicity of CAR T cells were measured by flow cytometry 72h post co-culture set up. Each condition was tested with 3 donors (n=3), with median indicated. All data was normalised to NT T cells. Co-cultures were set up with an E:T ratio of 1:4. SupT1 NT target cells were used in the left column, SupT1 CD19^{Mid} target cells were used in the middle column and SupT1 CD19^{Low} target cells were used in the right column. Supernatant taken at 72h post co-culture set up was analysed by ELISA for the presence of IFN-γ (d-f) or IL-2 (g-i). For the cytotoxicity assay (a-c), IFN-γ (d-f) and IL-2 (g-i) release, all constructs were compared to LT22 CAR alone condition (red squares) by one-way ANOVA statistical analysis. *P<0.05, **P<0.01, ***P<0.001, ****P<0.0001.

5.3.3 dnCSK: CAT19 CAR

5.3.3.1 CAT19-dnCSK CAR constructs: structure and transduction efficiency

To investigate the effect of the dnCSK modules in an alternative clinically relevant anti-CD19 CAR, I chose the CAT19 CAR (Roddie et al. 2021; Ghorashian et al. 2019), a second generation CAR composed of the CAT19 scFv, CD8α spacer and TM domain with a 4-1BB co-stimulatory domain and CD3ζ signalling domain (Figure 28a and b). The RQR8 transduction marker was placed upstream of the CAR transgene and the CAR was individually expressed with dnCSK constructs described in the previous section. A construct expressing the CAR alongside wtCSK was again included as a negative control expected to show a suppressed CAR function. To confirm the surface expression of the CAT19 CAR in PBMCs, all cells were labelled with sCD19 as well as an anti-CD34 antibody for the detection of the RQR8 marker (Figure 28c).

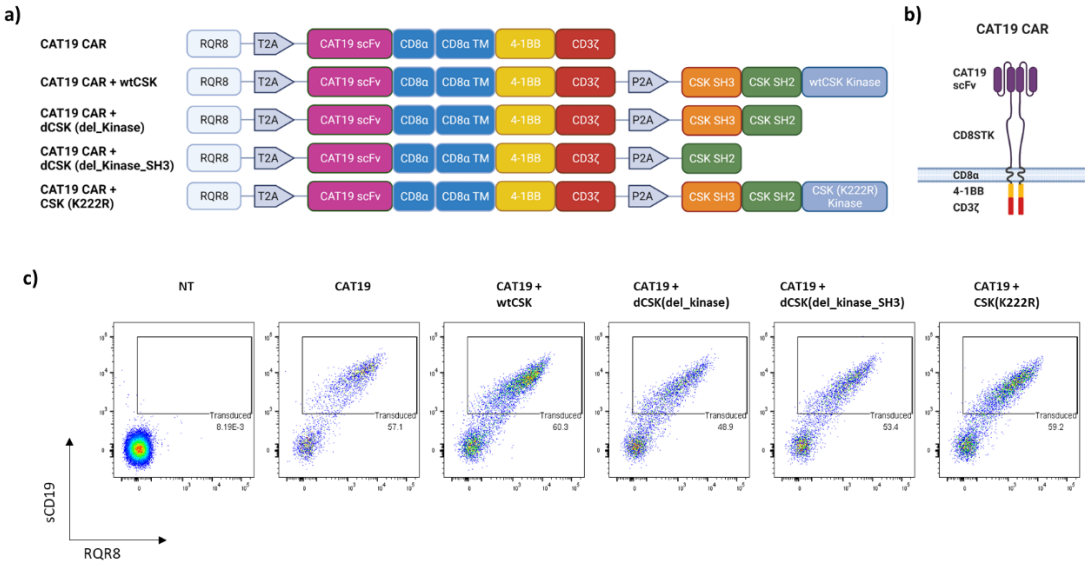

Figure 28. CAT19-dnCSK CAR constructs: Structure and transduction efficiency. a) The maps of the CAT19 CAR constructs, displaying the CAT19 CAR alone, co-expressing wtCSK, or co-expressing one of the three dnCSK modules. The RQR8 transduction marker is expressed in all constructs upstream of the CAR. b) Schematic of the CAT19 CAR. c) CAT19 CAR and RQR8 expression on the surface of one representative PBMC donor. PBMCs were labelled with sCD19 to test for expression of the CAT19 CAR. For detection of RQR8, PBMCs were labelled with an anti-Human CD34 antibody.

5.3.3.2 CD19 targets antigen density: Mid (b) and Low (b)

Two CD19^{+} target cell lines were engineered to express mid and low densities of antigen (Figure 29). I obtained SupT1 cells expressing antigen densities of 16,357 molecules/cell and 4,754 molecules/cell. These cell lines are distinct from the CD19^{+} cells outlined in Figure 26, thus will be referred to as CD19$^{Mid(b)}$ and CD19$^{Low(b)}$, respectively.

a)

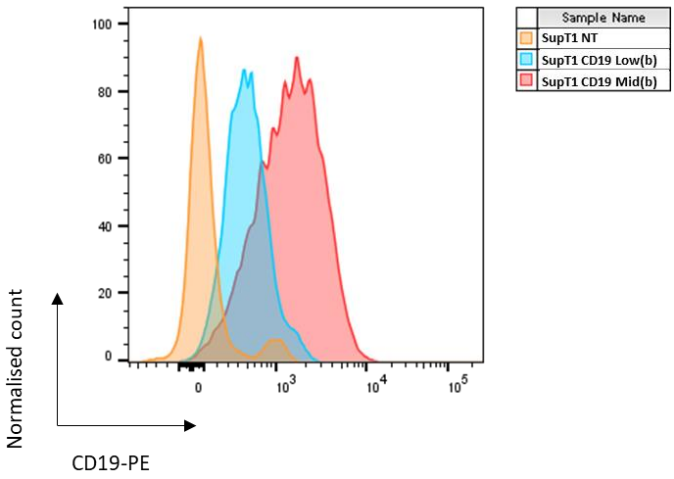

b)

Target cell line	CD19/cell
SupT1 NT	0
SupT1 CD19$^{Mid(b)}$	16,357
SupT1 CD19$^{Low(b)}$	4,754

Figure 29. dnCSK: Antigen density of SupT1 CD19 target cells. a) SupT1 cell lines were labelled with an anti-CD19-PE antibody to verify the expression of CD19 on the cell surface. b) Quantibrite^{TM} beads were used to quantify the CD19 antigen density. Based on the MFI and the Quantibrite^{TM} standard curve, the density of the cell lines was calculated by deducting the isotype from the CD19^{+} signal. I obtained a CD19$^{Mid(b)}$ and CD19$^{Low(b)}$ cell lines expressing 16,357 and 4,754 molecules/cell, respectively.

5.3.3.3 CAT19-dnCSK CAR function

Compared to the CAT19 CAR T cells, all of the dnCSK modules improved cytotoxic capacity against antigen-expressing cells. Significance was reached when CAR T cells expressing the dCSK(del_kinase) module were challenged with the $CD19^{Mid(b)}$ target cells, decreasing median target cell survival from 11.7% to 2.3% (Figure 30b). Against the $CD19^{Low(b)}$ targets, the dCSK(del_kinase_SH3) module had the biggest impact on cytotoxicity compared to the CAT19 CAR, decreasing median target cell survival by 20.9% (Figure 30c).

Compared to CAT19 CAR T cells, CAR T cells bearing the dCSK(del_kinase_SH3) module displayed significantly increased levels of IFN-γ release (3.9-fold) when challenged with SupT1 $CD19^{Low(b)}$ targets (Figure 30f) and significantly increased levels of IL-2 release when challenged with $CD19^{Mid(b)}$ or $CD19^{Low(b)}$ targets (Figure 30h and i). The biggest increase in IL-2 release was observed against the $CD19^{Low(b)}$ targets, where the dCSK(del_kinase_SH3) CAR T cells produced a 3.7-fold increase in IL-2 compared to the CAT19 CAR alone control (Figure 30i).

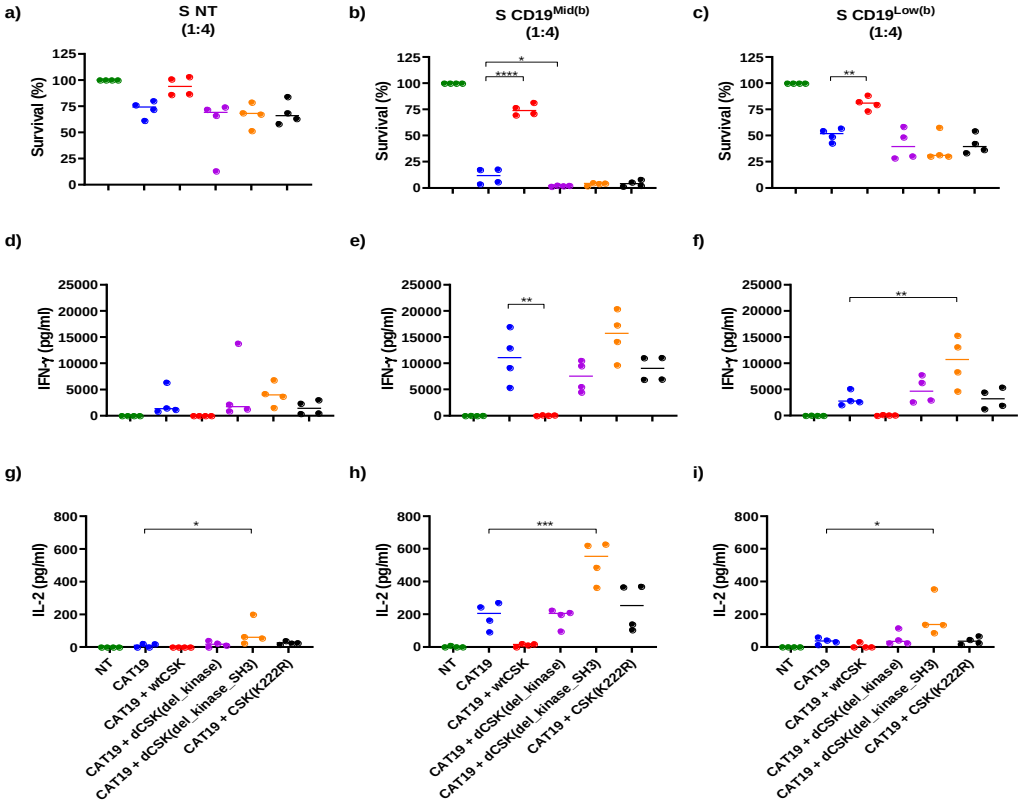

Figure 30. Cytotoxicity and cytokine production of CAT19-dnCSK CAR T cells. Cytotoxicity of the CAR T cells challenged against a) SupT1 NT, b) SupT1 CD19$^{Mid(b)}$ and c) SupT1 CD19$^{Low(b)}$ cells was measured by flow cytometry at 72h post co-culture set up. Each condition was tested with 4 donors (n=4), with median indicated. All data was normalised to NT T cells. Co-cultures were set up with an E:T ratio of 1:4. SupT1 NT target cells were used in the left column, SupT1 CD19$^{Mid(b)}$ target cells were used in the middle column and SupT1 CD19$^{Low(b)}$ target cells were used in the right column. 72h post co-culture set up, supernatant was analysed by ELISA for the presence of IFN-γ (d-f) or IL-2 (g-i). All constructs were compared to LT22 CAR alone condition (red squares) by one-way ANOVA statistical analysis. *P<0.05, **P<0.01, ***P<0.001, ****P<0.0001.

5.4 Summary

There is a clinical need to improve the sensitivity of CAR T cells to target cells with low antigen density. The importance of antigen density was highlighted by Fry and colleagues, who reported in a phase 1 trial that the CD22 CAR failed to recognise density below 2,839 molecules/cell leading to relapse (Fry et al. 2018; Shah et al. 2020). Moreover, in another clinical trial, the relapse of one patient was partly attributed to dimming of CD22 expression (Cordoba et al. 2021).

CAR sensitivity is integral when targeting antigens that are expressed at low densities. Watanabe and colleagues demonstrated that the antigen density required for CAR T cell cytotoxicity *in vitro* was as low as 240 molecules/cell, while for IFN-γ production 5,320 molecules/cell were required. Additionally, efficient CAR-mediated lysis of targets displaying antigen density below 1,000 molecules/cell was not associated with IFN-γ production or CAR T cell proliferation (Watanabe et al. 2015). This emphasizes the importance of a strategy to lower the activation threshold of CAR T cells, enabling efficient cytotoxicity and cytokine release in response to low antigen density targets.

In order to increase CAR T sensitivity, I co-expressed one of three dnCSK modules alongside either the CD22 targeting LT22 CAR or the CD19 targeting FMC63 or CAT19 CARs in T cells. Two of the dnCSK modules were either truncated by removal of the CSK kinase domain (dCSK(del_kinase)) or the removal of both the kinase domain and the SH3 domain (dCSK(del_kinase_SH3)). A third dnCSK module was also tested, which was a full length but catalytically inactive CSK mutant (CSK(K222R)) (Figure 23c). In all cases, the SH2 domain of CSK was retained in order to block endogenous CSK binding a membrane anchor, thus creating the dominant-negative effect (Figure 23d).

In light of CD22 down-regulation after CAR T therapy, the anti-CD22 LT22 CAR platform was an obvious choice as a model to test the effect of the dnCSK modules on CAR sensitivity. The co-expression of wtCSK had a profound effect on the release of IFN-γ and IL-2, with any production completely ablated (Figure 24e and h). This inhibition of CAR T cell function was likely facilitated by a reservoir of membrane

anchors that were unbound by endogenous CSK (Schoenborn et al. 2011; Sabe et al. 1994; Pfrepper et al. 2001; Cao, Courchesne, and Mastick 2002; Xu et al. 2005). Therefore, wtCSK expressed in CAR T cells was able to bind via its SH2 domain to any unoccupied membrane anchors, localizing to lipid rafts in the cell membrane and into the proximity of Lck. wtCSK could then phosphorylate the inhibitory tyrosine of Lck, rendering it inactive and inhibiting downstream signalling.

All dnCSK modules investigated were observed to improve the functional response of the LT22 CAR T cells, improving cytotoxicity and cytokine release against SupT1 target cells expressing as low as 1,968 CD22 molecules/cell (Figure 24). Conversely to the expression of wtCSK, it is reasonable to assume that the expression of a dnCSK module led to competition with endogenous CSK for binding to membrane anchors. Less CSK associated with these membrane anchors would lead to a larger pool of activated Lck, in turn lowering the activation threshold of CAR T cells. As discussed above, one clinical trial saw anti-CD22 CAR T cells to lack efficacy against blasts with a median antigen density of 2,839 molecules/cell (Fry et al. 2018). Therefore, it was promising to see the dnCSK modules improve CAR T cell function against target cells with an antigen density below this threshold.

I went on to investigate whether the dnCSK modules could be utilised in a CD19 targeting CAR as it is a well characterised target. Additionally, although the main cause of CD19 CAR therapy relapse is loss of CD19 expression (Grupp et al. 2015; Cordoba et al. 2021; Turtle et al. 2016), it has been suggested that inter- and intra-patient heterogeneity of CD19 expression in some B cell malignancies could enable tumour escape due to diminished antigen density (Majzner et al. 2020). Therefore, I next chose to test the dnCSK modules alongside the CD19 targeting FMC63 CAR. Of the dnCSK modules tested, only the dCSK(del_kinase) module improved CAR T cell function, with modest increases in IFN-γ observed against both the $CD19^{Mid}$ and $CD19^{Low}$ targets (Figure 27e and f).

A reason why the dnCSK modules only showed a modest impact in FMC63 CAR T cells could be that the CAR-mediated cytotoxicity and cytokine production was already close to the maximum levels achievable by these CAR T cells in response to the antigen densities tested. To investigate whether the function of an alternative,

clinically relevant, CD19 targeting CAR T cell platform could be increased, the dnCSK modules were co-expressed alongside the CAT19 CAR. In the context of the CAT19 CAR, the dCSK(del_kinase_SH3) module improved cytotoxicity comparably to the other dnCSK modules but was superior in augmenting cytokine release (Figure 30).

I believe the dnCSK modules could constitute an agnostic approach to lower the activation threshold of CAR T cells with suboptimal function against low antigen density targets. In particular, the dCSK(del_kinase_SH3) was able to improve the cytotoxicity of both the LT22 and CAT19 CARs when challenged against low antigen density targets, causing a reduction in median target cell survival by 17% (Figure 24c) and 20.9% (Figure 30c), respectively.

The dCSK(del_kinase_SH3) module also significantly improved cytokine release in response to low antigen density targets. The LT22 CAR bearing this module displayed a 15.8-fold increase in IFN-γ production (Figure 24f), whereas it increased the CAT19 CAR production by 3.9-fold (Figure 30f). Furthermore, in the CAT19 CAR platform, dCSK(del_kinase_SH3) led to a significant increase in IL-2 release against both the $CD19^{Mid(b)}$ (Figure 30h) and $CD19^{Low(b)}$ targets (Figure 30i). A key difference between the dCSK(del_kinase_SH3) module and the other dnCSK modules is the deletion of the SH3 domain of CSK, which enables association with the phosphatase PTPN22, which is another negative T cell regulator (Wu et al. 2006; Cloutier and Veillette 1999). Thus, removal of the SH3 domain and subsequent reduction in PTPN22 localisation to the plasma membrane could have enabled an increase in the pool of activated Lck and ZAP-70, lowering the activation threshold.

There are a number of different strategies implemented to improve CAR T cell sensitivity. Re-engineering of the CAR architecture to express two copies of the CD3ζ chain or a CD28 hinge/transmembrane were both shown to improve CAR T cell sensitivity (Majzner et al. 2020).

Another strategy is to tune the affinity of the CAR, with many groups reporting an increase in affinity leads to an increase in sensitivity to low antigen density targets (Hudecek et al. 2013; Chames et al. 2002; Lynn et al. 2016; Caruso et al. 2015; Liu et al. 2015; Chmielewski et al. 2004). However, these studies possess a number of

caveats, such as the comparison of affinity based off CARs with different scFv clones, a small number of CARs compared in each study and comparing scFvs with potentially different stabilities. Moreover, one study has reported the opposite relationship between CAR affinity and sensitivity, with low-affinity CARs demonstrating superior function against low-density targets (Turatti et al. 2007).

An advantage of the dnCSK technology over other strategies to improve sensitivity is that it does not require modification to the CAR architecture. As they require no re-engineering of the CAR in order to improve CAR T cell function, I believe the co-expression of a dnCSK module in CAR T cells, either through co-transduction or through the same construct via a 2A peptide, presents a practical solution to improve CAR T cell sensitivity.

6 RESULTS: TUNING OF LT22 CAR T CELL FUNCTION

6.1 Introduction

The success of CAR T cell therapy for the treatment of blood cancers, such as MM, B-ALL, NHL, DLBCL and MCL has led to numerous FDA-approved products (Maude et al. 2018; Neelapu et al. 2017; Wang et al. 2022; Abramson et al. 2020; Munshi et al. 2021). Despite this clinical success, the transition of CAR T cell therapy into treatment for solid tumours remains problematic. One of the main challenges hindering more widespread use of CAR T cell therapy is on-target off-tumour toxicity. Due to a lack of tumour specific antigens, many candidate antigens for solid tumours are also expressed on healthy tissues. The shared antigens on malignant and healthy tissues increases the risk of on-target off-tumour toxicity and has been observed with HER2 (Morgan et al. 2010), CEACAM5 (Thistlethwaite et al. 2017) and CAIX targeting CAR T cells (Lamers et al. 2013).

The risk of on-target off-tumour toxicity has led to the development of various safety strategies to be implemented in CAR T cells. One approach to tackling on-target off-tumour toxicity is the development of “suicide switches”. In cases where toxicity arises, such switches permit irreversible ablation of CAR T cells in response to an external trigger such as the administration of a small molecule drug or monoclonal antibody (Straathof et al. 2005; Philip et al. 2014; Paszkiewicz et al. 2016; Stavrou et al. 2018). However, a major drawback of suicide switches is that they cause permanent elimination of CAR T cells, thus also eliminating the antitumour response of the CAR T cells.

An alternative strategy to lower the risk of toxicity is by tuning the CAR affinity. Different groups have exhibited that tuning CARs to possess lower affinity results in CAR T cells being able to discriminate between targets expressing either high- or low-antigen density (Caruso et al. 2015; Liu et al. 2015). One of these groups demonstrated that a 10-fold decrease in affinity (1.8nM compared to 21nM) of CAR T cells targeting EGFR, provoked significant decreases in the lysis of antigen presenting targets with reduced EGFR expression (≤ 30,899 molecules/cell) (Caruso

et al. 2015). This approach not only requires the challenging engineering of the CAR affinity, but getting the affinity just right for the optimal density range required for each specific antigen is stochastic and improbable. Plus, the literature regarding affinity and CAR function is controversial. Finally, reducing the affinity below a threshold could hinder CAR T cells efficacy and enable tumour escape.

To increase specificity to tumour cells and reduce the risk of on-target off-tumour toxicity, numerous research groups have applied Boolean logic gating to CAR T cells. These strategies allow for more accurate differentiation between tumour cells and healthy tissue by requiring the recognition of a combination of antigens to initiate CAR activation (Kloss et al. 2013; He et al. 2020; Lajoie et al. 2020; Lanitis et al. 2013; Fedorov, Themeli, and Sadelain 2013; Srivastava et al. 2019; Roybal et al. 2016). The major caveat of these strategies is that they all require re-engineering of the CAR architecture so are not easily adapted for use in existing CAR platforms.

Other caveats of logic gates include reliance on transcriptional changes to elicit a functional response to antigen, which require hours to come into effect (Roybal et al. 2016). Moreover, Srivastava and colleagues demonstrated a logic gate system that also required spatial segregation of healthy tissue and tumour cells to avoid CAR-mediated on-target off-tumour toxicity (Srivastava et al. 2019).

An alternative safety strategy is the engineering of tuneable CAR T cell platforms, the efficacy of which can be regulated by the administration of a small molecule drug. There have been several different iterations of such tuneable CAR platforms. Some are drug-ON systems, wherein presence of both antigen and the small molecule drug are required for CAR functionality (Wu et al. 2015; Juillerat et al. 2016; Leung et al. 2019; Labanieh et al. 2022; Sahillioglu et al. 2021). Conversely, other tuneable CARs are drug-OFF systems, in which the presence of a small molecule drug disrupts CAR T cell function (Juillerat et al. 2019; Sun et al. 2020; Giordano-Attianese et al. 2020; Hotblack et al. 2021).

Logic gate and tuneable CAR platforms provide an advantage over suicide switches as a strategy to mitigate toxicity, as they avoid permanent ablation of T cells and can therefore retain antitumour efficacy. Furthermore, the dose-dependent manner in

which tuneable CAR platforms can be regulated allows for efficacy to be maintained whilst avoiding toxicity. However, as with the logic gate platforms, the majority of tuneable systems require altering of the CAR architecture, which can result in CAR T cells that are less efficacious than those expressing conventional CARs. Other limitations of current tuneable systems include reduced surface expression compared to conventional CARs (Leung et al. 2019; Hotblack et al. 2021; Giordano-Attianese et al. 2020), the use of immunosuppressive drugs like rapamycin (Juillerat et al. 2016; Wu et al. 2015; Sun et al. 2020; Leung et al. 2019) and/or the incorporation of potentially immunogenic components (Juillerat et al. 2019; Labanieh et al. 2022; Sahillioglu et al. 2021; Hotblack et al. 2021).

In Chapter 4, I observed that wtCSK is capable of impairing the efficacy of different CAR platforms. Then in Chapter 5 I demonstrated that co-expression of dnCSK modules in CAR T cells has the potential to improve sensitivity against low antigen density targets. Both observations indicated that CSK could be a promising candidate to serve as the foundation of an tuneable CAR system.

I aimed to develop a CSK-based tuneable system regulated by a small molecule drug, with the capacity to be efficacious towards low antigen density targets (dnCSK effect) but also able to be dampened to mitigate for toxicity (wtCSK effect). To this end, I exploited a published CSK mutant that is tuneable through the application of a small molecule drug. Schoenborn and colleagues generated an analogue-sensitive CSK (CSK^{AS}) by substituting a threonine (T) residue at position 266 for a glycine (G) residue. This substitution, located in the ATP-binding pocket, enabled CSK^{AS} to be tuneable, wherein the kinase activity can be inhibited by 3-iodo-benzyl-PP1 (3-IB-PP1). 3-IB-PP1 is an analogue of the nonselective kinase inhibitor PP1 and selectively inhibits CSK^{AS} (Schoenborn et al. 2011). This group also generated a second CSK^{AS} in which the eleven N-terminal amino acid residues of Lck (MGCVCSSNPED) were fused to CSK^{AS}, enforcing its localisation to the plasma membrane via association with the CD4 and CD8 co-receptors or in lipid rafts. This membrane localised CSK^{AS} is referred to as $mCSK^{AS}$.

6.2 Aim

Firstly, I aimed to investigate whether the expression of CSK^{AS} and $mCSK^{AS}$ in T cells could enable functional tuning of TCR-activated T cells. Secondly, I aimed to investigate the co-expression of CSK^{AS} and $mCSK^{AS}$ in LT22 CAR T cells as means to tune CAR T cell function in response to a small molecule drug.

6.3 Results

6.3.1 Expression of CSK^{AS} and $mCSK^{AS}$ in T cells

In order to validate the use of CSK^{AS} or $mCSK^{AS}$ as a means to control CAR T cell function, I first investigated whether the CSK^{AS} system could enable tuneable control of T cells activated via their native TCRs. To this end, both CSK^{AS} and $mCSK^{AS}$ were transduced in PBMCs, with the RQR8 marker included to determine transduction efficiency (Figure 31a). The RQR8 marker also enabled sorting of the transduced PBMCs using anti-CD34 bead selection kit, resulting in a highly transduced PBMC population (Figure 31b).

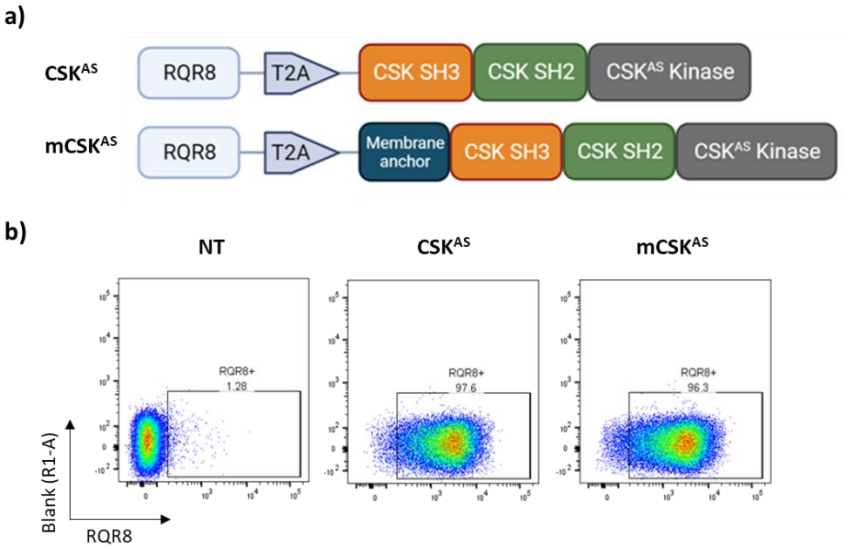

Figure 31. CSK^{AS} and mCSK^{AS} constructs: Structure and transduction efficiency. a) Construct maps of the CSK^{AS} and mCSK^{AS} modules. The RQR8 transduction marker included upstream of each module. b) Constructs were transduced into PBMCs (one representative donor shown). PBMCs were labelled with an anti-CD34 antibody to detect the RQR8 transduction marker.

6.3.2 IFN-γ production of T cells expressing either the CSK^{AS} or mCSK^{AS} module

To test the effect of the CSK^{AS} and mCSK^{AS} modules on TCR stimulated T cells, transduced T cells were added to wells of a 96-well plate coated with an anti-CD3 antibody at a range of concentrations (0-10 µg/ml). Each condition was set up in the absence of the CSK^{AS} inhibitor, 3-IB-PP1 (referred to hereafter as the drug), or with increasing concentrations of drug (0.1-10 µM) (Figure 32). Analysis of IFN-γ production showed NT T cells to produce more IFN-γ in response to increasing concentrations of aCD3, with increasing concentrations of drug bearing no impact (Figure 32a). In the condition when T cells were activated with 5 µg/ml plate-bound aCD3 antibody with no drug present, CSK^{AS} expressing cells displayed 31% less mean IFN-γ production than the NT cells (Figure 32b), yet the mCSK^{AS} cells dampened the mean IFN-γ production by 82% (Figure 32c). In the presence of 10 µM drug, mean IFN-γ production by CSK^{AS} cells was 1.5-fold higher compared to NT cells, whereas IFN-γ production by mCSK^{AS} cells was 2.3-fold higher. As the expression of either cytoplasmic CSK^{AS} or mCSK^{AS} enabled the function of TCR-activated T cells to be altered in the presence or absence of the drug, I next investigated whether these modules could also permit tuneable control of CAR T cells.

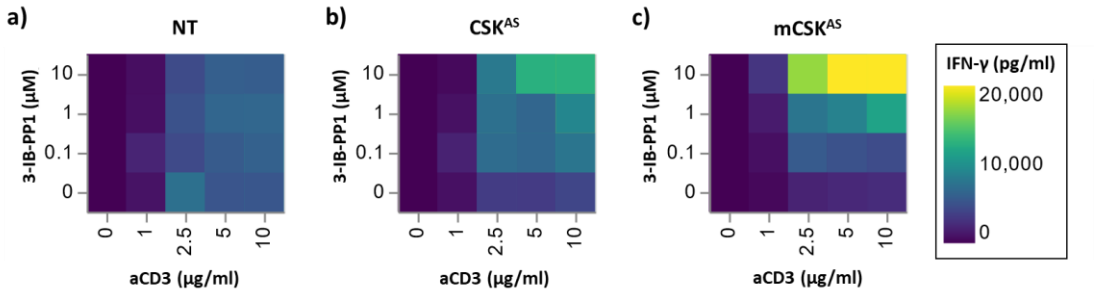

Figure 32. Heat maps of IFN-γ production by T cells expressing either CSK^{AS} or mCSK^{AS}. NT T cells (a), CSK^{AS} T cells (b) and mCSK^{AS} T cells (c) were stimulated with plate-bound OKT3 antibody ranging in concentration from 0-10 µg/ml. Reactions were set up in media (R10) or in media supplemented with 3-IB-PP1 (0.1-10 µM). Supernatant taken 24h post assay initiation was analysed by ELISA for the presence of IFN-γ. Each condition was tested with a minimum of 4 donors (n=4), mean values indicated.

6.3.3 LT22 CSK^{AS} CAR constructs: structure and transduction efficiency

To investigate the capacity of CSK^{AS} and mCSK^{AS} to enable tuneable control of CAR T cell function, I co-expressed each module alongside the LT22 CAR (previously described in 4.3.1.1) (Figure 33a). I transduced PBMCs with these constructs, as well as two control constructs expressing the LT22 CAR alone or the LT22 CAR and the wtCSK module (Figure 33b). The CSK^{AS} and mCSK^{AS} modules contain the SH3, and SH2 domains of wtCSK but the kinase domain has a single amino acid mutation (T266G) permitting inhibition of kinase activity by the administration of 3-IB-PP1 (Figure 33c).

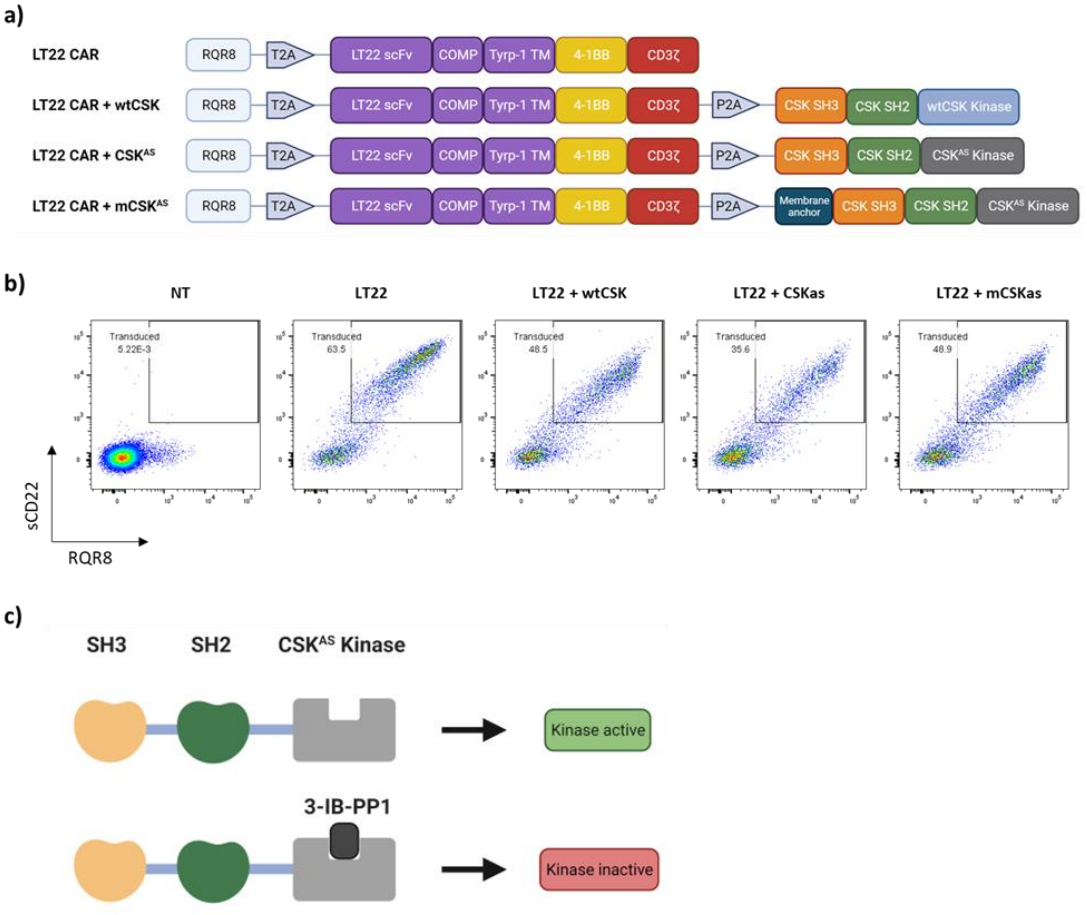

Figure 33. LT22 CSK^{AS} CAR constructs: Structure and transduction efficiency. a) Construct maps of the LT22 CAR, LT22 CAR co-expressing wtCSK, CSK^{AS} or mCSK^{AS}. All constructs included the RQR8 transduction marker upstream of the CAR. b) All constructs were successfully transduced into PBMCs. PBMCs were labelled with sCD22 to test for expression of the LT22 CAR and an anti-CD34 antibody to detect the RQR8 transduction marker. One representative donor is shown. c) Schematic depicting the inhibition of CSK^{AS} kinase activity via the administration of 3-IB-PP1.

6.3.4 CD22 targets antigen density: High, low, and very low (VL)

In section 4.3.2.3, I engineered SupT1 $CD22^{+}$ target cell lines expressing antigen densities of 6,309 or 1,968 molecules/cell. However, I wanted to challenge the CSK^{AS} and $mCSK^{AS}$ expressing CAR T cells against targets with a wider range of antigen density. Therefore, I engineered SupT1 $CD22^{High}$ and $CD22^{VL}$ cells, expressing 53,866 and 284 molecules/cell, respectively (Figure 34). The $CD22^{Low}$ cell lines used in this section expressed similar levels of antigen to the $CD22^{Low}$ cells described in 4.3.2.3 (1,946 and 1,968, respectively). However, as they are distinct cell lines, the former is hereafter referred to as $CD22^{Low(b)}$.

a)

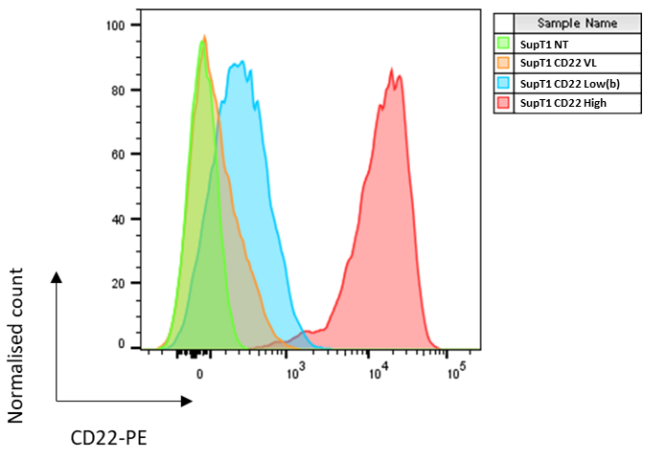

b)

Target cell line	CD22/cell
SupT1 NT	0
SupT1 CD22^{High}	53,866
SupT1 CD22$^{Low(b)}$	1,946
SupT1 CD22^{VL}	284

Figure 34. Antigen density of SupT1 CD22 target cells: High, low(b), and very low. SupT1 cells were transduced with a retroviral vector to express a chimeric CD22 antigen, with CD22 ectodomain and CD19 TM and endo-domains. a) The CD22 antigen density on three engineered target cell lines was verified by labelling the cells with an anti-CD22-PE antibody. b) Quantibrite^{TM} beads were used to create a standard curve on PE MFI and molecules/cell, enabling quantification of the CD22 antigen density.

6.3.5 LT22 CSK^{AS} CAR T cell characterisation

6.3.5.1 LT22-CAR: CSK^{AS} Vs mCSK^{AS}

To test whether the CSK^{AS} and mCSK^{AS} modules could enable drug-mediated control of CAR T cell function, 72-hour co-cultures were set up challenging LT22 CAR T cells expressing CSK^{AS} or mCSK^{AS} against SupT1 CD22^{High}, CD22$^{Low(b)}$ and CD22^{VL} target cells. The cells were cultured in the presence or absence of 10 µM CSK^{AS} inhibitor, 3-IB-PP1. There was a small amount of background lysis observed when the LT22 CAR T cells were co-cultured with SupT1 NT control targets (Figure 35a). Co-expression of CSK^{AS} or mCSK^{AS} reduced this background kill when no drug was present.

The LT22 CAR T cells moderately lysed the CD22^{VL} target cells, with a mean target cell survival of 35.6% (Figure 35a). Unexpectedly, increasing the CD22 density on SupT1 targets led to a decrease in cytotoxicity, with a mean target cell survival of 50.8% and 48.2% observed for the CD22$^{Low(b)}$ and CD22^{High} targets, respectively. The addition of the drug led to a decrease in cytotoxicity of the LT22 CAR T cells when challenged against any of the CD22^{+} target cells. The largest difference observed was a 10.9% decrease in cytotoxicity when challenged against the CD22^{High} cells (Figure 35a).

In the absence of drug, the co-expression of CSK^{AS} significantly inhibited the cytotoxicity of the LT22 CAR T cells against all the target cell lines (Figure 35a and Figure 35d). Compared to the LT22 CAR T cells, the addition of the drug to CSK^{AS} bearing cells led to significant increases in the lysis of the CD22^{VL} and CD22$^{Low(b)}$ targets, with a 26.2% and 29.4% decrease in target cell survival, respectively. Against the CD22^{High} targets an 11.6% decrease in cell survival was observed (Figure 35a).

As observed with the CSK^{AS} module, co-expression of mCSK^{AS} also led to significant decreases in CAR T cell cytotoxicity against all target cell lines, compared to the LT22 CAR T cells (Figure 35a). In the presence of drug, mCSK^{AS} bearing cells were more cytotoxic than the LT22 CAR T cells, with a significant increase in cytotoxicity observed against the CD22$^{Low(b)}$ targets (Figure 35d).

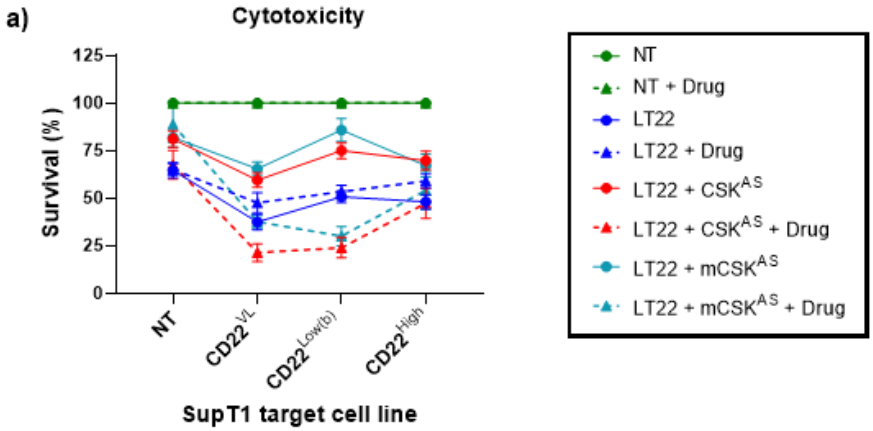

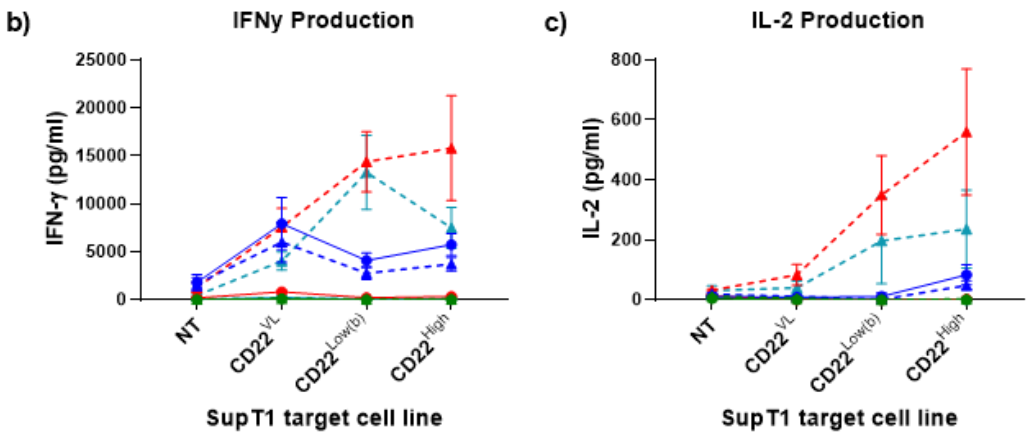

d)

		SupT1 NT		CD22VL		CD22Low(b)		CD22High	
		No Drug	+ Drug	No Drug	+ Drug	No Drug	+ Drug	No Drug	+ Drug
Cytotoxicity	LT22 Vs LT22 + CSKAS	*	ns	**	**	***	***	**	ns
	LT22 Vs LT22 + mCSKAS	*	ns	**	ns	****	*	*	ns
IFN-γ	LT22 Vs LT22 + CSKAS	ns	ns	*	ns	****	**	***	ns
	LT22 Vs LT22 + mCSKAS	ns	ns	*	ns	***	*	***	ns
IL-2	LT22 Vs LT22 + CSKAS	ns	ns	ns	ns	ns	*	*	*
	LT22 Vs LT22 + mCSKAS	ns	ns	ns	ns	ns	ns	ns	ns

Figure 35. Cytotoxicity and cytokine production of LT22 CSK^{AS} CAR T cells. a) 72h post co-culture initiation CAR T cell cytotoxicity was analysed by flow cytometry. Each condition was tested with a minimum of 4 donors (n=4-8), with mean (with SEM) indicated. All data was normalised to NT T cells. Co-cultures were set up with an E:T ratio of 1:4. CAR T cells were challenged against SupT1 NT target cells and three SupT1 CD22^{+} cell lines expressing antigen from 284-53,886 molecules/cell. Co-cultures were set up in media or media supplemented with 10 µM 3-IB-PP1 (+ Drug). Supernatant taken at 72h post co-culture set up was analysed by ELISA for the presence of IFN-γ (b) or IL-2 (c). d) For cytotoxicity, IFN-γ and IL-2 production, statistical analysis was performed by one-way ANOVA with Dunnett's post-test comparing LT22 CAR against CSK^{AS} and mCSK^{AS} bearing CARs within each condition. *P<0.05, **P<0.01, ***P<0.001, ****P<0.0001.

72h post co-culture initiation, supernatants were analysed by ELISA for the presence of either IFN-γ (Figure 35b) or IL-2 (Figure 35c). The addition of drug to the LT22 CAR T cells impaired function, with a 24.2% decrease in IFN-γ released observed when challenged against the $GD2^{VL}$ target cells (Figure 35b). In the absence of drug, CAR T cells bearing CSK^{AS} produced significantly less IFN-γ when challenged against each of the $CD22^{+}$ targets, compared to the LT22 CAR T cells (Figure 35b and Figure 35d). In the presence of drug, IFN-γ release by CSK^{AS} bearing cells when challenged against the $CD22^{VL}$ targets was restored to levels comparable to the LT22 CAR T cells. However, against the $CD22^{Low(b)}$ and $CD22^{High}$ targets, CSK^{AS} expression led to marked increases in IFN-γ release compared to the LT22 CAR (5.2- and 4.2-fold increase, respectively) (Figure 35b).

CAT T cells expressing $mCSK^{AS}$ had significantly reduced IFN-γ production compared to LT22 CAR T cells when challenged against $CD22^{+}$ target cells. Against the $CD22^{VL}$ targets, the addition of drug was not able to restore the level of IFN-γ production by $mCSK^{AS}$ bearing cells to levels achieved by the LT22 CAR T cells (Figure 35b). Conversely, against the $CD22^{Low(b)}$ targets, $mCSK^{AS}$ bearing cells in the presence of drug achieved significantly higher levels of IFN-γ compared to the LT22 CAR T cells (4.8-fold increase). When challenged against the $CD22^{High}$ targets, a more modest increase in IFN-γ was observed (2-fold) (Figure 35b).

The baseline levels of IL-2 release observed were consistently low for the LT22 CAR T cells regardless the antigen density (Figure 35c). Against the $CD22^{High}$ targets, the modest IL-2 release by the LT22 CAR T cells was abrogated in cells co-expressing either CSK^{AS} or $mCSK^{AS}$.

With the addition of the drug, CAR T cells bearing CSK^{AS} demonstrated significant increases in IL-2 release against both the $CD22^{Low(b)}$ and $CD22^{High}$ targets, compared to the LT22 CAR T cells (Figure 35c). CAR T cells expressing $mCSK^{AS}$ also achieved marked increases in IFN-γ production compared to the LT22 CAR T cells against these two target cell lines, but these increases did not reach significance (Figure 35c and Figure 35d).

In summary, both CSK^{AS} and $mCSK^{AS}$ modules were able to inhibit CAR T cell function, with the addition of drug leading to improved CAR T cell cytotoxicity and cytokine production. The most profound effect between the two modules was observed with regards to cytokine production, which showed that when T cells bearing the CSK^{AS} module were challenged against $CD22^{+}$ targets, they elicited higher levels of both IFN-γ (Figure 35b) and IL-2 (Figure 35c) production than cells expressing the $mCSK^{AS}$ module. To examine the difference between the two modules further I conducted a Western blot assay in Jurkat cells, a human leukemic T cell line with well characterised signalling pathways (Abraham and Weiss 2004).

6.3.5.1.1 Western blots: CSK^{AS} Vs $mCSK^{AS}$

An immunoblot of activated Jurkat cells expressing the LT22 CAR and either the CSK^{AS} or $mCSK^{AS}$ module demonstrated that the presence of the drug led to an increase in ZAP-70 phosphorylation (Y319) (Figure 36). In agreement with the higher levels of cytokine production observed in CSK^{AS} bearing CAR T cells (Figure 35b and c), Jurkat cells expressing the CSK^{AS} module showed increased ZAP-70 phosphorylation compared to cells expressing the $mCSK^{AS}$ module. As the CSK^{AS} module enabled greater cytokine release and ZAP-70 phosphorylation than the $mCSK^{AS}$ module, I chose to only continue with further characterisation of the CSK^{AS} module.

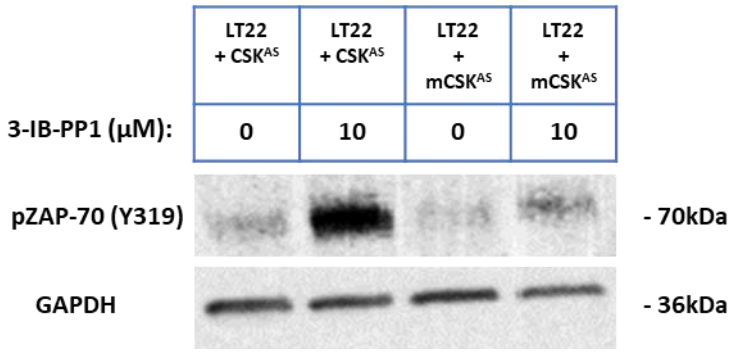

Figure 36. Effect of CSK^{AS} and mCSK^{AS} modules on ZAP-70 phosphorylation in Jurkat cells. Jurkat cells expressing the LT22 CAR and either the CSK^{AS} or mCSK^{AS} module were incubated at 37°C for 30 minutes in either plain media or media supplemented with 3-IB-PP1 (10 µM). The Jurkat cells were then activated with sCD22 (8 µg/ml). Activation was stopped after 2 minutes, and cells were then lysed. Tyrosine phosphorylation of ZAP-70 (Y319) was assessed by Western blotting (n = 1). The presence of total GAPDH was detected as a loading control.

6.3.5.2 LT22 CSK^{AS} CAR: Drug titration

A system to control CAR T cell function via the administration of a small molecule drug is more desirable if the response to the drug is dose dependant, as it allows for more sensitive tuning of CAR T cell activation. To this end, I investigated the cytotoxicity and cytokine release of CAR T cells expressing CSK^{AS} in response to increasing concentrations of the CSK^{AS} inhibitory drug, 3-IB-PP1 (0-10 µM). Co-cultures were set up challenging the T cells against SupT1 NT, CD22^{High} and CD22$^{Low(b)}$ target cells (Figure 37). There was some background cytotoxicity observed by the LT22 CAR T cells against the SupT1 NT targets in the absence of drug. However, the inclusion of CSK^{AS} reduced this background toxicity by 33% (Figure 37a). CSK^{AS} expression also markedly reduced background cytokine release, with IFN-γ decreasing by 94% (Figure 37d) and IL-2 decreasing by 90% (Figure 37g).

Against the CD22^{High} targets, LT22 CAR cytotoxicity was decreased by 10.6% upon co-expression of CSK^{AS} (Figure 37b). Addition of the drug led to CSK^{AS} expressing CAR T cells demonstrating subtly improved cytotoxicity compared to the LT22 CAR, at all the drug concentrations tested. As the cytotoxicity of the CSK^{AS} CAR T cells was consistently high, increases in cytotoxicity after increasing the drug concentration were small (increasing drug concentration from 0.156-10 µM led to a decrease in target cell survival from 7.6% to 4.9%).

Against the SupT1 CD22$^{Low(b)}$ targets and in the absence of drug, CSK^{AS} inhibited target cell lysis by 18.3% (Figure 37b). After drug administration, CSK^{AS} increased cytotoxicity compared to the LT22 CAR alone cells, with drug concentrations of 0.156 µM and 1.25 µM increasing target cell lysis by 14.4% and 25.8%, respectively (Figure 37c). The cytotoxic response of the CSK^{AS} bearing cells then plateaued at drug concentrations above 1.25 µM, not eliciting further increases in target cell lysis.

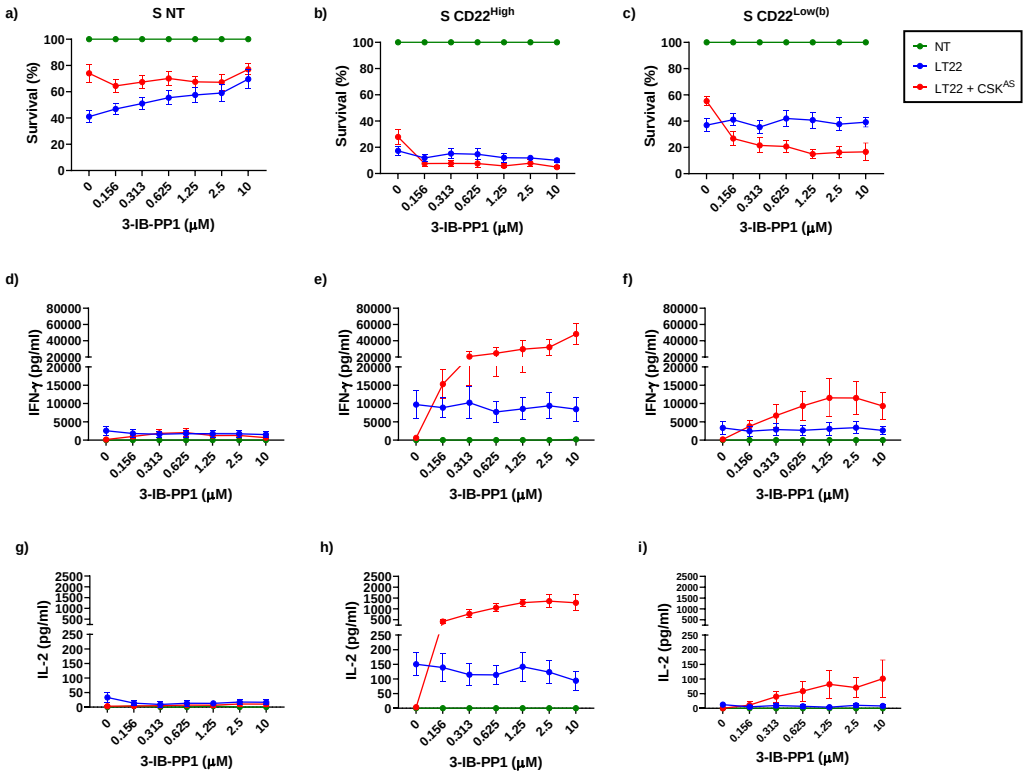

Figure 37. Cytotoxicity and cytokine production of LT22 CSK^{AS} CAR T cells in response to drug titration. a-c) CAR T cell cytotoxicity was analysed by flow cytometry 72h after co-culture set up. Each condition was tested with a minimum of 6 donors (n=6), with mean indicated. All data was normalised to NT T cells. Co-cultures were set up with an E:T ratio of 1:4. SupT1 NT target cells were used in the left column, SupT1 CD22^{High} (53,886 molecules/cell) target cells were used in the middle column and SupT1 CD22$^{Low(b)}$ (1,946 molecules/cell) target cells were used in the right column. 72h post co-culture set up, supernatant was analysed by ELISA for the presence of IFN-γ (d-f) or IL-2 (g-i).

The production of the cytokines IFN-γ (Figure 37d-f) and IL-2 (Figure 37g-i) was analysed 72-hours after co-culture initiation. In the absence of drug, no cytokine production was detected by the LT22 CSK^{AS} CAR T cells when challenged against either the $CD22^{High}$ or $CD22^{Low(b)}$ targets. As the concentration of drug increased, the general trend observed was that secretion of cytokines by CSK^{AS} bearing cells also increased. Against the $CD22^{High}$ target cells, the addition of 0.156 µM drug resulted in LT22 CSK^{AS} T cells producing 1.7-fold more IFN-γ (Figure 37e) and 3-fold more IL-2 (Figure 37h) compared to the LT22 CAR T cells. When the concentration of drug present was increased to 10 µM, LT22 CSK^{AS} T cells produced 5.7-fold more IFN-γ (Figure 37e) and 13.6-fold more IL-2 (Figure 37h) compared to the LT22 CAR T cells.

Overall, these data indicate that the CSK^{AS} module could be further explored as a tuneable CAR switch. However, the optimal drug concentration can vary depending on the functional readout. Moreover, the dynamic range for cytotoxicity was relatively narrow, with near maximal functional response achieved in the presence of 1.25 µM drug (Figure 37b and c). Therefore, to gain a clearer picture of the dose-response relationship, testing a more comprehensive range of drug concentrations between 0-1.25 µM would be beneficial.

6.3.5.3 LT22 CSK^{AS} CAR: Proliferation

The proliferative capacity of CAR T cells is an important feature for predicting persistence and antitumour effect after adoptive transfer (Porter et al. 2011; Kalos et al. 2011; Ghorashian et al. 2019). Therefore, I investigated the impact of the CSK^{AS} on CAR T cell proliferation. As described in 3.2.7.3, CAR T cells were labelled with the CTV proliferation dye prior to co-culture set up. CAR T cells expressing the LT22 CAR, LT22 CAR + wtCSK or LT22 CAR + CSK^{AS} were co-cultured as before with either SupT1 NT, SupT1 $CD22^{High}$, or SupT1 $CD22^{Low(b)}$ target cells (Figure 38).

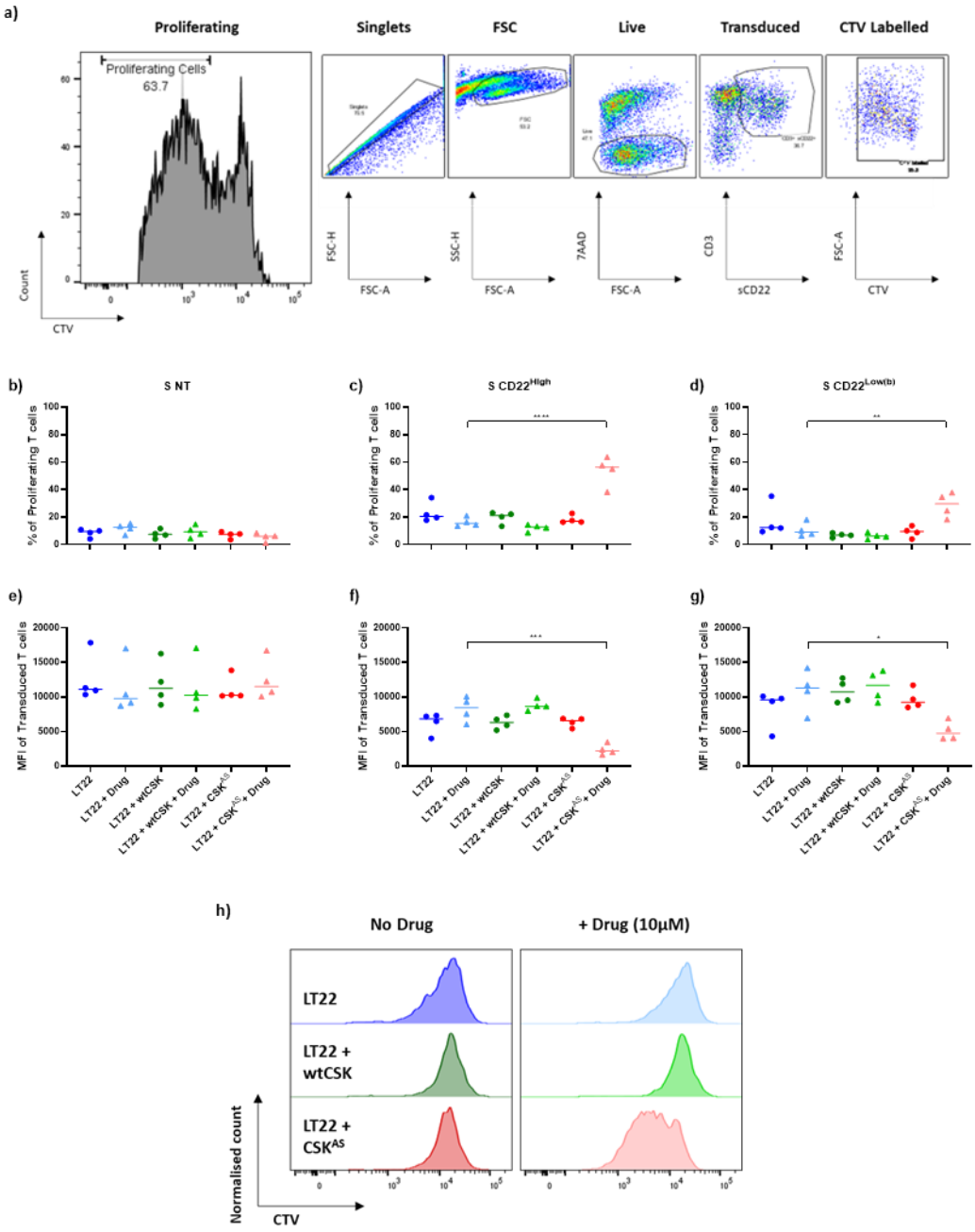

Figure 38. Proliferation of LT22 CSK^{AS} CAR T cells. a) Example gating strategy to plot the percentage of proliferating CAR T cells. b-g) Transduced CAR T cells labelled with CTV were challenged against SupT1 NT target cells (b and e), SupT1 CD22^{High} (53,886 molecules/cell) target cells (c and f) and SupT1 CD22$^{Low(b)}$ (1,946 molecules/cell) target cells (d and g). Co-cultures were set up with an E:T ratio of 1:2 in media or media supplemented with 10 µM 3-IB-PP1 (+ Drug). Proliferation was analysed by flow cytometry on day 7 post co-culture set up. Each condition was tested with a minimum of 4 donors (n=4), with median indicated. Statistical analysis was performed by one-way ANOVA with Dunnett's post-test comparing LT22 CAR against wtCSK and CSK^{AS} bearing CARs within each condition (no drug or + drug). *P<0.05, **P<0.01, ***P<0.001, ****P<0.0001. b-d) Plots showing the % of proliferating CTV^{+} transduced T cells. e-g) Plots showing the MFI of all transduced and CTV^{+} T cells. h) Representative histogram plots of CTV dilution from CAR T cells co-cultured with CD22$^{Low(b)}$ targets (f).

On day 7 post co-culture initiation I analysed the percentage of proliferating T cells (Figure 38a-d). Against the SupT1 NT target cells, no background proliferation was observed (Figure 38b). When challenged against either the $CD22^{High}$ or $CD22^{Low(b)}$ targets, LT22 CAR T cells displayed only marginal levels of proliferation. Thus, LT22 CAR T cells bearing the wtCSK or CSK^{AS} module had only negligible dampening effects compared to the LT22 CAR T cells (Figure 38c and d). In co-cultures supplemented with drug, CAR T cells expressing the CSK^{AS} module displayed significantly higher percentage of proliferating cells compared to the LT22 CAR. Against the $CD22^{High}$ targets a 41% increase was observed (Figure 38c) and against the $CD22^{Low(b)}$ targets, a 20.7% increase was observed (Figure 38d).

Another measure of proliferation is the reduction of the MFI of CTV caused by dilution of the dye as cells divide (Figure 38e-h). Analysis of CTV MFI showed that when challenged against the $CD22^{High}$ targets, CAR T cells expressing either the wtCSK or CSK^{AS} displayed no dampening effect (Figure 38f). As mentioned above, this was likely due to the low baseline levels of proliferation achieved by the LT22 CAR T cells.

When challenged against the $CD22^{Low(b)}$ targets, wtCSK bearing cells elicited a small dampening response, with median CTV levels 11.9% higher than the LT22 CAR T cells (Figure 38g). Analysis of CTV MFI indicated that CAR T cells expressing CSK^{AS} were not observed to dampen proliferation, again likely due to the already low proliferation observed by the LT22 CAR T cells. Interestingly, we observed an inhibitory effect of the drug itself, which resulted in higher median CTV levels after exposure to $CD22^{+}$ target cells (Figure 38f and g). In the presence of drug, CSK^{AS} expressing CAR T cells significantly increased proliferation against both the $CD22^{High}$ and $CD22^{Low(b)}$ targets, eliciting a 74% and 58% reduction in median CTV, respectively (Figure 38f and g).

6.3.5.4 LT22 CSK^{AS} CAR: Memory phenotype

CAR T cells with a more undifferentiated memory/stem like phenotype are associated with improved persistence and efficacy (Gattinoni et al. 2011; Louis et al. 2011; Xu et al. 2014). This considered, a higher proportion of more terminally differentiated T cells is undesirable. As the CSK^{AS} module has been shown to dampen CAR T cell activation, it has the potential to delay differentiation. Conversely, in the presence of

drug, CSK^{AS} expressing CAR T cells may be vulnerable to early or disproportionate terminal differentiation. To determine whether this theory is correct, I assessed the impact of the CSK^{AS} module on CAR T cell differentiation by analysing the expression of CCR7 and CD45RA (Figure 39), allowing identification of the four subsets of T cell memory phenotype: Tn, Tcm, Tem and Teff (described in 3.2.7.4).

When challenged against the SupT1 NT target cells, the subsets of the $CD4^+$ CAR T cells were comparable, regardless of wtCSK or CSK^{AS} expression (Figure 39b). However, in the $CD8^+$ populations, expression of wtCSK or CSK^{AS} subtly increased the proportion of Tcm cells to Teff cells compared to the LT22 CAR T cells (Figure 39e). For both the $CD4^+$ and $CD8^+$ populations, addition of the drug bore little impact on the differentiation of T cells challenged against SupT1 NT target cells (Figure 39b and e).

As observed when challenged with the SupT1 NT target cells, T cell subsets of CD4+ CAR T cells were comparable after being challenged against the $CD22^{Low(b)}$ or $CD22^{VL}$ targets, irrespective of the expression of wtCSK or CSK^{AS} (Figure 39c and d). Moreover, in these conditions the addition of the drug had little impact on cell phenotype.

Minor differences in phenotype were observed for $CD8^+$ CAR T cells upon stimulation with targets: when challenged with the $CD22^{VL}$ targets in absence of drug, co-expression of wtCSK and CSK^{AS} marginally increased the mean proportion of Tcm T cells compared to the LT22 CAR T cells (15.8% and 7.2% increase, respectively) (Figure 39g). Statistical analysis (one-way ANOVA) comparing the wtCSK or CSK^{AS} expressing cells to the LT22 CAR alone cells, found these increases in the Tcm populations to not be significant. Interestingly the addition of drug had an impact on the LT22 CAR T cells when challenged against the $CD22^{Low(b)}$ targets, decreasing the mean proportion of Tcm cells by 9% (unpaired t-test, *P = 0.0176) and increasing the proportion of Tem cells by 13.4% (unpaired t-test, ****P < 0.0001) (Figure 39f).

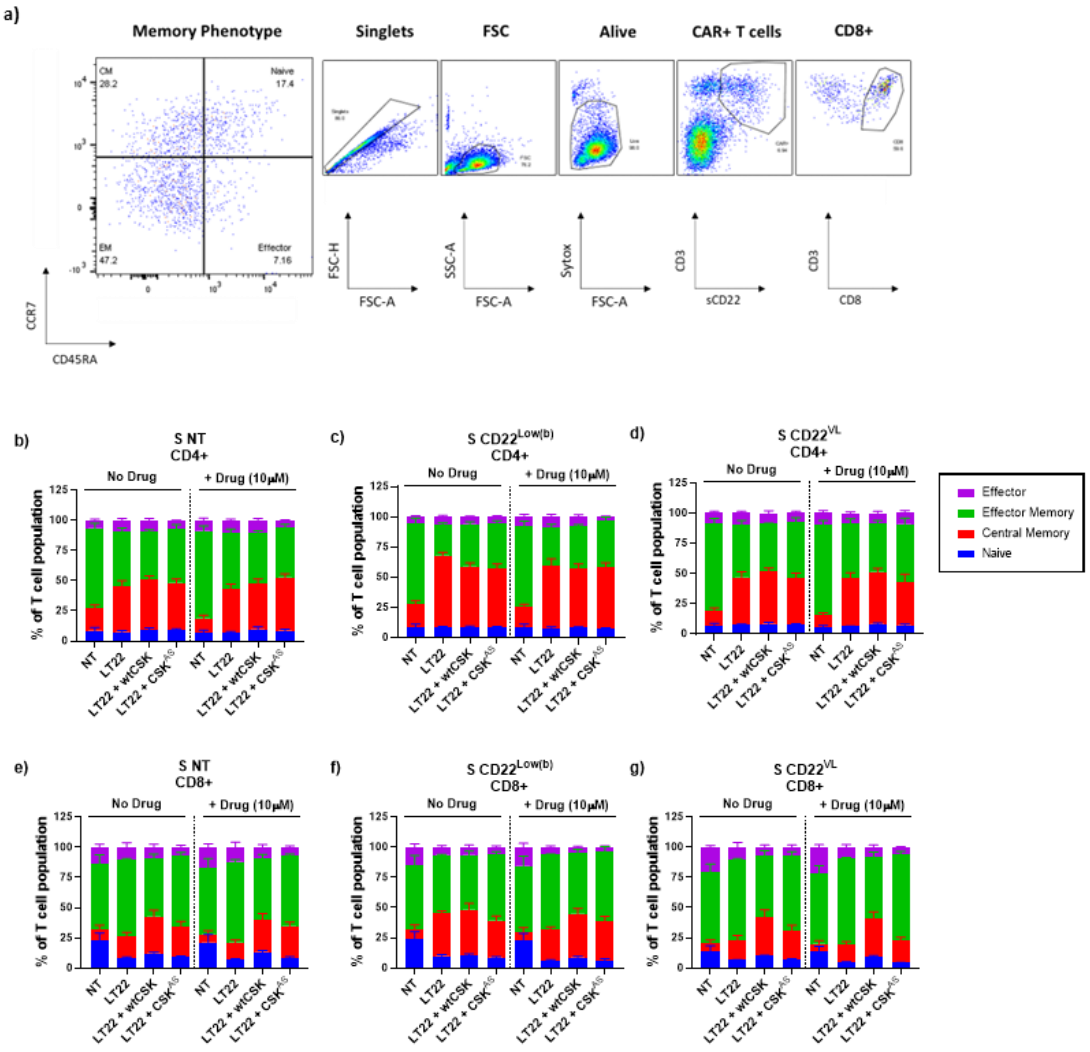

Figure 39. Memory phenotype of LT22 CSK^{AS} CAR T cells. a) Example gating strategy for the analysis of CCR7 and CD45RA expression on T cells. b-g) T cells were co-cultured with either SupT1 NT (b and e), SupT1 CD22$^{Low(b)}$ (c and f) or SupT2 CD22^{VL} (d and g) target cells at an E:T ratio of 1:2. Co-cultures were set up in media with no 3-IB-PP1 (no drug) or in media supplemented with 10 μM 3-IB-PP1 (+ drug). On day 4 post co-culture set up, T cells were analysed for the expression of CCR7 and CD45RA to determine their memory phenotype. The bar charts display the mean percentages of each memory phenotype population (n=4).

6.3.5.5 LT22 CSK^{AS} CAR: Exhaustion phenotype

T cell exhaustion, a phenomenon first described by Zajac and colleagues (Zajac et al. 1998), refers to dysfunctional T cells which have lost functions such as cytotoxicity and cytokine release. CAR T cell exhaustion has been identified as a key factor limiting antitumour efficacy (Eyquem et al. 2017; Fraietta et al. 2018; Long et al. 2015). Phenotypic markers of T cell exhaustion are Tim-3, Lag-3, and PD-1, with double and triple positive phenotypes indicative of more severe exhaustion (Grosso et al. 2009; Fourcade et al. 2010; Sakuishi et al. 2010). To further characterise the impact of CSK^{AS} on CAR T cells, I sought to investigate the expression of these exhaustion markers on CAR T cells post co-culture with antigen positive target cells (Figure 40). Four different exhaustion phenotype populations were analysed: cells expressing none of the exhaustion markers (triple negative), cells expressing one marker (single positive), cells expressing two markers (double positive) and cells expressing all three markers (triple positive).

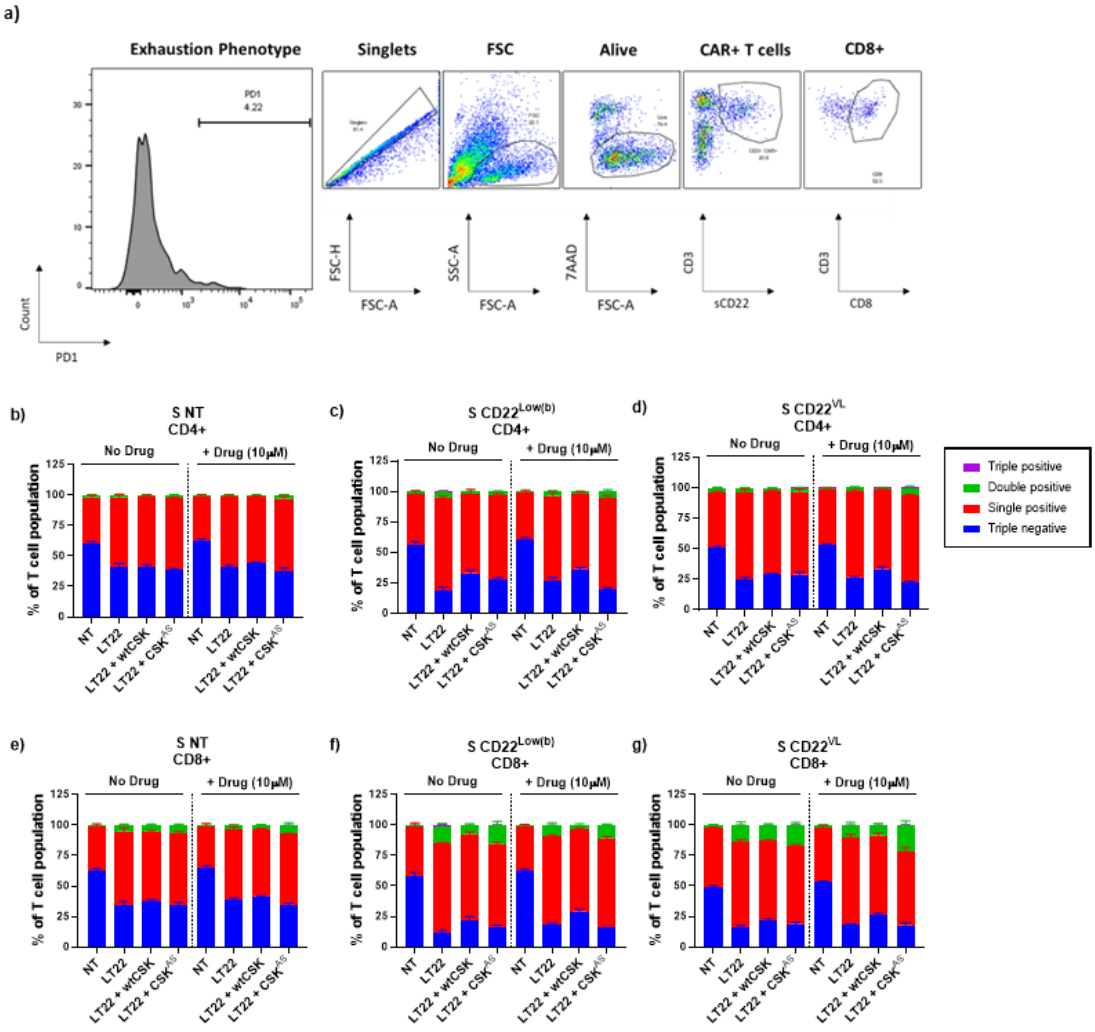

Figure 40. Exhaustion phenotype of LT22 CSK^{AS} CAR T cells. a) Example gating strategy for the analysis of the expression markers Tim-3, Lag-3, and PD-1 on T cells. b-g) T cells were co-cultured with either SupT1 NT (b and e), SupT1 CD22$^{Low(b)}$ (c and f) or SupT2 CD22^{VL} (d and g) target cells at an E:T ratio of 1:2. Co-cultures were set up in media with no 3-IB-PP1 (no drug) or in media supplemented with 10 µM 3-IB-PP1 (+ drug). On day 4 post co-culture set up, T cells were analysed for the expression of Tim-3, Lag-3, and PD-1 to determine their exhaustion phenotype. The bar charts display the mean percentages of different exhaustion phenotype populations (n=4).

When challenged with SupT1 NT target cells, the co-expression of wtCSK or CSK^{AS} had a negligible impact on the proportion of cells expressing at least one exhaustion marker, irrespective of the presence of drug (Figure 40b and e). In the absence of drug, CAR T cells bearing either wtCSK or CSK^{AS} displayed a higher proportion of triple negative cells than the LT22 CAR T cells when challenged against $CD22^{+}$ targets, with those expressing wtCSK consistently having a larger proportion of triple negative cells than CSK^{AS} bearing cells. Specifically, against the $CD22^{Low(b)}$ targets, 11.2% of $CD8^{+}$ LT22 CAR T cells were triple negative, whereas 21.9% of LT22 wtCSK cells and 15.5% of CSK^{AS} expressing cells were triple negative (Figure 40f). However, after analysis using a one-way ANOVA comparing the wtCSK or CSK^{AS} expressing cells to the LT22 CAR alone cells, the increase in the triple negative population achieved by co-expression of wtCSK reached significance (*P = 0.0333), whereas the increase in those co-expressing CSK^{AS} did not (P = 0.4321).

For CAR T cells expressing CSK^{AS}, there was a trend that addition of drug led to an increase in the proportion of cells expressing one or more exhaustion marker. For example, when challenged against $CD22^{VL}$ targets in the absence of drug (Figure 40g), $CD8^{+}$ LT22 CSK^{AS} CAR T cells had a 3.3% larger double positive population than the LT22 CAR T cells. Yet, In the presence of drug this difference rose to 11.1%. However, the difference in the number of double positive cells in the $CD8^{+}$ LT22 CSK^{AS} CAR T populations between conditions in which drug was present or not, was not found to be significant (unpaired t-test, P = 0.2909).

6.3.5.6 LT22 CSK^{AS} CAR: Kinase activity profiling

Protein tyrosine phosphorylation is fundamental to T cell signalling and function. Immunoblot analysis has shown that the addition of the CSK^{AS} inhibitor drug led to a marked increase in ZAP-70 phosphorylation (Y319) in activated Jurkats expressing the LT22 CSK^{AS} CAR (Figure 36). This result indicates that the improved functionality observed in CSK^{AS} bearing CAR T cells in the presence of drug is due to an increase in the activation of kinases involved in proximal T cell signalling events. In order to establish a more in-depth analysis of the protein tyrosine kinase (PTK) activity within LT22 and LT22 CSK^{AS} CAR T cells in response to the drug, I sent samples to be run on peptide microarrays, a service provided by PamGene.

LT22 and LT22 CSK^{AS} CAR T cells were incubated in plain media (R10), or media supplemented with drug (10 µM 3-IB-PP1) (as described in 3.3.3). After incubation, all cells were activated with sCD22 for 15 minutes. Cell pellets of six biological replicates (n=6) were sent to PamGene for lysis and subsequent running of lysates on the PamChip® microarrays. The PamChip® microarrays contain peptides representative of kinase targets/substrates (phosphosites) covalently immobilised in a porous matrix (Hilhorst et al. 2013). The active kinases in each sample phosphorylate the phosphosites within the PamChip® arrays. Fluorescently labelled antibodies that recognize phosphorylated residues are added to the arrays, enabling quantification of the extent to which each phosphosite has been phosphorylated (Figure 41).

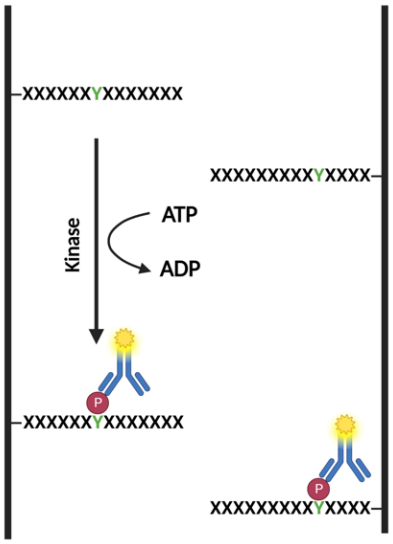

Figure 41. Schematic of the PamChip® peptide microarray reaction. Cell lysate samples are passed through the porous array in the presence of ATP to facilitate the phosphorylation of the phosphosites by the activated kinases in each sample. The phosphorylation of the phosphosites is detected by fluorescently labelled antibodies.

After running all the samples on the PamChip®, the difference in phosphorylation of each phosphosite was compared between different conditions: LT22 Vs LT22 CSK^{AS} (no drug), LT22 Vs LT22 CSK^{AS} (+ drug), + drug Vs no drug (LT22) or + drug Vs no drug (LT22 + CSK^{AS}) (Table 20).

In the CAR alone to CSK^{AS} comparison in the absence of drug, 66 phosphosites showed less kinase activity. This list included phosphosites belonging to kinase targets known to play a role in T cell receptor signalling (CD3ζ, Lck, ZAP-70, PLC-γ1). However, when comparing the CAR to the addition of the CSK^{AS} module in the presence of drug, 49 phosphosites showed an increase in kinase activity.

The effect of the drug treatment on either LT22 or LT22 CSK^{AS} CAR T cells was also investigated. Interestingly, when comparing the presence to absence of drug for the LT22 CAR, the drug had an inhibitory effect, with 56 phosphosites showing a decrease in kinase activity. Conversely, the comparison between the +/- drug conditions for the LT22 CSK^{AS} CAR showed 108 phosphosites to have higher kinase activity in the presence of drug.

Table 20. Phosphosite analysis

Comparison	Up	Down
LT22 Vs LT22 + CSK^{AS} (no drug)[a]	0	66
LT22 Vs LT22 + CSK^{AS} (+ drug)[a]	49	1
+ drug Vs no drug (LT22)[b]	0	56
+ drug Vs no drug (LT22 + CSK^{AS})[b]	108	0

[a]Significance was obtained using a two-sided unpaired Student's t-test, $p<0.05$
[b]Significance was obtained using a two-sided paired Student's t-test, $p<0.05$

The signal of each specific phosphosite is the result of the overall phosphorylation caused by the activity of one or multiple kinases. Furthermore, kinases in the cell lysates phosphorylate multiple phosphosites. To determine which kinases are responsible for the differences in phosphosite phosphorylation in each condition, PamGene performed Upstream Kinase Analysis (UKA). Using sets of phosphosites, for each condition the UKA algorithm predicts differential kinase activity in the test

condition compared to the control. In total, 83 kinases were analysed in each condition but in Table 21, Table 22, Table 23 and Table 24 the kinases with the top 20 mean final score are shown. The final score values are a combination of the significance of the result with the specificity, with a high final score indicating a higher probability of being differentially active within the test condition. The kinase statistic represents change in kinase activity (< 0 = inhibition, > 0 = activation).

Table 21. Kinase score table: LT22 Vs LT22 + CSK^{AS} (no drug)

Rank	Kinase Name	Kinase Family	Mean Final Score	Mean Kinase Statistic
1	Lck	Src	4.49	-1.03
2	Src	Src	4.30	-0.95
3	BLK	Src	3.67	-0.99
4	Lyn	Src	3.59	-0.97
5	KDR	VEGFR	3.12	-0.94
6	Srm	Src	3.17	-0.90
7	CHK1	CAMKL	3.13	-1.16
8	Abl	Abl	3.05	-0.87
9	FRK	Src	3.07	-0.89
10	Fyn	Src	3.10	-0.93
11	ROR1	Ror	2.93	-1.12
12	EphA1	Eph	2.72	-1.04
13	Ron	Met	2.64	-0.96
14	Tyro3/Sky	Axl	2.65	-0.85
15	Yes	Src	2.54	-0.87
16	TXK	Tec	2.45	-0.86
17	Axl	Axl	2.51	-0.83
18	HCK	Src	2.37	-0.84
19	Syk	Syk	2.33	-0.81
20	IGF1R	InsR	2.29	-0.87

In the absence of drug when CSK^{AS} should play an inhibitory role on T cell signalling, the module bearing T cells showed a substantial decrease in overall kinase activity compared to the CAR alone (Table 21). Many SFK members showed the largest decreases in activity. This was expected as CSK directly inhibits SFKs via phosphorylation of the conserved C-terminal inhibitory tyrosine residue (Okada et al. 1991; Okada 2012). Furthermore, kinases involved in proximal T cell signalling displayed decreases in activity, such as Lck (mean kinase statistic of -1.03) and ZAP-

70 (Zap-70 was ranked 33 with a mean final score of 1.87 and mean kinase statistic of -0.78).

Table 22. Kinase score table: LT22 Vs LT22 + CSK^{AS} (+ drug)

Rank	Kinase Name	Kinase Family	Mean Final Score	Mean Kinase Statistic
1	CTK	Csk	4.23	1.32
2	FAK1	Fak	4.70	1.14
3	FAK2	Fak	3.96	1.07
4	Fgr	Src	3.60	1.55
5	Yes	Src	4.41	1.31
6	HCK	Src	3.13	1.00
7	FGFR4	FGFR	3.13	1.02
8	InSR	InsR	2.78	0.94
9	EphA8	Eph	3.23	1.03
10	ALK	Alk	3.29	0.96
11	FGFR3	FGFR	3.10	1.04
12	HER3	EGFR	3.11	0.97
13	FGFR1	FGFR	3.08	1.03
14	LTK	Alk	2.64	0.91
15	Tyk2	JakA	2.62	1.03
16	FGFR2	FGFR	2.82	0.97
17	TRKC	Trk	2.55	0.91
18	Ros	Sev	2.24	0.84
19	ZAP70	Syk	2.16	0.79
20	TRKB	Trk	2.24	0.83

LT22 CAR T cells were also compared to CSK^{AS} bearing CAR T cells in the presence of the CSK^{AS} inhibitor drug (Table 22). In CSK^{AS} bearing cells there was a substantial increase in overall kinase activity. Notably, many SFKs showed an increase in kinase activity such as Fgr, Yes and HCK (Lck was ranked 57 with a mean kinase statistic of 0.54). Interestingly, many of the kinases with the largest increase in activity such as FAK1, FAK2 and FGFR4 play roles in pathways such as PI3-AKT signalling and MAPK signalling.

When comparing LT22 and LT22 CSK^{AS} CAR T cells, I previously observed the addition of drug to elicit and increase in ZAP-70 phosphorylation (Figure 36). This finding was supported by the data generated from the peptide microarrays, which also saw an increase in ZAP-70 activity (Table 22).

An interesting finding from this particular comparison was that CSK-Type protein tyrosine Kinase (CTK) displayed the highest level of increased kinase activity. CTK is very similar in structure to CSK and also phosphorylates the conserved inhibitory C-terminal tyrosine residue of the SFKs (Klages et al. 1994; Hirao et al. 1997). The addition of the drug to inhibit CSK^{AS} in CAR T cells in turn reduces the inhibitory capacity of CSK, by blocking accessibility to membrane anchors such as PAG. Thus, the increase in kinase activity of CTK may be a cellular response to attempt to regulate the equilibrium between positive and negative regulators of T cell signalling.

Table 23. Kinase score table: + drug Vs no drug (LT22)

Rank	Kinase Name	Kinase Family	Mean Final Score	Mean Kinase Statistic
1	Met	Met	3.64	-0.70
2	HCK	Src	2.70	-0.67
3	Syk	Syk	2.77	-0.63
4	Yes	Src	3.01	-0.68
5	BLK	Src	2.70	-0.69
6	Axl	Axl	2.47	-0.63
7	Src	Src	2.60	-0.65
8	ZAP70	Syk	2.39	-0.63
9	Srm	Src	2.07	-0.64
10	Fgr	Src	2.09	-0.69
11	Tyro3/Sky	Axl	1.92	-0.63
12	Fyn	Src	2.05	-0.66
13	HER2	EGFR	1.93	-0.64
14	RYK	Ryk	1.93	-0.70
15	Kit	PDGFR	2.09	-0.68
16	CTK	Csk	2.11	-0.65
17	Mer	Axl	1.84	-0.63
18	FRK	Src	1.86	-0.63
19	PDGFR[beta]	PDGFR	1.76	-0.64
20	FGFR4	FGFR	1.73	-0.63

The addition of the drug had an inhibitory effect on the LT22 CAR T cells, resulting in an overall decrease in kinase activity (Table 23). The kinase activity of several SFKs, such as HCK, Yes, BLK and Src was reduced (Lck was ranked 25 with a mean kinase statistic of -0.64). Notably, ZAP-70 also displayed a reduction in kinase activity. However, the inhibitory effect of drug administration was less that that observed

after co-expression of CSK^{AS} in the absence of drug (in this instance, Lck had a mean kinase statistic of -1.03) (Table 21).

Table 24. Kinase score table: + drug Vs no drug (LT22 CSK^{AS})

Rank	Kinase Name	Kinase Family	Mean Final Score	Mean Kinase Statistic
1	Yes	Src	5.07	1.42
2	InSR	InsR	4.15	1.27
3	HCK	Src	4.14	1.25
4	TRKC	Trk	4.11	1.22
5	TRKB	Trk	3.59	1.18
6	Fyn	Src	3.50	1.15
7	IRR	InsR	2.72	1.05
8	Src	Src	3.60	1.08
9	LTK	Alk	2.95	1.03
10	CTK	Csk	3.53	1.13
11	Syk	Syk	3.05	0.98
12	TRKA	Trk	2.85	1.06
13	CHK1	CAMKL	3.22	1.52
14	IGF1R	InsR	2.93	1.09
15	FAK2	Fak	2.85	1.03
16	BLK	Src	3.24	1.14
17	HER3	EGFR	2.84	0.99
18	ZAP70	Syk	2.72	0.97
19	ALK	Alk	2.69	0.98
20	FAK1	Fak	2.91	1.02

The addition of the drug to the LT22 CAR T cells co-expressing CSK^{AS}, resulted in a strong overall increase in kinase activity (Table 24). Many SFKs displayed increased activity, including Yes, HCK, Fyn and Src. Kinases that play a role in proximal T cell signalling also showed an increase in kinase activity, such as ZAP-70 (mean kinase statistic of 0.97) and Lck (rank 26 with a mean kinase statistic of 0.98).

6.3.5.7 LT22 CSK^{AS} CAR: *In vivo* function

I observed the co-expression of CSK^{AS} in LT22-CAR T cells to enable tuning of CAR T cell functioning *in vitro* in response to a small molecule drug, 3-IB-PP1. Next, I aimed to demonstrate this mechanism *in vivo*.

6.3.5.7.1 3-IB-PP1 toxicology *in vivo*

Prior to carrying out a CAR T cell efficacy *in vivo* model, a preliminary study was conducted to determine whether 3-IB-PP1 is tolerated well in NSG mice (Figure 42). Three times a week, NSG mice were administered 3-IB-PP1 via IP injection, with different groups receiving a different dose of drug (1-500 ng/g). Control groups were also included which received IP injections of RPMI containing DMSO at equivalent percentages as three of the 3-IB-PP1 concentrations tested. There were 3 mice in each group (n=3) and all mice were weighed regularly, with weight loss considered a sign of toxicity. Any mouse with sudden body weight loss of ≥ 20% would have been culled. Additionally, mice were monitored for changes in physical appearance or behaviour as signs of toxicity.

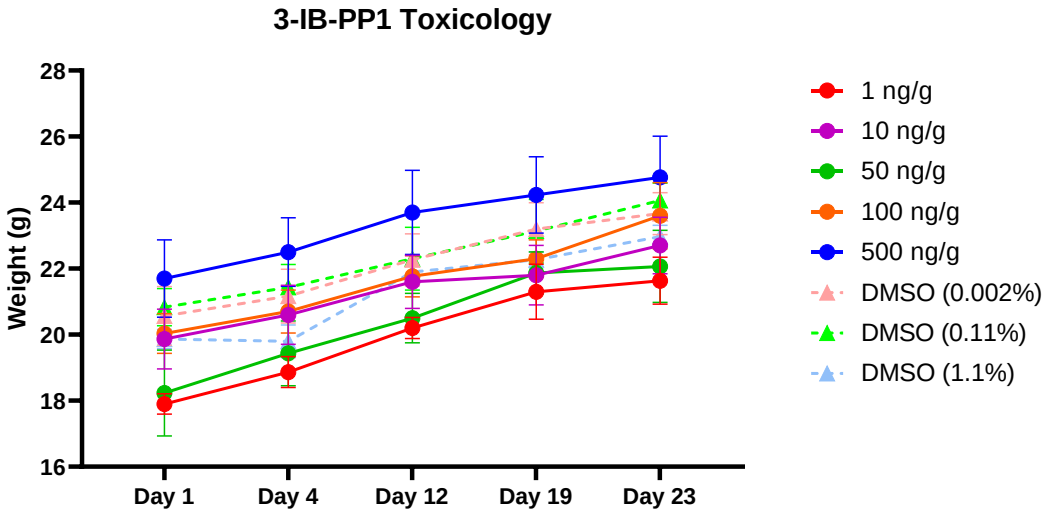

Figure 42. Toxicology of 3-IB-PP1 *in vivo*. 3-IB-PP1 was administered to NSG mice via IP injection three times a week for up to 23 days. Control groups were also included which were had DMSO (in RPMI) administered IP at representative concentrations of some of the 3-IB-PP1 doses: 1 ng/g = 0.002% DMSO, 50 ng/g = 0.11% DMSO and 500 ng/g = 1.1% DMSO. The weight of each mouse was recorded at the timepoints indicated. Plots displayed are the mean values of 3 replicates (n=3).

3-IB-PP1 was tolerated well in NSG mice at all the doses tested (Figure 42). Overall, all groups steadily gained weight over the course of the study, with no group showing any mean weight loss. DMSO, in which 3-IB-PP1 is reconstituted, was also well tolerated. As the drug was seen to be well tolerated in NSG mice, I next carried out a mouse model to investigate the functionality of LT22 and LT22 CSK^{AS} CAR T cells *in vivo*.

6.3.5.7.2 LT22 CSK^{AS} CAR function *in vivo*

I have observed inhibition of the CSK^{AS} module to augment CAR T cell function *in vitro*. Therefore, I envisioned that it may also provide improved CAR T cell functioning *in vivo*. Since, CD22 CAR patient relapses have been attributed to density lower than 2,839 molecules/cell (Fry et al. 2018), ideally we would show anti-tumour efficacy below this threshold. For the *in vivo* model I generated Nalm6 cells with reduced CD22 site density compared to Nalm6 WT cells (Figure 43a). To generate the Nalm6 $CD22^{Low}$ cell line, an in house CD19/CD22 double KO Nalm6 line was transduced with a plasmid encoding CD22 downstream of a STOPSKIP sequence, as described in 3.2.3.1. Using this approach, I generated the Nalm6 $CD22^{Low}$ cell line (referred to as Nalm6 cells hereafter) which had an antigen density of 1,641 CD22 molecules/cell. The Nalm6 cells were engineered to express firefly luciferase (FLuc), allowing for detection by BLI after IP injections of luciferin.

a)

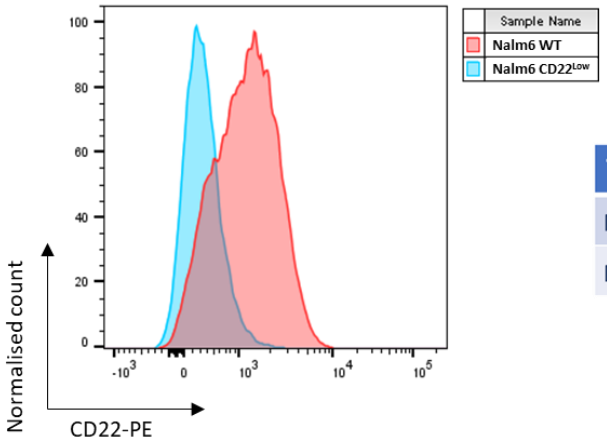

Target cell line	CD22/cell
Nalm6 WT	7,016
Nalm6 CD22^{Low}	1,641

b)

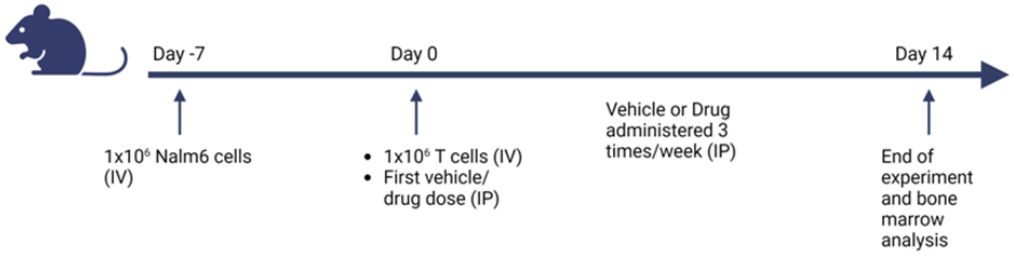

Figure 43. Nalm6 cells and *in vivo* model outline. a) The antigen density of CD22 on Nalm6 WT cells and Nalm6 CD22^{Low} cells. b) On day -7, 6–8-week-old female NSG mice were injected with 1x10^6 Nalm6 cells via tail vein IV injection. On day 0, 1x10^6 transduced CAR T cells (40% transduced, therefore 2.5x10^6 total cells) were administered IV. Mice were injected (IP) with their first dose of either vehicle (1.1% DMSO in RPMI) or drug (500 ng/g) on day 0 and three times a week thereafter. On day 14, all surviving mice were culled and both hind limbs harvested for bone marrow analysis.

The experimental outline is shown in Figure 43b. On day -7, NSG mice were injected (IV) with $1x10^6$ Nalm6 cells. There were six groups containing six mice per group, those groups comprised mice bearing NT, LT22 or LT22 CSK^{AS} CART that received the drug or vehicle as a negative control. On day 0 the mice were injected (IV) with $1x10^6$ CAR T cells. On day 0 the mice also received their first dose of either vehicle or drug, which they received three times per week until day 14.

The anti-tumour response was measured by BLI. In the cohorts that received the vehicle instead of the drug, mice that received LT22 CAR T cells showed a reduction in tumour burden compared to the NT cohort (Figure 44a). The LT22 CSK^{AS} cohort displayed an increase in tumour burden compared to mice in the LT22 CAR cohort. This result resembled the dampening effect of CSK^{AS} seen on CAR T cell cytotoxicity and cytokine production *in vitro* (Figure 35).

In the cohorts that the drug was administrated to, the LT22 CAR displayed a reduced tumour burden compared to both the NT and the LT22 CSK^{AS} cohort. This result differed from what had been observed *in vitro*, wherein drug administration to CSK^{AS} bearing cells was associated with improved cytotoxicity, cytokine release (Figure 37) and proliferation (Figure 38) of the LT22 CAR T cells.

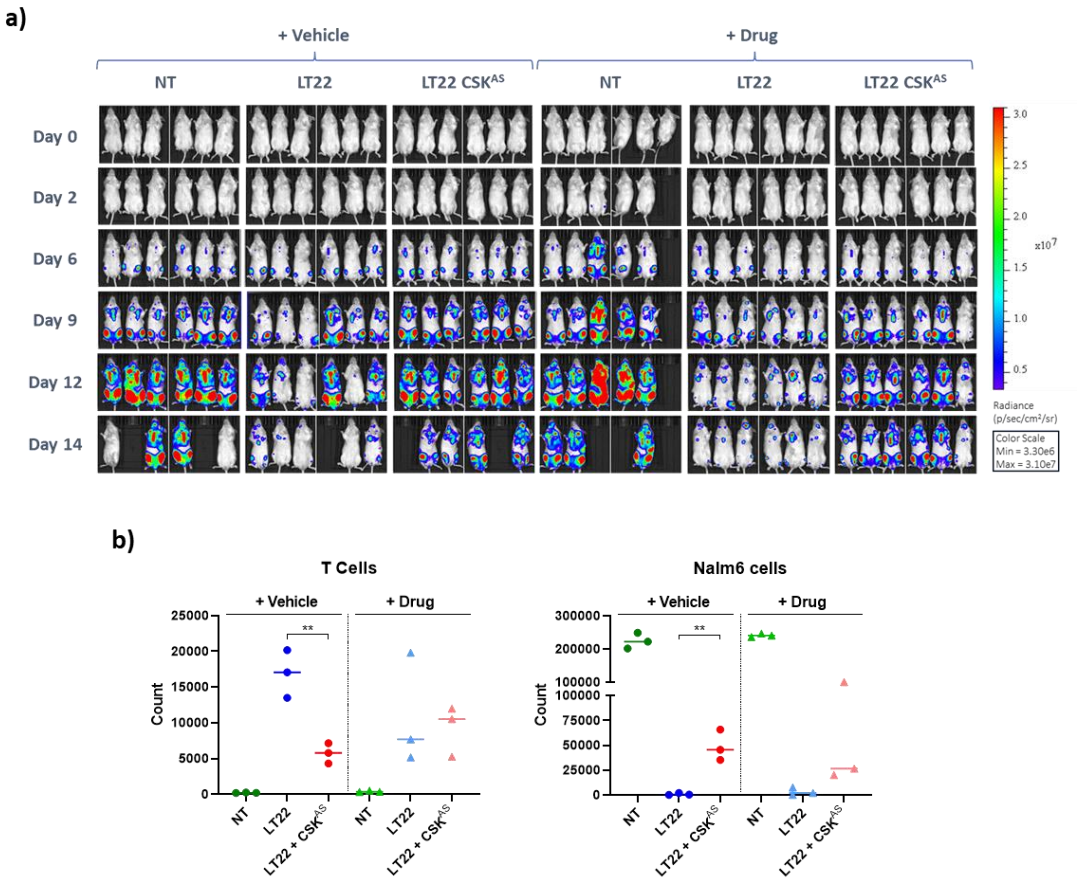

Figure 44. LT22 and LT22 CSK^{AS} CAR T cell function *in vivo*. a) Bioluminescence of Nalm6 tumours in mice. On day -7, mice were injected (IP) with 1x10^6 Nalm6 cells. On day 0, mice were injected (IV) with 2.5x10^6 NT T cells, LT22 and LT22 CSK^{AS} CAR T cells (CAR T cells were 40% transduced). From the first dose on day 0, groups were administered (IP) either vehicle (1.1% DMSO in RPMI) or drug (500 ng/g 3-IB-PP1 in RPMI) three times a week until the end of the study on day 14. b) T cells (left) and Nalm6 cells (right) in bone marrow on day 14. Three mice from each group were analysed (n=3) with the median counts indicated by horizontal lines. **P = 0.0059, unpaired t-test.

On day 14 of the Nalm6 model, the total number of T cells and Nalm6 cells in the bone marrow was analysed (Figure 44b). There were significantly less LT22 CSK^{AS} CAR T cells in bone marrow compared to LT22 CAR T cells (median count decreased by 66%). However, in the groups which received regular administrations of drug, there was a 1.4-fold increase in median number of CSK^{AS} bearing cells compared to CAR alone cells.

In agreement with the BLI readings (Figure 44a), the LT22 CAR cleared Nalm6 cells most efficiently (Figure 44b, right). In groups that received injections of vehicle, the LT22 CSK^{AS} CAR T cells significantly reduced tumour clearance compared to the LT22 CAR T cells, resulting in an 87.2-fold increase in median number of Nalm6 cells. Although the administration of the drug resulted in improved number of LT22 CSK^{AS} CAR T cells, this did not result in superior tumour clearance, as the median number of Nalm6 cells was 12.5-fold higher compared to the LT22 CAR T cell group. Interestingly, although administration of the drug reduced the number of LT22 CAR T cells by 55% (Figure 44b, left), the LT22 CAR-mediated tumour clearance was comparable between the vehicle and drug groups.

6.4 Summary

In this chapter I aimed to characterise the use of CSK^{AS} as a module to tune CAR T cell function. I envisioned that this module would help address two challenges facing CAR T cell therapies: suboptimal function against low antigen density targets and on-target off-tumour toxicity.

CSK^{AS} was developed by Schoenborn and colleagues, and is specifically inhibited by the PP1 analogue, 3-IB-PP1. Reporting on the impact of CSK^{AS} and $mCSK^{AS}$ on T cell signalling, this group observed $mCSK^{AS}$ to elicit a more potent dampening effect in Jurkat cells than the CSK^{AS} module. Moreover, after stimulation through the TCR and in the presence of drug, the magnitude of CD3ζ chain phosphorylation was 5- to 10-fold higher in the $mCSK^{AS}$ containing cells (Schoenborn et al. 2011). In agreement with this study, I observed the $mCSK^{AS}$ module to elicit greater dampening and augmentation of IFN-γ release by TCR-stimulated T cells than the CSK^{AS} module (Figure 32).

In a clinical trial wherein the LT22 CAR was the CD22 targeting component of a CD19/CD22 bispecific CAR platform, one patient relapsed with CD19-negative disease and dimming of CD22 expression from 4,649 molecules/cell before CAR T cell treatment to 1,416 molecules/cell post treatment (Cordoba et al. 2021). This suggested that increasing the sensitivity of the LT22 CAR would be beneficial.

As I observed the expression of wtCSK to dampen LT22 CAR T cell function (chapter 4) and the expression of dnCSK modules to augment function (chapter 5), I initially compared the effect of co-expressing CSK^{AS} or $mCSK^{AS}$ in the LT22 CAR T cell platform (Figure 35). The inhibitory capacity of the CSK^{AS} and $mCSK^{AS}$ modules were comparable against target cells expressing a range of antigen densities. However, in the presence of the drug, against the $CD22^{VL}$ targets cells, LT22 CAR T cells bearing CSK^{AS} elicited a significant increase in mean target cell lysis of 26.2%, whereas the $mCSK^{AS}$ T cells achieved a more modest increase of 10% compared to the LT22 CAR control (Figure 35a).

The addition of the drug also led to notably higher levels of IFN-γ (Figure 35b) and IL-2 (Figure 35c) being produced by both CSK^{AS} and $mCSK^{AS}$ bearing cells compared to the LT22 CAR T cells. With regards to IFN-γ production, the increases observed for both the CSK^{AS} and $mCSK^{AS}$ bearing cells in response to $CD22^{Low(b)}$ targets reached significance. However, against the $CD22^{Low(b)}$ and $CD22^{High}$ targets, only the CSK^{AS} bearing cells and not those co-expressing $mCSK^{AS}$ significantly increased IL-2 production (Figure 35d). The superior functional capacity of the CSK^{AS} in response to drug was supported by immunoblot analysis, which showed CSK^{AS} expressing Jurkats to have increased levels of phosphorylated ZAP-70 compared to $mCSK^{AS}$ expressing cells (Figure 36).

Contrary to what I observed in TCR activated T cells, the drug-mediated inhibition of the CSK^{AS} module in CAR activated T cells allowed for a greater augmentation of T cell function than the $mCSK^{AS}$ module. Therefore, I selected CSK^{AS} as the module to further characterise in the LT22 CAR platform. A possible explanation for the difference I observed between the CSK^{AS} and $mCSK^{AS}$ modules could be that CSK^{AS} is able to freely bind membrane anchors such as DOK1 (Schoenborn et al. 2011), SIT1 (Pfrepper et al. 2001), LIME (Brdicková et al. 2003) and caveolin-1 (Cao, Courchesne,

and Mastick 2002), blocking endogenous CSK from binding. Whereas $mCSK^{AS}$ is constitutively localised to the membrane and thus its SH2 domain may not be able to bind other membrane anchors as efficiently due to steric hindrance, leading to a greater pool of endogenous CSK free to occupy the membrane anchors and in turn inhibit signalling.

However, I observed the $mCSK^{AS}$ module to be more efficient than CSK^{AS} in TCR stimulated T cells (Figure 32). Therefore, the variance in the efficiency between the $mCSK^{AS}$ and CSK^{AS} modules could be explained by fundamental differences between TCR- and CAR- mediated activation of T cells, such as the disparity in IS organisation. TCRs form an IS which is enriched with Lck, whereas Lck localisation in CAR synapses is more disorganised (Davenport et al. 2018). As the $mCSK^{AS}$ module is localised to the membrane via the N-terminal domain of Lck (Schoenborn et al. 2011), it would be reasonable to presume that $mCSK^{AS}$ is enriched to a greater extent than CSK^{AS} in synapses formed after TCRs engagement.

After demonstrating the CSK^{AS} module was able to improve LT22 CAR T cell cytotoxicity and cytokine release in response to the administration of the CSK^{AS} inhibitor drug (Figure 35), I next explored the relationship between the concentration of the drug and magnitude of functional augmentation (Figure 37). As expected, the inhibitory effects of the CSK^{AS} module were seen in the absence of drug.

Increasing drug concentration increased the cytotoxicity and cytokine release of CSK^{AS} expressing CAR T cells when challenged with antigen positive targets. Against the $CD22^{High}$ targets, the CAR function reached a plateau at lower drug concentration compared to the $CD22^{Low(b)}$ targets (Figure 37). This saturation effect is presumably due to the higher antigen density on target cells resulting in a stronger activation signal, thus less drug is required in order to achieve maximal activation. The drug concentrations used in these titration experiments did not enable a clear conclusion to be formed on the dose-response relationship, as in the cytotoxicity assays a near maximal response was achieved in response to a drug concentration of 1.25 µM (Figure 37c). Thus, to better understand the relationship between CSK^{AS} expressing CAR T cells and the drug, a more comprehensive range of concentrations between 0-1.25 µM would be required.

An interesting observation regarding the dominant-negative effect of CSK^{AS} is that in response to $CD22^{Low(b)}$ targets, although IFN-γ reached a plateau at 1.25 µM of drug, IL-2 failed to reach a plateau at 10 µM (Figure 37l; Figure 37f). This is consistent with literature claiming that the threshold of activation for IL-2 release is higher than IFN-γ (Watanabe et al. 2015).

Against the $CD22^{Low(b)}$ targets, a subtle decrease in IFN-γ was observed in response to drug concentrations above 1.25 µM (Figure 37f), possibly due to the CSK^{AS} system becoming saturated and the drug itself having an inhibitory effect on T cells. Supporting this, cytotoxicity (Figure 35a) and proliferation (Figure 38f and g) were also observed to be inhibited by the addition of the drug. Taken together, this suggests that the CSK^{AS} inhibitor drug, 3-IB-PP1, has a non-specific inhibitory effect on T cells.

PP1 is an inhibitor of SFKs (Hanke et al. 1996). Bishop and colleagues demonstrated that the I338G mutation in the active site of v-Src enabled accommodation of a bulky PP1 analogue inhibitor and reasoned that mutation at the corresponding position in other kinases would also enable inhibition via a PP1 analogue (Bishop et al. 2000). CSK^{AS} was generated by introducing the T266G mutation in its active site, with the PP1 analogue, 3-IB-PP1, identified as a selective inhibitor of CSK^{AS} (Schoenborn et al. 2011).

However, the inhibition of CAR T cell function I observed upon the administration of 3-IB-PP1 indicates that it still possesses the ability to inhibit kinases involved in T cell signalling. Despite this inhibitory effect, I chose to use the drug at the highest concentration tested (10 µM), as for CAR T cells co-expressing CSK^{AS}, the inhibitory effect of the drug was overcome and significant increases in cytotoxicity, IFN-γ and IL-2 production were observed (Figure 35). Additionally, in response to drug, LT22 CSK^{AS} T cells showed significant increases in the percentage of proliferating CAR T cells (Figure 38).

Another benefit of CSK^{AS} expression was highlighted in the absence of drug, wherein CAR T cells bearing CSK^{AS} reduced tonic signalling (Figure 37). Moreover, expression of CSK^{AS} in $CD8^{+}$ CAR T cells led to a small increase in the proportion of cells with a

memory-like phenotype when challenged against antigen negative targets (Figure 39e) or $CD22^{+}$ targets (Figure 39g). This promotion of a memory-like phenotype is desirable as it has previously been shown to enhance T cell persistence and efficacy (Gattinoni et al. 2011; Louis et al. 2011; Xu et al. 2014).

To better understand the mechanism of the CSK^{AS} module, cell lysates were sent to be run on peptide microarrays to analyse PTK activity (6.3.5.6). As CSK inhibits SFKs, many of which play key roles in proximal T cell signalling, it was unsurprising that the co-expression of CSK^{AS} in LT22 CAR T cells was shown to have an inhibitory effect on the overall kinase activity. In total, 66 phosphosites were shown to have less kinase activity (Table 20), many of which belonged to kinase targets involved in TCR signalling, such as CD3ζ, Lck, ZAP-70 and PLC-γ1. A number of the kinases identified to have had a decrease in activity are known substrates of CSK such as the SFK members, Lck and Fyn (Okada et al. 1991; Okada 2012) (Table 21). In turn, ZAP-70 was also observed to be less active. These data suggest that CAR T cells function through the same proximal signalling networks utilised by the TCR. In support of this, a recent study showed that near complete abrogation of CAR T cell activity was achieved by knocking out molecules involved in proximal T cell signalling (Lck, ZAP-70, LAT and SLP-76) (Tousley et al. 2023).

When comparing LT22 CAR T cells and LT22 CSK^{AS} CAR T cells in the presence of drug (Table 22), there was a marked increase in overall kinase activity in CSK^{AS} bearing cells, with many SFKs and ZAP-70 showing higher activity. This finding is consistent with my observation that drug-mediated inhibition of CSK^{AS} resulted in greater phosphorylation of ZAP-70 (Y319) in Jurkats (Figure 36). Moreover, research by Manz and colleagues showed that T cells expressing CSK^{AS} stimulated by either anti-CD3 antibodies or peptide-MHC bore marked increases in the phosphorylation of ZAP-70 and it's substrates (LAT and PLC-γ1) after the addition of the CSK^{AS} inhibitor drug (Manz et al. 2015).

Interestingly, the administration of drug to LT22 CSK^{AS} CAR T cells saw a prominent increase in the activity of the focal adhesion kinases, FAK1 (FAK) and FAK2 (Table 22). Dephosphorylation of the C-terminal regulatory tyrosine residue of Src (an SFK), promotes its localisation to FAK (Kaplan et al. 1994). This binding of Src results in

increased activation of FAK, with the Src/FAK complex able to promote cell survival and proliferation via the PI3K/AKT signalling pathway (Siesser and Hanks 2006). The dominant-negative effect of CSK^{AS} in the presence of the drug causes an overall decrease in phosphorylation of the inhibitory tyrosine residues on SFKs by endogenous CSK, leading to a greater pool of active SFKs. Thus, more active Src results in a higher proportion of activated FAK, explaining the results seen in Table 22.

As discussed above, the addition of the drug elicited low-level inhibition of LT22 CAR T cell cytotoxicity (Figure 35a), IFN-γ production (Figure 35b) and proliferation (Figure 38f and g). To investigate the cellular mechanism behind this inhibition I compared the kinase activity of LT22 CAR T cells with and without the drug. In response to the drug there was an overall decrease in kinase activity, with 56 phosphosites showing a decrease in activity (Table 20). Of the kinases with the largest decrease in activity, 8 of the top 20 belonged to the Src family of kinases (Table 23), further supporting the suggestion that 3-IB-PP1 is not entirely selective for CSK^{AS} and retains some of the SFK inhibitory capabilities of PP1.

In a Nalm6 NSG mouse model, LT22 CAR T cells demonstrated better tumour clearance than LT22 CSK^{AS} CAR T cells (Figure 44), which was consistent with the dampening effect of CSK^{AS} observed *in vitro*. Compared to the cohorts which received injections of vehicle, regular IP injections of drug saw a 1.8-fold increase in the median number of CSK^{AS} bearing T cells and a subsequent 41% decrease in Nalm6 cells (Figure 44b). However, the addition of drug did not result in LT22 CSK^{AS} CAR T cells achieving superior tumour clearance compared to the conventional LT22 CAR T cells *in vivo*.

Interestingly, administration of drug inhibited the proliferation of LT22 CAR T cells *in vivo*, causing a 55% decrease in the median number of cells (Figure 44b, left). Despite this, LT22 CAR T cells still efficiently cleared tumour in the presence of drug (Figure 44b, right).

In addition to the inhibitory effect of the drug on T cells, there are a number of other possible reasons for the modest tuning of CSK^{AS} CAR T cell function *in vivo*, such as

potential poor tissue penetration of the drug, sequestration, or half-life of the drug. This makes *in vivo* administration of the drug complex, as there is a balance to be made between the drug being administered regularly enough and at a sufficient concentration to inhibit the CSK^{AS} module, yet not too regularly/high concentration as to have an inhibitory effect on the T cells. Moreover, when the drug has been metabolised and excreted from the mice, CSK^{AS} bearing cells are being dampened. In this model, it is clear that the optimal drug dosing frequency and concentration were not identified, which may explain the reduced antitumour efficacy of CSK^{AS} CAR T cells compared to the CAR alone cohort after drug administration.

Furthermore, as the T cells administered were only 40% transduced (total of $1x10^6$ transduced T cells) there may have been insufficient numbers of CSK^{AS} expressing cells to enable efficient tuning of CAR T cells *in vivo*. These points highlight the need for optimisation of this Nalm6 NSG mouse model, particularly in terms of drug concentration and dosing. To do so, I suggest running a number of parallel *in vivo* models in which the concentration of drug varies between each model as well as the frequency and/or method of drug delivery. Alternative options for drug delivery include the insertion of an osmotic pump, drinking water supplemented with the drug or IV injections.

In this chapter I demonstrated that the function of CSK^{AS} expressing CAR T cells could be tuned *in vitro* and *in vivo* (albeit modestly). The CSK^{AS} module represents a potential strategy to tune CAR T cells to transiently reduce efficacy or to boost cytokine release and proliferative capacity. Therefore, this system could be utilised to improve CAR T cell sensitivity, improving function against low antigen density targets, yet the same system also allows for sensitivity to be reduced, protecting against on-target off-tumour toxicity.

To date, there have been numerous strategies developed that enable tuneable control over CAR T cell function. However, many of these approaches require re-engineering of the CAR architecture, which in some instances has led to reduced expression of CAR on the cell surface and inferior functionality compared to conventional CARs (Leung et al. 2019; Hotblack et al. 2021; Giordano-Attianese et al. 2020). In comparison, the CSK^{AS} module characterised in this chapter permits

tuneable control of CAR T cell function without the need to alter CAR architecture and displays similar levels of expression to conventional CAR constructs.

7 RESULTS: TUNING OF 14G2A CAR T CELL FUNCTION

7.1 Introduction

The overall aim of this project was to develop a strategy that would enable tuneable control of CAR T cell function. To address both the issue of on-target off-tumour toxicity and of suboptimal CAR T cell sensitivity. In chapter 6 the CSK^{AS} module was characterised in the context of a CD22 targeting CAR platform. The co-expression of CSK^{AS} in LT22 CAR T cells dampened T cell function, with drug-mediated inhibition of CSK^{AS} shown to improve *in vitro* function beyond baseline levels of the conventional CAR. In this setting, the augmentation of CAR T cell function was more relevant than the dampening effect of CSK^{AS}, as data from clinical trials highlighted that relapses after anti-CD22 CAR T cell treatment was due to dimming of CD22 antigen (Fry et al. 2018; Shah et al. 2020; Cordoba et al. 2021).

To demonstrate that the CSK^{AS} system could be applied to another CAR platform I chose to characterise it in a CAR platform targeting the disialoganglioside GD2 (GD2). GD2 is overexpressed on several solid tumours and hence a number of CAR T cell therapies have been developed for the treatment of these tumours, such as melanoma (Gargett et al. 2016), small cell lung cancer (Reppel et al. 2022) and neuroblastoma (Pule et al. 2008; Louis et al. 2011; Heczey et al. 2017; Quintarelli et al. 2018; Straathof et al. 2020). However, as GD2 is also expressed at low levels on tissues of the central nervous system (CNS) (Lammie et al. 1993), it has the potential to cause on-target off-tumour toxicity. In a study comparing two anti-GD2 CARs in a neuroblastoma mouse model, enhanced antitumour activity was associated with lethal on-target off-tumour toxicity, in which CAR T cells targeted the CNS, leading to neuronal destruction (Richman et al. 2018). Moreover, treatment with anti-GD2 antibodies has often been accompanied with side effects of neuropathic pain (Ladenstein et al. 2018; Yu et al. 2010; Navid et al. 2014; Cheung et al. 2012).

In the context of an anti-GD2 CAR, the dampening effect of CSK^{AS} is required to lessen the risk of on-target off-tumour toxicity, while the tuneable control of CAR T cell function is also required to maintain an antitumour response. Thus, in the absence of

the small molecule drug I envisioned co-expression of CSK^{AS} in anti-GD2 CAR T cells to enable efficient lysis of high expressing target cells (representative of tumour cells), whilst sparing low-antigen density targets (representative of healthy cells). In the presence of drug, the activation threshold of CSK^{AS} bearing cells would be lowered, permitting targeting of targets with a lower antigen density.

The anti-GD2 CAR platform I chose to test the CSK^{AS} module in contained a scFv derived from the 14G2a antibody (14G2a CAR). The murine anti-GD2 monoclonal antibody (mAb) 14G2a was identified in 1987 and facilitated lysis of human neuroblastoma cells *in vitro* and suppressed growth of neuroblastoma tumours in immunodeficient mice (Mujoo et al. 1987). Since then, the 14G2a-derived scFv has been utilised in a number of CAR T cell therapies for the treatment of neuroblastoma (Rossig et al. 2001; Pule et al. 2008; 2005; Quintarelli et al. 2018; Louis et al. 2011; Heczey et al. 2017).

7.2 Aim

I have shown the CSK^{AS}-based tuneable system to enable drug-mediated control of LT22 CAR T cell function. However, in this chapter the aim was to utilise the CSK^{AS} module in a CAR platform in which on-target off-tumour toxicity is a more prominent risk. To this end, I aimed to characterise the co-expression of CSK^{AS} in the GD2 targeting platform, 14G2a CAR.

7.3 Results

7.3.1 14G2a CSK^{AS} CAR constructs: structure and transduction efficiency

To investigate the generalisability of the CSK^{AS} system I co-expressed it with two different GD2-specific CARs. Both CARs had the 14G2a scFv, with one CAR containing a CD28 co-stimulatory domain and the other containing a 4-1BB co-stimulatory domain (Figure 45a). PBMCs were successfully transduced with each construct (Figure 45b).

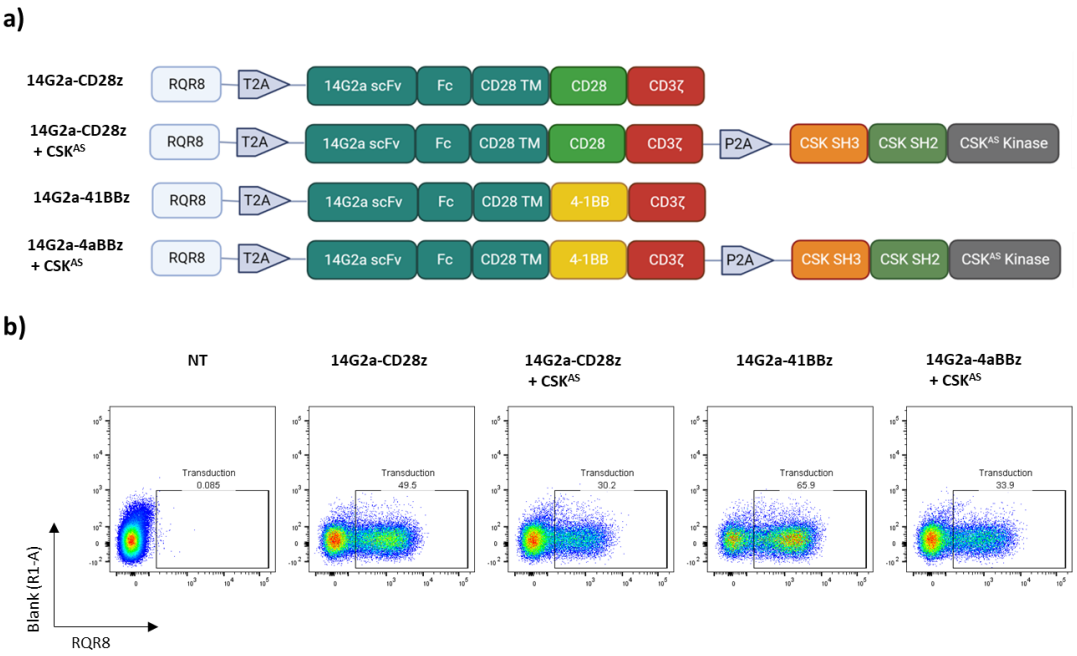

Figure 45. 14G2a CSK^{AS} CAR constructs: Structure and transduction efficiency. a) Construct maps of 14G2a CARs with CD28 or 4-1BB endodomains and either expressed as a conventional CAR or co-expressing CSK^{AS}. All constructs included the RQR8 transduction marker upstream of the CAR. b) Constructs were successfully transduced into PBMCs (one representative donor shown). PBMCs were labelled with an anti-CD34 antibody to detect the RQR8 transduction marker.

7.3.2 GD2 targets antigen density

Most studies measuring the expression of GD2 on tumours and healthy tissue use ELISAs and immunohistochemical stains, making it hard to quantify the antigen density on the cell surface (Terzic et al. 2018; Mujoo et al. 1987; Lammie et al. 1993). GD2 expression on human neuroblastoma cell lines has been shown to range from approximately 4,357-599,163 molecules/cell (Zirngibl et al. 2021). Therefore, to robustly characterise the CSK^{AS} module in CAR T cells targeting GD2, SupT1 target cells with a large range of antigen density were engineered (Figure 46).

a)

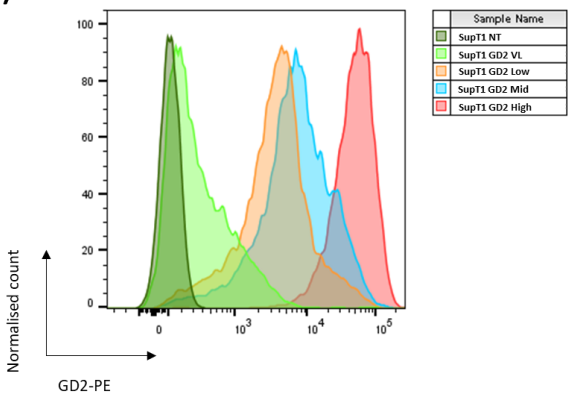

b)

Target cell line	GD2/cell
SupT1 NT	0
SupT1 GD2^{High}	220,834
SupT1 GD2^{Mid}	28,903
SupT1 GD2^{Low}	14,920
SupT1 GD2^{VL}	415

Figure 46. Antigen density of SupT1 GD2 target cells. a) SupT1 cells were transduced to express a GD2 (SupT1 GD2^{High}), these cells were transduced with a plasmid encoding Beta-1,3-galactosyltransferase 4 (B3GALT4) which uses GD2 as a substrate, therefore reducing its expression on the cell surface. The B3GALT4 cells were then sorted on the FACSMelody™ cell sorter for cells expressing high and medium levels of the B3GALT4 plasmid. These sorted cell lines were then single cell cloned by limiting dilution, generating the SupT1 GD2^{mid}, GD2^{Low} and GD2^{VL} cell lines. b) The GD2 surface density was quantified for each cell line using Quantibrite^{TM}.

7.3.3 14G2a CSK^{AS} CAR T cell characterisation

7.3.3.1 14G2a CSK^{AS} CAR: Cytotoxicity and cytokine production of 14G2a CAR T cells with either CD28 or 4-1BB co-stimulatory domains

To test the generalisability of the CSK^{AS} module, it was co-expressed in PBMCs alongside 14G2a CARs containing either CD28 or 4-1BB co-stimulatory domains alongside CD3ζ. T cells were challenged against SupT1 target cells expressing a range of GD2 antigen densities (415-220,834 molecules/cell) in R10 media or R10 media supplemented with 10 µM of the CSK^{AS} inhibitor drug. 72 hours after co-culture initiation, CAR T cell cytotoxicity and cytokine production was analysed (Figure 47).

The expression of CSK^{AS} in 14G2a CD28z CAR T cells markedly reduced background lysis of the GD2 negative SupT1 NT targets, irrespective of the presence of drug (Figure 47a). Against both the GD2^{VL} and GD2^{Low} targets, CSK^{AS} expression significantly dampened cytotoxicity (by 46% and 27%, respectively), yet against the GD2^{High} targets, dampening was not observed. This was likely due to high antigen density leading to a potent activation signal, which was difficult for the CSK^{AS} module to counteract. The addition of drug improved the cytotoxicity of CSK^{AS} expressing CAR T cells when challenged against the GD2^{VL} and GD2^{Low} targets to levels comparable to the 14G2a CD28z control CAR T cells.

Analysis of supernatant from the co-cultures revealed negligible levels of IFN-γ production by 14G2a CD28z CAR T cells when challenged with the SupT1 NT targets (Figure 47c). Against the GD2^{VL}, GD2^{Low} and GD2^{High} targets, CSK^{AS} expressing CAR T cells consistently released less IFN-γ than CAR T cells not expressing CSK^{AS}. Specifically, IFN-γ production was reduced by >95% against both the GD2^{VL} and GD2^{Low} targets and reduced by 68% against the GD2^{High} targets. After the addition of drug, IFN-γ production by CSK^{AS} expressing CAR T cells was restored to levels comparable to the 14G2a CD28z CAR control T cells. The trend observed for IL-2 production (Figure 47e) was similar to that of IFN-γ, with the expression of CSK^{AS} dampening the release of cytokine in response to all target cell lines. Interestingly, the addition of drug was unable to fully restore IL-2 production by CSK^{AS} expressing cells to levels comparable to that achieved by the 14G2a CAR T cells.

14G2a CAR T cells with a 4-1BB co-stimulatory domain achieved only modest lysis of the $GD2^{VL}$ and $GD2^{Low}$ targets (Figure 47b). Hence, co-expression of CSK^{AS} only led to modest dampening of cytotoxicity, reducing target cell lysis by 9% and 14%, respectively. CSK^{AS} expression was not able to dampen cytotoxicity against the $GD2^{High}$ targets. The addition of the drug significantly improved the cytotoxicity of CSK^{AS} expressing CAR T cells, with $GD2^{VL}$ target cell survival decreasing by 43% and $GD2^{Low}$ target cell survival decreasing by 53% compared to the 14G2a 4-1BBz CAR T cells. Almost all (>98%) of the $GD2^{High}$ target cells were lysed by T cells expressing the 14G2a 4-1BBz CAR, regardless of CSK^{AS} expression or the presence or absence of drug.

Against all the target cell lines, production of IFN-γ by 14G2a 4-1BBz CAR T cells expressing CSK^{AS} was reduced compared to the 14G2a control CAR T cells. Significant reduction in IFN-γ release was observed against all $GD2^{+}$ targets, with the largest reduction seen against the $GD2^{High}$ targets (Figure 47d and g). Conversely, in the presence of drug, CSK^{AS} expression in 14G2a 4-1BBz CAR T cells had significantly higher levels of IFN-γ production than the 14G2a 4-1BBz control CAR T cells after being challenged with $GD2^{Low}$ or $GD2^{High}$ target cells.

Against the NT and $GD2^{VL}$ targets, both the 14G2a 4-1BBz control CAR T cells and those bearing CSK^{AS} produced no detectable IL-2 (Figure 47f). However, against the $GD2^{High}$ target cells, 14G2a 4-1BBz CAR T cells produced a mean IL-2 value of 5,340pg/ml. In 14G2a 4-1BBz CAR T cells expressing CSK^{AS}, this value dropped by 90% to 520pg/ml, yet drug administration not only restored the IL-2 production, but CSK^{AS} bearing T cells produced significantly more IL-2 than the 14G2a 4-1BBz control CAR T cells (1.5-fold higher).

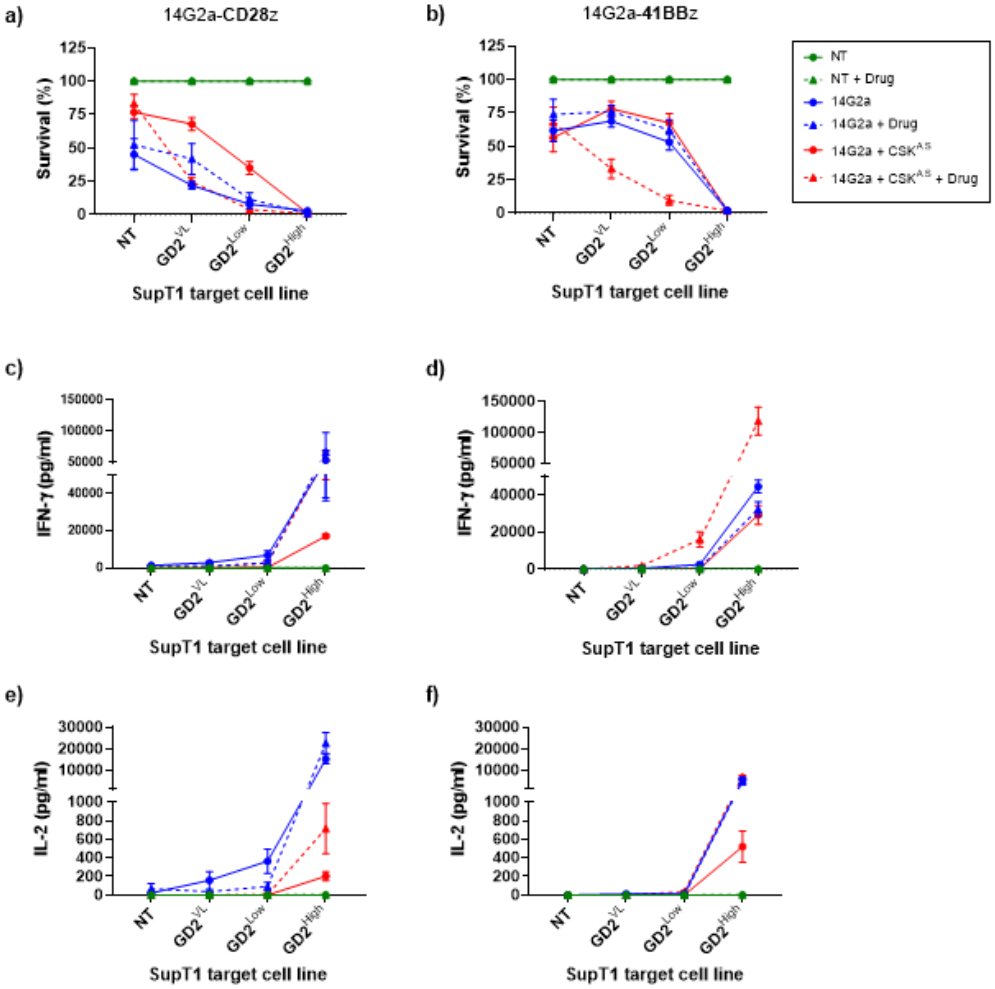

g)

		SupT1 NT		GD2^{VL}		GD2^{Low}		GD2^{High}	
		No Drug	+ Drug	No Drug	+ Drug	No Drug	+ Drug	No Drug	+ Drug
Cytotoxicity	14G2a CD28 Vs 14G2a CD28 + CSK^{AS}	*	ns	***	ns	**	ns	ns	ns
	14G2a 4-1BB Vs 14G2a 4-1BB + CSK^{AS}	ns	ns	ns	**	ns	***	ns	ns
IFN-γ	14G2a CD28 Vs 14G2a CD28 + CSK^{AS}	**	*	***	ns	*	ns	ns	ns
	14G2a 4-1BB Vs 14G2a 4-1BB + CSK^{AS}	ns	ns	*	ns	*	*	***	*
IL-2	14G2a CD28 Vs 14G2a CD28 + CSK^{AS}	ns	ns	ns	**	*	ns	***	**
	14G2a 4-1BB Vs 14G2a 4-1BB + CSK^{AS}	ns	ns	ns	ns	ns	*	**	ns

Figure 47. Cytotoxicity and cytokine production of 14G2a CSK^{AS} CAR T cells with either CD29 or 4-1BB endodomains. a-b) CAR T cells were challenged against SupT1 NT target cells and three SupT1 GD2^{+} cell lines expressing antigen from 415-220,834 molecules/cell. CAR T cell cytotoxicity was analysed by flow cytometry 72h after co-culture set up. The % of target cell survival was calculated. Each condition was tested with 4 donors (n=4), with mean indicated (error bars represent SEM). All data was normalised to NT T cells. Co-cultures were set up with an E:T ratio of 1:2 and in media or media supplemented with 10 µM 3-IB-PP1 (+ Drug). Supernatant taken at 72h after co-culture set up was analysed by ELISA for the presence of IFN-γ (c-d) or IL-2 (e-g) For cytotoxicity, IFN-γ and IL-2 production, statistical analysis was performed using unpaired t-tests to compare the impact of CSK^{AS} co-expression in each condition. * P<0.05, **P<0.01, ***P<0.001, ****P<0.0001.

Comparison of 14G2a CD28z to 14G2a 4-1BBz CAR showed that the former was markedly more cytotoxic than the latter. This difference in potency between the two CARs affected the dynamic range of CSK^{AS} bearing cells. For instance, against the $GD2^{Low}$ targets, the co-expression of CSK^{AS} in 14G2a CD28z CAR T cells dampened mean target cell survival from 7.9% to 35% (Figure 47a). Whereas cytotoxicity of 14G2a 4-1BBz CAR T cells was dampened from 53.1% to 67.5% (Figure 47b). This highlights that with regards to the dampening capacity of CSK^{AS}, the dynamic range was restricted when co-expressed in 14G2a 4-1BB CAR T cells as target cell lysis was modest to begin with.

On the other hand, the increase of function after the addition of drug to CSK^{AS} expressing cells was more pronounced in the 14G2a 4-1BBz CAR T cells. For example, when challenged against the $GD2^{Low}$ targets, the addition of drug to 14G2a CD28 CSK^{AS} T cells saw an 7.7% increase in target cell lysis compared to the 14G2a CD28 T cells (Figure 47a). Whereas, for the 14G2a 4-1BB CSK^{AS} T cells, a 52.7% increase in target cell lysis was observed (Figure 47b).

A similar trend was observed for cytokine release, in which the addition of drug to CSK^{AS} expressing 14G2a 4-1BBz CAR T cells augmented cytokine release (Figure 47d and f), whereas for 14G2a CD28 CAR T cells, cytokine production was comparable or less than the control CAR T cells (Figure 47c and e). This effect is likely because the 14G2a CD28 CAR T cells are more efficient than the 4-1BB CAR T cells, producing close to maximal functional output in response each target cell line. Thus, as the 14G2a 4-1BB CAR T cells are less efficient, there is more room for improvement.

Consequently, the dynamic range of 14G2a 4-1BB CAR T cells expressing CSK^{AS} is wider than that of 14G2a CD28 CSK^{AS} cells. This larger dynamic range makes the 14G2a 4-1BB construct more suitable to demonstrate the capacity of a module for tuning CAR T cell function. Therefore, further characterisation of the CSK^{AS} module was only carried out in the 14G2a 4-1BB CAR T cells (referred to as 14G2a CAR T cells hereafter).

7.3.3.2 14G2a CSK^{AS} CAR: Drug titration

To investigate whether the function of 14G2a CAR T cells bearing the CSK^{AS} module could be regulated by the drug in a dose dependant manner, I analysed T cell cytotoxicity and cytokine release in response to increasing concentrations of the drug (Figure 48). Co-cultures were set up with T cells challenged against SupT1 NT targets, GD2^{Mid} targets and GD2^{VL} target cells.

In the absence of drug, there was background cytotoxicity observed against the NT target cells by the 14G2a T cells, however this was dampened upon co-expression of CSK^{AS}, which led to a 16.2% increase in mean target cell survival (Figure 48a).

When challenged against the GD2^{Mid} target cells, both the 14G2a and 14G2a CSK^{AS} T cells efficiently lysed > 95% of target cells, regardless of the presence or absence of drug (Figure 48b). Interestingly, despite no inhibition of cytotoxicity observed against the GD2^{Mid} targets, co-expression of the CSK^{AS} dampened both IFN-γ (Figure 48e) and IL-2 (Figure 48h) production, by 56.3% and 75.8%, respectively.

In the presence of drug, mean IFN-γ production by the 14G2a CAR T cells fluctuated between 32,885 and 49,080 pg/ml. In the CSK^{AS} expressing cells, mean IFN-γ production peaked at 77,855 pg/ml after the addition of drug at a concentration of 1.25 µM before plateauing. At this concentration, the CSK^{AS} expressing CAR T cells produced 2.3-fold more IFN-γ than the 14G2a control CAR T cells (Figure 48e). A similar trend was observed with regards to IL-2 production, but in this case cytokine production by the CSK^{AS} expressing cells peaked earlier, after the addition of 0.313 µM drug. At this concentration of drug, CSK^{AS} expressing CAR T cells produced 1.6-fold more IL-2 than the 14G2a control CAR T cells (Figure 48h).

Against the GD2^{VL} cell line, expression of CSK^{AS} dampened the modest cytotoxicity of the 14G2a CAR T cells, resulting in an 18.9% increase in target cell survival (Figure 48c). Increasing the concentration of the drug from 0.156 µM to 10 µM improved the cytotoxicity of 14G2a CSK^{AS} T cells, with mean target cell survival decreasing from 44.2% to 13.7%. The biggest increase in cytotoxicity of the CSK^{AS} expressing cells was observed in response to 10 µM drug, which led to a 36.4% increase in mean target cell lysis compared to the 14G2a CAR T cells.

In addition to dampening of cytotoxicity, co-expression of CSK^{AS} completely abolished IFN-γ production against the $GD2^{VL}$ targets (Figure 48f). When co-cultures were supplemented with 0.156 µM of the drug, CSK^{AS} expressing CAR T cells improved IFN-γ production by 3-fold compared to the 14G2a CAR T cells. Increasing the concentration of the drug to 1.25 µM led to a 5.6-fold higher level of IFN-γ production, but the response to drug then plateaued. Against the $GD2^{VL}$ target cells, only negligible levels of IL-2 production were detected by the CAR T cells, irrespective of CSK^{AS} expression or drug concentration (Figure 48i).

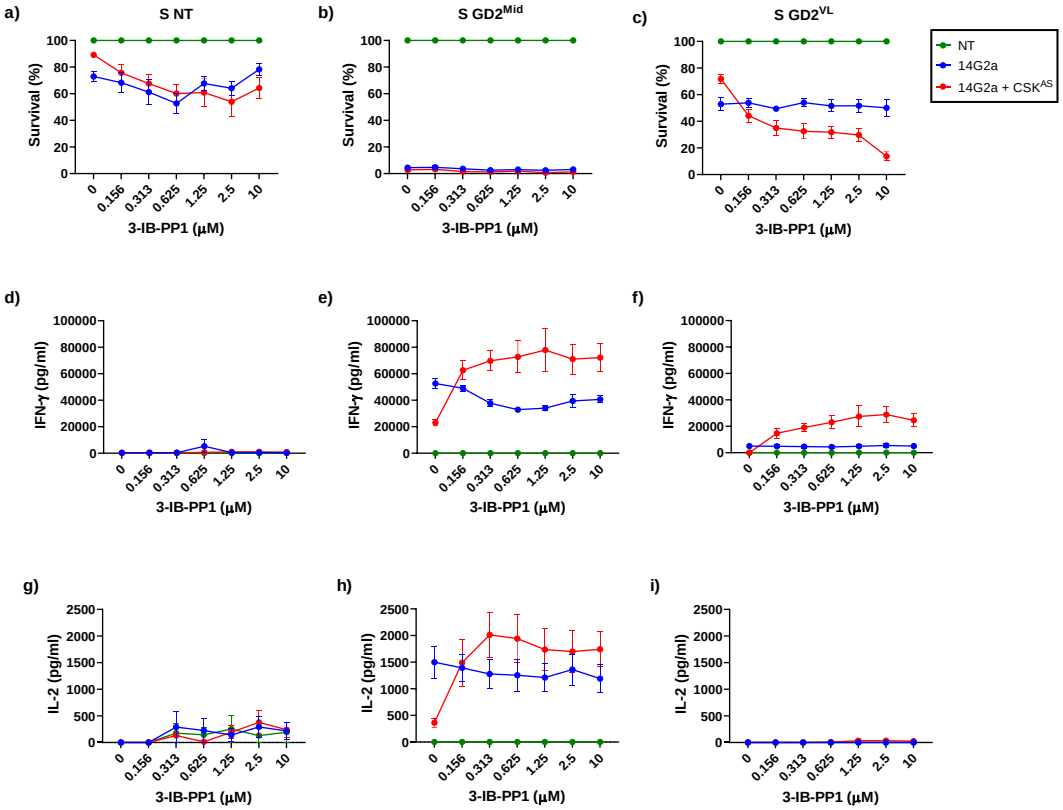

Figure 48. 14G2a CSK^{AS} CAR T cell function in response to drug titration. a-c) Co-cultures were set up with an E:T ratio of 1:4. T cells were challenged against SupT1 NTs (left column), SupT1 GD2^{Mid} (28,903 molecules/cell) (middle column) and SupT1 GD2^{VL} (415 molecules/cell) target cells (right column). On day 3 after co-culture set up, CAR T cell cytotoxicity was analysed by flow cytometry. Each condition was tested with 4 donors (n=4), with mean indicated. All data was normalised to NT T cells. 72h post co-culture set up, supernatant was analysed by ELISA for the presence of IFN-γ (d-f) or IL-2 (g-i).

7.3.3.3 14G2a CSK^{AS} CAR: Proliferation

The ability for CAR T cells to proliferate is a key component of effective CAR T cell function. To investigate the proliferative capacity of the 14G2a CSK^{AS} CAR T cells, co-cultures were set up challenging transduced T cells against either SupT1 NT or GD2^{VL} target cells. Prior to assay set up, all T cells were labelled with the proliferative dye, CTV.

Against the antigen negative SupT1 NT target cells, the addition of drug to CSK^{AS} bearing T cells unexpectedly led to a higher percentage of proliferation than that seen for the 14G2a control CAR T cells (Figure 49b). This was possibly due to the drug-mediated inhibition of CSK^{AS} lowering the T cell activation threshold, resulting in some tonic signalling. However, this observation was not supported when I analysed the CTV MFI, which showed that in the addition of drug to CSK^{AS} expressing cells led to higher levels of CTV, indicating less proliferating cells in this population than the 14G2a CAR T cell control population (Figure 49d).

When challenged against GD2^{VL} target cells, CSK^{AS} bearing T cells showed 9.4% lower proliferation compared to the 14G2a control CAR T cells. However, after drug administration, CAR T cells expressing CSK^{AS} showed a 20.0% increase in proliferation (Figure 49c). Analysis of the MFI of CTV demonstrated that 14G2a CSK^{AS} CAR T cells challenged against the GD2^{VL} targets had 1.4-fold higher MFI than the 14G2a CAR T cells, indicating a dampening effect. Whilst in the presence of the drug, a 0.6-fold reduction in MFI was observed compared to the 14G2a CAR T cells, demonstrating an increase in proliferation (Figure 49e).

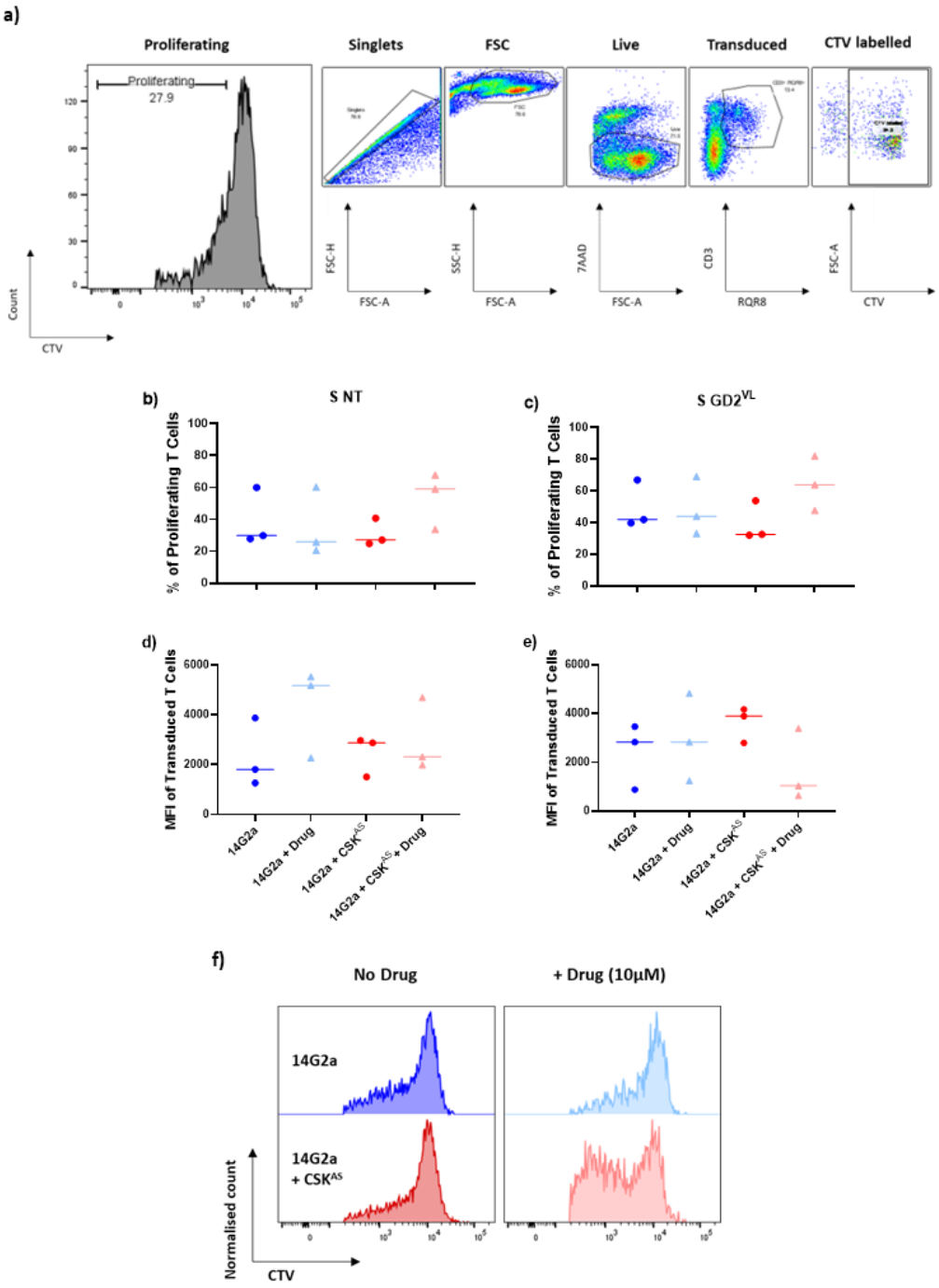

Figure 49. Proliferation of 14G2a CSK^{AS} CAR T cells. a) Example gating strategy to plot the percentage of proliferating CAR T cells. b-g) CAR T cells labelled with CTV were challenged against SupT1 NT (b and d) or SupT1 GD2^{VL} (415 molecules/cell) target cells (c and e). Proliferation was analysed by flow cytometry on day 7 post co-culture set up and each condition was tested with a minimum of 3 donors (n=3). Median indicated by horizontal lines. Statistical analysis was performed by using unpaired t-tests (*P<0.05, **P<0.01, ***P<0.001, ****P<0.0001) comparing 14G2a CAR against 14G2a CSK^{AS} CAR T cells within each condition (no drug or + drug) and comparing the effect of the drug. However, none of the comparisons reached significance. b-c) Plots of the % of proliferating transduced and CTV^{+} T cells. d-e) Plots showing the MFI of all transduced and CTV^{+} T cells. f) Representative histogram plots of CTV dilution from CAR T cells co-cultured with GD2^{VL} targets (e).

7.3.3.4 14G2a CSK^{AS} CAR: Memory phenotype

As previously mentioned (6.3.5.4), a more undifferentiated memory/stem like phenotype is associated with improved persistence and efficacy in CAR T cells (Gattinoni et al. 2011; Louis et al. 2011; Xu et al. 2014). The memory phenotype of 14G2a CAR T cells with and without CSK^{AS} was analysed after the initiation of co-cultures with SupT1 NT, GD2^{Low} and GD2^{VL} target cells. CD4^{+} and CD8^{+} T cell subsets were analysed for expression of CCR7 and CD45RA to determine the proportion of each memory phenotype in the cell population (Figure 50).

Against the SupT1 NT target cells, CSK^{AS} expressing cells showed very marginal increases of naïve and central memory cells compared to control CAR T cells. In the absence of drug, the CD4^{+} 14G2a CAR T cells expressing CSK^{AS} had a 4.6% larger Tn cell population than the 14G2a control CAR T cells (unpaired t-test, **P = 0.0032) (Figure 50b), with the CD8^{+} cells having 4.5% more Tn cells (unpaired t-test, *P = 0.0211) (Figure 50e). In the presence of drug, CSK^{AS} bearing CD4^{+} 14G2a CAR T cells had 6.9% larger Tcm population than the control 14G2a CAR T cells (unpaired t-test, ns, P = 0.0803) (Figure 50b).

When challenged against the GD2^{Low} cell lines, the CD4^{+} 14G2a and 14G2a CSK^{AS} CAR T cells had comparable proportions of each memory phenotype subset (Figure 50c). Moreover, in this CD4^{+} subset, the addition of the drug bore little impact on CAR T cell differentiation. However, in the CD8^{+} subset, the addition of drug to CSK^{AS} expressing cells led to a 7.6% increase in the proportion of Teff cells (unpaired t-test, *P = 0.0148) (Figure 50f). Against the GD2^{VL} target cells, the expression of CSK^{AS} was seen to have negligible impact on the memory phenotype of 14G2a CAR T cells, regardless of the presence or absence of drug (Figure 50d and g).

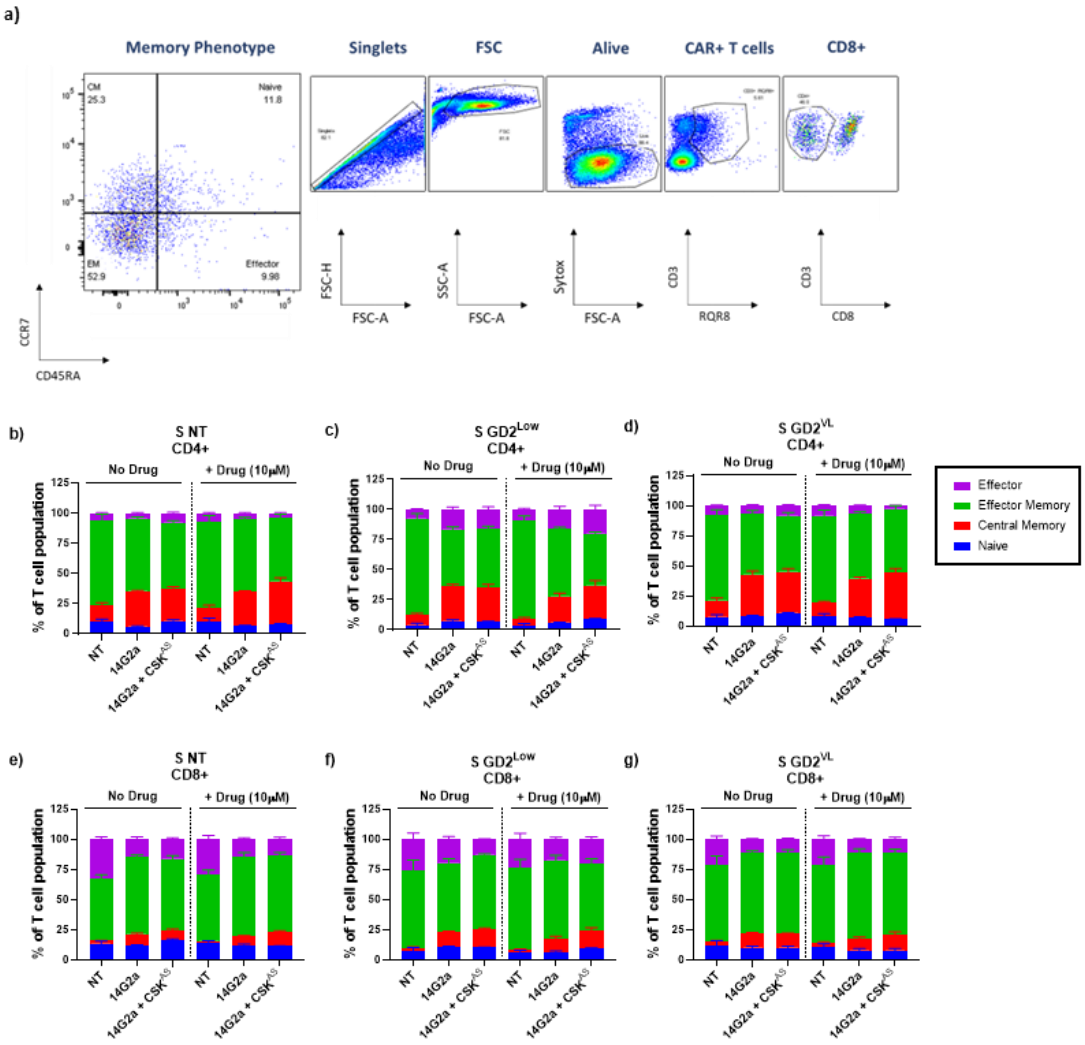

Figure 50. Memory phenotype of 14G2a CSK^{AS} CAR T cells. a) Gating strategy to determine the memory phenotype of the T cell populations. b-g) T cells were co-cultured with either SupT1 NT (b and e), SupT1 GD2^{Low} (c and f) or SupT2 GD2^{VL} (d and g) target cells at an E:T ratio of 1:2. Co-cultures were set up in media with no 3-IB-PP1 (no drug) or in media supplemented with 10 μM 3-IB-PP1 (+ drug). On day 4 after assay set up, T cells were analysed for the expression of CCR7 and CD45RA to determine their memory phenotype. The bar charts display the mean percentages of each memory phenotype population (n=4).

7.3.3.5 14G2a CSK^{AS} CAR: Exhaustion phenotype

Characterisation of T cell exhaustion is of importance as it has been linked to poor antitumour efficacy (Eyquem et al. 2017; Fraietta et al. 2018; Long et al. 2015). The drug-mediated inhibition of CSK^{AS} in CAR T cells has been shown to lower their activation threshold, improving their function against low antigen density target cells (Figure 47). However, lowering the activation threshold of CAR T cells may also increase their propensity to become exhausted. The expression of PD-1, Tim-3 and Lag-3 on the cell surface are all indicators of exhaustion. Therefore, I analysed the expression of these markers in 14G2a and 14G2a CSK^{AS} T cells after 4-day co-cultures (Figure 51).

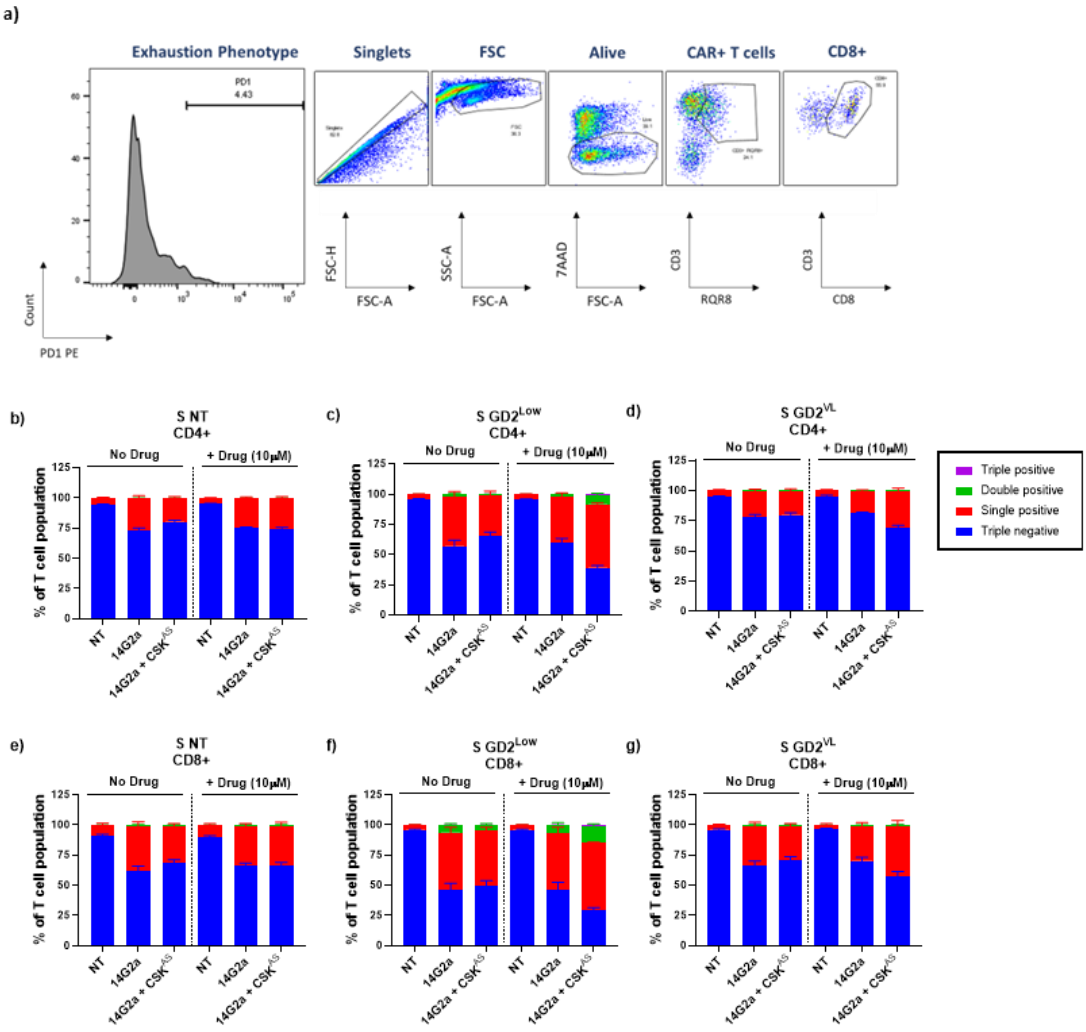

Figure 51. Exhaustion phenotype of 14G2a CSK^{AS} CAR T cells. Example gating strategy for the analysis of the expression markers Tim-3, Lag-3, and PD-1 on T cells. b-g) T cells were co-cultured with either SupT1 NT (b and e), SupT1 GD2^{Low} (c and f) or SupT2 GD2^{VL} (d and g) target cells at an E:T ratio of 1:2. Co-cultures were set up in media with no 3-IB-PP1 (no drug) or in media supplemented with 10 µM 3-IB-PP1 (+ drug). On day 4 after assay set up, T cells were analysed for the expression of Tim-3, Lag-3, and PD-1 to determine their exhaustion phenotype. The bar charts display the mean percentages of different exhaustion phenotype populations (n=4).

When challenged against SupT1 NT cells, CAR T cells expressing CSK^{AS} had a similar exhaustion phenotype to the 14G2a control CAR T cells in both the $CD4^+$ (Figure 51b) and $CD8^+$ (Figure 51e) subsets. However, in the absence of drug, the CSK^{AS} expressing cells had a 7% bigger triple negative population than the 14G2a CAR T cells in the $CD4^+$ subset (unpaired t-test, *P = 0.0410) (Figure 51b), and 6.8% more triple negative cells in the $CD8^+$ subset (unpaired t-test, ns, P = 0.2395) (Figure 51e).

Against the $GD2^{Low}$ target cells, in co-cultures with no drug, 14G2a and 14G2a CSK^{AS} T cells displayed comparable levels of exhaustion markers expressed on their surface (Figure 51c and f). Interestingly, the triple negative population was again observed to be higher in CSK^{AS} expressing cells. CAR T cells bearing CSK^{AS} had 8.3% more triple negative cells than the 14G2a CAR T cells in the $CD4^+$ subset (unpaired t-test, ns, P = 0.2242) (Figure 51c) and a marginal increase of 3.9% was observed in the $CD8^+$ subset (unpaired t-test, ns, P = 0.6212) (Figure 51f).

The addition of the drug to 14G2a CSK^{AS} T cells increased the mean proportion of single positive cells by 18.5% in the $CD4^+$ subset (unpaired t-test, **P = 0.0022) (Figure 51c) and 10.3% in the $CD8^+$ subset (unpaired t-test, **P = 0.0161) (Figure 51f). Moreover, the mean proportion of double positive cells increased 6.7% (unpaired t-test, **P = 0.0065) and 9.1% (unpaired t-test, **P = 0.0042), respectively.

A similar trend was observed when 14G2a CSK^{AS} T cells were challenged against the $GD2^{VL}$ targets; in the presence of the drug, the mean proportion of single positive cells increased 11.1% in the $CD4^+$ subset (unpaired t-test, *P = 0.0101), (Figure 51d) and 14.6% in the $CD8^+$ subset (unpaired t-test, *P = 0.0261) (Figure 51g). However, unlike against the $GD2^{Low}$ targets, when challenged against the $GD2^{VL}$ cell line there was no increase in the proportion of double positive cells (Figure 51g and g). This is likely due to the $GD2^{VL}$ target cells having a lower antigen density than the $GD2^{Low}$ cell line, resulting in less activated CAR T cells and subsequently a lower proportion of exhausted cells.

7.4 Summary

GD2 is overexpressed on a number of solid tumours such as melanoma, small cell lung cancer and neuroblastoma, making it an attractive target for CAR T cell therapies

(Gargett et al. 2016; Reppel et al. 2022; Pule et al. 2008; Louis et al. 2011; Heczey et al. 2017; Quintarelli et al. 2018; Straathof et al. 2020). Although GD2 constitutes a promising target for CAR T cells, it is also expressed at low-level on tissues within the CNS. Hence, on-target off-tumour toxicity is a potential risk of anti-GD2 CAR T cell therapies (Lammie et al. 1993; Richman et al. 2018).

In this chapter I aimed to investigate the CSK^{AS} module as a means of tuning 14G2a CAR T cell function to avoid CAR-mediated on-target off-tumour toxicity. There have been a number of studies with CAR T cells containing the 14G2a scFv for the treatment of neuroblastoma. Initially, first generation CARs with only a CD3ζ endodomain were tested, demonstrating the feasibility of targeting GD2 for treatment of neuroblastoma, but the CAR T cells lacked sufficient proliferative capacity in response to antigen (Rossig et al. 2001). To improve CAR T cell function, a number of 14G2a-based CARs have since been developed containing different combinations of co-stimulatory domains (Pule et al. 2005; Heczey et al. 2017; Quintarelli et al. 2018). Thus, in order to investigate whether the CSK^{AS} module is generalisable and can be utilised in CARs with different endodomains, I expressed it alongside 14G2a CAR T cells with either a CD28 or 4-1BB co-stimulatory domain.

Co-expression of CSK^{AS} inhibited the function of 14G2a CD28 and 14G2a 4-1BB CAR T cells (Figure 47), and whilst inhibition of CSK^{AS} enabled augmentation of 4-1BB CAR T cell function, it only led to restoration of CD28 CAR T cells to baseline levels. This lack of functional augmentation could be due to the potent baseline level of functionality achieved by CAR T cells with the CD28 co-stimulatory domain. Whereas the 14G2a 4-1BB CAR T cells were less potent and displayed only modest cytotoxicity against both the $GD2^{VL}$ and $GD2^{Low}$ targets. Therefore, the inhibition of CSK^{AS} enabled improvement of cytotoxicity over a larger dynamic range compared to the 14G2a CD28 CAR T cells.

These data are in line with a previous study in which CD28 CAR T cells showed enhanced cytotoxicity and cytokine release compared to 4-1BB CAR T cells when challenged against targets with low antigen density (Majzner et al. 2020). This difference in CAR sensitivity has been attributed to higher basal phosphorylation of CAR-associated CD3ζ chains and Lck in CD28 CARs leading to faster and more

pronounced phosphorylation of proximal T cell signalling molecules, such as ZAP-70 and PLC-γ1 (Salter et al. 2018). As the co-expression of CSK^{AS} in 14G2a 4-1BB CAR T cells enabled drug-mediated control over a larger dynamic range than the 14G2a CD28 CAR T cells it was considered more suited to demonstrating the capacity of a module for the tuning of CAR T cell function. For this reason, along with the lower levels of tonic signalling, only the 14G2a 4-1BB CAR was taken forward for further characterisation.

Drug-mediated inhibition of the CSK^{AS} module in 14G2a CAR T cells led to improved cytotoxicity, cytokine release (Figure 48) and proliferation (Figure 49) compared to conventional 14G2a CAR T cells. I believe this augmentation of function in response to antigen is predominantly due to a dominant-negative effect of the drug inhibited CSK^{AS} module, whereby CSK^{AS} binds membrane anchors in lipid rafts, blocking endogenous CSK localising to the membrane and inhibiting T cell signalling.

However, the increased intensity and sensitivity of the CSK^{AS} bearing GD2 CAR T cells could also be attributed to a reduction in tonic signalling. In the absence of drug, CSK^{AS} reduced cytotoxicity against SupT1 NT target cells (Figure 48a) and reduced the basal expression of exhaustion markers on 14G2a 41BB CAR T cells, eliciting a 8.3% decrease in the proportion of $CD8^+$ cells expressing at least one marker (Figure 51e). In support of these data, research by Weber and colleagues has shown that intermittent dampening of CAR signalling resulted in improved functionality (Weber et al. 2021). In this study, CAR signalling was transiently inhibited by either drug-regulated reduction of CAR expression or via administration of an Src kinase inhibitor drug (dasatinib). Exhausted CAR T cells or CAR T cells undergoing *ex vivo* expansion that were subjected to periods of signal inhibition, or “rest”, had reduced expression of exhaustion markers and demonstrated improved function *in vitro* and *in vivo* (Weber et al. 2021).

In response to $GD2^{Low}$ target cells, drug administration led to a subtle increase in exhaustion markers on the surface of CSK^{AS} expressing 14G2a CAR T cells, with the mean proportion of double positive cells increasing 6.7% in the $CD4^+$ subset (Figure 51c) and 9.1% in the $CD8^+$ subset (Figure 51f). This increase in exhaustion markers was not seen to be associated with poor CAR T cell function *in vitro*, as the drug-

mediated inhibition of CSK^{AS} permitted improved cytotoxicity (Figure 47b), IFN-γ release (Figure 47d) and proliferation (Figure 49c and e) of 14G2a CAR T cells against $GD2^{+}$ targets. However, the timeframe of these functional readouts may not be long enough (all ≤ 4 days) to make a conclusion on the impact CSK^{AS} has on CAR T cell exhaustion. To investigate this in the future, assays whereby CSK^{AS} bearing CAR T cells undergo multiple stimulations with antigen positive target cells over a number of weeks would be more appropriate.

A plethora of strategies have been developed to reduce the risk of CAR-mediated on-target off-tumour toxicity, such as tuning the CAR affinity, logic gates and tuneable CARs. However, a caveat of these strategies is that they require reengineering of current CAR platforms. The CSK^{AS} module on the other hand, can be co-expressed alongside a CAR without requiring a change in the CAR architecture. Co-expression of CSK^{AS} is capable of dampening CAR T cell efficacy against low antigen density targets whilst maintaining efficacy against high antigen density target cells (Figure 47).

Despite the concern of CAR-mediated on-target off-tumour toxicity, a number of anti-GD2 CAR T cell clinical trials have proven to be safe (Pule et al. 2008; Louis et al. 2011; Heczey et al. 2017; Straathof et al. 2020; Quintarelli et al. 2018). Yet, poor expansion, persistence and antitumour efficacy remain challenges of anti-GD2 CAR T cell therapies. Drug-mediated inhibition of CSK^{AS} enabled augmentation of CAR T cell cytotoxicity (Figure 48c) and IFN-γ production (Figure 48f) against targets expressing as low as 415 molecules/cell. As drug-mediated inhibition of CSK^{AS} has been shown to improve CAR T cell function, it has the potential to improve the persistence of such anti-GD2 CARs.

8 DISCUSSION

8.1 dnCSK: Improving CAR T cell sensitivity

In clinical trials of CAR T cells targeting CD22 for the treatment of B-ALL, patient relapse has been attributed to inefficient tumour eradication due to low antigen density, highlighting a need to improve CAR T cell sensitivity (Fry et al. 2018; Shah et al. 2020; Cordoba et al. 2021).

It has been approximated that CAR T cell sensitivity is 100- to 1,000-times lower than the TCR (Burton et al. 2023). Engagement of the TCR with a single pMHC complex is sufficient to activate the T cell and induce cytokine production (Sykulev et al. 1996; Huang et al. 2013), whereas CAR T cells require an antigen density in the range of 770-5,320 molecules/cell to produce cytokines (Stone et al. 2012; Watanabe et al. 2015). There are a number of differences between CAR- and TCR-mediated signalling that could explain the discrepancy in sensitivity. Compared to the immunological synapse formed after TCR engagement with pMHC complexes, CAR T cells form disorganised microclusters with no distinct LFA-1 enriched region (Davenport et al. 2018). Moreover, a recent study has shown that inefficient utilisation of adhesion receptors such as LFA-1 (and CD2) by CARs contributes to their inferior sensitivity (Burton et al. 2023). Research groups have also found that ITAMS within the cytoplasmic tails of the CD3 chains, as well as ZAP-70 and LAT were all phosphorylated to a lesser degree after CAR stimulation (Gudipati et al. 2020; Salter et al. 2021).

To improve the sensitivity of CAR T cells, various strategies have been employed and numerous studies have demonstrated that increasing CAR affinity can improve sensitivity (Hudecek et al. 2013; Chames et al. 2002; Lynn et al. 2016; Caruso et al. 2015; Liu et al. 2015; Chmielewski et al. 2004). However, the process of increasing affinity is challenging, and excessively high affinity CARs can limit T cell proliferation due to AICD (Watanabe et al. 2014). Additionally, one research group demonstrated a negative correlation between CAR affinity and sensitivity, with low affinity CARs associated with higher sensitivity (Turatti et al. 2007). It was suggested that the low affinity CAR performed better than the high affinity CAR due to a shorter duration of

CAR-antigen binding, allowing for serial triggering which in turn may amplify signalling to enable CAR T cell activation. This is supported by data from a clinical study in which a low affinity CD19 targeting CAR was associated with better expansion and longer persistence in patients with ALL (Ghorashian et al. 2019). The contradictory data and complex relationship between CAR affinity and sensitivity make it a difficult strategy to utilise to improve CAR function against low antigen density targets.

Other strategies to improve CAR sensitivity include changing of the CAR hinge/transmembrane domain and altering the signalling domains. Majzner and colleagues demonstrated that CARs with a CD28 hinge/transmembrane domain had a lower antigen density threshold for activation than CARs bearing a CD8 hinge/transmembrane domain (Majzner et al. 2020). The same group also demonstrated that expression of two CD3ζ chains in tandem also lowered the CAR T cell activation threshold, improving function against low antigen density targets both *in vitro* and *in vivo*. By expressing a truncated form of the CD3ε chain or the SH2 domain from GRB2 (an adapter molecule that aids the activation of LAT) in the endodomain of CAR T cells, Salter and colleagues also demonstrated that altering the signalling domain of CARs could improve sensitivity (Salter et al. 2021). Modifying CAR architecture to improve sensitivity is an important consideration in the design and optimisation of new CAR platforms, but for existing CAR platforms such structural alterations are less practical. Therefore, there is a need for an alternative strategy to improve the sensitivity of CAR T cells without changing the CAR architecture.

Recently identified CSK-specific inhibitors have the potential to improve the sensitivity of CAR T cells. Although they are yet to be investigated clinically, when administered to mice, two compounds identified by O'Malley and colleagues were shown to elicit significant reductions in the phosphorylation of the inhibitory tyrosine residue on Lck (Y505) (O'Malley et al. 2019). This reduction of Lck inhibition would increase the pool of Lck in an active state, in turn lowering the activation threshold of T cells and enhancing function against low antigen density targets. The administration of a CSK inhibitor could thus be used to "release the breaks" of CAR T cells, and this approach to improving CAR T cell sensitivity would not require re-

engineering of CAR architecture. However, administration of a CSK inhibitor drug would not be specific to CAR T cells and would affect other immune cells such as NK cells, T cells and B cells. As CRS is a common adverse effect of CAR T cell therapy, lowering the threshold of activation of these immune cells may exacerbate this systemic inflammatory toxicity.

To address the issue of CAR T cell sensitivity I aimed to develop a module that is co-expressed independently of the CAR. In chapter 4, I validated the inhibitory effect of CSK on CAR T cells. This was an important step as it demonstrated that CSK was a viable candidate to exploit in order to manipulate CAR T cell function. Then in chapter 5 I focused on engineering dnCSK modules. I tested three distinct dnCSK modules by co-expressing them in different CAR T cell platforms, with two of the modules being truncated forms of CSK and the third dnCSK a catalytically inactive mutant. All of the modules retained the SH2 domain of CSK which is required for the dominant-negative effect, as it enables binding to membrane anchors and subsequently blocks localisation of endogenous CSK to the plasma membrane.

I found that co-expression of the dnCSK modules improved the cytotoxicity and cytokine release of LT22 (Figure 24) and CAT19 (Figure 30) CAR T cells against low antigen density targets, with the most notable changes observed in CAR T cells co-expressing the dCSK(del_kinase_SH3). Interestingly, when expressed in FMC63 CAR T cells, expression of any of the dnCSK modules elicited only minimal improvement to CAR T cell function (Figure 27). This could be because against the target cells lines tested, the FMC63 CAR T cells were already producing close to their maximum functional response. This highlights a caveat of the dnCSK modules, in that they are not able to improve the sensitivity of efficient CAR platforms.

The dnCSK modules, specifically dCSK(del_kinase_SH3), represent a viable strategy to improve CAR T cell sensitivity, possessing an advantage over existing approaches in that they are expressed as a standalone module and require no modification of the CAR architecture. Thus, they represent agnostic modules that could be easily implemented into existing CAR platforms.

8.2 CSK^{AS} as a module to tune CAR T cell function

The scarcity of tumour-specific antigens has led to numerous CAR T cell therapies being developed that target antigens which are commonly expressed at high density on tumour cells but also expressed at low density on healthy tissues. The expression of antigen on both tumour cells and healthy tissues increases the risk of CAR-mediated on-target off-tumour toxicity (Morgan et al. 2010; Thistlethwaite et al. 2017; Lamers et al. 2013), which has led to the development of a number of different strategies aimed at reducing this risk.

Affinity tuning CARs to enable differentiation between targets with either high or low antigen expression levels is a strategy suggested by some groups to avoid on-target off-tumour toxicity (Caruso et al. 2015; Liu et al. 2015; Park et al. 2017). These studies show that lower affinity CAR T cells are able to efficiently target tumour cells expressing a high antigen density while sparing cells with low antigen density. However, achieving the balance between antitumour activity and avoiding on-target off-tumour toxicity via affinity tuning is challenging, as the optimal antigen density threshold varies between different diseases and also between patients. Moreover, lowering the affinity of the CAR scFv potentially reduces the sensitivity of the CAR, which could enable tumour escape.

CAR T cell platforms applying Boolean logic gating allows for the activation of CAR T cells only in response to a specific combination of antigens, with numerous research groups having employed logic gate strategies to improve CAR T cell specificity and reduce the risk of on-target off-tumour toxicity (Kloss et al. 2013; He et al. 2020; Lajoie et al. 2020; Lanitis et al. 2013; Fedorov, Themeli, and Sadelain 2013; Srivastava et al. 2019; Roybal et al. 2016; Tousley et al. 2023). In some cases, a split CAR approach is taken, with two CARs expressed that target different antigens, with one CAR expressing the CD3ζ chain and the other CAR expressing a co-stimulatory domain (Lanitis et al. 2013). Although such an approach reduces the risk of on-target off-tumour toxicity it does not eliminate it, as CARs expressing CD3ζ alone are able to trigger an activation response (Eshhar et al. 1993).

A recent study by Tousley and colleagues elegantly described a logic gate CAR termed "LINK CAR", in which LAT and SLP-76 are utilised as the signalling domains of two CARs specific for independent targets (Tousley et al. 2023). LINK CAR T cells demonstrated high specificity *in vitro* and *in vivo*, with CAR T cells only becoming functionally activated in response to double positive targets. However, the issue of CAR sensitivity was not addressed in this study. Therefore, despite reducing the risk of on-target off-tumour toxicity through improved specificity, a potential lack of sensitivity to low antigen density targets could allow for tumour escape.

Another approach to safeguard against CAR-associated toxicities is the engineering of suicide switches. Suicide switches are activated once toxicities have developed and permanently delete the engineered T cells. The expression of surface molecules such as EGFRt (Wang et al. 2011; Paszkiewicz et al. 2016) and RQR8 (Philip et al. 2014) on CAR T cells has been shown as an effective strategy to selectively clear CAR T cells in response to the onset of adverse events. The administration of antibodies specific for these surface markers (cetuximab and rituximab, respectively) enables the elimination of CAR T cells via Complement-Dependent Cytotoxicity (CDC) or Antibody-Dependent Cell-Mediated Cytotoxicity (ADCC). Alternative suicide switches have also been engineered that cause apoptosis after the drug-mediated dimerization of caspase-9 containing monomers (Straathof et al. 2005; Stavrou et al. 2018). Although suicide switches constitute an efficient strategy to manage CAR T cell-mediated toxicities, the CAR T cell elimination also entails the loss of the antitumour effect.

As mentioned above, activation of suicide switches results in the permanent ablation of CAR T cells and thus also eradicates antitumour efficacy. This highlights the need for an approach that allows for reversible and temporal control of CAR activation. To this end, there have been numerous iterations of tuneable CAR systems developed, which can be broadly grouped into either drug-ON systems in which both antigen and drug are needed for activation (Wu et al. 2015; Juillerat et al. 2016; Leung et al. 2019; Labanieh et al. 2022; Sahillioglu et al. 2021), or drug-OFF systems wherein the administration of the drug reduces CAR T cell function (Juillerat et al. 2019; Sun et al. 2020; Giordano-Attianese et al. 2020; Hotblack et al. 2021).

Despite their elegant engineering, tuneable CAR platforms have a number of different limitations. These include the use of immunosuppressive drugs (Juillerat et al. 2016; Wu et al. 2015; Sun et al. 2020; Leung et al. 2019), and the incorporation of potentially immunosuppressive components such as the virally derived NS3 protease (Wu et al. 2015; Juillerat et al. 2019; Labanieh et al. 2022; Sahillioglu et al. 2021) or the tetracycline repressor protein which is of bacterial origin (Hotblack et al. 2021). Additionally, some tuneable CARs have shown inferior IL-2 production compared to conventional CAR T cells (Wu et al. 2015; Giordano-Attianese et al. 2020).

In splitting the CAR so that the binding domain and signalling domain are expressed as separate peptides, some groups have observed a negative impact on the stability of these tuneable CARs which has led to lower surface expression compared to conventional CARs (Leung et al. 2019; Hotblack et al. 2021; Giordano-Attianese et al. 2020). Although lower levels of CAR expression on the T cell surface may reduce sensitivity to antigen, high CAR expression is associated with increased tonic signalling and AICD (Gomes-Silva et al. 2017). CAR T cells with a low CAR expression have demonstrated improved engraftment, persistence and tumour clearance in mice compared to cells with high CAR expression (Frigault et al. 2015). This finding is supported by recent clinical data, in which patients that demonstrated a partial or no response to CAR T cell treatment were found to have a higher proportion of CAR T cells with high CAR density than patients that achieved a complete response (Rodriguez-Marquez et al. 2022).

In addition to the caveats mentioned above, affinity tuned CARs, logic gates, and the majority of tuneable CARs require reengineering of the CAR architecture, rendering the implementation into existing CAR platforms cumbersome. Therefore, in this project I aimed to develop and characterise a standalone module that permits tuneable control of CAR T cell function in response to a small molecule drug. To this end, I utilised the CSK mutant CSK^{AS}, the kinase activity of which can be switched off by the administration of 3-IB-PP1, an analogue of the kinase inhibitor PP1.

Co-expression of the CSK^{AS} module in LT22 and 14G2a CAR T cell platforms enabled dampening of CAR T cell function against low antigen density targets whilst maintaining a functional response against high antigen density targets. This highlighted the potential of CSK^{AS} as a module to lessen the risk of on-target off-tumour toxicity, but in a similar manner to affinity tuning, dampening CAR T cell sensitivity may increase the risk of tumour escape.

The ability to control CAR function in response to drug administration is key to achieving the balance between limiting toxicity yet maintaining efficacy. The addition of the CSK^{AS} inhibitor drug improved CAR T cell sensitivity, augmenting cytotoxicity and cytokine release in response to cell lines with a low antigen density. Additionally, the administration of drug to LT22 CSK^{AS} T cells led to significant increases in the percentage of proliferating CAR T cells compared to the LT22 CAR T cells, which displayed negligible levels of proliferation (Figure 38). The capacity for CSK^{AS} expression in CAR T cells to enable drug-mediated augmentation of cytokine release and proliferation is extremely promising, as they are important characteristics of CAR T cells which have been linked to improved persistence in patients (Ghorashian et al. 2019).

This functional augmentation was likely due to a dominant-negative effect, wherein drug-inhibited CSK^{AS} bound to membrane anchors such as PAG blocked endogenous CSK from localising to the membrane. With the ability to both dampen and augment function, the expression of the CSK^{AS} module was found to widen the dynamic range of CAR T cells, highlighting this approach as one that could be used to limit CAR-mediated toxicity whilst maintaining efficacy.

Moreover, I demonstrated that the CSK^{AS} module was able to permit tuneable control of T cells activated via the TCR, supporting research done by Manz and colleagues which showed that drug-mediated inhibition of CSK^{AS} lowered the activation threshold of TCR-activated T cells (Manz et al. 2015). This illustrates that the scope of the CSK^{AS} module reaches beyond CARs and has the potential to benefit TCR-based immunotherapies.

The main benefits of this module over other approaches aimed at tuning CAR T cell function is that it does not comprise potentially immunogenic components or require reengineering of the CAR architecture, making it straightforward to implement into existing CAR T cell platforms.

Dasatinib, the FDA-approved SFK inhibitor, is another way in which CAR T cell function can be tuned without altering the CAR structure. Dasatinib has been shown to efficiently and reversibly dampen CAR T cell function *in vitro* and *in vivo* (Weber et al. 2019; Mestermann et al. 2019). Moreover, in a patient who experienced grade 3 CRS and grade 4 ICANS after CAR T cell infusion, administration of dasatinib in combination with tocilizumab led to significant clinical improvement, reducing the CAR T cell-associated toxicities (Baur et al. 2022).

A caveat of dasatinib for treatment of on-target off-tumour toxicity is that after cessation of administration, CAR T cells were shown to rapidly return to displaying antitumour function (Mestermann et al. 2019). Therefore, regular administrations of dasatinib would be required to avoid toxicity. This considered, dasatinib may not be a suitable long-term solution for the treatment of on-target off-tumour toxicity. Whereas co-expression of the CSK^{AS} module in CAR T cells shifts the threshold for activation, enabling healthy tissue expressing low density antigen to be spared.

A major caveat of the CSK^{AS} system as an approach to tune CAR T cell function is the CSK^{AS} inhibitor drug, 3-IB-PP1. Firstly, as 3-IB-PP1 is not a clinically approved drug, the CSK^{AS} system in its current iteration could not be translated into a clinical setting. Secondly, I observed the drug to have an inhibitory effect on T cell function. When administered to CSK^{AS} expressing CAR T cells *in vitro*, the drug-mediated inhibitory effect was overcome by the strength of the dominant-negative effect caused by the CSK^{AS} module, resulting in an overall improvement in CAR T cell function. However, when the drug was administered to CAR T cells bearing CSK^{AS} *in vivo*, I was not able to identify the optimal drug dose to restore antitumour effect to levels achieved by the conventional CAR T cells.

Another caveat of the CSK^{AS} module is that it is a drug-ON system, meaning that in order to maintain functional efficacy against low antigen targets, the CSK^{AS} inhibitor

drug would need to be continuously administered. In a clinical setting wherein the antigen density of malignant cells is very high, administration of drug to inhibit CSK^{AS} may not be necessary, as the inhibitory signal of CSK^{AS} may be overcome by the strong activation signal triggered by the high density of antigen. However, if the antigen density of malignant cells is low, the continuous administration of drug to maintain functional efficacy whilst avoiding on-target off-tumour toxicity would be a difficult balance to find.

Despite the caveats of the CSK^{AS} system, this project has highlighted the potential of an agnostic CSK-based platform to improve the sensitivity of CAR T cells whilst permitting tuneable control of CAR T cell function. Future research aimed towards the development of such a system that could be dampened in response to the administration of a clinically approved drug (drug-OFF system) would be a worthwhile venture.

REFERENCES

Abate-Daga, Daniel, Kiran H. Lagisetty, Eric Tran, Zhili Zheng, Luca Gattinoni, Zhiya Yu, William R. Burns, et al. 2014. 'A Novel Chimeric Antigen Receptor Against Prostate Stem Cell Antigen Mediates Tumor Destruction in a Humanized Mouse Model of Pancreatic Cancer'. *Human Gene Therapy* 25 (12): 1003–12. https://doi.org/10.1089/hum.2013.209.

Abraham, Robert T., and Arthur Weiss. 2004. 'Jurkat T Cells and Development of the T-Cell Receptor Signalling Paradigm'. *Nature Reviews Immunology* 4 (4): 301–8. https://doi.org/10.1038/nri1330.

Abramson, Jeremy S., M. Lia Palomba, Leo I. Gordon, Matthew A. Lunning, Michael Wang, Jon Arnason, Amitkumar Mehta, et al. 2020. 'Lisocabtagene Maraleucel for Patients with Relapsed or Refractory Large B-Cell Lymphomas (TRANSCEND NHL 001): A Multicentre Seamless Design Study'. *The Lancet* 396 (10254): 839–52. https://doi.org/10.1016/S0140-6736(20)31366-0.

Acuto, Oreste, and Frédérique Michel. 2003. 'CD28-Mediated Co-Stimulation: A Quantitative Support for TCR Signalling'. *Nature Reviews Immunology* 3 (12): 939–51. https://doi.org/10.1038/nri1248.

Agarwal, Manju, Timothy W. Austin, Franck Morel, Jingyi Chen, Ernst Böhnlein, and Ivan Plavec. 1998. 'Scaffold Attachment Region-Mediated Enhancement of Retroviral Vector Expression in Primary T Cells'. *Journal of Virology* 72 (5): 3720–28.

Ahmed, Nabil, Vita S. Brawley, Meenakshi Hegde, Catherine Robertson, Alexia Ghazi, Claudia Gerken, Enli Liu, et al. 2015. 'Human Epidermal Growth Factor Receptor 2 (HER2) - Specific Chimeric Antigen Receptor-Modified T Cells for the Immunotherapy of HER2-Positive Sarcoma'. *Journal of Clinical Oncology: Official Journal of the American Society of Clinical Oncology* 33 (15): 1688–96. https://doi.org/10.1200/JCO.2014.58.0225.

Aivazian, D., and L. J. Stern. 2000. 'Phosphorylation of T Cell Receptor Zeta Is Regulated by a Lipid Dependent Folding Transition'. *Nature Structural Biology* 7 (11): 1023–26. https://doi.org/10.1038/80930.

Aleksic, Milos, Nathaniel Liddy, Peter E. Molloy, Nick Pumphrey, Annelise Vuidepot, Kyong-Mi Chang, and Bent K. Jakobsen. 2012. 'Different Affinity Windows for Virus and Cancer-Specific T-Cell Receptors: Implications for Therapeutic Strategies'. *European Journal of Immunology* 42 (12): 3174–79. https://doi.org/10.1002/eji.201242606.

Andersen, Rikke, Marie Christine Wulff Westergaard, Julie Westerlin Kjeldsen, Anja Müller, Natasja Wulff Pedersen, Sine Reker Hadrup, Özcan Met, et al. 2018. 'T-Cell Responses in the Microenvironment of Primary Renal Cell Carcinoma-Implications for Adoptive Cell Therapy'. *Cancer Immunology Research* 6 (2): 222–35. https://doi.org/10.1158/2326-6066.CIR-17-0467.

Au-Yeung, Byron B., Sebastian Deindl, Lih-Yun Hsu, Emil H. Palacios, Susan E. Levin, John Kuriyan, and Arthur Weiss. 2009. 'The Structure, Regulation, and Function of ZAP-70'. *Immunological Reviews* 228 (1): 41–57. https://doi.org/10.1111/j.1600-065X.2008.00753.x.

Baker, J. E., R. Majeti, S. G. Tangye, and A. Weiss. 2001. 'Protein Tyrosine Phosphatase CD148-Mediated Inhibition of T-Cell Receptor Signal Transduction Is Associated with Reduced LAT and Phospholipase Cgamma1 Phosphorylation'. *Molecular and Cellular Biology* 21 (7): 2393–2403. https://doi.org/10.1128/MCB.21.7.2393-2403.2001.

Battula, Venkata Lokesh, Yuexi Shi, Kurt W. Evans, Rui-Yu Wang, Erika L. Spaeth, Rodrigo O. Jacamo, Rudy Guerra, et al. 2012. 'Ganglioside GD2 Identifies Breast Cancer Stem Cells and Promotes Tumorigenesis'. *The Journal of Clinical Investigation* 122 (6): 2066–78. https://doi.org/10.1172/JCI59735.

Baur, Katharina, Dominik Heim, Astrid Beerlage, Anna S. Poerings, Bastian Kopp, Michael Medinger, Jan C. Dirks, Jakob R. Passweg, and Andreas Holbro. 2022. 'Dasatinib for Treatment of CAR T-Cell Therapy-Related Complications'. *Journal for ImmunoTherapy of Cancer* 10 (12): e005956. https://doi.org/10.1136/jitc-2022-005956.

Ben-Avi, Ronny, Ronit Farhi, Alon Ben-Nun, Marina Gorodner, Eyal Greenberg, Gal Markel, Jacob Schachter, Orit Itzhaki, and Michal J. Besser. 2018. 'Establishment of Adoptive Cell Therapy with Tumor Infiltrating Lymphocytes for Non-Small Cell Lung Cancer Patients'. *Cancer Immunology, Immunotherapy: CII* 67 (8): 1221–30. https://doi.org/10.1007/s00262-018-2174-4.

Bendle, Gavin M., Carsten Linnemann, Anna I. Hooijkaas, Laura Bies, Moniek A. de Witte, Annelies Jorritsma, Andrew D. M. Kaiser, et al. 2010. 'Lethal Graft-versus-Host Disease in Mouse Models of T Cell Receptor Gene Therapy'. *Nature Medicine* 16 (5): 565–70. https://doi.org/10.1038/nm.2128.

Berdeja, Jesus G., Deepu Madduri, Saad Z. Usmani, Andrzej Jakubowiak, Mounzer Agha, Adam D. Cohen, A. Keith Stewart, et al. 2021. 'Ciltacabtagene Autoleucel, a B-Cell Maturation Antigen-Directed Chimeric Antigen Receptor T-Cell Therapy in Patients with Relapsed or Refractory Multiple Myeloma (CARTITUDE-1): A Phase 1b/2 Open-Label Study'. *The Lancet* 398 (10297): 314–24. https://doi.org/10.1016/S0140-6736(21)00933-8.

Bergman, M., V. Joukov, I. Virtanen, and K. Alitalo. 1995. 'Overexpressed Csk Tyrosine Kinase Is Localized in Focal Adhesions, Causes Reorganization of Alpha v Beta 5 Integrin, and Interferes with HeLa Cell Spreading'. *Molecular and Cellular Biology* 15 (2): 711–22. https://doi.org/10.1128/mcb.15.2.711.

Bergman, M., T. Mustelin, C. Oetken, J. Partanen, N. A. Flint, K. E. Amrein, M. Autero, P. Burn, and K. Alitalo. 1992. 'The Human P50csk Tyrosine Kinase Phosphorylates P56lck at Tyr-505 and down Regulates Its Catalytic Activity'. *The EMBO Journal* 11 (8): 2919–24.

Bishop, A. C., J. A. Ubersax, D. T. Petsch, D. P. Matheos, N. S. Gray, J. Blethrow, E. Shimizu, et al. 2000. 'A Chemical Switch for Inhibitor-Sensitive Alleles of Any Protein Kinase'. *Nature* 407 (6802): 395–401. https://doi.org/10.1038/35030148.

Brdicka, T., D. Pavlistová, A. Leo, E. Bruyns, V. Korínek, P. Angelisová, J. Scherer, et al. 2000. 'Phosphoprotein Associated with Glycosphingolipid-Enriched Microdomains (PAG), a Novel Ubiquitously Expressed Transmembrane Adaptor Protein, Binds the Protein Tyrosine Kinase Csk and Is Involved in Regulation of T Cell Activation'. *The Journal of Experimental Medicine* 191 (9): 1591–1604. https://doi.org/10.1084/jem.191.9.1591.

Brdicková, Nadezda, Tomás Brdicka, Pavla Angelisová, Ondrej Horváth, Jiri Spicka, Ivan Hilgert, Jan Paces, et al. 2003. 'LIME: A New Membrane Raft-Associated Adaptor Protein Involved in CD4 and CD8 Coreceptor Signaling'. *The Journal of Experimental Medicine* 198 (10): 1453–62. https://doi.org/10.1084/jem.20031484.

Brenner, M. B., J. McLean, D. P. Dialynas, J. L. Strominger, J. A. Smith, F. L. Owen, J. G. Seidman, S. Ip, F. Rosen, and M. S. Krangel. 1986. 'Identification of a Putative Second T-Cell Receptor'. *Nature* 322 (6075): 145–49. https://doi.org/10.1038/322145a0.

Brocker, T., and K. Karjalainen. 1995. 'Signals through T Cell Receptor-Zeta Chain Alone Are Insufficient to Prime Resting T Lymphocytes'. *The Journal of Experimental Medicine* 181 (5): 1653–59. https://doi.org/10.1084/jem.181.5.1653.

Brocker, Thomas. 2000. 'Chimeric Fv-ζ or Fv-ε Receptors Are Not Sufficient to Induce Activation or Cytokine Production in Peripheral T Cells'. *Blood* 96 (5): 1999–2001. https://doi.org/10.1182/blood.V96.5.1999.

Bromley, Shannon K., W. Richard Burack, Kenneth G. Johnson, Kristina Somersalo, Tasha N. Sims, Cenk Sumen, Mark M. Davis, Andrey S. Shaw, Paul M. Allen, and Michael L. Dustin. 2001. 'The Immunological Synapse'. *Annual Review of Immunology* 19 (1): 375–96. https://doi.org/10.1146/annurev.immunol.19.1.375.

Büeler, H., and R. C. Mulligan. 1996. 'Induction of Antigen-Specific Tumor Immunity by Genetic and Cellular Vaccines against MAGE: Enhanced Tumor Protection by Coexpression of Granulocyte-Macrophage Colony-Stimulating Factor and B7-1'. *Molecular Medicine (Cambridge, Mass.)* 2 (5): 545–55.

Burton, Jake, Jesús A. Siller-Farfán, Johannes Pettmann, Benjamin Salzer, Mikhail Kutuzov, P. Anton van der Merwe, and Omer Dushek. 2023. 'Inefficient Exploitation of Accessory Receptors Reduces the Sensitivity of Chimeric Antigen Receptors'. *Proceedings of the National Academy of Sciences* 120 (2): e2216352120. https://doi.org/10.1073/pnas.2216352120.

Cao, Haiming, William E. Courchesne, and Cynthia Corley Mastick. 2002. 'A Phosphotyrosine-Dependent Protein Interaction Screen Reveals a Role for Phosphorylation of Caveolin-1 on Tyrosine 14: RECRUITMENT OF C-TERMINAL Src KINASE *'. *Journal of Biological Chemistry* 277 (11): 8771–74. https://doi.org/10.1074/jbc.C100661200.

Carpenito, Carmine, Michael C. Milone, Raffit Hassan, Jacqueline C. Simonet, Mehdi Lakhal, Megan M. Suhoski, Angel Varela-Rohena, et al. 2009. 'Control of Large, Established Tumor Xenografts with Genetically Retargeted Human T Cells Containing CD28 and CD137 Domains'. *Proceedings of the National Academy of Sciences of the United States of America* 106 (9): 3360–65. https://doi.org/10.1073/pnas.0813101106.

Caruso, Hillary G., Lenka V. Hurton, Amer Najjar, David Rushworth, Sonny Ang, Simon Olivares, Tiejuan Mi, et al. 2015. 'Tuning Sensitivity of CAR to EGFR Density Limits Recognition of Normal Tissue While Maintaining Potent Antitumor Activity'. *Cancer Research* 75 (17): 3505–18. https://doi.org/10.1158/0008-5472.CAN-15-0139.

Casas, Javier, Joanna Brzostek, Veronika I. Zarnitsyna, Jin-sung Hong, Qianru Wei, John A. H. Hoerter, Guo Fu, et al. 2014. 'Ligand-Engaged TCR Is Triggered by Lck Not Associated with CD8 Coreceptor'. *Nature Communications* 5 (November): 5624. https://doi.org/10.1038/ncomms6624.

Cassan, M., and J. P. Rousset. 2001. 'UAG Readthrough in Mammalian Cells: Effect of Upstream and Downstream Stop Codon Contexts Reveal Different Signals'. *BMC Molecular Biology* 2: 3. https://doi.org/10.1186/1471-2199-2-3.

Chames, Patrick, Ralph A. Willemsen, Gertrudis Rojas, Detlef Dieckmann, Louise Rem, Gerold Schuler, Reinder L. Bolhuis, and Hennie R. Hoogenboom. 2002. 'TCR-like Human Antibodies Expressed on Human CTLs Mediate Antibody Affinity-Dependent Cytolytic Activity'. *Journal of Immunology (Baltimore, Md.: 1950)* 169 (2): 1110–18. https://doi.org/10.4049/jimmunol.169.2.1110.

Chan, A. C., M. Dalton, R. Johnson, G. H. Kong, T. Wang, R. Thoma, and T. Kurosaki. 1995. 'Activation of ZAP-70 Kinase Activity by Phosphorylation of Tyrosine 493 Is Required for Lymphocyte Antigen Receptor Function'. *The EMBO Journal* 14 (11): 2499–2508.

Chan, A. C., M. Iwashima, C. W. Turck, and A. Weiss. 1992. 'ZAP-70: A 70 Kd Protein-Tyrosine Kinase That Associates with the TCR Zeta Chain'. *Cell* 71 (4): 649–62. https://doi.org/10.1016/0092-8674(92)90598-7.

Chandran, Smita S., Robert P.T. Somerville, James C. Yang, Richard M. Sherry, Christopher A. Klebanoff, Stephanie L. Goff, John R. Wunderlich, et al. 2017. 'Treatment of Metastatic Uveal Melanoma with Adoptive Transfer of Tumor Infiltrating Lymphocytes: A Single-Center Phase 2 Study'. *The Lancet. Oncology* 18 (6): 792–802. https://doi.org/10.1016/S1470-2045(17)30251-6.

Chaplin, David D. 2010. 'Overview of the Immune Response'. *The Journal of Allergy and Clinical Immunology* 125 (2 Suppl 2): S3-23. https://doi.org/10.1016/j.jaci.2009.12.980.

Cheung, Nai-Kong V., Irene Y. Cheung, Brian H. Kushner, Irina Ostrovnaya, Elizabeth Chamberlain, Kim Kramer, and Shakeel Modak. 2012. 'Murine Anti-GD2 Monoclonal Antibody 3F8 Combined With Granulocyte-Macrophage Colony-Stimulating Factor and 13-Cis-Retinoic Acid in High-Risk Patients With Stage 4 Neuroblastoma in First Remission'. *Journal of Clinical Oncology* 30 (26): 3264–70. https://doi.org/10.1200/JCO.2011.41.3807.

Chmielewski, Markus, Andreas A. Hombach, and Hinrich Abken. 2013. 'Antigen-Specific T-Cell Activation Independently of the MHC: Chimeric Antigen Receptor-Redirected T Cells'. *Frontiers in Immunology* 4 (November). https://doi.org/10.3389/fimmu.2013.00371.

Chmielewski, Markus, Andreas Hombach, Claudia Heuser, Gregory P. Adams, and Hinrich Abken. 2004. 'T Cell Activation by Antibody-like Immunoreceptors: Increase in Affinity of the Single-Chain Fragment Domain above Threshold Does Not Increase T Cell Activation against Antigen-Positive Target Cells but Decreases Selectivity'. *Journal of Immunology (Baltimore, Md.: 1950)* 173 (12): 7647–53. https://doi.org/10.4049/jimmunol.173.12.7647.

Chmielewski, Markus, Caroline Kopecky, Andreas A. Hombach, and Hinrich Abken. 2011. 'IL-12 Release by Engineered T Cells Expressing Chimeric Antigen Receptors Can Effectively Muster an Antigen-Independent Macrophage Response on Tumor Cells That Have Shut down Tumor Antigen Expression'. *Cancer Research* 71 (17): 5697–5706. https://doi.org/10.1158/0008-5472.CAN-11-0103.

Chothia, C, D R Boswell, and A M Lesk. 1988. 'The Outline Structure of the T-Cell Alpha Beta Receptor.' *The EMBO Journal* 7 (12): 3745–55.

Chow, Lionel M. L., Marielle Fournel, Dominique Davidson, and André Veillette. 1993. 'Negative Regulation of T-Cell Receptor Signalling by Tyrosine Protein Kinase P50csk'. *Nature* 365 (6442): 156–60. https://doi.org/10.1038/365156a0.

Ciceri, Fabio, Chiara Bonini, Maria Teresa Lupo Stanghellini, Attilio Bondanza, Catia Traversari, Monica Salomoni, Lucia Turchetto, et al. 2009. 'Infusion of Suicide-Gene-Engineered Donor Lymphocytes after Family Haploidentical Haemopoietic Stem-Cell Transplantation for Leukaemia (the TK007 Trial): A Non-Randomised Phase I–II Study'. *The Lancet Oncology* 10 (5): 489–500. https://doi.org/10.1016/S1470-2045(09)70074-9.

Clevers, H., B. Alarcon, T. Wileman, and C. Terhorst. 1988. 'The T Cell Receptor/CD3 Complex: A Dynamic Protein Ensemble'. *Annual Review of Immunology* 6: 629–62. https://doi.org/10.1146/annurev.iy.06.040188.003213.

Cloutier, and A Veillette. 1996. 'Association of Inhibitory Tyrosine Protein Kinase P50csk with Protein Tyrosine Phosphatase PEP in T Cells and Other Hemopoietic Cells.' *The EMBO Journal* 15 (18): 4909–18.

Cloutier, and André Veillette. 1999. 'Cooperative Inhibition of T-Cell Antigen Receptor Signaling by a Complex between a Kinase and a Phosphatase'. *The Journal of Experimental Medicine* 189 (1): 111–21.

Cohen, S., H. Dadi, E. Shaoul, N. Sharfe, and C. M. Roifman. 1999. 'Cloning and Characterization of a Lymphoid-Specific, Inducible Human Protein Tyrosine Phosphatase, Lyp'. *Blood* 93 (6): 2013–24.

Cooper, R. D. Peterson, and R. A. Good. 1965. 'Delineation of the Thymic and Bursal Lymphoid Systems in the Chicken'. *Nature* 205 (January): 143–46. https://doi.org/10.1038/205143a0.

Cooper, Raymond D. A. Peterson, Mary Ann South, and Robert A. Good. 1966. 'The Functions of the Thymus System and the Bursa System in the Chicken'. *The Journal of Experimental Medicine* 123 (1): 75–102.

Cordoba, Shaun-Paul, Kaushik Choudhuri, Hao Zhang, Marcus Bridge, Alp Bugra Basat, Michael L. Dustin, and P. Anton van der Merwe. 2013. 'The Large Ectodomains of CD45 and CD148 Regulate Their Segregation from and Inhibition of Ligated T-Cell Receptor'. *Blood* 121 (21): 4295–4302. https://doi.org/10.1182/blood-2012-07-442251.

Cordoba, Shaun-Paul, Shimobi Onuoha, Simon Thomas, Daniela Soriano Pignataro, Rachael Hough, Sara Ghorashian, Ajay Vora, et al. 2021. 'CAR T Cells with Dual Targeting of CD19 and CD22 in Pediatric and Young Adult Patients with Relapsed or Refractory B Cell Acute Lymphoblastic Leukemia: A Phase 1 Trial'. *Nature Medicine* 27 (10): 1797–1805. https://doi.org/10.1038/s41591-021-01497-1.

Courtney, Adam H., Wan-Lin Lo, and Arthur Weiss. 2018. 'TCR Signaling: Mechanisms of Initiation and Propagation'. *Trends in Biochemical Sciences* 43 (2): 108–23. https://doi.org/10.1016/j.tibs.2017.11.008.

Courtney, Adam H., Alexey A. Shvets, Wen Lu, Gloria Griffante, Marianne Mollenauer, Veronika Horkova, Wan-Lin Lo, et al. 2019. 'CD45 Functions as a Signaling Gatekeeper in T Cells'. *Science Signaling* 12 (604). https://doi.org/10.1126/scisignal.aaw8151.

Dadmarz, R., M. K. Sgagias, S. A. Rosenberg, and D. J. Schwartzentruber. 1995. 'CD4+ T Lymphocytes Infiltrating Human Breast Cancer Recognise Autologous Tumor in an MHC-Class-II Restricted Fashion'. *Cancer Immunology, Immunotherapy: CII* 40 (1): 1–9. https://doi.org/10.1007/BF01517229.

Davenport, A. J., R. S. Cross, K. A. Watson, Y. Liao, W. Shi, H. M. Prince, P. A. Beavis, et al. 2018. 'Chimeric Antigen Receptor T Cells Form Nonclassical and Potent Immune Synapses Driving Rapid Cytotoxicity'. *Proceedings of the National Academy of Sciences* 115 (9): E2068–76. https://doi.org/10.1073/pnas.1716266115.

Davidson, D., Marcin Bakinowski, Matthew L. Thomas, Vaclav Horejsi, and André Veillette. 2003. 'Phosphorylation-Dependent Regulation of T-Cell Activation by PAG/Cbp, a Lipid Raft-Associated Transmembrane Adaptor'. *Molecular and Cellular Biology* 23 (6): 2017–28. https://doi.org/10.1128/mcb.23.6.2017-2028.2003.

Davila, Marco L., Isabelle Riviere, Xiuyan Wang, Shirley Bartido, Jae Park, Kevin Curran, Stephen S. Chung, et al. 2014. 'Efficacy and Toxicity Management of 19-28z CAR T Cell Therapy in B Cell Acute Lymphoblastic Leukemia'. *Science Translational Medicine* 6 (224): 224ra25. https://doi.org/10.1126/scitranslmed.3008226.

Davis, and P. J. Bjorkman. 1988. 'T-Cell Antigen Receptor Genes and T-Cell Recognition'. *Nature* 334 (6181): 395–402. https://doi.org/10.1038/334395a0.

Davis, J. J. Boniface, Z. Reich, D. Lyons, J. Hampl, B. Arden, and Y. Chien. 1998. 'Ligand Recognition by Alpha Beta T Cell Receptors'. *Annual Review of Immunology* 16: 523–44. https://doi.org/10.1146/annurev.immunol.16.1.523.

Davis, and PA van der Merwe. 2006. 'The Kinetic-Segregation Model: TCR Triggering and Beyond'. *Nature Immunology* 7 (8): 803–9. https://doi.org/10.1038/ni1369.

Desai, D.m., J. Sap, O. Silvennoinen, J. Schlessinger, and A. Weiss. 1994. 'The Catalytic Activity of the CD45 Membrane-Proximal Phosphatase Domain Is Required for TCR Signaling and Regulation.' *The EMBO Journal* 13 (17): 4002–10. https://doi.org/10.1002/j.1460-2075.1994.tb06716.x.

Di Bartolo, V., D. Mège, V. Germain, M. Pelosi, E. Dufour, F. Michel, G. Magistrelli, A. Isacchi, and O. Acuto. 1999. 'Tyrosine 319, a Newly Identified Phosphorylation Site of ZAP-70, Plays a Critical Role in T Cell Antigen Receptor Signaling'. *The Journal of Biological Chemistry* 274 (10): 6285–94. https://doi.org/10.1074/jbc.274.10.6285.

Djenidi, Fayçal, Julien Adam, Aïcha Goubar, Aurélie Durgeau, Guillaume Meurice, Vincent de Montpréville, Pierre Validire, Benjamin Besse, and Fathia Mami-Chouaib. 2015. 'CD8+CD103+ Tumor-Infiltrating Lymphocytes Are Tumor-Specific Tissue-Resident Memory T Cells and a Prognostic Factor for Survival in Lung Cancer Patients'. *Journal of Immunology (Baltimore, Md.: 1950)* 194 (7): 3475–86. https://doi.org/10.4049/jimmunol.1402711.

Duan, Lei, Alagarsamy Lakku Reddi, Amiya Ghosh, Manjari Dimri, and Hamid Band. 2004. 'The Cbl Family and Other Ubiquitin Ligases: Destructive Forces in Control of Antigen Receptor Signaling'. *Immunity* 21 (1): 7–17. https://doi.org/10.1016/j.immuni.2004.06.012.

Eshhar, Z., T. Waks, G. Gross, and D. G. Schindler. 1993. 'Specific Activation and Targeting of Cytotoxic Lymphocytes through Chimeric Single Chains Consisting of Antibody-Binding Domains and the Gamma or Zeta Subunits of the Immunoglobulin and T-Cell Receptors'. *Proceedings of the National Academy of Sciences of the United States of America* 90 (2): 720–24. https://doi.org/10.1073/pnas.90.2.720.

Eyquem, Justin, Jorge Mansilla-Soto, Theodoros Giavridis, Sjoukje J. C. van der Stegen, Mohamad Hamieh, Kristen M. Cunanan, Ashlesha Odak, Mithat Gönen, and Michel Sadelain. 2017. 'Targeting a CAR to the TRAC Locus with CRISPR/Cas9 Enhances Tumour Rejection'. *Nature* 543 (7643): 113–17. https://doi.org/10.1038/nature21405.

Fedorov, Victor D., Maria Themeli, and Michel Sadelain. 2013. 'PD-1– and CTLA-4–Based Inhibitory Chimeric Antigen Receptors (ICARs) Divert Off-Target Immunotherapy Responses'. *Science Translational Medicine* 5 (215): 215ra172. https://doi.org/10.1126/scitranslmed.3006597.

Feucht, Judith, Jie Sun, Justin Eyquem, Yu-Jui Ho, Zeguo Zhao, Josef Leibold, Anton Dobrin, Annalisa Cabriolu, Mohamad Hamieh, and Michel Sadelain. 2019. 'Calibration of CAR Activation Potential Directs Alternative T Cell Fates and Therapeutic Potency'. *Nature Medicine* 25 (1): 82–88. https://doi.org/10.1038/s41591-018-0290-5.

Filipp, Dominik, Jenny Zhang, Bernadine L. Leung, Andrey Shaw, Steven D. Levin, Andre Veillette, and Michael Julius. 2003. 'Regulation of Fyn through Translocation of Activated Lck into Lipid Rafts'. *The Journal of Experimental Medicine* 197 (9): 1221–27. https://doi.org/10.1084/jem.20022112.

Finney, Helene M., Arne N. Akbar, and Alastair D. G. Lawson. 2004. 'Activation of Resting Human Primary T Cells with Chimeric Receptors: Costimulation from CD28, Inducible Costimulator, CD134, and CD137 in Series with Signals from the TCR Zeta Chain'. *Journal of Immunology (Baltimore, Md.: 1950)* 172 (1): 104–13. https://doi.org/10.4049/jimmunol.172.1.104.

Fourcade, Julien, Zhaojun Sun, Mourad Benallaoua, Philippe Guillaume, Immanuel F. Luescher, Cindy Sander, John M. Kirkwood, Vijay Kuchroo, and Hassane M. Zarour. 2010. 'Upregulation of Tim-3 and PD-1 Expression Is Associated with Tumor Antigen–Specific

CD8+ T Cell Dysfunction in Melanoma Patients'. *The Journal of Experimental Medicine* 207 (10): 2175–86. https://doi.org/10.1084/jem.20100637.

Fraietta, Joseph A., Simon F. Lacey, Elena J. Orlando, Iulian Pruteanu-Malinici, Mercy Gohil, Stefan Lundh, Alina C. Boesteanu, et al. 2018. 'Determinants of Response and Resistance to CD19 Chimeric Antigen Receptor (CAR) T Cell Therapy of Chronic Lymphocytic Leukemia'. *Nature Medicine* 24 (5): 563–71. https://doi.org/10.1038/s41591-018-0010-1.

Freiberg, Benjamin A., Hannah Kupfer, William Maslanik, Joe Delli, John Kappler, Dennis M. Zaller, and Abraham Kupfer. 2002. 'Staging and Resetting T Cell Activation in SMACs'. *Nature Immunology* 3 (10): 911–17. https://doi.org/10.1038/ni836.

Frigault, Matthew J, Jihyun Lee, Maria Ciocca Basil, Carmine Carpenito, Shinichiro Motohashi, John Scholler, Omkar U. Kawalekar, et al. 2015. 'Identification of Chimeric Antigen Receptors That Mediate Constitutive or Inducible Proliferation of T Cells'. *Cancer Immunology Research* 3 (4): 356–67. https://doi.org/10.1158/2326-6066.CIR-14-0186.

Fry, Terry J., Nirali N. Shah, Rimas J. Orentas, Maryalice Stetler-Stevenson, Constance M. Yuan, Sneha Ramakrishna, Pamela Wolters, et al. 2018. 'CD22-Targeted CAR T Cells Induce Remission in B-ALL That Is Naive or Resistant to CD19-Targeted CAR Immunotherapy'. *Nature Medicine* 24 (1): 20–28. https://doi.org/10.1038/nm.4441.

Fugmann, Sebastian D., Alfred Ian Lee, Penny E. Shockett, Isabelle J. Villey, and David G. Schatz. 2000. 'The RAG Proteins and V(D)J Recombination: Complexes, Ends, and Transposition'. *Annual Review of Immunology* 18: 495–527.

Furukawa, T., M. Itoh, N. X. Krueger, M. Streuli, and H. Saito. 1994. 'Specific Interaction of the CD45 Protein-Tyrosine Phosphatase with Tyrosine-Phosphorylated CD3 Zeta Chain'. *Proceedings of the National Academy of Sciences of the United States of America* 91 (23): 10928–32. https://doi.org/10.1073/pnas.91.23.10928.

Gan, Hui K., Andrew H. Kaye, and Rodney B. Luwor. 2009. 'The EGFRvIII Variant in Glioblastoma Multiforme'. *Journal of Clinical Neuroscience* 16 (6): 748–54. https://doi.org/10.1016/j.jocn.2008.12.005.

Garfall, Alfred L., Marcela V. Maus, Wei-Ting Hwang, Simon F. Lacey, Yolanda D. Mahnke, J. Joseph Melenhorst, Zhaohui Zheng, et al. 2015. 'Chimeric Antigen Receptor T Cells against CD19 for Multiple Myeloma'. *New England Journal of Medicine* 373 (11): 1040–47. https://doi.org/10.1056/NEJMoa1504542.

Gargett, Tessa, Wenbo Yu, Gianpietro Dotti, Eric S Yvon, Susan N Christo, John D Hayball, Ian D Lewis, Malcolm K Brenner, and Michael P Brown. 2016. 'GD2-Specific CAR T Cells Undergo Potent Activation and Deletion Following Antigen Encounter but Can Be Protected From Activation-Induced Cell Death by PD-1 Blockade'. *Molecular Therapy* 24 (6): 1135–49. https://doi.org/10.1038/mt.2016.63.

Gattinoni, Luca, Enrico Lugli, Yun Ji, Zoltan Pos, Chrystal M. Paulos, Máire F. Quigley, Jorge R. Almeida, et al. 2011. 'A Human Memory T Cell Subset with Stem Cell–like Properties'. *Nature Medicine* 17 (10): 1290–97. https://doi.org/10.1038/nm.2446.

Gauen, A N Kong, L E Samelson, and A S Shaw. 1992. 'P59fyn Tyrosine Kinase Associates with Multiple T-Cell Receptor Subunits through Its Unique Amino-Terminal Domain.' *Molecular and Cellular Biology* 12 (12): 5438–46.

Gauen, Y. Zhu, F. Letourneur, Q. Hu, J. B. Bolen, L. A. Matis, R. D. Klausner, and A. S. Shaw. 1994. 'Interactions of P59fyn and ZAP-70 with T-Cell Receptor Activation Motifs: Defining the Nature of a Signalling Motif'. *Molecular and Cellular Biology* 14 (6): 3729–41. https://doi.org/10.1128/mcb.14.6.3729.

Ghorashian, Sara, Anne Marijn Kramer, Shimobi Onuoha, Gary Wright, Jack Bartram, Rachel Richardson, Sarah J. Albon, et al. 2019. 'Enhanced CAR T Cell Expansion and Prolonged Persistence in Pediatric Patients with ALL Treated with a Low-Affinity CD19 CAR'. *Nature Medicine* 25 (9): 1408–14. https://doi.org/10.1038/s41591-019-0549-5.

Gil, Diana, Wolfgang W. A. Schamel, María Montoya, Francisco Sánchez-Madrid, and Balbino Alarcón. 2002. 'Recruitment of Nck by CD3 Epsilon Reveals a Ligand-Induced Conformational Change Essential for T Cell Receptor Signaling and Synapse Formation'. *Cell* 109 (7): 901–12. https://doi.org/10.1016/s0092-8674(02)00799-7.

Ginaldi, L., M. De Martinis, E. Matutes, N. Farahat, R. Morilla, and D. Catovsky. 1998. 'Levels of Expression of CD19 and CD20 in Chronic B Cell Leukaemias.' *Journal of Clinical Pathology* 51 (5): 364–69. https://doi.org/10.1136/jcp.51.5.364.

Giordano-Attianese, Greta, Pablo Gainza, Elise Gray-Gaillard, Elisabetta Cribioli, Sailan Shui, Seonghoon Kim, Mi-Jeong Kwak, et al. 2020. 'A Computationally Designed Chimeric Antigen Receptor Provides a Small-Molecule Safety Switch for T-Cell Therapy'. *Nature Biotechnology* 38 (4): 426–32. https://doi.org/10.1038/s41587-019-0403-9.

Gjörloff-Wingren, Anette, Manju Saxena, Scott Williams, Don Hammi, and Tomas Mustelin. 1999. 'Characterization of TCR-Induced Receptor-Proximal Signaling Events Negatively Regulated by the Protein Tyrosine Phosphatase PEP'. *European Journal of Immunology* 29 (12): 3845–54. https://doi.org/10.1002/(SICI)1521-4141(199912)29:12<3845::AID-IMMU3845>3.0.CO;2-U.

Gomes-Silva, Diogo, Malini Mukherjee, Madhuwanti Srinivasan, Giedre Krenciute, Olga Dakhova, Yueting Zheng, Joaquim M. S. Cabral, et al. 2017. 'Tonic 4-1BB Costimulation in Chimeric Antigen Receptors Impedes T Cell Survival and Is Vector-Dependent'. *Cell Reports* 21 (1): 17–26. https://doi.org/10.1016/j.celrep.2017.09.015.

Gong, M. C., J. B. Latouche, A. Krause, W. D. Heston, N. H. Bander, and M. Sadelain. 1999. 'Cancer Patient T Cells Genetically Targeted to Prostate-Specific Membrane Antigen Specifically Lyse Prostate Cancer Cells and Release Cytokines in Response to Prostate-Specific Membrane Antigen'. *Neoplasia (New York, N.Y.)* 1 (2): 123–27. https://doi.org/10.1038/sj.neo.7900018.

Grosso, Joseph F., Monica V. Goldberg, Derese Getnet, Tullia C. Bruno, Hung-Rong Yen, Kristin J. Pyle, Edward Hipkiss, Dario A. A. Vignali, Drew M. Pardoll, and Charles G. Drake. 2009. 'Functionally Distinct LAG-3 and PD-1 Subsets on Activated and Chronically Stimulated CD8 T Cells'. *Journal of Immunology (Baltimore, Md. : 1950)* 182 (11): 6659–69. https://doi.org/10.4049/jimmunol.0804211.

Grupp, Stephan A., Michael Kalos, David Barrett, Richard Aplenc, David L. Porter, Susan R. Rheingold, David T. Teachey, et al. 2013. 'Chimeric Antigen Receptor–Modified T Cells for Acute Lymphoid Leukemia'. *New England Journal of Medicine* 368 (16): 1509–18. https://doi.org/10.1056/NEJMoa1215134.

Grupp, Stephan A., Shannon L Maude, Pamela A Shaw, Richard Aplenc, David M. Barrett, Colleen Callahan, Simon F. Lacey, et al. 2015. 'Durable Remissions in Children with Relapsed/Refractory ALL Treated with T Cells Engineered with a CD19-Targeted Chimeric Antigen Receptor (CTL019)'. *Blood* 126 (23): 681. https://doi.org/10.1182/blood.V126.23.681.681.

Gudipati, Venugopal, Julian Rydzek, Iago Doel-Perez, Vasco Dos Reis Gonçalves, Lydia Scharf, Sebastian Königsberger, Elisabeth Lobner, et al. 2020. 'Inefficient CAR-Proximal Signaling Blunts Antigen Sensitivity'. *Nature Immunology*, July. https://doi.org/10.1038/s41590-020-0719-0.

Guest, Ryan D., Robert E. Hawkins, Natalia Kirillova, Eleanor J. Cheadle, Jennifer Arnold, Allison O'Neill, Joely Irlam, et al. 2005. 'The Role of Extracellular Spacer Regions in the Optimal Design of Chimeric Immune Receptors: Evaluation of Four Different ScFvs and Antigens'. *Journal of Immunotherapy* 28 (3): 203–211. https://doi.org/10.1097/01.cji.0000161397.96582.59.

Hanada, K., D. M. Perry-Lalley, G. A. Ohnmacht, M. P. Bettinotti, and J. C. Yang. 2001. 'Identification of Fibroblast Growth Factor-5 as an Overexpressed Antigen in Multiple Human Adenocarcinomas'. *Cancer Research* 61 (14): 5511–16.

Hanke, Jeffrey H., Joseph P. Gardner, Robert L. Dow, Paul S. Changelian, William H. Brissette, Elora J. Weringer, Brian A. Pollok, and Patricia A. Connelly. 1996. 'Discovery of a Novel, Potent, and Src Family-Selective Tyrosine Kinase Inhibitor STUDY OF Lck- AND FynT-DEPENDENT T CELL ACTIVATION'. *Journal of Biological Chemistry* 271 (2): 695–701. https://doi.org/10.1074/jbc.271.2.695.

Harris, L. Haynes, P. C. Sayles, D. K. Duso, S. M. Eaton, N. M. Lepak, L. L. Johnson, S. L. Swain, and F. E. Lund. 2000. 'Reciprocal Regulation of Polarized Cytokine Production by Effector B and T Cells'. *Nature Immunology* 1 (6): 475–82. https://doi.org/10.1038/82717.

Harris, and David M. Kranz. 2016. 'Adoptive T Cell Therapies: A Comparison of T Cell Receptors and Chimeric Antigen Receptors'. *Trends in Pharmacological Sciences* 37 (3): 220–30. https://doi.org/10.1016/j.tips.2015.11.004.

He, Xin, Zijie Feng, Jian Ma, Sunbin Ling, Yan Cao, Buddha Gurung, Yuan Wu, et al. 2020. 'Bispecific and Split CAR T Cells Targeting CD13 and TIM3 Eradicate Acute Myeloid Leukemia'. *Blood* 135 (10): 713–23. https://doi.org/10.1182/blood.2019002779.

Heczey, Andras, Chrystal U. Louis, Barbara Savoldo, Olga Dakhova, April Durett, Bambi Grilley, Hao Liu, et al. 2017. 'CAR T Cells Administered in Combination with Lymphodepletion and PD-1 Inhibition to Patients with Neuroblastoma'. *Molecular Therapy* 25 (9): 2214–24. https://doi.org/10.1016/j.ymthe.2017.05.012.

Hennecke, Jens, and Don C. Wiley. 2001. 'T Cell Receptor–MHC Interactions up Close'. *Cell* 104 (1): 1–4. https://doi.org/10.1016/S0092-8674(01)00185-4.

Hermiston, Michelle L., Zheng Xu, Ravindra Majeti, and Arthur Weiss. 2002. 'Reciprocal Regulation of Lymphocyte Activation by Tyrosine Kinases and Phosphatases'. *The Journal of Clinical Investigation* 109 (1): 9–14. https://doi.org/10.1172/JCI14794.

Hermiston, Michelle L., Zheng Xu, and Arthur Weiss. 2003. 'CD45: A Critical Regulator of Signaling Thresholds in Immune Cells'. *Annual Review of Immunology* 21: 107–37. https://doi.org/10.1146/annurev.immunol.21.120601.140946.

Hermiston, Michelle L., Julie Zikherman, and Jing W. Zhu. 2009. 'CD45, CD148, and Lyp/Pep: Critical Phosphatases Regulating Src Family Kinase Signaling Networks in Immune Cells'. *Immunological Reviews* 228 (1): 288–311. https://doi.org/10.1111/j.1600-065X.2008.00752.x.

Hilhorst, Riet, Liesbeth Houkes, Monique Mommersteeg, Joyce Musch, Adriënne van den Berg, and Rob Ruijtenbeek. 2013. 'Peptide Microarrays for Profiling of Serine/Threonine Kinase Activity of Recombinant Kinases and Lysates of Cells and Tissue Samples'. In *Gene Regulation: Methods and Protocols*, edited by Minou Bina, 259–71. Methods in Molecular Biology. Totowa, NJ: Humana Press. https://doi.org/10.1007/978-1-62703-284-1_21.

Hirao, A, I Hamaguchi, T Suda, and N Yamaguchi. 1997. 'Translocation of the Csk Homologous Kinase (Chk/Hyl) Controls Activity of CD36-Anchored Lyn Tyrosine Kinase in Thrombin-

Stimulated Platelets.' *The EMBO Journal* 16 (9): 2342–51. https://doi.org/10.1093/emboj/16.9.2342.

Hombach, Andreas A., Verena Schildgen, Claudia Heuser, Ricarda Finnern, David E. Gilham, and Hinrich Abken. 2007. 'T Cell Activation by Antibody-like Immunoreceptors: The Position of the Binding Epitope within the Target Molecule Determines the Efficiency of Activation of Redirected T Cells'. *Journal of Immunology (Baltimore, Md.: 1950)* 178 (7): 4650–57. https://doi.org/10.4049/jimmunol.178.7.4650.

Hotblack, Alastair, Evangelia K. Kokalaki, Morgan J. Palton, Gordon Weng-Kit Cheung, Iwan P. Williams, Somayya Manzoor, Thomas I. Grothier, et al. 2021. 'Tunable Control of CAR T Cell Activity through Tetracycline Mediated Disruption of Protein–Protein Interaction'. *Scientific Reports* 11 (1): 21902. https://doi.org/10.1038/s41598-021-01418-9.

Huang, Jun, Mario Brameshuber, Xun Zeng, Jianming Xie, Qi-jing Li, Yueh-hsiu Chien, Salvatore Valitutti, and Mark M. Davis. 2013. 'A Single Peptide-Major Histocompatibility Complex Ligand Triggers Digital Cytokine Secretion in CD4(+) T Cells'. *Immunity* 39 (5): 846–57. https://doi.org/10.1016/j.immuni.2013.08.036.

Hudecek, Michael, Maria-Teresa Lupo-Stanghellini, Paula L. Kosasih, Daniel Sommermeyer, Michael C. Jensen, Christoph Rader, and Stanley R. Riddell. 2013. 'Receptor Affinity and Extracellular Domain Modifications Affect Tumor Recognition by ROR1-Specific Chimeric Antigen Receptor T Cells'. *Clinical Cancer Research: An Official Journal of the American Association for Cancer Research* 19 (12): 3153–64. https://doi.org/10.1158/1078-0432.CCR-13-0330.

Hui, Enfu, and Ronald D. Vale. 2014. 'In Vitro Membrane Reconstitution of the T-Cell Receptor Proximal Signaling Network'. *Nature Structural & Molecular Biology* 21 (2): 133–42. https://doi.org/10.1038/nsmb.2762.

Huppa, Johannes B., Michael Gleimer, Cenk Sumen, and Mark M. Davis. 2003. 'Continuous T Cell Receptor Signaling Required for Synapse Maintenance and Full Effector Potential'. *Nature Immunology* 4 (8): 749–55. https://doi.org/10.1038/ni951.

Imbert, V, J F Peyron, D Farahi Far, B Mari, P Auberger, and B Rossi. 1994. 'Induction of Tyrosine Phosphorylation and T-Cell Activation by Vanadate Peroxide, an Inhibitor of Protein Tyrosine Phosphatases.' *Biochemical Journal* 297 (Pt 1): 163–73.

Irles, Claudine, Antony Symons, Frédérique Michel, Talitha R. Bakker, P. Anton van der Merwe, and Oreste Acuto. 2003. 'CD45 Ectodomain Controls Interaction with GEMs and Lck Activity for Optimal TCR Signaling'. *Nature Immunology* 4 (2): 189–97. https://doi.org/10.1038/ni877.

Irving, B. A., and Arthur Weiss. 1991. 'The Cytoplasmic Domain of the T Cell Receptor ζ Chain Is Sufficient to Couple to Receptor-Associated Signal Transduction Pathways'. *Cell* 64 (5): 891–901. https://doi.org/10.1016/0092-8674(91)90314-O.

James, Scott E., Philip D. Greenberg, Michael C. Jensen, Yukang Lin, Jinjuan Wang, Brian G. Till, Andrew A. Raubitschek, Stephen J. Forman, and Oliver W. Press. 2008. 'Antigen Sensitivity of CD22-Specific Chimeric TCR Is Modulated by Target Epitope Distance from the Cell Membrane'. *Journal of Immunology (Baltimore, Md.: 1950)* 180 (10): 7028–38. https://doi.org/10.4049/jimmunol.180.10.7028.

Janes, Peter W., Steven C. Ley, Anthony I. Magee, and Panagiotis S. Kabouridis. 2000. 'The Role of Lipid Rafts in T Cell Antigen Receptor (TCR) Signalling'. *Seminars in Immunology* 12 (1): 23–34. https://doi.org/10.1006/smim.2000.0204.

Johnson, Laura A., John Scholler, Takayuki Ohkuri, Akemi Kosaka, Prachi R. Patel, Shannon E. McGettigan, Arben K. Nace, et al. 2015. 'Rational Development and Characterization of Humanized Anti-EGFR Variant III Chimeric Antigen Receptor T Cells for Glioblastoma'. *Science Translational Medicine* 7 (275): 275ra22. https://doi.org/10.1126/scitranslmed.aaa4963.

Juillerat, Alexandre, Alan Marechal, Jean-Marie Filhol, Julien Valton, Aymeric Duclert, Laurent Poirot, and Philippe Duchateau. 2016. 'Design of Chimeric Antigen Receptors with Integrated Controllable Transient Functions'. *Scientific Reports* 6 (1): 18950. https://doi.org/10.1038/srep18950.

Juillerat, Alexandre, Diane Tkach, Brian W. Busser, Sonal Temburni, Julien Valton, Aymeric Duclert, Laurent Poirot, Stéphane Depil, and Philippe Duchateau. 2019. 'Modulation of Chimeric Antigen Receptor Surface Expression by a Small Molecule Switch'. *BMC Biotechnology* 19 (1): 44. https://doi.org/10.1186/s12896-019-0537-3.

June, C H, J A Ledbetter, M M Gillespie, T Lindsten, and C B Thompson. 1987. 'T-Cell Proliferation Involving the CD28 Pathway Is Associated with Cyclosporine-Resistant Interleukin 2 Gene Expression.' *Molecular and Cellular Biology* 7 (12): 4472–81.

Junghans, Richard P., Qiangzhong Ma, Ritesh Rathore, Erica M. Gomes, Anthony J. Bais, Agnes S.Y. Lo, Mehrdad Abedi, et al. 2016. 'Phase I Trial of Anti-PSMA Designer CAR-T Cells in Prostate Cancer: Possible Role for Interacting Interleukin 2-T Cell Pharmacodynamics as a Determinant of Clinical Response'. *The Prostate* 76 (14): 1257–70. https://doi.org/10.1002/pros.23214.

Kalos, Michael, Bruce L. Levine, David L. Porter, Sharyn Katz, Stephan A. Grupp, Adam Bagg, and Carl H. June. 2011. 'T Cells with Chimeric Antigen Receptors Have Potent Antitumor Effects and Can Establish Memory in Patients with Advanced Leukemia'. *Science Translational Medicine* 3 (95): 95ra73. https://doi.org/10.1126/scitranslmed.3002842.

Kaplan, K. B., K. B. Bibbins, J. R. Swedlow, M. Arnaud, D. O. Morgan, and H. E. Varmus. 1994. 'Association of the Amino-Terminal Half of c-Src with Focal Adhesions Alters Their Properties and Is Regulated by Phosphorylation of Tyrosine 527'. *The EMBO Journal* 13 (20): 4745–56. https://doi.org/10.1002/j.1460-2075.1994.tb06800.x.

Kershaw, Michael H., Jennifer A. Westwood, Linda L. Parker, Gang Wang, Zelig Eshhar, Sharon A. Mavroukakis, Donald E. White, et al. 2006. 'A Phase I Study on Adoptive Immunotherapy Using Gene-Modified T Cells for Ovarian Cancer'. *Clinical Cancer Research : An Official Journal of the American Association for Cancer Research* 12 (20 Pt 1): 6106–15. https://doi.org/10.1158/1078-0432.CCR-06-1183.

Klages, S, D Adam, K Class, J Fargnoli, J B Bolen, and R C Penhallow. 1994. 'Ctk: A Protein-Tyrosine Kinase Related to Csk That Defines an Enzyme Family.' *Proceedings of the National Academy of Sciences of the United States of America* 91 (7): 2597–2601.

Kloss, Christopher C., Maud Condomines, Marc Cartellieri, Michael Bachmann, and Michel Sadelain. 2013. 'Combinatorial Antigen Recognition with Balanced Signaling Promotes Selective Tumor Eradication by Engineered T Cells'. *Nature Biotechnology* 31 (1): 71–75. https://doi.org/10.1038/nbt.2459.

Kochenderfer, James N., Mark E. Dudley, Sadik H. Kassim, Robert P. T. Somerville, Robert O. Carpenter, Maryalice Stetler-Stevenson, James C. Yang, et al. 2015. 'Chemotherapy-Refractory Diffuse Large B-Cell Lymphoma and Indolent B-Cell Malignancies Can Be Effectively Treated with Autologous T Cells Expressing an Anti-CD19 Chimeric Antigen

Receptor'. *Journal of Clinical Oncology: Official Journal of the American Society of Clinical Oncology* 33 (6): 540–49. https://doi.org/10.1200/JCO.2014.56.2025.

Kochenderfer, James N., Steven A. Feldman, Yangbing Zhao, Hui Xu, Mary A. Black, Richard A. Morgan, Wyndham H. Wilson, and Steven A. Rosenberg. 2009. 'Construction and Pre-Clinical Evaluation of an Anti-CD19 Chimeric Antigen Receptor'. *Journal of Immunotherapy (Hagerstown, Md. : 1997)* 32 (7): 689–702. https://doi.org/10.1097/CJI.0b013e3181ac6138.

Kokalaki, Evangelia, Biao Ma, Mathieu Ferrari, Thomas Grothier, Warren Hazelton, Somayya Manzoor, Eren Costu, et al. 2023. 'Dual Targeting of CD19 and CD22 against B-ALL Using a Novel High-Sensitivity ACD22 CAR'. *Molecular Therapy* 0 (0). https://doi.org/10.1016/j.ymthe.2023.03.020.

Labanieh, Louai, Robbie G. Majzner, Dorota Klysz, Elena Sotillo, Chris J. Fisher, José G. Vilches-Moure, Kaithlen Zen B. Pacheco, et al. 2022. 'Enhanced Safety and Efficacy of Protease-Regulated CAR-T Cell Receptors'. *Cell* 185 (10): 1745-1763.e22. https://doi.org/10.1016/j.cell.2022.03.041.

Ladenstein, Ruth, Ulrike Pötschger, Dominique Valteau-Couanet, Roberto Luksch, Victoria Castel, Isaac Yaniv, Genevieve Laureys, et al. 2018. 'Interleukin 2 with Anti-GD2 Antibody Ch14.18/CHO (Dinutuximab Beta) in Patients with High-Risk Neuroblastoma (HR-NBL1/SIOPEN): A Multicentre, Randomised, Phase 3 Trial'. *The Lancet. Oncology* 19 (12): 1617–29. https://doi.org/10.1016/S1470-2045(18)30578-3.

Lafferty, K. J., and A. J. Cunningham. 1975. 'A New Analysis of Allogeneic Interactions'. *The Australian Journal of Experimental Biology and Medical Science* 53 (1): 27–42. https://doi.org/10.1038/icb.1975.3.

Lajoie, Marc J., Scott E. Boyken, Alexander I. Salter, Jilliane Bruffey, Anusha Rajan, Robert A. Langan, Audrey Olshefsky, et al. 2020. 'Designed Protein Logic to Target Cells with Precise Combinations of Surface Antigens'. *Science (New York, N.Y.)* 369 (6511): 1637–43. https://doi.org/10.1126/science.aba6527.

Lamers, Cor HJ, Stefan Sleijfer, Sabine van Steenbergen, Pascal van Elzakker, Brigitte van Krimpen, Corrien Groot, Arnold Vulto, et al. 2013. 'Treatment of Metastatic Renal Cell Carcinoma With CAIX CAR-Engineered T Cells: Clinical Evaluation and Management of On-Target Toxicity'. *Molecular Therapy* 21 (4): 904–12. https://doi.org/10.1038/mt.2013.17.

Lammie, G., N. Cheung, W. Gerald, M. Rosenblum, and C. Cordoncardo. 1993. 'Ganglioside Gd(2) Expression in the Human Nervous-System and in Neuroblastomas - an Immunohistochemical Study'. *International Journal of Oncology* 3 (5): 909–15. https://doi.org/10.3892/ijo.3.5.909.

Lanitis, Evripidis, Mathilde Poussin, Alex W. Klattenhoff, Degang Song, Raphael Sandaltzopoulos, Carl H. June, and Daniel J. Powell. 2013. 'Chimeric Antigen Receptor T Cells with Dissociated Signaling Domains Exhibit Focused Anti-Tumor Activity with Reduced Potential for Toxicity in Vivo'. *Cancer Immunology Research* 1 (1): 43–53. https://doi.org/10.1158/2326-6066.CIR-13-0008.

Lee, Rebecca Gardner, David L. Porter, Chrystal U. Louis, Nabil Ahmed, Michael Jensen, Stephan A. Grupp, and Crystal L. Mackall. 2014. 'Current Concepts in the Diagnosis and Management of Cytokine Release Syndrome'. *Blood* 124 (2): 188–95. https://doi.org/10.1182/blood-2014-05-552729.

Lee, Young-Ae Kim, Chan Kyu Sim, Sun-Hee Heo, In Hye Song, Hye Seon Park, Suk Young Park, et al. 2017. 'Expansion of Tumor-Infiltrating Lymphocytes and Their Potential for

Application as Adoptive Cell Transfer Therapy in Human Breast Cancer'. *Oncotarget* 8 (69): 113345–59. https://doi.org/10.18632/oncotarget.23007.

Lee, Su-Jung Park, Beom K. Choi, Hyun Hwa Kim, Kyung-Ok Nam, and Byoung S. Kwon. 2002. '4-1BB Promotes the Survival of CD8+ T Lymphocytes by Increasing Expression of Bcl-XL and Bfl-1'. *Journal of Immunology (Baltimore, Md.: 1950)* 169 (9): 4882–88. https://doi.org/10.4049/jimmunol.169.9.4882.

Leung, Wai-Hang, Joel Gay, Unja Martin, Tracy E. Garrett, Holly M. Horton, Michael T. Certo, Bruce R. Blazar, et al. 2019. 'Sensitive and Adaptable Pharmacological Control of CAR T Cells through Extracellular Receptor Dimerization'. *JCI Insight* 5. https://doi.org/10.1172/jci.insight.124430.

Ley, S. C., M. Marsh, C. R. Bebbington, K. Proudfoot, and P. Jordan. 1994. 'Distinct Intracellular Localization of Lck and Fyn Protein Tyrosine Kinases in Human T Lymphocytes'. *The Journal of Cell Biology* 125 (3): 639–49. https://doi.org/10.1083/jcb.125.3.639.

Lin, Joseph, and Arthur Weiss. 2003. 'The Tyrosine Phosphatase CD148 Is Excluded from the Immunologic Synapse and Down-Regulates Prolonged T Cell Signaling'. *The Journal of Cell Biology* 162 (4): 673–82. https://doi.org/10.1083/jcb.200303040.

Linette, Gerald P., Edward A. Stadtmauer, Marcela V. Maus, Aaron P. Rapoport, Bruce L. Levine, Lyndsey Emery, Leslie Litzky, et al. 2013. 'Cardiovascular Toxicity and Titin Cross-Reactivity of Affinity-Enhanced T Cells in Myeloma and Melanoma'. *Blood* 122 (6): 863–71. https://doi.org/10.1182/blood-2013-03-490565.

Liu, Olivia Chen, J. Blake Joseph Wall, Michael Zheng, Yang Zhou, Li Wang, Haley Ruth Vaseghi, Li Qian, and Jiandong Liu. 2017. 'Systematic Comparison of 2A Peptides for Cloning Multi-Genes in a Polycistronic Vector'. *Scientific Reports* 7 (1): 1–9. https://doi.org/10.1038/s41598-017-02460-2.

Liu, Shuguang Jiang, Chongyun Fang, Shiyu Yang, Devvora Olalere, Edward C. Pequignot, Alexandria P. Cogdill, et al. 2015. 'Affinity-Tuned ErbB2 or EGFR Chimeric Antigen Receptor T Cells Exhibit an Increased Therapeutic Index against Tumors in Mice'. *Cancer Research* 75 (17): 3596–3607. https://doi.org/10.1158/0008-5472.CAN-15-0159.

Long, Adrienne H., Waleed M. Haso, Jack F. Shern, Kelsey M. Wanhainen, Meera Murgai, Maria Ingaramo, Jillian P. Smith, et al. 2015. '4-1BB Costimulation Ameliorates T Cell Exhaustion Induced by Tonic Signaling of Chimeric Antigen Receptors'. *Nature Medicine* 21 (6): 581–90. https://doi.org/10.1038/nm.3838.

Loughran, Gary, Ming-Yuan Chou, Ivaylo P. Ivanov, Irwin Jungreis, Manolis Kellis, Anmol M. Kiran, Pavel V. Baranov, and John F. Atkins. 2014. 'Evidence of Efficient Stop Codon Readthrough in Four Mammalian Genes'. *Nucleic Acids Research* 42 (14): 8928–38. https://doi.org/10.1093/nar/gku608.

Louis, Chrystal U., Barbara Savoldo, Gianpietro Dotti, Martin Pule, Eric Yvon, G. Doug Myers, Claudia Rossig, et al. 2011. 'Antitumor Activity and Long-Term Fate of Chimeric Antigen Receptor–Positive T Cells in Patients with Neuroblastoma'. *Blood* 118 (23): 6050–56. https://doi.org/10.1182/blood-2011-05-354449.

Love, Paul E., and Sandra M. Hayes. 2010. 'ITAM-Mediated Signaling by the T-Cell Antigen Receptor'. *Cold Spring Harbor Perspectives in Biology* 2 (6): a002485. https://doi.org/10.1101/cshperspect.a002485.

Love, Paul E., and Elizabeth W. Shores. 2000. 'ITAM Multiplicity and Thymocyte Selection: How Low Can You Go?' *Immunity* 12 (6): 591–97. https://doi.org/10.1016/S1074-7613(00)80210-1.

Lupher, M. L., Z. Songyang, S. E. Shoelson, L. C. Cantley, and H. Band. 1997. 'The Cbl Phosphotyrosine-Binding Domain Selects a D(N/D)XpY Motif and Binds to the Tyr292 Negative Regulatory Phosphorylation Site of ZAP-70'. *The Journal of Biological Chemistry* 272 (52): 33140–44. https://doi.org/10.1074/jbc.272.52.33140.

Lynn, Rachel C, Yang Feng, Keith Schutsky, Mathilde Poussin, Anna Kalota, Dimiter S Dimitrov, and Daniel J Powell. 2016. 'High Affinity FRβ-Specific CAR T Cells Eradicate AML and Normal Yeloid Lineage without HSC Toxicity'. *Leukemia* 30 (6): 1355–64. https://doi.org/10.1038/leu.2016.35.

Maher, John, Renier J. Brentjens, Gertrude Gunset, Isabelle Rivière, and Michel Sadelain. 2002. 'Human T-Lymphocyte Cytotoxicity and Proliferation Directed by a Single Chimeric TCRzeta /CD28 Receptor'. *Nature Biotechnology* 20 (1): 70–75. https://doi.org/10.1038/nbt0102-70.

Majzner, Robbie G., Skyler P. Rietberg, Elena Sotillo, Rui Dong, Vipul T. Vachharajani, Louai Labanieh, June H. Myklebust, et al. 2020. 'Tuning the Antigen Density Requirement for CAR T Cell Activity'. *Cancer Discovery*, January. https://doi.org/10.1158/2159-8290.CD-19-0945.

Manz, Boryana N, Ying Xim Tan, Adam H Courtney, Florentine Rutaganira, Ed Palmer, Kevan M Shokat, and Arthur Weiss. 2015. 'Small Molecule Inhibition of Csk Alters Affinity Recognition by T Cells'. *ELife* 4 (August). https://doi.org/10.7554/eLife.08088.

Marofi, Faroogh, Roza Motavalli, Vladimir A. Safonov, Lakshmi Thangavelu, Alexei Valerievich Yumashev, Markov Alexander, Navid Shomali, et al. 2021. 'CAR T Cells in Solid Tumors: Challenges and Opportunities'. *Stem Cell Research & Therapy* 12 (1): 81. https://doi.org/10.1186/s13287-020-02128-1.

Marth, J. D., J. A. Cooper, C. S. King, S. F. Ziegler, D. A. Tinker, R. W. Overell, E. G. Krebs, and R. M. Perlmutter. 1988. 'Neoplastic Transformation Induced by an Activated Lymphocyte-Specific Protein Tyrosine Kinase (Pp56lck)'. *Molecular and Cellular Biology* 8 (2): 540–50. https://doi.org/10.1128/mcb.8.2.540.

Matthews, R. J., D. B. Bowne, E. Flores, and M. L. Thomas. 1992. 'Characterization of Hematopoietic Intracellular Protein Tyrosine Phosphatases: Description of a Phosphatase Containing an SH2 Domain and Another Enriched in Proline-, Glutamic Acid-, Serine-, and Threonine-Rich Sequences'. *Molecular and Cellular Biology* 12 (5): 2396–2405. https://doi.org/10.1128/mcb.12.5.2396.

Maude, Shannon L., Noelle Frey, Pamela A. Shaw, Richard Aplenc, David M. Barrett, Nancy J. Bunin, Anne Chew, et al. 2014. 'Chimeric Antigen Receptor T Cells for Sustained Remissions in Leukemia'. *New England Journal of Medicine* 371 (16): 1507–17. https://doi.org/10.1056/NEJMoa1407222.

Maude, Shannon L., Theodore W. Laetsch, Jochen Buechner, Susana Rives, Michael Boyer, Henrique Bittencourt, Peter Bader, et al. 2018. 'Tisagenlecleucel in Children and Young Adults with B-Cell Lymphoblastic Leukemia'. *New England Journal of Medicine* 378 (5): 439–48. https://doi.org/10.1056/NEJMoa1709866.

McCall, M. N., D. M. Shotton, and A. N. Barclay. 1992. 'Expression of Soluble Isoforms of Rat CD45. Analysis by Electron Microscopy and Use in Epitope Mapping of Anti-CD45R Monoclonal Antibodies'. *Immunology* 76 (2): 310–17.

McFarland, T. R. Hurley, J. T. Pingel, B. M. Sefton, A. Shaw, and M. L. Thomas. 1993. 'Correlation between Src Family Member Regulation by the Protein-Tyrosine-Phosphatase CD45 and Transmembrane Signaling through the T-Cell Receptor'.

Proceedings of the National Academy of Sciences of the United States of America 90 (4): 1402–6. https://doi.org/10.1073/pnas.90.4.1402.

McNeill, Louise, Robert J. Salmond, Joanne C. Cooper, Céline K. Carret, Robin L. Cassady-Cain, Marta Roche-Molina, Panna Tandon, Nick Holmes, and Denis R. Alexander. 2007. 'The Differential Regulation of Lck Kinase Phosphorylation Sites by CD45 Is Critical for T Cell Receptor Signaling Responses'. *Immunity* 27 (3): 425–37. https://doi.org/10.1016/j.immuni.2007.07.015.

Merwe, PA van der, S. J. Davis, A. S. Shaw, and M. L. Dustin. 2000. 'Cytoskeletal Polarization and Redistribution of Cell-Surface Molecules during T Cell Antigen Recognition'. *Seminars in Immunology* 12 (1): 5–21. https://doi.org/10.1006/smim.2000.0203.

Merwe, PA van der, Peter N. McNamee, Elizabeth A. Davies, A. Neil Barclay, and Simon J. Davis. 1995. 'Topology of the CD2–CD48 Cell-Adhesion Molecule Complex: Implications for Antigen Recognition by T Cells'. *Current Biology* 5 (1): 74–84. https://doi.org/10.1016/S0960-9822(95)00019-4.

Mestermann, Katrin, Theodoros Giavridis, Justus Weber, Julian Rydzek, Silke Frenz, Thomas Nerreter, Andreas Mades, Michel Sadelain, Hermann Einsele, and Michael Hudecek. 2019. 'The Tyrosine Kinase Inhibitor Dasatinib Acts as a Pharmacologic on/off Switch for CAR T Cells'. *Science Translational Medicine* 11 (499). https://doi.org/10.1126/scitranslmed.aau5907.

Milone, Michael C., Jonathan D. Fish, Carmine Carpenito, Richard G. Carroll, Gwendolyn K. Binder, David Teachey, Minu Samanta, et al. 2009. 'Chimeric Receptors Containing CD137 Signal Transduction Domains Mediate Enhanced Survival of T Cells and Increased Antileukemic Efficacy in Vivo'. *Molecular Therapy: The Journal of the American Society of Gene Therapy* 17 (8): 1453–64. https://doi.org/10.1038/mt.2009.83.

Mingueneau, Michaël, Amandine Sansoni, Claude Grégoire, Romain Roncagalli, Enrique Aguado, Arthur Weiss, Marie Malissen, and Bernard Malissen. 2008. 'The Proline-Rich Sequence of CD3epsilon Controls T Cell Antigen Receptor Expression on and Signaling Potency in Preselection CD4+CD8+ Thymocytes'. *Nature Immunology* 9 (5): 522–32. https://doi.org/10.1038/ni.1608.

Mitchell, C. D., S. M. Richards, S. E. Kinsey, J. Lilleyman, A. Vora, and T. O. B. Eden. 2005. 'Benefit of Dexamethasone Compared with Prednisolone for Childhood Acute Lymphoblastic Leukaemia: Results of the UK Medical Research Council ALL97 Randomized Trial'. *British Journal of Haematology* 129 (6): 734–45. https://doi.org/10.1111/j.1365-2141.2005.05509.x.

Monks, Colin R. F., Benjamin A. Freiberg, Hannah Kupfer, Noah Sciaky, and Abraham Kupfer. 1998. 'Three-Dimensional Segregation of Supramolecular Activation Clusters in T Cells'. *Nature* 395 (6697): 82–86. https://doi.org/10.1038/25764.

Morgan, Richard A., Nachimuthu Chinnasamy, Daniel D Abate-Daga, Alena Gros, Paul F. Robbins, Zhili Zheng, Steven A. Feldman, et al. 2013. 'Cancer Regression and Neurologic Toxicity Following Anti-MAGE-A3 TCR Gene Therapy'. *Journal of Immunotherapy (Hagerstown, Md. : 1997)* 36 (2): 133–51. https://doi.org/10.1097/CJI.0b013e3182829903.

Morgan, Richard A., Mark E. Dudley, John R. Wunderlich, Marybeth S. Hughes, James C. Yang, Richard M. Sherry, Richard E. Royal, et al. 2006. 'Cancer Regression in Patients after Transfer of Genetically Engineered Lymphocytes'. *Science (New York, N.Y.)* 314 (5796): 126–29. https://doi.org/10.1126/science.1129003.

Morgan, Richard A, James C Yang, Mio Kitano, Mark E Dudley, Carolyn M Laurencot, and Steven A Rosenberg. 2010. 'Case Report of a Serious Adverse Event Following the Administration of T Cells Transduced With a Chimeric Antigen Receptor Recognizing ERBB2'. *Molecular Therapy* 18 (4): 843–51. https://doi.org/10.1038/mt.2010.24.

Mueller, D. L., M. K. Jenkins, and R. H. Schwartz. 1989. 'Clonal Expansion versus Functional Clonal Inactivation: A Costimulatory Signalling Pathway Determines the Outcome of T Cell Antigen Receptor Occupancy'. *Annual Review of Immunology* 7: 445–80. https://doi.org/10.1146/annurev.iy.07.040189.002305.

Mujoo, Kalpana, David A. Cheresh, Hsin Ming Yang, and Ralph A. Reisfeld. 1987. 'Disialoganglioside GD2 on Human Neuroblastoma Cells: Target Antigen for Monoclonal Antibody-Mediated Cytolysis and Suppression of Tumor Growth1'. *Cancer Research* 47 (4): 1098–1104.

Munshi, Nikhil C., Larry D. Anderson, Nina Shah, Deepu Madduri, Jesús Berdeja, Sagar Lonial, Noopur Raje, et al. 2021. 'Idecabtagene Vicleucel in Relapsed and Refractory Multiple Myeloma'. *New England Journal of Medicine* 384 (8): 705–16. https://doi.org/10.1056/NEJMoa2024850.

Mustelin, T., K. M. Coggeshall, and A. Altman. 1989. 'Rapid Activation of the T-Cell Tyrosine Protein Kinase Pp56lck by the CD45 Phosphotyrosine Phosphatase'. *Proceedings of the National Academy of Sciences of the United States of America* 86 (16): 6302–6. https://doi.org/10.1073/pnas.86.16.6302.

Mustelin, T., T. Pessa-Morikawa, M. Autero, M. Gassmann, L. C. Andersson, C. G. Gahmberg, and P. Burn. 1992. 'Regulation of the P59fyn Protein Tyrosine Kinase by the CD45 Phosphotyrosine Phosphatase'. *European Journal of Immunology* 22 (5): 1173–78. https://doi.org/10.1002/eji.1830220510.

Nada, S., M. Okada, A. MacAuley, J. A. Cooper, and H. Nakagawa. 1991. 'Cloning of a Complementary DNA for a Protein-Tyrosine Kinase That Specifically Phosphorylates a Negative Regulatory Site of P60c-Src'. *Nature* 351 (6321): 69–72. https://doi.org/10.1038/351069a0.

Nada, S., T. Yagi, H. Takeda, T. Tokunaga, H. Nakagawa, Y. Ikawa, M. Okada, and S. Aizawa. 1993. 'Constitutive Activation of Src Family Kinases in Mouse Embryos That Lack Csk'. *Cell* 73 (6): 1125–35. https://doi.org/10.1016/0092-8674(93)90642-4.

Navid, Fariba, Paul M. Sondel, Raymond Barfield, Barry L. Shulkin, Robert A. Kaufman, Jim A. Allay, Jacek Gan, et al. 2014. 'Phase I Trial of a Novel Anti-GD2 Monoclonal Antibody, Hu14.18K322A, Designed to Decrease Toxicity in Children with Refractory or Recurrent Neuroblastoma'. *Journal of Clinical Oncology: Official Journal of the American Society of Clinical Oncology* 32 (14): 1445–52. https://doi.org/10.1200/JCO.2013.50.4423.

Neelapu, Sattva S., Frederick L. Locke, Nancy L. Bartlett, Lazaros J. Lekakis, David B. Miklos, Caron A. Jacobson, Ira Braunschweig, et al. 2017. 'Axicabtagene Ciloleucel CAR T-Cell Therapy in Refractory Large B-Cell Lymphoma'. *New England Journal of Medicine* 377 (26): 2531–44. https://doi.org/10.1056/NEJMoa1707447.

Neelapu, Sattva S., Sudhakar Tummala, Partow Kebriaei, William Wierda, Cristina Gutierrez, Frederick L. Locke, Krishna V. Komanduri, et al. 2018. 'Chimeric Antigen Receptor T-Cell Therapy - Assessment and Management of Toxicities'. *Nature Reviews. Clinical Oncology* 15 (1): 47–62. https://doi.org/10.1038/nrclinonc.2017.148.

Nicholson, I. C., K. A. Lenton, D. J. Little, T. Decorso, F. T. Lee, A. M. Scott, H. Zola, and A. W. Hohmann. 1997. 'Construction and Characterisation of a Functional CD19 Specific Single Chain Fv Fragment for Immunotherapy of B Lineage Leukaemia and Lymphoma'.

Molecular Immunology 34 (16–17): 1157–65. https://doi.org/10.1016/s0161-5890(97)00144-2.

Nika, Konstantina, Cristiana Soldani, Mogjiborahman Salek, Wolfgang Paster, Adrian Gray, Ruth Etzensperger, Lars Fugger, et al. 2010. 'Constitutively Active Lck Kinase in T Cells Drives Antigen Receptor Signal Transduction'. *Immunity* 32 (6): 766–77. https://doi.org/10.1016/j.immuni.2010.05.011.

Nothwehr, S. F., and J. I. Gordon. 1990. 'Targeting of Proteins into the Eukaryotic Secretory Pathway: Signal Peptide Structure/Function Relationships'. *BioEssays: News and Reviews in Molecular, Cellular and Developmental Biology* 12 (10): 479–84. https://doi.org/10.1002/bies.950121005.

Ogawa, Akira, Yoshiharu Takayama, Hiroaki Sakai, Khoon Tee Chong, Satoru Takeuchi, Atsushi Nakagawa, Shigeyuki Nada, Masato Okada, and Tomitake Tsukihara. 2002. 'Structure of the Carboxyl-Terminal Src Kinase, Csk'. *Journal of Biological Chemistry* 277 (17): 14351–54. https://doi.org/10.1074/jbc.C200086200.

Okada, M. 2012. 'Regulation of the Src Family Kinases by Csk'. *International Journal of Biological Sciences* 8 (10): 1385–97. https://doi.org/10.7150/ijbs.5141.

Okada, M., S. Nada, Y. Yamanashi, T. Yamamoto, and H. Nakagawa. 1991. 'CSK: A Protein-Tyrosine Kinase Involved in Regulation of Src Family Kinases.' *Journal of Biological Chemistry* 266 (36): 24249–52.

O'Malley, Daniel P., Vijay Ahuja, Brian Fink, Carolyn Cao, Cindy Wang, Jesse Swanson, Susan Wee, et al. 2019. 'Discovery of Pyridazinone and Pyrazolo[1,5-a]Pyridine Inhibitors of C-Terminal Src Kinase'. *ACS Medicinal Chemistry Letters* 10 (10): 1486–91. https://doi.org/10.1021/acsmedchemlett.9b00354.

O'Shea, J. J., D. W. McVicar, T. L. Bailey, C. Burns, and M. J. Smyth. 1992. 'Activation of Human Peripheral Blood T Lymphocytes by Pharmacological Induction of Protein-Tyrosine Phosphorylation'. *Proceedings of the National Academy of Sciences of the United States of America* 89 (21): 10306–10. https://doi.org/10.1073/pnas.89.21.10306.

Ostman, A., Q. Yang, and N. K. Tonks. 1994. 'Expression of DEP-1, a Receptor-like Protein-Tyrosine-Phosphatase, Is Enhanced with Increasing Cell Density'. *Proceedings of the National Academy of Sciences of the United States of America* 91 (21): 9680–84. https://doi.org/10.1073/pnas.91.21.9680.

Palacios, Emil H., and Arthur Weiss. 2004. 'Function of the Src-Family Kinases, Lck and Fyn, in T-Cell Development and Activation'. *Oncogene* 23 (48): 7990–8000. https://doi.org/10.1038/sj.onc.1208074.

Pardoll, Drew. 2003. 'Does the Immune System See Tumors as Foreign or Self?' *Annual Review of Immunology* 21: 807–39. https://doi.org/10.1146/annurev.immunol.21.120601.141135.

Park, David L. Digiusto, Marilyn Slovak, Christine Wright, Araceli Naranjo, Jamie Wagner, Hunsar B. Meechoovet, et al. 2007. 'Adoptive Transfer of Chimeric Antigen Receptor Re-Directed Cytolytic T Lymphocyte Clones in Patients with Neuroblastoma'. *Molecular Therapy: The Journal of the American Society of Gene Therapy* 15 (4): 825–33. https://doi.org/10.1038/sj.mt.6300104.

Park, Enda Shevlin, Yogindra Vedvyas, Marjan Zaman, Susan Park, Yen-Michael S. Hsu, Irene M. Min, and Moonsoo M. Jin. 2017. 'Micromolar Affinity CAR T Cells to ICAM-1 Achieves Rapid Tumor Elimination While Avoiding Systemic Toxicity'. *Scientific Reports* 7 (1): 14366. https://doi.org/10.1038/s41598-017-14749-3.

Parkhurst, Maria R, James C Yang, Russell C Langan, Mark E Dudley, Debbie-Ann N Nathan, Steven A Feldman, Jeremy L Davis, et al. 2011. 'T Cells Targeting Carcinoembryonic Antigen Can Mediate Regression of Metastatic Colorectal Cancer but Induce Severe Transient Colitis'. *Molecular Therapy* 19 (3): 620–26. https://doi.org/10.1038/mt.2010.272.

Parnes, J. R. 1989. 'Molecular Biology and Function of CD4 and CD8'. *Advances in Immunology* 44: 265–311. https://doi.org/10.1016/s0065-2776(08)60644-6.

Parry, Richard V., Karin Reif, Graham Smith, David M. Sansom, Brian A. Hemmings, and Stephen G. Ward. 1997. 'Ligation of the T Cell Co-Stimulatory Receptor CD28 Activates the Serine-Threonine Protein Kinase Protein Kinase B'. *European Journal of Immunology* 27 (10): 2495–2501. https://doi.org/10.1002/eji.1830271006.

Paszkiewicz, Paulina J., Simon P. Fräßle, Shivani Srivastava, Daniel Sommermeyer, Michael Hudecek, Ingo Drexler, Michel Sadelain, et al. 2016. 'Targeted Antibody-Mediated Depletion of Murine CD19 CAR T Cells Permanently Reverses B Cell Aplasia'. *The Journal of Clinical Investigation* 126 (11): 4262–72. https://doi.org/10.1172/JCI84813.

Pfrepper, Klaus-Ingmar, Anne Marie-Cardine, Luca Simeoni, Yasuhiro Kuramitsu, Albrecht Leo, Jiri Spicka, Ivan Hilgert, Jeanette Scherer, and Burkhart Schraven. 2001. 'Structural and Functional Dissection of the Cytoplasmic Domain of the Transmembrane Adaptor Protein SIT (SHP2-Interacting Transmembrane Adaptor Protein)'. *European Journal of Immunology* 31 (6): 1825–36. https://doi.org/10.1002/1521-4141(200106)31:6<1825::AID-IMMU1825>3.0.CO;2-V.

Philip, Brian, Evangelia Kokalaki, Leila Mekkaoui, Simon Thomas, Karin Straathof, Barry Flutter, Virna Marin, et al. 2014. 'A Highly Compact Epitope-Based Marker/Suicide Gene for Easier and Safer T-Cell Therapy'. *Blood* 124 (8): 1277–87. https://doi.org/10.1182/blood-2014-01-545020.

Pingel, J. T., and M. L. Thomas. 1989. 'Evidence That the Leukocyte-Common Antigen Is Required for Antigen-Induced T Lymphocyte Proliferation'. *Cell* 58 (6): 1055–65. https://doi.org/10.1016/0092-8674(89)90504-7.

Porter, David L., Wei-Ting Hwang, Noelle V. Frey, Simon F. Lacey, Pamela A. Shaw, Alison W. Loren, Adam Bagg, et al. 2015. 'Chimeric Antigen Receptor T Cells Persist and Induce Sustained Remissions in Relapsed Refractory Chronic Lymphocytic Leukemia'. *Science Translational Medicine* 7 (303): 303ra139-303ra139. https://doi.org/10.1126/scitranslmed.aac5415.

Porter, David L., Bruce L. Levine, Michael Kalos, Adam Bagg, and Carl H. June. 2011. 'Chimeric Antigen Receptor-Modified T Cells in Chronic Lymphoid Leukemia'. *The New England Journal of Medicine* 365 (8): 725–33. https://doi.org/10.1056/NEJMoa1103849.

Poschke, Isabel C., Jessica C. Hassel, Aaron Rodriguez-Ehrenfried, Katharina A. M. Lindner, Ignacio Heras-Murillo, Lena M. Appel, Johanna Lehmann, et al. 2020. 'The Outcome of Ex Vivo TIL Expansion Is Highly Influenced by Spatial Heterogeneity of the Tumor T-Cell Repertoire and Differences in Intrinsic In Vitro Growth Capacity between T-Cell Clones'. *Clinical Cancer Research: An Official Journal of the American Association for Cancer Research* 26 (16): 4289–4301. https://doi.org/10.1158/1078-0432.CCR-19-3845.

Pule, Martin A., Barbara Savoldo, G. Doug Myers, Claudia Rossig, Heidi V. Russell, Gianpietro Dotti, M. Helen Huls, et al. 2008. 'Virus-Specific T Cells Engineered to Coexpress Tumor-Specific Receptors: Persistence and Antitumor Activity in Individuals with

Neuroblastoma'. *Nature Medicine* 14 (11): 1264–70. https://doi.org/10.1038/nm.1882.

Pule, Martin A., Karin C. Straathof, Gianpietro Dotti, Helen E. Heslop, Cliona M. Rooney, and Malcolm K. Brenner. 2005. 'A Chimeric T Cell Antigen Receptor That Augments Cytokine Release and Supports Clonal Expansion of Primary Human T Cells'. *Molecular Therapy: The Journal of the American Society of Gene Therapy* 12 (5): 933–41. https://doi.org/10.1016/j.ymthe.2005.04.016.

Qian, D., S. Lev, N. S. van Oers, I. Dikic, J. Schlessinger, and A. Weiss. 1997. 'Tyrosine Phosphorylation of Pyk2 Is Selectively Regulated by Fyn during TCR Signaling'. *The Journal of Experimental Medicine* 185 (7): 1253–59. https://doi.org/10.1084/jem.185.7.1253.

Quintarelli, Concetta, Domenico Orlando, Iolanda Boffa, Marika Guercio, Vinicia Assunta Polito, Andrea Petretto, Chiara Lavarello, et al. 2018. 'Choice of Costimulatory Domains and of Cytokines Determines CAR T-Cell Activity in Neuroblastoma'. *OncoImmunology* 7 (6): e1433518. https://doi.org/10.1080/2162402X.2018.1433518.

Raje, Noopur, Jesus Berdeja, Yi Lin, David Siegel, Sundar Jagannath, Deepu Madduri, Michaela Liedtke, et al. 2019. 'Anti-BCMA CAR T-Cell Therapy Bb2121 in Relapsed or Refractory Multiple Myeloma'. *New England Journal of Medicine* 380 (18): 1726–37. https://doi.org/10.1056/NEJMoa1817226.

Rapoport, Aaron P., Edward A. Stadtmauer, Gwendolyn K. Binder-Scholl, Olga Goloubeva, Dan T. Vogl, Simon F. Lacey, Ashraf Z. Badros, et al. 2015. 'NY-ESO-1-Specific TCR-Engineered T Cells Mediate Sustained Antigen-Specific Antitumor Effects in Myeloma'. *Nature Medicine* 21 (8): 914–21. https://doi.org/10.1038/nm.3910.

Reinherz, Ellis L., and Stuart F. Schlossman. 1980. 'The Differentiation and Function of Human T Lymphocytes'. *Cell* 19 (4): 821–27. https://doi.org/10.1016/0092-8674(80)90072-0.

Reppel, Loïc, Ourania Tsahouridis, Jason Akulian, Ian J. Davis, Hong Lee, Giovanni Fucà, Jared Weiss, Gianpietro Dotti, Chad V. Pecot, and Barbara Savoldo. 2022. 'Targeting Disialoganglioside GD2 with Chimeric Antigen Receptor-Redirected T Cells in Lung Cancer'. *Journal for Immunotherapy of Cancer* 10 (1). https://doi.org/10.1136/jitc-2021-003897.

Reth, M. 1989. 'Antigen Receptor Tail Clue'. *Nature* 338 (6214): 383–84. https://doi.org/10.1038/338383b0.

Richman, Sarah A., Selene Nunez-Cruz, Babak Moghimi, Lucy Z. Li, Zachary T. Gershenson, Zissimos Mourelatos, David M. Barrett, Stephan A. Grupp, and Michael C. Milone. 2018. 'High-Affinity GD2-Specific CAR T Cells Induce Fatal Encephalitis in a Preclinical Neuroblastoma Model'. *Cancer Immunology Research* 6 (1): 36–46. https://doi.org/10.1158/2326-6066.CIR-17-0211.

Robinson, James, Jason A. Halliwell, James D. Hayhurst, Paul Flicek, Peter Parham, and Steven G. E. Marsh. 2015. 'The IPD and IMGT/HLA Database: Allele Variant Databases'. *Nucleic Acids Research* 43 (D1): D423–31. https://doi.org/10.1093/nar/gku1161.

Rock, Kenneth L., Eric Reits, and Jacques Neefjes. 2016. 'Present Yourself! By MHC Class I and MHC Class II Molecules'. *Trends in Immunology* 37 (11): 724–37. https://doi.org/10.1016/j.it.2016.08.010.

Roddie, Claire, Juliana Dias, Maeve A. O'Reilly, Mahnaz Abbasian, Amaia Cadinanos-Garai, Ketki Vispute, Leticia Bosshard-Carter, et al. 2021. 'Durable Responses and Low Toxicity After Fast Off-Rate CD19 Chimeric Antigen Receptor-T Therapy in Adults With

Relapsed or Refractory B-Cell Acute Lymphoblastic Leukemia'. *Journal of Clinical Oncology* 39 (30): 3352–63. https://doi.org/10.1200/JCO.21.00917.

Rodriguez-Marquez, Paula, Maria E. Calleja-Cervantes, Guillermo Serrano, Aina Oliver-Caldes, Maria L. Palacios-Berraquero, Angel Martin-Mallo, Cristina Calviño, et al. 2022. 'CAR Density Influences Antitumoral Efficacy of BCMA CAR T Cells and Correlates with Clinical Outcome'. *Science Advances* 8 (39): eabo0514. https://doi.org/10.1126/sciadv.abo0514.

Rogers, Paul R, Jianxun Song, Irene Gramaglia, Nigel Killeen, and Michael Croft. 2001. 'OX40 Promotes Bcl-XL and Bcl-2 Expression and Is Essential for Long-Term Survival of CD4 T Cells'. *Immunity* 15 (3): 445–55. https://doi.org/10.1016/S1074-7613(01)00191-1.

Rosenberg, S. A., B. S. Packard, P. M. Aebersold, D. Solomon, S. L. Topalian, S. T. Toy, P. Simon, M. T. Lotze, J. C. Yang, and C. A. Seipp. 1988. 'Use of Tumor-Infiltrating Lymphocytes and Interleukin-2 in the Immunotherapy of Patients with Metastatic Melanoma. A Preliminary Report'. *The New England Journal of Medicine* 319 (25): 1676–80. https://doi.org/10.1056/NEJM198812223192527.

Rossig, Claudia, Catherine M. Bollard, Jed G. Nuchtern, Durriya A. Merchant, and Malcolm K. Brenner. 2001. 'Targeting of GD2-Positive Tumor Cells by Human T Lymphocytes Engineered to Express Chimeric T-Cell Receptor Genes'. *International Journal of Cancer* 94 (2): 228–36. https://doi.org/10.1002/ijc.1457.

Roybal, Kole T., Levi J. Rupp, Leonardo Morsut, Whitney J. Walker, Krista A. McNally, Jason S. Park, and Wendell A. Lim. 2016. 'Precision Tumor Recognition by T Cells With Combinatorial Antigen Sensing Circuits'. *Cell* 164 (4): 770–79. https://doi.org/10.1016/j.cell.2016.01.011.

Rudd, C. E., J. M. Trevillyan, J. D. Dasgupta, L. L. Wong, and S. F. Schlossman. 1988. 'The CD4 Receptor Is Complexed in Detergent Lysates to a Protein-Tyrosine Kinase (Pp58) from Human T Lymphocytes'. *Proceedings of the National Academy of Sciences* 85 (14): 5190–94. https://doi.org/10.1073/pnas.85.14.5190.

Sabe, H., A. Hata, M. Okada, H. Nakagawa, and H. Hanafusa. 1994. 'Analysis of the Binding of the Src Homology 2 Domain of Csk to Tyrosine-Phosphorylated Proteins in the Suppression and Mitotic Activation of c-Src'. *Proceedings of the National Academy of Sciences of the United States of America* 91 (9): 3984–88. https://doi.org/10.1073/pnas.91.9.3984.

Sahillioglu, Ali Can, Mireille Toebes, Georgi Apriamashvili, Raquel Gomez, and Ton N. Schumacher. 2021. 'CRASH-IT Switch Enables Reversible and Dose-Dependent Control of TCR and CAR T-Cell Function'. *Cancer Immunology Research* 9 (9): 999–1007. https://doi.org/10.1158/2326-6066.CIR-21-0095.

Sakuishi, Kaori, Lionel Apetoh, Jenna M. Sullivan, Bruce R. Blazar, Vijay K. Kuchroo, and Ana C. Anderson. 2010. 'Targeting Tim-3 and PD-1 Pathways to Reverse T Cell Exhaustion and Restore Anti-Tumor Immunity'. *The Journal of Experimental Medicine* 207 (10): 2187–94. https://doi.org/10.1084/jem.20100643.

Salter, Alexander I., Richard G. Ivey, Jacob J. Kennedy, Valentin Voillet, Anusha Rajan, Eva J. Alderman, Uliana J. Voytovich, et al. 2018. 'Phosphoproteomic Analysis of Chimeric Antigen Receptor Signaling Reveals Kinetic and Quantitative Differences That Affect Cell Function'. *Science Signaling* 11 (544). https://doi.org/10.1126/scisignal.aat6753.

Salter, Alexander I., Anusha Rajan, Jacob J. Kennedy, Richard G. Ivey, Sarah A. Shelby, Isabel Leung, Megan L. Templeton, et al. 2021. 'Comparative Analysis of TCR and CAR

Signaling Informs CAR Designs with Superior Antigen Sensitivity and in Vivo Function'. *Science Signaling* 14 (697): eabe2606. https://doi.org/10.1126/scisignal.abe2606.

Samelson, L. E., A. F. Phillips, E. T. Luong, and R. D. Klausner. 1990. 'Association of the Fyn Protein-Tyrosine Kinase with the T-Cell Antigen Receptor'. *Proceedings of the National Academy of Sciences of the United States of America* 87 (11): 4358–62. https://doi.org/10.1073/pnas.87.11.4358.

Sampson, John H., Bryan D. Choi, Luis Sanchez-Perez, Carter M. Suryadevara, David J. Snyder, Catherine T. Flores, Robert J. Schmittling, et al. 2014. 'EGFRvIII MCAR-Modified T-Cell Therapy Cures Mice with Established Intracerebral Glioma and Generates Host Immunity against Tumor-Antigen Loss'. *Clinical Cancer Research* 20 (4): 972–84. https://doi.org/10.1158/1078-0432.CCR-13-0709.

Schoenborn, Jamie R., Ying Xim Tan, Chao Zhang, Kevan M. Shokat, and Arthur Weiss. 2011. 'Feedback Circuits Monitor and Adjust Basal Lck-Dependent Events in T Cell Receptor Signaling'. *Science Signaling* 4 (190): ra59–ra59. https://doi.org/10.1126/scisignal.2001893.

Secrist, J. P., L. A. Burns, L. Karnitz, G. A. Koretzky, and R. T. Abraham. 1993. 'Stimulatory Effects of the Protein Tyrosine Phosphatase Inhibitor, Pervanadate, on T-Cell Activation Events'. *The Journal of Biological Chemistry* 268 (8): 5886–93.

Shah, Michael Russell Bishop, Olalekan O. Oluwole, Aaron Logan, Maria R. Baer, William Bruce Donnellan, Kristen Marie Carr-O'Dwyer, et al. 2019. 'End of Phase I Results of ZUMA-3, a Phase 1/2 Study of KTE-X19, Anti-CD19 Chimeric Antigen Receptor (CAR) T Cell Therapy, in Adult Patients (Pts) with Relapsed/Refractory (R/R) Acute Lymphoblastic Leukemia (ALL).' *Journal of Clinical Oncology* 37 (15_suppl): 7006–7006. https://doi.org/10.1200/JCO.2019.37.15_suppl.7006.

Shah, Steven L. Highfill, Haneen Shalabi, Bonnie Yates, Jianjian Jin, Pamela L. Wolters, Amanda Ombrello, et al. 2020. 'CD4/CD8 T-Cell Selection Affects Chimeric Antigen Receptor (CAR) T-Cell Potency and Toxicity: Updated Results From a Phase I Anti-CD22 CAR T-Cell Trial'. *Journal of Clinical Oncology* 38 (17): 1938–50. https://doi.org/10.1200/JCO.19.03279.

Shah, Daniel W. Lee, Bonnie Yates, Constance M. Yuan, Haneen Shalabi, Staci Martin, Pamela L. Wolters, et al. 2021. 'Long-Term Follow-Up of CD19-CAR T-Cell Therapy in Children and Young Adults With B-ALL'. *Journal of Clinical Oncology: Official Journal of the American Society of Clinical Oncology* 39 (15): 1650–59. https://doi.org/10.1200/JCO.20.02262.

Sharpe, Arlene H., and Gordon J. Freeman. 2002. 'The B7–CD28 Superfamily'. *Nature Reviews Immunology* 2 (2): 116–26. https://doi.org/10.1038/nri727.

Sieh, M., J. B. Bolen, and A. Weiss. 1993. 'CD45 Specifically Modulates Binding of Lck to a Phosphopeptide Encompassing the Negative Regulatory Tyrosine of Lck'. *The EMBO Journal* 12 (1): 315–21.

Siesser, Priscila M.F., and Steven K. Hanks. 2006. 'The Signaling and Biological Implications of FAK Overexpression in Cancer'. *Clinical Cancer Research* 12 (11): 3233–37. https://doi.org/10.1158/1078-0432.CCR-06-0456.

Sillibourne, James E, Giulia Agliardi, Matteo Righi, Katerina Smetanova, Grant Rowley, Simon Speller, Abigail Dolor, et al. 2022. 'A Compact and Simple Method of Achieving Differential Transgene Expression by Exploiting Translational Readthrough'. *BioTechniques* 72 (4): 143–54. https://doi.org/10.2144/btn-2021-0079.

Song, De-Gang, Qunrui Ye, Carmine Carpenito, Mathilde Poussin, Li-Ping Wang, Chunyan Ji, Mariangela Figini, Carl H. June, George Coukos, and Daniel J. Powell. 2011. 'In Vivo Persistence, Tumor Localization, and Antitumor Activity of CAR-Engineered T Cells Is Enhanced by Costimulatory Signaling through CD137 (4-1BB)'. *Cancer Research* 71 (13): 4617–27. https://doi.org/10.1158/0008-5472.CAN-11-0422.

Srivastava, Shivani, Alexander I. Salter, Denny Liggitt, Sushma Yechan-Gunja, Megha Sarvothama, Kirsten Cooper, Kimberly S. Smythe, et al. 2019. 'Logic-Gated ROR1 Chimeric Antigen Receptor Expression Rescues T Cell-Mediated Toxicity to Normal Tissues and Enables Selective Tumor Targeting'. *Cancer Cell* 35 (3): 489-503.e8. https://doi.org/10.1016/j.ccell.2019.02.003.

Stavrou, Maria, Brian Philip, Charlotte Traynor-White, Christopher G. Davis, Shimobi Onuoha, Shaun Cordoba, Simon Thomas, and Martin Pule. 2018. 'A Rapamycin-Activated Caspase 9-Based Suicide Gene'. *Molecular Therapy: The Journal of the American Society of Gene Therapy* 26 (5): 1266–76. https://doi.org/10.1016/j.ymthe.2018.03.001.

Stepanek, Ondrej, Tomas Kalina, Peter Draber, Tereza Skopcova, Karel Svojgr, Pavla Angelisova, Vaclav Horejsi, Arthur Weiss, and Tomas Brdicka. 2011. 'Regulation of Src Family Kinases Involved in T Cell Receptor Signaling by Protein-Tyrosine Phosphatase CD148'. *The Journal of Biological Chemistry* 286 (25): 22101–12. https://doi.org/10.1074/jbc.M110.196733.

Stone, Jennifer D., David H. Aggen, Andrea Schietinger, Hans Schreiber, and David M. Kranz. 2012. 'A Sensitivity Scale for Targeting T Cells with Chimeric Antigen Receptors (CARs) and Bispecific T-Cell Engagers (BiTEs)'. *Oncoimmunology* 1 (6): 863–73. https://doi.org/10.4161/onci.20592.

Straathof, Barry Flutter, Rebecca Wallace, Neha Jain, Thalia Loka, Sarita Depani, Gary Wright, et al. 2020. 'Antitumor Activity without On-Target off-Tumor Toxicity of GD2-Chimeric Antigen Receptor T Cells in Patients with Neuroblastoma'. *Science Translational Medicine* 12 (571): eabd6169. https://doi.org/10.1126/scitranslmed.abd6169.

Straathof, Martin A. Pulè, Patricia Yotnda, Gianpietro Dotti, Elio F. Vanin, Malcolm K. Brenner, Helen E. Heslop, David M. Spencer, and Cliona M. Rooney. 2005. 'An Inducible Caspase 9 Safety Switch for T-Cell Therapy'. *Blood* 105 (11): 4247. https://doi.org/10.1182/blood-2004-11-4564.

Straus, D. B., and A. Weiss. 1992. 'Genetic Evidence for the Involvement of the Lck Tyrosine Kinase in Signal Transduction through the T Cell Antigen Receptor'. *Cell* 70 (4): 585–93. https://doi.org/10.1016/0092-8674(92)90428-f.

Sun, Chuang, Peishun Shou, Hongwei Du, Koichi Hirabayashi, Yuhui Chen, Laura E. Herring, Sarah Ahn, et al. 2020. 'THEMIS-SHP1 Recruitment by 4-1BB Tunes LCK-Mediated Priming of Chimeric Antigen Receptor-Redirected T Cells'. *Cancer Cell* 37 (2): 216-225.e6. https://doi.org/10.1016/j.ccell.2019.12.014.

Sykulev, Yuri, Michael Joo, Irina Vturina, Theodore J. Tsomides, and Herman N. Eisen. 1996. 'Evidence That a Single Peptide–MHC Complex on a Target Cell Can Elicit a Cytolytic T Cell Response'. *Immunity* 4 (6): 565–71. https://doi.org/10.1016/S1074-7613(00)80483-5.

Szymczak, Andrea L., Creg J. Workman, Diana Gil, Smaroula Dilioglou, Kate M. Vignali, Ed Palmer, and Dario A. A. Vignali. 2005. 'The CD3ε Proline-Rich Sequence, and Its Interaction with Nck, Is Not Required for T Cell Development and Function'. *The Journal of Immunology* 175 (1): 270–75. https://doi.org/10.4049/jimmunol.175.1.270.

Tanaka, S., L. Neff, R. Baron, and J. B. Levy. 1995. 'Tyrosine Phosphorylation and Translocation of the C-Cbl Protein after Activation of Tyrosine Kinase Signaling Pathways'. *The Journal of Biological Chemistry* 270 (24): 14347–51. https://doi.org/10.1074/jbc.270.24.14347.

Tangye, S. G., J. Wu, G. Aversa, J. E. de Vries, L. L. Lanier, and J. H. Phillips. 1998. 'Negative Regulation of Human T Cell Activation by the Receptor-Type Protein Tyrosine Phosphatase CD148'. *Journal of Immunology (Baltimore, Md.: 1950)* 161 (8): 3803–7.

Teachey, David T., Simon F. Lacey, Pamela A. Shaw, J. Joseph Melenhorst, Shannon L. Maude, Noelle Frey, Edward Pequignot, et al. 2016. 'Identification of Predictive Biomarkers for Cytokine Release Syndrome after Chimeric Antigen Receptor T-Cell Therapy for Acute Lymphoblastic Leukemia'. *Cancer Discovery* 6 (6): 664–79. https://doi.org/10.1158/2159-8290.CD-16-0040.

Terzic, Tatjana, Martine Cordeau, Sabine Herblot, Pierre Teira, Sonia Cournoyer, Mona Beaunoyer, Michel Peuchmaur, Michel Duval, and Herve Sartelet. 2018. 'Expression of Disialoganglioside (GD2) in Neuroblastic Tumors: A Prognostic Value for Patients Treated With Anti-GD2 Immunotherapy'. *Pediatric and Developmental Pathology* 21 (4): 355–62. https://doi.org/10.1177/1093526617723972.

Thien, Christine B. F., and Wallace Y. Langdon. 2005. 'C-Cbl and Cbl-b Ubiquitin Ligases: Substrate Diversity and the Negative Regulation of Signalling Responses'. *The Biochemical Journal* 391 (Pt 2): 153–66. https://doi.org/10.1042/BJ20050892.

Thistlethwaite, Fiona C., David E. Gilham, Ryan D. Guest, Dominic G. Rothwell, Manon Pillai, Deborah J. Burt, Andrea J. Byatte, et al. 2017. 'The Clinical Efficacy of First-Generation Carcinoembryonic Antigen (CEACAM5)-Specific CAR T Cells Is Limited by Poor Persistence and Transient Pre-Conditioning-Dependent Respiratory Toxicity'. *Cancer Immunology, Immunotherapy* 66 (11): 1425–36. https://doi.org/10.1007/s00262-017-2034-7.

Thomas, and Joan S. Brugge. 1997. 'Cellular Functions Regulated by Src Family Kinases'. *Annual Review of Cell and Developmental Biology* 13 (1): 513–609. https://doi.org/10.1146/annurev.cellbio.13.1.513.

Thomas, M. L. 1989. 'The Leukocyte Common Antigen Family'. *Annual Review of Immunology* 7: 339–69. https://doi.org/10.1146/annurev.iy.07.040189.002011.

Thomas, M. L., and L. Lefrançois. 1988. 'Differential Expression of the Leucocyte-Common Antigen Family'. *Immunology Today* 9 (10): 320–26. https://doi.org/10.1016/0167-5699(88)91326-6.

Till, Brian G., Michael C. Jensen, Jinjuan Wang, Eric Y. Chen, Brent L. Wood, Harvey A. Greisman, Xiaojun Qian, et al. 2008. 'Adoptive Immunotherapy for Indolent Non-Hodgkin Lymphoma and Mantle Cell Lymphoma Using Genetically Modified Autologous CD20-Specific T Cells'. *Blood* 112 (6): 2261–71. https://doi.org/10.1182/blood-2007-12-128843.

Tokarski, John S., John A. Newitt, Chieh Ying J. Chang, Janet D. Cheng, Michael Wittekind, Susan E. Kiefer, Kevin Kish, et al. 2006. 'The Structure of Dasatinib (BMS-354825) Bound to Activated ABL Kinase Domain Elucidates Its Inhibitory Activity against Imatinib-Resistant ABL Mutants'. *Cancer Research* 66 (11): 5790–97. https://doi.org/10.1158/0008-5472.CAN-05-4187.

Topp, M.S., N. Gökbuget, G. Zugmaier, P. Klappers, M. Stelljes, S. Neumann, A. Viardot, et al. 2014. 'Phase II Trial of the Anti-CD19 Bispecific T Cell-Engager Blinatumomab Shows Hematologic and Molecular Remissions in Patients with Relapsed or Refractory B-

Precursor Acute Lymphoblastic Leukemia'. *Journal of Clinical Oncology* 32 (36): 4134–40. https://doi.org/10.1200/JCO.2014.56.3247.

Tousley, Aidan M., Maria Caterina Rotiroti, Louai Labanieh, Lea Wenting Rysavy, Won-Ju Kim, Caleb Lareau, Elena Sotillo, et al. 2023. 'Co-Opting Signalling Molecules Enables Logic-Gated Control of CAR T Cells'. *Nature*, March, 1–10. https://doi.org/10.1038/s41586-023-05778-2.

Tsimberidou, Apostolia-Maria, Karlyle Van Morris, Henry Hiep Vo, Stephen Eck, Yu-Feng Lin, Jorge Mauricio Rivas, and Borje S. Andersson. 2021. 'T-Cell Receptor-Based Therapy: An Innovative Therapeutic Approach for Solid Tumors'. *Journal of Hematology & Oncology* 14 (1): 1–22. https://doi.org/10.1186/s13045-021-01115-0.

Turatti, Fabio, Mariangela Figini, Emanuela Balladore, Paola Alberti, Patrizia Casalini, James D. Marks, Silvana Canevari, and Delia Mezzanzanica. 2007. 'Redirected Activity of Human Antitumor Chimeric Immune Receptors Is Governed by Antigen and Receptor Expression Levels and Affinity of Interaction'. *Journal of Immunotherapy (Hagerstown, Md.: 1997)* 30 (7): 684–93. https://doi.org/10.1097/CJI.0b013e3180de5d90.

Turcotte, Simon, Alena Gros, Eric Tran, Chyi-Chia R. Lee, John R. Wunderlich, Paul F. Robbins, and Steven A. Rosenberg. 2014. 'Tumor-Reactive CD8+ T Cells in Metastatic Gastrointestinal Cancer Refractory to Chemotherapy'. *Clinical Cancer Research: An Official Journal of the American Association for Cancer Research* 20 (2): 331–43. https://doi.org/10.1158/1078-0432.CCR-13-1736.

Turtle, Cameron J., Laïla-Aïcha Hanafi, Carolina Berger, Theodore A. Gooley, Sindhu Cherian, Michael Hudecek, Daniel Sommermeyer, et al. 2016. 'CD19 CAR-T Cells of Defined CD4+:CD8+ Composition in Adult B Cell ALL Patients'. *The Journal of Clinical Investigation* 126 (6): 2123–38. https://doi.org/10.1172/JCI85309.

Vang, Torkel, Knut Martin Torgersen, Vibeke Sundvold, Manju Saxena, Finn Olav Levy, Bjørn S. Skålhegg, Vidar Hansson, Tomas Mustelin, and Kjetil Taskén. 2001. 'Activation of the Cooh-Terminal Src Kinase (Csk) by Camp-Dependent Protein Kinase Inhibits Signaling through the T Cell Receptor'. *The Journal of Experimental Medicine* 193 (4): 497–508.

Veillette, André, Michael A. Bookman, Eva M. Horak, and Joseph B. Bolen. 1988. 'The CD4 and CD8 T Cell Surface Antigens Are Associated with the Internal Membrane Tyrosine-Protein Kinase P56lck'. *Cell* 55 (2): 301–8. https://doi.org/10.1016/0092-8674(88)90053-0.

Wang, Yoav Altman, Deyu Fang, Chris Elly, Yang Dai, Yuan Shao, and Yun-Cai Liu. 2001. 'Cbl Promotes Ubiquitination of the T Cell Receptor ζ through an Adaptor Function of Zap-70'. *Journal of Biological Chemistry* 276 (28): 26004–11. https://doi.org/10.1074/jbc.M010738200.

Wang, Wen-Chung Chang, ChingLam W. Wong, David Colcher, Mark Sherman, Julie R. Ostberg, Stephen J. Forman, Stanley R. Riddell, and Michael C. Jensen. 2011. 'A Transgene-Encoded Cell Surface Polypeptide for Selection, in Vivo Tracking, and Ablation of Engineered Cells'. *Blood* 118 (5): 1255–63. https://doi.org/10.1182/blood-2011-02-337360.

Wang, Javier Munoz, Andre Goy, Frederick L. Locke, Caron A. Jacobson, Brian T. Hill, John M. Timmerman, et al. 2020. 'KTE-X19 CAR T-Cell Therapy in Relapsed or Refractory Mantle-Cell Lymphoma'. *The New England Journal of Medicine* 382 (14): 1331–42. https://doi.org/10.1056/NEJMoa1914347.

———. 2022. ‘Three-Year Follow-Up of KTE-X19 in Patients With Relapsed/Refractory Mantle Cell Lymphoma, Including High-Risk Subgroups, in the ZUMA-2 Study’. *Journal of Clinical Oncology*, June, JCO.21.02370. https://doi.org/10.1200/JCO.21.02370.

Wang, Guoqing Wei, and Delong Liu. 2012. ‘CD19: A Biomarker for B Cell Development, Lymphoma Diagnosis and Therapy’. *Experimental Hematology & Oncology* 1 (1): 36. https://doi.org/10.1186/2162-3619-1-36.

Wange, R. L. 2000. ‘LAT, the Linker for Activation of T Cells: A Bridge between T Cell-Specific and General Signaling Pathways’. *Science’s STKE: Signal Transduction Knowledge Environment* 2000 (63): re1. https://doi.org/10.1126/stke.2000.63.re1.

Watanabe, Keisuke, Seitaro Terakura, Anton C. Martens, Tom van Meerten, Susumu Uchiyama, Misa Imai, Reona Sakemura, et al. 2015. ‘Target Antigen Density Governs the Efficacy of Anti-CD20-CD28-CD3 ζ Chimeric Antigen Receptor-Modified Effector CD8+ T Cells’. *Journal of Immunology (Baltimore, Md.: 1950)* 194 (3): 911–20. https://doi.org/10.4049/jimmunol.1402346.

Watanabe, Keisuke, Seitaro Terakura, Susumu Uchiyama, Anton C. Martens, Tom van Meerten, Hitoshi Kiyoi, Tetsuya Nishida, Tomoki Naoe, and Makoto Murata. 2014. ‘Excessively High-Affinity Single-Chain Fragment Variable Region in a Chimeric Antigen Receptor Can Counteract T-Cell Proliferation’. *Blood* 124 (21): 4799. https://doi.org/10.1182/blood.V124.21.4799.4799.

Weber, Evan W., Rachel C. Lynn, Elena Sotillo, John Lattin, Peng Xu, and Crystal L. Mackall. 2019. ‘Pharmacologic Control of CAR-T Cell Function Using Dasatinib’. *Blood Advances* 3 (5): 711–17. https://doi.org/10.1182/bloodadvances.2018028720.

Weber, Evan W., Kevin R. Parker, Elena Sotillo, Rachel C. Lynn, Hima Anbunathan, John Lattin, Zinaida Good, et al. 2021. ‘Transient “Rest” Restores Functionality in Exhausted CAR-T Cells via Epigenetic Remodeling’. *Science (New York, N.Y.)* 372 (6537). https://doi.org/10.1126/science.aba1786.

Weiss, Arthur, and Dan R. Littman. 1994. ‘Signal Transduction by Lymphocyte Antigen Receptors’. *Cell* 76 (2): 263–74. https://doi.org/10.1016/0092-8674(94)90334-4.

Wilkie, Scott, Gianfranco Picco, Julie Foster, David M. Davies, Sylvain Julien, Lucienne Cooper, Sefina Arif, et al. 2008. ‘Retargeting of Human T Cells to Tumor-Associated MUC1: The Evolution of a Chimeric Antigen Receptor’. *Journal of Immunology (Baltimore, Md.: 1950)* 180 (7): 4901–9. https://doi.org/10.4049/jimmunol.180.7.4901.

Williams, Matthew A., and Michael J. Bevan. 2007. ‘Effector and Memory CTL Differentiation’. *Annual Review of Immunology* 25 (1): 171–92. https://doi.org/10.1146/annurev.immunol.25.022106.141548.

Wooldridge, Linda, Hugo A. van den Berg, Meir Glick, Emma Gostick, Bruno Laugel, Sarah L. Hutchinson, Anita Milicic, et al. 2005. ‘Interaction between the CD8 Coreceptor and Major Histocompatibility Complex Class I Stabilizes T Cell Receptor-Antigen Complexes at the Cell Surface’. *The Journal of Biological Chemistry* 280 (30): 27491–501. https://doi.org/10.1074/jbc.M500555200.

Wu, Anjali Katrekar, Lee A. Honigberg, Ashley M. Smith, Marion T. Conn, Jie Tang, Doug Jeffery, et al. 2006. ‘Identification of Substrates of Human Protein-Tyrosine Phosphatase PTPN22’. *Journal of Biological Chemistry* 281 (16): 11002–10. https://doi.org/10.1074/jbc.M600498200.

Wu, Kole T. Roybal, Elias M. Puchner, James Onuffer, and Wendell A. Lim. 2015. ‘Remote Control of Therapeutic T Cells through a Small Molecule-Gated Chimeric Receptor’.

Science (New York, N.Y.) 350 (6258): aab4077. https://doi.org/10.1126/science.aab4077.

Wucherpfennig, Kai W., Etienne Gagnon, Melissa J. Call, Eric S. Huseby, and Matthew E. Call. 2010. 'Structural Biology of the T-Cell Receptor: Insights into Receptor Assembly, Ligand Recognition, and Initiation of Signaling'. *Cold Spring Harbor Perspectives in Biology* 2 (4): a005140. https://doi.org/10.1101/cshperspect.a005140.

Xiao, Qian, Xinyan Zhang, Liqun Tu, Jian Cao, Christian S. Hinrichs, and Xiaolei Su. 2022. 'Size-Dependent Activation of CAR-T Cells'. *Science Immunology* 7 (74): eabl3995. https://doi.org/10.1126/sciimmunol.abl3995.

Xu, Amish Doshi, Ming Lei, Michael J Eck, and Stephen C Harrison. 1999. 'Crystal Structures of C-Src Reveal Features of Its Autoinhibitory Mechanism'. *Molecular Cell* 3 (5): 629–38. https://doi.org/10.1016/S1097-2765(00)80356-1.

Xu, Jianxin Huo, Joy En-Lin Tan, and Kong-Peng Lam. 2005. 'Cbp Deficiency Alters Csk Localization in Lipid Rafts but Does Not Affect T-Cell Development'. *Molecular and Cellular Biology* 25 (19): 8486–95. https://doi.org/10.1128/MCB.25.19.8486-8495.2005.

Xu, Ming Zhang, Carlos A. Ramos, April Durett, Enli Liu, Olga Dakhova, Hao Liu, et al. 2014. 'Closely Related T-Memory Stem Cells Correlate with in Vivo Expansion of CAR.CD19-T Cells and Are Preserved by IL-7 and IL-15'. *Blood* 123 (24): 3750–59. https://doi.org/10.1182/blood-2014-01-552174.

Yamaguchi, Hiroto, and Wayne A. Hendrickson. 1996. 'Structural Basis for Activation of Human Lymphocyte Kinase Lck upon Tyrosine Phosphorylation'. *Nature* 384 (6608): 484–89. https://doi.org/10.1038/384484a0.

Ying, Zhitao, Ting He, Xiaopei Wang, Wen Zheng, Ningjing Lin, Meifeng Tu, Yan Xie, et al. 2019. 'Parallel Comparison of 4-1BB or CD28 Co-Stimulated CD19-Targeted CAR-T Cells for B Cell Non-Hodgkin's Lymphoma'. *Molecular Therapy - Oncolytics* 15 (December): 60–68. https://doi.org/10.1016/j.omto.2019.08.002.

Yu, Alice L., Andrew L. Gilman, M. Fevzi Ozkaynak, Wendy B. London, Susan G. Kreissman, Helen X. Chen, Malcolm Smith, et al. 2010. 'Anti-GD2 Antibody with GM-CSF, Interleukin-2, and Isotretinoin for Neuroblastoma'. *The New England Journal of Medicine* 363 (14): 1324–34. https://doi.org/10.1056/NEJMoa0911123.

Zajac, Allan J., Joseph N. Blattman, Kaja Murali-Krishna, David J.D. Sourdive, M. Suresh, John D. Altman, and Rafi Ahmed. 1998. 'Viral Immune Evasion Due to Persistence of Activated T Cells Without Effector Function'. *The Journal of Experimental Medicine* 188 (12): 2205–13.

Zhang, Joanne Sloan-Lancaster, Jason Kitchen, Ronald P Trible, and Lawrence E Samelson. 1998. 'LAT: The ZAP-70 Tyrosine Kinase Substrate That Links T Cell Receptor to Cellular Activation'. *Cell* 92 (1): 83–92. https://doi.org/10.1016/S0092-8674(00)80901-0.

Zhang, Zhiwei, Duqing Jiang, Huan Yang, Zhou He, Xiangzhen Liu, Wenxia Qin, Linfang Li, et al. 2019. 'Modified CAR T Cells Targeting Membrane-Proximal Epitope of Mesothelin Enhances the Antitumor Function against Large Solid Tumor'. *Cell Death & Disease* 10 (7): 1–12. https://doi.org/10.1038/s41419-019-1711-1.

Zhao, Xiangyu, Junfang Yang, Xian Zhang, Xin-An Lu, Min Xiong, Jianping Zhang, Xiaosu Zhou, et al. 2020. 'Efficacy and Safety of CD28- or 4-1BB-Based CD19 CAR-T Cells in B Cell Acute Lymphoblastic Leukemia'. *Molecular Therapy Oncolytics* 18 (June): 272–81. https://doi.org/10.1016/j.omto.2020.06.016.

Zhong, Xiao-Song, Maiko Matsushita, Jason Plotkin, Isabelle Riviere, and Michel Sadelain. 2010. 'Chimeric Antigen Receptors Combining 4-1BB and CD28 Signaling Domains Augment PI3kinase/AKT/Bcl-XL Activation and CD8+ T Cell–Mediated Tumor Eradication'. *Molecular Therapy* 18 (2): 413–20. https://doi.org/10.1038/mt.2009.210.

Zhou, Ru, Mahboubeh Yazdanifar, Lopamudra Das Roy, Lynsey M. Whilding, Artemis Gavrill, John Maher, and Pinku Mukherjee. 2019. 'CAR T Cells Targeting the Tumor MUC1 Glycoprotein Reduce Triple-Negative Breast Cancer Growth'. *Frontiers in Immunology* 10 (May). https://doi.org/10.3389/fimmu.2019.01149.

Zikherman, Julie, Michelle Hermiston, David Steiner, Kiminori Hasegawa, Andrew Chan, and Arthur Weiss. 2009. 'PTPN22 Deficiency Cooperates with the CD45 E613R Allele to Break Tolerance on a Non-Autoimmune Background'. *The Journal of Immunology* 182 (7): 4093–4106. https://doi.org/10.4049/jimmunol.0803317.

Zikherman, Julie, Craig Jenne, Susan Watson, Kristin Doan, William Raschke, Christopher C. Goodnow, and Arthur Weiss. 2010. 'CD45-Csk Phosphatase-Kinase Titration Uncouples Basal and Inducible T Cell Receptor Signaling during Thymic Development'. *Immunity* 32 (3): 342–54. https://doi.org/10.1016/j.immuni.2010.03.006.

Zirngibl, Felix, Sara M Ivasko, Laura Grunewald, Anika Klaus, Silke Schwiebert, Peter Ruf, Horst Lindhofer, et al. 2021. 'GD2-Directed Bispecific Trifunctional Antibody Outperforms Dinutuximab Beta in a Murine Model for Aggressive Metastasized Neuroblastoma'. *Journal for Immunotherapy of Cancer* 9 (7): e002923. https://doi.org/10.1136/jitc-2021-002923.